UCSF
UC San Francisco Electronic Theses and Dissertations

Title
Differentiation of Caudal Interneuron Populations from Human Pluripotent Stem Cells

Permalink
https://escholarship.org/uc/item/38445035

Author
Butts, Jessica

Publication Date
2018

Peer reviewed|Thesis/dissertation

eScholarship.org Powered by the California Digital Library
University of California

Differentiation of Caudal Interneuron Populations from Human Pluripotent Stem Cells

by

Jessica C. Butts

DISSERTATION

Submitted in partial satisfaction of the requirements for the degree of

DOCTOR OF PHILOSOPHY

in

Bioengineering

in the

GRADUATE DIVISION

of the

UNIVERSITY OF CALIFORNIA, SAN FRANCISCO

AND

UNIVERSITY OF CALIFORNIA, BERKELEY

Copyright 2018
by
Jessica Butts

Dedicated to my nieces Layla Christine and Evelyn Nicole
&
my godson Evan James.

May your love for your adventure and learning never cease and may you know your family will always support your dreams.

ACKNOWLEDGEMENTS

I have thoroughly enjoyed my time as a graduate student. I will always be thankful for the opportunities I have been giving to learn, to gain friendships and mentors, to live in and travel to new places, and to push myself to become a better scientist. Even when experiments were not cooperating, I always had an incredible support system to keep me motivated.

I would first like to thank Dr. Shelly Sakiyama-Elbert for taking a chance on me as an undergraduate by giving me my first research experience. My first few years of college were rough and I was heavily questioning if I was cut out for biomedical engineering. My motivation was restored once I experienced the gratification of scientific discovery. I have to also thank the entire SSE lab – Nithya Jesuraj, Dylan McCreedy, Laura Marquardt, Thomas Willems, Xi Lu, Nisha Iyer, Hao Xu, and my research partner in crime – Chelsea Brown for showing me what strong lab comradery looks like and for your all you continued support throughout my time in graduate school. I also have to thank Dr. Amy Harkins for all the mentorship and guidance as I applied to graduate schools. Thank you for encouraging me to cold call professors, to add my race results to the bottom of what was a very brief CV at the time, and to sign my Georgia Tech acceptance letter in the break room on April 15th 2013. Without these things, I would have never joined the McDevitt Lab, which has been an incredible experience.

I would like to thank my advisor, Dr. Todd McDevitt, for the unwavering support throughout the past 5 years. From the very first meeting that occurred before I even began graduate school, he was supportive of and excited by new ideas. I will be forever grateful for the amount of trust and independence Todd gave me to start a new project in the lab. I

learned so much from Todd during the move from Atlanta to San Francisco. Todd is such a caring person that he made it a priority to ensure that each individual in the lab was taken care of during the move. I have learned many lessons from him that will be key to my future success including thinking more big picture, writing more concisely (still working on it), and learning to be more flexible. In addition to supporting my science, Todd always encouraged my passion for community outreach. I am thankful to have been trained by someone who recognizes the broader impacts of our research.

I would like to thank my committee members, Dr. David Schaffer, Dr. Yadong Huang, Dr. Tejal Desai, Dr. Linda Noble, and Dr. Shelly Sakiyama-Elbert for their intellectual support of my thesis work. I feel very lucky to have the opportunity to get feedback from the leaders in the field. Beyond my thesis work, my committee members have also ensured my future career goals are in place and have provided support in me moving on to my next position.

I'd like to thank my second mentor, Dr. Robert Mahley, for welcoming me into the Gladstone community. After the move to San Francisco, Dr. Mahley was a key component in helping me settle into the new environment. Anyone who knows Dr. Mahley knows that he can put a smile on your face by just a quick passing in the hall. In addition, the career advice he has provided me over the past three years is invaluable. Dr. Mahley has spent many hours with me going over presentation slides and he is not afraid to tell me when a slide needs improvement. From chalk talk pointers to advice on how to be a good mentor and mentee, I am a better scientist and trainee because of Dr. Mahley.

The past 5 years would not have been as enjoyable with out my fantastic lab mates. When I joined the lab at Georgia Tech it was quite large but still had great sense of

community and pride. This was thanks to the graduate students at the time who were incredibly welcoming and provided me with an easy transition to my graduate work.

As I began working with human cells, I also started working with Dr. Tracy Hookway, an incredible post-doc in the lab. If you know Tracy, you know that she is a great mentor. Even though I was a first year graduate student, she immediately treated me like her equal and we quickly began to learn from each other. She was such a rock for the whole lab to lean on during the transition phase of the lab and we all owe a lot to her. Not only is she a great person inside of the lab but we also became good friends outside of the lab.

The decision to leave Atlanta and my friends was very hard but I know scientifically it was the right choice. I am very thankful for the other lab members who made the move to the Gladstone – Dr. Tracy Hookway, Dr. Yun Wang, Dr. Jenna Quinto, and Dr. Josh Zimmermann as well as Oriane Matthys who was the first new person to join the lab in San Francisco and my now husband, Dr. Dylan McCreedy. Setting up a new lab space was a lot of work but also a great learning experience! I am very thankful to everyone at Gladstone for being so welcoming and making the transition very smooth. I was culturing cells just a week after moving! The lab quickly expanded in San Francisco with the addition of new graduate students (Ashley Libby, Ariel Kauss, David Joy, Ana Silva), post docs and fellows (Dr. Vaishaali Natarajan, Dr. Diwakar Turaga, and Dr. Michael Kang), lab assistants (Nik Mendoza-Camacho and Eszter Mihaly) and our trusty lab managers – first Amy Foley and now Ron Manlapaz. I feel very lucky to have worked with such a talented group of scientists, each with their own strengths. I have learned so much from my lab members, and while we were working on different projects, my science was elevated because of their guidance. I have learned how important it is to have a strong support system when

experiments may not be going your way. The McDevitt lab has always been there to support and encourage each other and I am very excited for what future holds for the lab.

The quality of science and people at the Gladstone Institutes makes it a very special place to work. I interacted with many labs in both the Gladstone Institute of Cardiovascular Disease (GICD) and Gladstone Institute of Neurological Disease (GIND) that valued collaboration and helped pushed my science to the next level. At the heart of the great science at Gladstone is the support and guidance from the core facilities. The work that follows would not have been possible with out the resources provided by the Stem Cell Core, Microscopy and Histology core, Bioinformatics Core, Genomics Core, and the Communications team.

I have been very thankful for my friendships outside of lab that have kept my spirits lifted. To my Georgia Tech friends, Katy Lassahn, Chad Glen, Liane Tellier, Andrew Shockey, Muaz Rushdi, Michael "Sack" Lockard, Michael Nelson, and Kristin Nelson, you all are incredible people. I really enjoyed exploring Atlanta with you and thank you for humoring me with your participation in Drink Club. Even though I was only in Atlanta for a year and a half, we figured out the early years of graduate student life together and because of that, developed life-long friendships. Kyle, I'm sorry we never got our band off the ground but I am so thankful for our jamming nights and breakfast conversations. I am thankful for the continued support even though I moved across the country.

After moving to San Francisco, the McDevitt Lab 2.0 became close. Thank you to Tracy, Jenna, Josh, and Oriane for helping me settle into the new city by exploring new neighborhoods, having game nights, and going to Giants games. To Oriane Mattys, thank you for going to South East Asia and deferring your graduate school acceptance so that we

could be friends. You have been my swolemate, my GO co-chair, my cooking buddy, and overall just a great person. I was also very lucky that my family friends, The Smiths, also live in San Francisco. Ryan Smith is a big reason why I am who I am today. He's the reason I chose to pursue biomedical engineering, he introduced me to my first research advisor, and at the same time, unknowingly, introduced me to my husband. I have been so lucky to be able to spend the last 3 years in the same city with him and his wife, Kristin, and daughter, Athena. Also, after several years of being away at college, my best friend from childhood, Zach Smith and I were reunited in San Francisco. For a while, he actually worked next door to Gladstone! There is nothing like having the comfort of a conversation with a childhood friend and I can't be more thankful for his continued love and support. Though they haven't been in San Francisco with me, Maggie Causey and Hanna Wright have continued to be my cheerleaders from across the country.

While I am very passionate about my science, nothing comes before family. I would not be where I am today without my parents Dave and Janie Butts. From a young age, my parents fully supported both my academic and extracurricular activities. I am thankful for the many phone calls and conversations that encouraged me when things were not going great but also celebrated my accomplishments. I am also thankful for the support of my siblings and their growing families. Growing up, my siblings gave me a tough act to follow, as they were role all models for success. Thank you for all the love and encouragement you have given me through the past 5 years.

It only seems appropriate that Dylan and I met in the lab. I have really enjoyed being able to work with Dylan on this project but I am also thankful for his continued support outside of the lab. We have always approached our relationship as a team, picking each

other up when experiments get tough. It has been invaluable to have a partner that understands the ups and downs of a career in research. Thank you for the morning Philz dates, going to concerts with me, and playing board games late into the night when I could not get my mind off of my experiments. Dylan can be my biggest science critic but also my biggest fan and is continuously pushing me to be a better scientist and person.

The text of chapter 2 of this dissertation is a reprint of the material as it appears in Differentiation of V2a Interneurons from Human Pluripotent Stem Cells ". The co-author listed in this publication directed and supervised the research that forms the basis for the dissertation/thesis.

Abstract

Interneurons, the most abundant neuronal class in the CNS, are critical to transducing synaptic information within and between neural networks for proper neurologic function. In the hindbrain and spinal cord, ventral interneurons are key components of pattern generators that control respiration and locomotion. Disruption of the interneurons by disease or injury can disrupt the pattern generators and lead to debilitation. Elucidating how these interneuron populations develop, as well as their roles in pattern generation, can lead to potential repair strategies for damaged circuits. While murine models have provided insight on interneuron development and circuitry, human populations may develop and function differently. Human pluripotent stem cell (hPSC)-derived neural populations provide a source to study human development and circuitry when alternative tissues are unavailable. This dissertation describes three studies that derive caudal interneuron populations from hPSCs. In the first study, V2a interneurons, a population involved in respiratory control and left-right coordination are differentiated from hPSCs. The V2a interneurons appropriately mature and survive to form long extensions following transplantation into an uninjured murine spinal cord. In the second study, multiple interneuron populations critical to respiratory control are specified from hPSCs. This study demonstrates the ability to describe multiple tissue-specific populations from one combination of signaling molecules. In the final study, a respiratory organoid is described that contains populations critical to respiratory control. This model provides a platform to probe how disruption of neural networks leads to respiratory distress. Together, this work is the first to describe multiple interneuron populations from hPSCs. These caudal interneurons can be used to study human development, test new drugs, and

establish therapies to reconnect neural networks following injury or disease. Additionally, these studies provided a systematic approach to co-emerge multiple neural populations that could be broadly applied to describe other neural populations.

TABLE OF CONTENTS

Chapter 1: Introduction **1**

1.1 Overview 1

1.2 Neural Tube Development 3

1.2.1 Overview of Neural Tube Development 3

1.2.2 Ventrodorsal Specification of the Neural Tube 5

1.2.3 Rostrocaudal Specification of the Neural Tube 6

1.2.3 Notch Signaling During Neurogenesis 8

1.3 Directed Stem Cell Differentiation into Neuronal Phenotypes 10

1.3.1 Directing Stem Cells to Neural Phenotypes 11

1.3.2 Neural Phenotypes Differentiated from Pluripotent Stem Cells 16

1.3.3 Interneuron Phenotypes Described from Pluripotent Stem Cells 17

1.3.4 Nueral Organoid Culture Systems 20

1.4 Central Pattern Generators 22

1.4.1 Locomotor Central Pattern Generators 23

1.4.2 Role of Interneuron Subtypes in Locomotor Central Pattern Generators 24

1.4.3 Respiratory Central Pattern Generators 26

1.4.4 Role of Hindbrain Nuclei in Respiratory Central Pattern Generators 27

1.5 Concluding Remarks 30

1.6 Bibliography 32

Chapter 2: Specification of V2a interneurons from human pluripotent stem cells **44**

2.1 Introduction 44

2.2 Materials and Methods 46

2.2.1 Human Pluripotent Stem Cell Culture 46

2.2.2 V2a Interneuron Differentiation 46

2.2.3 Neuronal Maturation 47

2.2.4 Real Time Quantification Polymerase Chain Reaction 47

2.2.5 Flow Cytometry 48

2.2.6 *In Vitro* Immunocytochemistry and Imaging 49

2.2.7 Single Cell RNA sequencing 49

2.2.8 Calcium Imaging and Analysis 50

2.2.9 Electrophysiological Testing 50

2.2.10 Spinal Transplantation 51

2.2.11 Murine Tissue Processing and Immunofluorescence 52

2.2.12 Image Quantification 54

2.2.13 Cryopreservation 54

2.2.14 Statistical Analysis 55

2.3 Results 55

2.3.1 Induction of V2a Interneurons is Dependent on RA, Shh, and Inhibition of Notch 55

2.3.2 Differentiation of V2a Interneurons is Specific 60

2.3.3 Long-term culture increases the maturation profile of V2a interneurons 70

2.3.4 Transplanted hPSC Derived V2a Interneurons Survive and Mature in the Uninjured Murine Spinal Cord ____ 74

2.3.5 Cryopreservation of V2a Interneurons ____ 78

2.4 Discussion ____ 80

2.5 Conclusions ____ 85

2.6 Bibliography ____ 87

Chapter 3: Co-emergence of Respiratory Hindbrain Populations____91

3.1 Introduction ____ 91

3.2 Materials and Methods ____ 95

3.2.1 Human Pluripotent Stem Cell Culture____ 95

3.2.2 V2a Interneuron Differentiation____ 95

3.2.3 Dissociation of V2a Interneuron Cultures ____ 96

3.2.4 Enrichment with Replating ____ 96

3.2.5 WNT Treatment____ 97

3.2.6 Single Cell RNA Sequencing____ 97

3.2.7 Flow Cytometry ____ 98

3.2.8 *In Vitro* Immunocytochemistry and Imaging ____ 99

3.2.9 Statistical Analysis____ 99

3.3 Results ____100

3.3.1 V2a Interneuron Enrichment Through Replating and WNT Activation __100

3.3.2 Characterization of Heterogeneous V2a Interneuron Cultures ____104

3.3.3 Identification of Hindbrain Neuronal Populations____108

3.3.4 *In Vitro* Confirmation of Hindbrain Populations ____ 113

3.3.5 Manipulation of Hindbrain Interneuron Populations in Response to Shh and RA treatment ____ 115

3.4 Discussion ____ 116

3.5 Conclusions ____ 121

3.6 Bibliography ____ 122

Chapter 4: Generation of Respiratory Hindbrain Organoids ____ 127

4.1 Introduction ____ 127

4.2 Materials and Methods ____ 131

4.2.1 Human Pluripotent Stem Cell Culture ____ 131

4.2.2 V2a Interneuron Differentiation ____ 132

4.2.3 Dissociation of V2a Interneuron Organoid Cultures ____ 133

4.2.4 Neuronal Maturation ____ 133

4.2.5 Flow Cytometry ____ 133

4.2.6 Organoid Tissue Processing ____ 134

4.2.7 Histological Processing of Organoid Tissue Sections ____ 135

4.2.8 Immunocytochemistry and Imaging of Whole Mount Organoids ____ 136

4.2.9 Phase Imaging Quantification ____ 136

4.2.10 Calcium Imaging and Analysis ____ 138

4.2.11 Statistical Analysis ____ 138

4.3 Results ____ 139

4.3.1 3D Differentiation fo Hindbrain Respiratory Populations ____ 139

4.3.2 Modulation of V2a and V0 Interneurons in Response to Sonic Hedgehog Signaling ____ 141

4.3.3 Developmental Timeline of Organoid Culture ____ 143

4.3.4 Phenotypic Analysis of Maturing Organoid Cultures ____ 154

4.3.5 Functional Analysis of Maturing Orgnaoid Cultures ____ 159

4.3.6 Model of CCHS in Organoid Culture ____ 163

4.4 Discussion ____ 167

4.5 Conclusions ____ 171

4.6 Bibliography ____ 172

Chapter 5: Future Considerations ____ 176

5.1 Reporter Lines for Real-Time Differentiation Assessment ____ 177

5.2 Caudalization of Interneuron Phenotypes ____ 180

5.3 Optimization of Differentiation using Design of Experiment ____ 182

5.4 Conclusions ____ 183

5.5 Bibliography ____ 185

LIST OF TABLES

Table 2.1: Primer sequences for real-time quantitative PCR analysis_____ 53

Table 2.2: Antibodies used for flow cytometry and immunostaining _____ 53

Table 2.3: Top differentially expressed genes for each cluster from heatmap ____ 64

Table 2.4: Genes assessed following cryopreservation_____ 79

Table 3.1: Antibodies used for flow cytometry and immunostaining _____ 99

Table 3.2: Top differentially expressed genes for each cluster from heatmap ___110

Table 4.1: Antibodies used for flow cytometry and immunostaining _____137

LIST OF FIGURES

Figure 2.1: Morphogen concentrations modulate V2a interneuron population. ___ 56

Figure 2.2: DAPT concentration effects V2a interneuron yield. _____ 58

Figure 2.3: The V2a interneuron differentiation is reproducible in multiple cell lines. _____ 59

Figure 2.4: V2a interneuron protocol robustly increases hPSC neurogenesis. _____ 61

Figure 2.5: V2a interneuron protocol specifically increases V2a interneuron population. _____ 61

Figure 2.6: Single cell RNAseq of V2a interneuron cultures. _____ 63

Figure 2.7: Select violin plots of genes that identify cluster A and cluster B. _____ 65

Figure 2.8: Select violin plots of genes that identify cluster D and cluster E. _____ 66

Figure 2.9: Select violin plots of genes that identify cluster C, cluster F and, cluster G**.** _____ 67

Figure 2.10: Cluster interpretation of Single cell RNAseq of V2a interneuron cultures. _____ 68

Figure 2.11: V2a interneuron genes and cluster identity. _____ 69

Figure 2.12: V2a interneuron maturation *in vitro.* _____ 71

Figure 2.13: Quantification of *in vitro* maturation cultures.. _____ 72

Figure 2.14: Electrophysiological properties show increased maturation with culture duration. _____ 73

Figure 2.15: hPSC derived V2a interneurons survive and mature in the adult murine spinal cord. 75

Figure 2.16: Transplanted cultures are not pluripotent. 76

Figure 2.17: Transplanted cells extend projections and form putative synapses with host neurons. 77

Figure 2.18: V2a interneuron cultures can be cryopreserved. 79

Figure 3.1: Replating enhances the V2a interneuron population. 101

Figure 3.2: Early WNT activation enhances the V2a population. 103

Figure 3.3: Single Cell RNA sequencing of replated differentiation. 105

Figure 3.4: Imbalanced gene count between clusters. 105

Figure 3.5: Identification of V2a interneuron population. 106

Figure 3.6: HOX expression profile of V2a interneuron cultures. 107

Figure 3.7: Heatmap of genes that define each cluster. 109

Figure 3.8: Clusters contain populations involved with respiratory control. 111

Figure 3.9: Confirmation of respiratory phenotype. 112

Figure 3.10: Confirmation of hindbrain respiratory populations *in vitro*. 114

Figure 3.11: Modulation of V2a and V0 interneuron in response to purmorphamine and retinoic acid concentration. 115

Figure 4.1: Hindbrain organoid differentiation. 140

Figure 4.2: Cellular composition of the organoids is modulated by pur concentration. 142

Figure 4.3: Phase contrast and H&E of organoids throughout the differentiation. 145

Figure 4.4: Analysis of pluripotency and proliferation in organoid sections throughout differentiation. 147

Figure 4.5: Analysis of neurogenesis in organoid sections throughout differentiation. 149

Figure 4.6: Analysis of rosette formation in organoid sections throughout differentiation. 151

Figure 4.7: Analysis of committed phenotypes in organoid sections throughout differentiation. 152

Figure 4.8: Phase contrast and H&E of organoids during maturation. 155

Figure 4.9: Assessment of early maturation in sectioned organoids. 156

Figure 4.10: Assessment of maturation markers in 100 day old organoids. 158

Figure 4.11: Synchronous Ca^{2+} fluctuations in the organoids throughout maturation. 160

Figure 4.12: Synchronous Ca^{2+} fluctuations in the organoids are dependent on cellular composition. 162

Figure 4.13: Disease modeling in hindbrain organoids. 164

Figure 4.14: Synchronous Ca^{2+} fluctuations in PHOX2B mutant organoids. 166

Chapter 1: Introduction

1.1 Overview

The goal of this dissertation was to develop novel caudal interneuron systems from human pluripotent stem cells (hPSCs). Caudal interneurons, located in the hindbrain and spinal cord are critical populations in the control of motor functions including respiration and locomotion. Prior to these studies, there were no *in vitro* sources of the human caudal interneuron populations that could be used for developmental research, disease modeling, or to evaluate their therapeutic potential for neurodegenerative disorders and injury. To derive specific populations of interneurons, these studies then aimed to recapitulate the endogenous signaling environment of the developing neural tube by varying the concentration, duration, and type of pathway specific small molecule activators and inhibitors. The differentiation processes were explored both in two-dimensional and three-dimensional platforms and tested in animal and disease models.

The goal of the first study was to describe V2a interneurons from hPSCs. V2a interneurons are a critical long-descending glutamatergic phenotype located in the hindbrain and throughout the spinal cord. They are involved in respiration as well as left-right coordination and are a candidate cell type to relay long-distance propriospinal connections after spinal cord injury (Al-Mosawie, Wilson et al. 2007, Crone, Quinlan et al. 2008, Zhong, Droho et al. 2010). V2a interneurons were differentiated from hPSCs using activation of sonic hedgehog (Shh) and retinoic acid (RA) pathways as well as inhibition of Notch signaling. Human PSC-derived V2a interneurons matured into functional

glutamatergic interneurons *in vitro* as well as in the uninjured murine spinal cord. This study provided the first report of hPSC-derived V2a interneurons.

Although V2a interneurons could be reliable produced from hPSCs, the cultures were heterogeneous. Therefore, the second study of this dissertation proceeded to identify the additional populations in the V2a interneuron cultures. Using emerging single cell RNA sequencing techniques, the sub-populations of the culture were revealed to contain additional populations present in the hindbrain, including V0 interneurons and a chemosensing population. In development, V2a interneurons, V0 interneurons, and chemosensing neurons arise similarly where they function together as a circuit to control respiration. The presence of these populations *in vitro* was confirmed via flow cytometry and the relative proportions of the populations were modulated by varying Shh and RA concentration similar to developmental signaling gradients. This study is the first to report co-emergence of hindbrain populations involved in respiration from hPSCs providing a resource to study human development *in vitro*.

After determining that the monolayer cultures gave rise to multiple populations involved in respiratory control, the goal of the last study was to build a hindbrain organoid system that could be used to study developmental processes as well as respiratory diseases, such as congenital central hypoventilation syndrome (CCHS). Recent literature has demonstrated the ability to create "tissue-like" structures called organoids. These structures often recapitulate the particular cellular organization and function of respective native tissues. However, there has yet to be report of a hindbrain organoid. This study describes the ability to differentiate V2a and V0 interneurons as well as a chemosensing population in a 3D tissue-like aggregate. The organoid cultures mimic many aspects of

native development during the differentiation process as well as produce a synchronous periodic Ca^{2+} flux thus recapitulating a neural firing pattern similar to what is observed in native respiratory hindbrain regions.

This dissertation provides the first description of V2a interneurons from hPSCs, the first co-emergence of multiple hindbrain populations, and the first description of a hindbrain organoid that recapitulates some function of respiration. This work can be used to further the mechanistic understanding of the functional roles of these different populations and even lead to potential therapeutics for neurological disease, neurodegeneration, and injury. The following introduction discusses topics critical to the development of the aforementioned studies including neural tube development, directed differentiation into neural cell types, and central pattern generators for locomotion and respiration.

1.2 Neural Tube Development

Development of the nervous system is a very delicate and intricate process. A combination of signaling molecules works to define patterning in the neural tube of specific neural subtypes, which have been described in the ventrodorsal (front to back) and rostrocaudal (head to tail) directions. Researchers have begun to unravel the signaling mechanisms involved in these patterning events as further experimentation will continue to refine our understanding of the complex developmental program.

1.2.1 Overview of Neural Tube Development

Embryonic development is driven by robust cell patterning and migration events that are in part driven by complex yet controlled release of signaling morphogens. The neural tube, which gives rise to the brain and spinal cord, is formed through a process known as neurulation. During neurulation, the notochord provides signals to the ectoderm to thicken and flatten out thus forming the neural plate (Smith and Schoenwolf 1989) . The neural plate then folds inward in the dorsoventral direction and pinches closed (van Straaten, Hekking et al. 1988, Smith and Schoenwolf 1989). As the neural tube is closing, it also expands in the rostrocaudal direction to initiate formation of the spinal cord. There are several key factors that aid in the ventrodorsal and rostrocaudal patterning of the neural tube including sonic hedgehog (Shh)/bone morphogenic proteins (BMPs) and retinoic acid (RA), respectively (Patten and Placzek 2000, Wilson and Maden 2005). To pattern the neural cell types in the ventral neural tube, Shh is released from the notochord then subsequently from a glial structure on the ventral midline of the neural tube called the floorplate, effectively creating a ventral-to-dorsal gradient of Shh concentration (Patten and Placzek 2000). Similarly, BMPs are released from a structure at the dorsal midline of the neural tube called the roofplate creating a dorsal-to-ventral gradient of BMP concentration. This combination of opposing signaling molecules induces a specific organization of neural lineage specification in the neural tube, with the ventral half of the neural tube typically comprising neurons of the motor system and the dorsal half contributing to the sensory system (Wilson and Maden 2005). The rostrocaudal identity of developing neurons comprising the neural tube is partially established by RA release from somites, a mesoderm population that runs along the side of the neural tube (Maden, Sonneveld et al. 1998). RA signaling, peaking at the rostral spinal cord, grossly separates

brain from spinal cord development but is also important in neuronal specification within the spinal cord. While neural fate specification within the neural tube can be broadly defined by Shh/BMP and RA signaling, there are many intricate signaling relationships critical to proper development of one of the most complex mammalian organs.

1.2.2 Ventrodorsal Specification of the Neural Tube

The neural tube is delineated into a ventral and dorsal half where the ventral side is patterned by Shh and gives rise to cells involved in motor control and the dorsal side patterned by BMPs gives rise to cells involved in sensory control. Here, the role of Shh in patterning the ventral half of the neural tube will be discussed. In response to a combination of signaling events, mainly driven by Shh signaling, the ventral half of the neural tube organizes into five distinct progenitor domains (p3, pMN, p2, p1, and p0) that give rise to corresponding committed motor neuron and interneuron domains (V3, MN, V2, V1, and V0, respectively) (Marklund, Alekseenko et al. 2014). Shh, released from the notochord and floorplate, first bind the 12-pass transmembrane receptors, Patched1 and Patched2 (Ptc1/2). Activation of Ptc promotes translocation of the G-protein coupled receptor, Smoothened (Smo), into primary cilia (Eggenschwiler and Anderson 2007, Dessaud, McMahon et al. 2008) . Movement of Smo into the cilia activates the Gli family of transcription factors, which then modulates the activity of transcription factors that pattern the neuronal subtypes of the ventral neural tube. Gli activity is sensitive to not only to the amount of Shh signaling but also the duration of the signal (Dessaud, Yang et al. 2007). A higher concentration and longer duration of Shh signaling specifies the most ventral V3 domain compared to more dorsal domains. In one example, Shh signaling

initially turns on the pMN transcription factor, OLIG2, in ventral neural precursors. If Shh signaling is sustained, the OLIG2 expression expands dorsally and NKX2.2 expression is activated which in turn inhibits OLIG2 expression to ultimately define the p3 domain (Dessaud, Ribes et al. 2010). This ventral-dorsal activation and repression of specific transcription factors expands across different domains, and results in regionally distinct areas of opposing transcription factor expression that distinguishes the p3 to p0 progenitor domains. The ventrodorsal patterning described here occurs throughout the neural tube however; the rostrocaudal location is critical in defining the functional role of the neurons.

1.2.3 Rostrocaudal Specification of the Neural Tube

While Shh has been the main signaling factor implicated in dorsoventral patterning of the neural tube, several factors have been implicated in the rostrocaudal patterning including RA, fibroblast growth factors (FGFs), growth differentiation factors (GDFs) and by the Wingless-type MMTV integration site family (WNTs). The hindbrain, which controls autonomic function, and spinal cord, which controls locomotion, are regionally identified in the rostrocaudal axis by structural organization of rhombomeres and expression of Hox genes. Rhombomeres 1-8 (r1-r8) are segmented developmental units that have differential adhesion properties and give rise to the specific populations that develop into the pons, medulla, and cerebellum of the hindbrain (Guthrie, Prince et al. 1993, Wizenmann and Lumsden 1997). While the rhombomeres create defined boundary conditions, Hox expression is temporally and spatially dynamic throughout development thus there is overlap of genes that define regions of the hindbrain and spinal cord. The hindbrain is marked by the expression of Hox1 – Hox5 whereas spinal cord is further separated into

cervical (Hox4 – Hox8), thoracic (Hox8 – Hox9), lumbar (Hox9 – Hox11), and sacral regions (Hox12 –Hox13) (Philippidou and Dasen 2013).

The signals that regulate Hox expression include RA, FGFs, GDFs, and WNTs. RA, released from adjacent somites during elongation of the neural tube, is synthesized by the enzyme retinaldehyde dehydrogenase 2 encoded by the Raldh2 gene (Niederreither, McCaffery et al. 1997, Berggren, McCaffery et al. 1999). RA effects Hox patterning through RA receptors that bind directly to effector regions of Hox genes. RA signaling is present in a gradient determined by expression of Raldh2 in the somites where local concentrations peak in the caudal hindbrain/rostral spinal cord and decreases in both the rostral and caudal direction (Philippidou and Dasen 2013).

Simultaneous FGF signaling is an additional important caudalizing factor that activates Hox4 – Hox10 expression (Liu, Laufer et al. 2001). FGF influences Hox expression through induction of Cdx genes that then induce caudal Hox expression (Bel-Vialar, Itasaki et al. 2002) . The FGFs are expressed in neuromesodermal progenitors and expression appears to begin near Hox6 in the lower cervical region of the spinal cord and increase in the caudal direction. Lastly Gdf11 is necessary for expression of the most caudal Hox genes (Hox10 – Hox11) (Liu, Laufer et al. 2001).

WNT signaling is involved in a variety of neurodevelopmental processes including specification of neurons along the rostrocaudal axis. In the hindbrain, Wnt1, Wnt3a, Wnt8b, and Wnt10b are expressed at rhombomere boundaries (Pasini and Wilkinson 2002) and Wnt1 has been shown to promote hindbrain neurogenesis (Amoyel, Cheng et al. 2005). Further, the influence of WNT activation on rostrocaudal specification appears to depend on pairing with other caudalizing molecules. For example, WNT activation combined with

RA and FGF signaling specifies a caudal hindbrain phenotype, yet WNT activation with RA or FGF alone can specify the rostral spinal cord or caudal spinal cord respectively (Elkouby and Frank 2010). This is likely because interactions between WNT, RA, and FGFs interact with Cdx genes to prepare the cells for Hox patterning (Nordstrom, Maier et al. 2006).

Together, there are several signaling molecules including RA, FGFs, GDFs, and WNTs that interact to specify the rostrocaudal axis. Research continues to investigate the roles of these signaling molecules in rostocaudal patterning including how and which subtypes of FGFs are transcribed in the developing cord, the temporal dynamics of these signaling events, and how FGFs and RA interact with WNT to influence rhombomere and Hox gene expression.

1.2.4 Notch Signaling During Neurogenesis

The Notch signaling pathway is utilized in a variety of embryonic morphogenic events and has been evolutionarily conserved from worms to humans (Lai 2004). The conical Notch signaling pathway relies on the physical interaction between a ligand-presenting cell and a neighboring cell that expresses a Notch receptor. While the kinetics of a specific mammalian ligand (Dll1, Dll3, Dll4, Jag1, and Jag2) binding to a specific mammalian receptor (Notch1, Notch2, Notch3, or Notch4) is unknown, the structure of the ligands and receptors differ mainly by number of EGF-like repeats, which may play a role in binding affinity (Gordon, Arnett et al. 2008). Notch ligands can bind to any Notch receptor, and the physical interaction between the ligand and receptor initiates a gamma secretase-mediated cleavage of the Notch intracellular domain (NICD) (Mumm and Kopan 2000). The NICD is then translocated to the nucleus and activates a variety of transcription factor programs

depending on the developmental stage of the cells. In early neural fate decisions, NICD upregulates Hes and Hey genes that inhibit proneural genes, such as Ascl1 and Ngn2, and thus keeps cells in a neural progenitor state (Shimojo, Ohtsuka et al. 2008, Imayoshi, Isomura et al. 2013). Deletion of the Rbpj gene, which when transcribed becomes a target of the NICD, in embryonic and adult mouse brains results in early differentiation of neural progenitors into neurons further implicating the role of Notch signaling in neural progenitor maintenance (Imayoshi, Sakamoto et al. 2010). Together, Notch signaling promotes the maintenance of neural progenitors whereas the absence of Notch promotes progenitors to a neuronal cell fate.

Furthermore, Notch signaling plays a role in the commitment of specific neuronal subtypes, including V2a/V2b interneurons from p2 progenitors that express the Foxn4 transcription factor. Oscillating expression of proneural genes, Ascl1 and Neurog, in p2 progenitors leads to upregulation of Ascl1 in one subset of cells and upregulation of Neurog in a second subset. The Ascl1 expressing cells activate expression of Dll4 by binding to the Dll4 enhancer and the $Neurog^{+}$ cells inhibit Dll4 enhancer binding. The Dll4 expressing cells go on to become the V2a interneurons where neighboring cells receiving the Notch signaling become the V2b interneurons (Misra, Luo et al. 2014). Further, conditional $Notch1^{-/-}$ mice have an increased V2a population but at the expense of the V2b population (Del Barrio, Taveira-Marques et al. 2007). These studies support the idea the Notch signaling is necessary for V2b commitment and the absence of Notch increases the V2a population.

Kong et al described how Notch signaling effects Shh signaling. The study proposed that Notch signaling effects trafficking of Shh receptors, Ptc1/2 and Smo, to the cilia

thereby changing the cell's responsiveness to Shh and thus the relative size of progenitor domains in the neural tube. Further, Notch activation increased activation of Gli transcription factors thus increasing ventral progenitor domains. Similarly, the opposite is true that the inhibition of Notch increased the size of dorsal domains at the expense of ventral domains (Kong, Yang et al. 2015).

Together, researchers have identified the main signaling pathways critical to neural development including Shh, RA, WNTs and Notch. Understanding how signaling occurs during normal development is key to developing ways to correct signaling in a disease state but also key in directing cell fate in a dish.

1.3 Directed Stem Cell Differentiation into Neuronal Phenotypes

As the field has come to understand the endogenous signaling mechanisms that define neural development, there have also been advances in how to apply those signaling pathways *in vitro*. Many neural phenotypes have been differentiated from PSCs using signaling cues inspired by early development, yet identifying the appropriate concentration, duration, and combination of Shh, RA, WNT activators, and Notch inhibitors to produce a desired neural phenotype *in vitro* is still a major challenge. One large hurdle is that while it is known what signaling molecules are involved, the amount of signaling produced is typically described in relative proportions instead of in absolute amounts. Additionally, identifying how to recapitulate temporal duration of signaling *in vitro* can be difficult. Despite these challenges, obtaining hPSC-derived neuronal populations can be used for a variety of different applications including elucidating developmental processes,

modeling disease progression, testing novel drug compounds, and developing new cell therapies for neurodegeneration or disease. While progress has been made towards these applications, there are challenges that still remain. Neural structures in the brain and spinal cord are composed of many different neuronal and glial populations that work in tandem to carry out function. However, many directed differentiation protocols focus on derivation of a single cell type that is typically broadly characterized (i.e. excitatory or inhibitory). This poses an issue when trying to recapitulate development or disease in the brain or spinal cord, which is comprised of many different cell types. The ability to co-emerge multiple specific neuronal phenotypes from pluripotent stem cells would increase the capability to more accurately recapitulate developmental processes and diseased phenotypes.

1.3.1 Directing Stem Cells to Neural Phenotypes

Human embryonic stem cells (hESCs), derived from the inner cell mass of the blastocyst, can self renew and have the potential to differentiate into all of the germ layers with the potential to become any somatic cell of the body (Amit, Carpenter et al. 2000). More recently, induced pluripotent stem cells (iPSCs), virally or chemically reprogrammed somatic cells that hold similar differentiation potential to pluripotent cells (PSCs), have been used in place of hPSCs (Takahashi and Yamanaka 2006). Scientists have differentiated PSCs into all three-germ lineages by developing culture conditions that recapitulate specific aspects of the embryonic stage that gives rise to these layers. A variety of neural cell types have been differentiated from hPSCs, which provides an important source of cells to study developmental processes, design disease or drug testing models, and for use as therapeutics for injury and neurodegeneration. The signaling pathways that pattern neural

development *in vivo* were described above, however, to direct differentiation of PSCs, these signaling environments need to be recapitulated *in vitro.* Directed differentiation protocols can often be partitioned into steps that follow developmental stages including neuralization, ventrodorsal patterning, rostrocaudal specification, and subtype specification (Sances, Bruijn et al. 2016). Small molecules, a stable cost-effective alternative to recombinant growth factors, are used to activate and repress specific developmental pathways in a way that mimics the developmental gradients that lead to the different stages of neural development. The specific signaling molecules to recapitulate these different stages of development will be discussed in the following sections.

Previous methods to initiate neuralization in hPSCs include either formation of small cell clusters called embryoid bodies, culture with a feeder layer of cells, or hand picking of early ectoderm structures called rosettes from early neural cultures (Amoroso, Croft et al. 2013, Zhao, Ma et al. 2016, Cheng, Fass et al. 2017). Each of these strategies, however, are time consuming or inefficient at driving an early neural lineage (neuroectoderm) in the hPSCs. Chambers *et al.*, described how chemical inhibition of two SMAD signaling pathways, BMP and TGFβ, was able to induce neural fate commitment in hPSCs (Chambers, Fasano et al. 2009). This has become known as "Dual SMAD Inhibition" and can be carried out by small molecules including LDN 193189 to inhibit the BMP pathway through inhibiting transcription of BMP type 1 receptors ALK2 and ALK3 and SB 431542 to inhibit the Lefty/Activin/TGFβ pathways through inhibiting phosphorylayion of ALK4, ALK5, and ALK7 receptors. This combination of small molecules inhibits Smad1, Smad2, Smad5, and Smad8. Dual SMAD inhibition has now become common use in the start

of many neural differentiation protocols to prevent mesendoderm signaling and promote neuralization (Kirkeby, Grealish et al. 2012, Amoroso, Croft et al. 2013).

As previously described, Shh signaling is a key signaling molecule in the specification of dorsoventral patterning, and it has been added to directed differentiation cultures to pattern ventral subtypes. For example, recombinant Shh was initially used to direct mouse embryonic stem cells into motor neuron phenotypes (Wichterle, Lieberam et al. 2002). However, recombinant Shh proteins are large, variable, costly, and unstable in culture. Smoothened agonist (SAG) and purmorphamine (pur) are two Shh agonists that bind to the smoothened receptor to activate the Shh pathway. Pur has been described to be a milder agonist potentially due to different binding affinities for Smo and has been used to specify V2a interneurons, which are more dorsal to motor neuron phenotypes (Wichterle, Peljto et al. 2009, Brown, Butts et al. 2014). Li *et al.* reported that small molecule agonists of Shh could provide a more stable and reproducible alternative and were capable of inducing motor neurons from hPSCs (Li, Hu et al. 2008). Further, Amoroso *et al.* compared small molecule activation with SAG and pur in combination to recombinant Shh proteins in directed differentiation to motor neurons and determined the combination of SAG and pur resulted in a higher percentage of motorneurons at day 21 compared to recombinant Shh proteins (Amoroso, Croft et al. 2013) implicating that the small molecules can be more effective than the recombinant protein. These Shh agonists have been used at varying concentrations and signaling durations to define the respective neural progenitor domains as inspired by neural tube development (Brown, Butts et al. 2014, Iyer, Huettner et al. 2016, Butts, McCreedy et al. 2017). Additionally, the small molecule cyclopomine has been identified as a natural inhibitor of the Shh pathway and acts through binding smoothened

(Incardona, Gaffield et al. 1998, Cao, Hu et al. 2017). The development of small molecules that activate or inhibit the Shh pathway with a range of affinities has provided useful tools to mimic or interrogate the signaling that occurs during neural tube development to control the emergence of specific neuronal populations *in vitro*.

Different sets of small molecules have been used *in vitro* in attempts to recapitulate a targeted rostrocaudal specification. RA is one of the most common pro-neural and caudalizing molecules and is a naturally stable small molecule that is easily added to *in vitro* cultures (Jones-Villeneuve, Rudnicki et al. 1983). RA binds to nuclear RA receptors (RARs), which then dimerize and bind to RA-response elements (RAREs) to alter gene transcription. Genes that contain RAREs include proneural targets NeuroG2 and Pax6 as well as Hoxa1, Hoxb1, Hoxa4, Hoxd4, and Hoxb5, which promotes caudalizaiton (Rhinn and Dolle 2012). In early mouse embryonic stem cell literature, addition of RA was shown to generally promote a pro-neural and anti-mesodermal cell fate (Bain, Ray et al. 1996). Further, a study assessed the role of RA on the rostrocaudal identity of mouse embryonic stem cells and demonstrated that increasing concentrations of RA induced stepwise caudal identity where no RA resulted in a forebrain phenotype and increasing RA induced a hindbrain and spinal cord phenotype as reported by Hox expression (Okada, Shimazaki et al. 2004). Therefore, typically, the addition of RA to hPSCs is one main factor in differentiating a caudal (hindbrain and spinal cord) phenotype compared to a brain phenotype. To obtain a more caudal spinal phenotype (thoracic or lower), recombinant FGF8, which is abundant during spinal cord elongation (Diez Del Corral and Morales 2017), has been added to *in vitro* cultures to mimic the FGF gradient that begins at in the lower cervical region of the spinal cord and more caudally. The addition of FGF8 along with RA

has capable of producing neuroepithelium that expressed HoxC5 from hPSCs (Lippmann, Williams et al. 2015).

Perturbation of WNT signaling has been used to influence rostrocaudal specification in *in vitro* culture systems. WNT signaling is dependent on accumulation of β-catenin in the cytoplasm which then gets translocated to the nucleus to effect transcription. In the absence of WNT, β-catenin is degraded but a combination of proteins known as the destruction complex including glycogen synthase kinase 3 (GSK3). In the presence of WNT, the destruction complex is disrupted and β-catenin is collected in the cytoplasm. The WNT/β-catenin pathway has been activated *in vitro* through a variety of small molecules but the most widely used are small molecule inhibitors of glycogen synthase kinase 3 (GSK3) to prevent translocation of β-catenin into the nucleus thereby blocking changes in transcription activity. CHIR99021 is a common GSK3 inhibitor that has been used in motor neuron differentiation protocols as a caudalizing agent (Li, Sun et al. 2011, Lippmann, Williams et al. 2015). Conversely, inhibition of WNT to prevent caudalization in the differentiation of forebrain and midbrain phenotypes has often been achieved using the recombinant protein Dickkopf WNT signaling pathway inhibitor 1 (DKK1) which inhibits disruption of the destruction complex or the small molecule XAV939, which stimulates β-catenin degradation (Perrier, Tabar et al. 2004, Ribeiro, Ellwanger et al. 2011).

Notch signaling has been perturbed in *in vitro* culture systems to promote early neuralization and influence later stage subtype specification. Following Notch ligand and receptor binding as described above, cleaved of NICD traffics from the cytoplasm to the nucleus where it modulates transcriptional activity. There are many methods to inhibit but not agonize Notch signaling. One of the most common forms of inhibition is with small

molecule inhibitors of γ-secretase, which inhibit cleavage of the NICD, thereby stopping translocation to the nucleus where it can no longer initiate transcription activity directly. DAPT is the most common γ-secretase inhibitor and has been used to promote neurogenesis of embryonic stem cells *in vitro* (Crawford and Roelink 2007, Borghese, Dolezalova et al. 2010). In addition, it has also been used to increase the yield of mouse embryonic stem cell-derived V2a interneurons *in vitro* (Brown, Butts et al. 2014). Notch signaling, or the absence thereof, is critical to neural development. As such, inhibition of this pathway is a powerful tool to direct neuralization as well as neural sub-type specification.

1.3.2 Neural Phenotypes Differentiated from Pluripotent Stem Cells

Using the developmental signaling pathways described above, many neural cell types have been derived from hPSCs including oligodendrocyte progenitors (Douvaras and Fossati 2015), cortical neurons (Shi, Kirwan et al. 2012), dopaminergic neurons (Perrier, Tabar et al. 2004, Adil, Vazin et al. 2017), GABAergic brain interneurons (Nicholas, Chen et al. 2013) (Maroof, Keros et al. 2013), and spinal motor neurons (Li, Du et al. 2005) (Amoroso, Croft et al. 2013). These protocols have been developed based on manipulation of signals present during development and therefore differ mostly by the type and/or concentration of signaling molecule used to direct the differentiation. Generally, many neuronal directed differentiation protocols (with the exception of sensory phenotypes) add Shh agonists to drive ventral neural tube patterning. Differentiation of hPSCs into forebrain and midbrain phenotypes often do not use RA (Perrier, Tabar et al. 2004, Maroof, Keros et al. 2013) but addition of RA is used to specify the more caudal spinal motor neurons (Li, Hu

et al. 2008, Lippmann, Williams et al. 2015). Further, differentiation to forebrain phenotypes have inhibited WNT signaling (Maroof, Keros et al. 2013, Nicholas, Chen et al. 2013) while recent motor neuron protocols have been using WNT activation to enhance and caudalize the resultant population (Kirkeby, Grealish et al. 2012, Du, Chen et al. 2015). There historically has been a major focus on neuronal phenotypes however, glial populations should not be disregarded. Many differentiations into glial phenotypes, including oligodendrocytes (Hu, Du et al. 2009, Douvaras and Fossati 2015) and astrocytes (Krencik and Zhang 2011, Shaltouki, Peng et al. 2013), take longer periods of time (around 100 days for functional phenotypes, potentially reflecting human developmental timelines) and tend to focus more on the cocktail of recombinant growth factors including platelet-derived growth factor (PDGF), triiodothytonin (T3), neurotrophin 3 (NT-3), and insulin growth factor 1 (IGF-1) for oligodendrocytes was well as ciliary neurotrophic factor (CNTF) for astrocytes that are added during the maturation process rather than focusing early on neural induction. Directed differentiation protocols for neuronal and glial populations have been developed by recapitulating developmental signaling yet many focus on a broad class of neurons (i.e. excitatory or inhibitory) and lack information about specific subtypes possibly due to difficulty in specifying the differentiation or because the subtype a distinct subtype is unknown.

1.3.3 Interneuron Phenotypes Described from Pluripotent Stem Cells

While there has been a variety of neural cell types differentiated from PSCs, differentiation of interneurons have represented a smaller proportion of the literature even though they are the most abundant neuron subtype located throughout the central

nervous system. Broadly, an interneuron refers to a neuron that functionally connects two other neurons. Interneurons are critical in both sensory and motor circuits and can have a variety of functional phenotypes including excitatory (glutamatergic,) and inhibitory (GABAergic and glycinergic) cell types. Some interneuron populations have been described from PSCs including GABAergic interneurons of the medial ganglionic eminence (MGE), spinal sensory interneurons, and spinal motor interneurons (Maroof, Keros et al. 2013, Nicholas, Chen et al. 2013, Brown, Butts et al. 2014, Xu and Sakiyama-Elbert 2015, Iyer, Huettner et al. 2016, Gupta, Sivalingam et al. 2018).

The cortex contains a diverse class of GABAergic interneurons that initially arise from the MGE. Deficiencies in these inhibitory populations have been associated with neurodevelopment and neurodegenerative disorders (Chao, Chen et al. 2010, Cheah, Yu et al. 2012, Verret, Mann et al. 2012). Two groups reported the differentiation into $Nkx2.1^{+}$ MGE-like progenitors that matured into GABAergic interneuron subtypes using dual SMAD inhibition, WNT antagonism, and small molecule activation of Shh (Maroof, Keros et al. 2013, Nicholas, Chen et al. 2013). The absence of RA and the inhibition of WNT aids in the specification of a forebrain phenotype. Transplantation of the MGE-like interneurons in the lumbar enlargement of mice spinal cord injured at T13 differentiated into GABAergic neurons, integrated into endogenous spinal circuitry, and resulted in improved bladder function and a mitigated pain response (Fandel, Trivedi et al. 2016).

Sensory interneurons arise from the dorsal half of the neural tube and are critical to the transduction of pain information. Similar to the ventral half of the neural tube, the dorsal half of the neural tube is separated into distinct sub domains (dl0-dl3). A recent study was the first to report differentiated dl1 and dl3 sensory interneurons from hPSCs

using RA and BMP4 (Gupta, Sivalingam et al. 2018). The addition of RA specifies a caudal phenotype (spinal cord) and the presence of BMP4 mimics signaling that is released from the roof plate of the developing neural tube.

The ventral half of the neural tube gives rise to interneurons that play critical roles in motor control. V2a interneurons have been previously differentiated from mouse embryonic stem cells using pur, RA, and DAPT (Brown, Butts et al. 2014, Iyer, Huettner et al. 2016). RA specifies a caudal phenotype and the use of the milder Shh agonist, pur, induces a more dorsal subtype of interneurons, recapitulating what occurs developmentally. Further, the addition of DAPT inhibits Notch signaling to increase the population of V2a interneurons. V3 interneurons, which arise from the most ventral domain of the neural tube have been differentiated from mouse PSCs using RA and compared to published motoneuron and V2a interneuron protocol, a longer duration of the stronger Shh agonist, SAG (Xu and Sakiyama-Elbert 2015). The combination of timing and dosage of Shh was utilized to specify the interneuron subtype that arises from the ventral-most domain and therefore is exposed to the greatest concentration and duration of Shh during development. Recently, several ventral interneuron subtypes were differentiated within one embryoid body to create what the researchers called a "circuitoid" (Sternfeld, Hinckley et al. 2017). The relative proportions of V1, V2and V3 interneurons as well as motor neurons were modulated depending on the amount of Shh signaling with low concentrations of SAG resulting in high populations of V1 interneurons and high concentrations of SAG resulting in high populations of V3 interneurons. Due to the different electrophysiological properties of the interneuron subtypes, the functional output of the

circuitoid measured by calcium flux was altered with different ratios of excitatory to inhibitory interneuron populations.

While forebrain interneurons have been differentiated from human PSCs and caudal interneurons have been differentiated from mouse PSCs, the work presented in this dissertation represents the first description of caudal interneurons differentiated from human PSCs.

1.3.4. Neural Organoid Culture Systems

While 2D culture models have been successful in differentiating specific cell types, the cells are geometrically constrained to have limited cell-cell interactions. 3D culture models provide a platform for morphogenesis to occur into tissue systems more organically instead of as cells in isolation. Many neural differentiation protocols begin with small clusters of PSCs that form a 3D aggregate in efforts to mimic early embryo development. The 3D cell aggregates can be formed spontaneously by placing individual cells in a non-adherent dish, which gives rise to cell aggregates of heterogeneous sizes (Brown, Butts et al. 2014, McCreedy, Brown et al. 2014). An alternative method is to use microfabricated molds where dissociated PCS are seeded and centrifuged into an array of inverse pyramidal wells that self-condense over 16 to 24 hours to form homogenous spherical aggregates (Ungrin, Joshi et al. 2008, Hookway, Butts et al. 2016). While the latter results in more consistent aggregate formation, it is a more time-intensive process. When the neural induction process is performed in 3D, the aggregates are typically dissociated and replated in a monolayer to allow the neurons to mature (Amoroso, Croft et al. 2013, Butts, McCreedy et al. 2017). However, researchers have investigated both induction and

maturation in 3D culture to form what are now termed organoids. The goal of these 3D organoids are to recapitulate the native tissue, which contains a heterogeneous population of neurons and glial phenotypes. In some cases, the organoids self-organize into structures that resemble native tissue development. There have been reports of organoid cultures that resemble tissues of the retina, forebrain, midbrain, hypothalamus, and cerebellum (Eiraku, Watanabe et al. 2008, Wataya, Ando et al. 2008, Muguruma, Nishiyama et al. 2010, Kadoshima, Sakaguchi et al. 2013, Mariani, Coppola et al. 2015, Jo, Xiao et al. 2016) though the consistency in which the specific structure that recapitulates native tissue emerges can vary between organoids. Lancaster *et al*. was one of the first reported organoids with organized neural layers resembling cerebral development (Lancaster, Renner et al. 2013). The organoids cultured with RA to promote neuralization in a spinning flask bioreactor for up to 4 months,which ultimately led regions of the organoid that resembled the cerebral cortex as well as cortical development with layering of the subventricular zone and ventricular zone. One potential issue with organoids, which can reach over 1mm in diameter, is that nutrient deficiencies due to diffusion limitations and lack of vasculature can result in the formation of necrotic cores (Lancaster, Renner et al. 2013, Watanabe, Buth et al. 2017). Mansour et al., proposed a potential solution to this issue by imbedding human neural organoids into the retrosplenial cortex (Mansour, Goncalves et al. 2018). After 30 days post-implantation, the organoids became vascularized by the surrounding mouse tissue. Decreased cell death was observed with the organoids that were grafted and vascularized compared with time-matched organoids that were cultured *in vitro*. Additionally, there was increased neuronal maturation demonstrated by an increased percentage of NeuN-expressing cells in the grafted organoids compared to *in vitro* time-

matched controls. This platform provides a way to further mature the organoids to observe functions that may not be possible solely with *in vitro* culture platforms.

While these organoids form into organized structures, the significance is greater when they have a functional application such as modeling development and disease and/or as a platform for drug testing. To model disease, forebrain organoids have been used as models to test how Zika infection could lead to microencephaly. Following infection of Zika virus in forebrain organoids, increased cell death and reduced proliferation was observed, which are indications of microencephaly (Qian, Nguyen et al. 2016). Human neural organoids have been used as platform to test the toxicity of pharmacological agents, which provides a way to test new potential drugs in a more physiologically relevant way than monolayer cultures systems or murine animal models (Schwartz, Hou et al. 2015).

While many different types of organoids have been developed, there have yet to be examples of medullary and spinal cord organoids from hPSCs. These two structures have defined neural networks involved in autonomic and motor control that is difficult to recapitulate in 2D but may form in 3D. Organoid models would provide a platform to dissect the neuronal networks and potentially model what happens during respiratory or locomotor disease.

1.4 Central Pattern Generators

After differentiating neuronal cultures *in vitro,* the next step would be to interrogate how the neurons form networks. Central pattern generators (CPGs) in the hindbrain and spinal cord are composed of a network of neurons that work together in a series of

feedback loops to control a variety of coordinated movements including locomotion, respiration, swimming, and chewing. The CPG networks have the ability to initiate and modify motor behaviors in response to supraspinal and sensory input. Many researchers have worked to unravel the role of specific neuronal subtypes involved in these highly complex circuits.

1.4.1 Locomotor Central Pattern Generators

The locomotor CPG can be categorized into cells that control rhythmicity, coordination, and flexion/extension. As previously described, a combination of signaling molecules gives rise to progenitor domains that mature into V0 to V3 interneurons as well as motor neurons. Researchers have begun to define the role of these interneurons using murine genetic knock-out strategies and have proposed models of the CPG connectome through synaptic tracings and computational modeling. To begin to fit the interneurons into a model, there are two main considerations – the type of neurotransmitter that is released and the neurite extension properties. Ventral interneuron populations are both excitatory (V3, V2a, $V0_V$) and inhibitory (V2b, V1, $V0_D$). Extension pattern is another important characteristic of the different interneuron populations with V3, $V0_c$, $V0_D$ interneurons having commissural projections and V1, V2a, V2b interneurons having ipsilateral projections meaning they do or do not cross the midline of the spinal cord, respectively. The combination of excitability and extension properties poise the interneuron populations to have specific roles in the locomotor CPG (Rybak, Dougherty et al. 2015).

1.4.2 Role of interneuron subtypes in locomotor Central Pattern Generators

Commissural V0 interneurons arise from a common Dbx1 expressing progenitor but mature into glutamatergic $V0_V$, glycinergic/GABAergic $V0_D$, and the lesser studied cholinergic $V0_C$ populations. Dbx1 mutant mice which resulted in disrupted left-right coordination with first elucidated he role of V0 interneurons (Lanuza, Gosgnach et al. 2004). However, distinct roles of the sub species was revealed through ablation of the $V0_V$ and VO_D subtypes independently which showed the species are important for different speeds of locomotion where $V0_D$ interneurons are essential for left-right coordination at low speeds and $V0_V$ interneurons are essential for left-right coordination at high speeds (Lanuza, Gosgnach et al. 2004, Talpalar, Bouvier et al. 2013, Griener, Zhang et al. 2015). This data suggests that while two sub-species of the same interneuron subtype may be involved in a similar task, their role could be further specified when taking a closer look, in this case by looking at the speed of locomotion.

Ipsilateral glutamatergic V2a interneurons express Chx10 and have also been demonstrated to be important for forelimb reaching tasks (Azim, Jiang et al. 2014) and left-right coordination (Crone, Quinlan et al. 2008, Zhong, Droho et al. 2010). Their activity mirrors that of the $V0_v$ in that they play a role in left-right coordination specifically at high locomotor speeds. This mirrored activity suggests that the V2a and V0 are connected in the locomotor CPG. Anatomical tracing revealed that V2a provide the excitatory drive onto commissural V0 interneurons through identification of V2a synapses onto $V0_V$ soma (Crone, Quinlan et al. 2008). Additionally, a subpopulation of V2a interneurons receive rhythmic input during locomotion and recruit additional V2a interneurons at high frequencies of locomotion, indicating a compensatory mechanism of this population

(Zhong, Sharma et al. 2011). Similar to the V0 interneuron populations, there are sub species of V2a interneurons that have unique roles. Optogenetic silencing of a subpopulation of V2 interneurons that expressed Shox2 and not Chx10 disrupted rhythm generation, which makes the Shox2$^+$ cells a potential candidate to be the main generator of rhythm in the locomotor CPG (Dougherty, Zagoraiou et al. 2013).

Ipsilateral glycinergic/GABAergic V1 interneurons express En1 and are important in the flexion-extension behavior of locomotion. More specifically, ablation of V1 interneurons in the caudal spinal cord results in hyperflexion of hind limbs, thus suggesting that they are necessary for extension of hind limbs. The V1 interneurons are complementary to Gata3$^+$ ipsilateral glycinergic/GABAergic V2b interneurons, which are involved in flexion. Ablation of V2b interneurons in the caudal spinal cord results in hyperextension indicating they are necessary for flexion (Britz, Zhang et al. 2015). V1 and V2b interneurons interact with motor control as both populations have been shown to form inhibitory synapses directly onto the soma of hind limb motor neurons indicating they are key cell types for regulating locomotion (Zhang, Lanuza et al. 2014).

Commissural glutamatergic V3 interneurons express the Sim1 transcription factor. Inhibition of V3 synaptic output by introducing a tetanus toxin light chain (TeNT) under Sim1 expression revealed V3 interneurons are not involved in left-right coordination nor flexion-extension behaviors. However, it is proposed that the V3 interneurons aid in synchronizing the motor outputs from the two halves of the spinal cord to provide a more stable rhythm (Zhang, Narayan et al. 2008). A separate study proposes that a sub-population of ventrally-derived V3 interneurons mature and migrate dorsally into distinct populations that have different roles during running and swimming behaviors with the

dorsal population mediating sensory circuits and the ventral population influencing premotor activity (Borowska, Jones et al. 2013).

Overall, excitatory V0 and V2a interneurons provide left-right input into the locomotor CPG while inhibitory V2b and V1 provide control of flexion and extension. The V3 interneurons appear to provide stabilization to signaling originating in the two halves of the spinal cord. These findings suggest that the different interneuron populations play a distinct role in carrying out motor function. The field has characterized the role of the different interneurons using only a few transcription factors to identify each population. While a few subtypes have been identified like the $Shox2^{+}$ cells, as tools continue to get better at identifying transcriptional signatures of neuronal populations, it is possible that additional species will be identified to reveal the subtleties of the locomotors circuit. Similar to the discovery of V0 sub species that have different roles at varying speeds of locomotion, there may be additional sub species that have different roles in sub-categories of behavior such as range of flexion-extension or compensation for unbalanced movement.

1.4.3 Respiratory Central Pattern Generator

The hindbrain is composed of the pons, medulla, and cerebellum and controls critical autonomic functions including heart rate and respiration. The respiratory CPG, similar to the locomotor CPG in that it is a neural network that responds to external cues but controls rate of respiration instead of locomotion. However, unlike the locomotor CPG, the components of the respiratory CPG were initially defined by specific regions in the hindbrain instead of by specific neuronal subtypes identified by transcription factor expression (Feldman, Del Negro et al. 2013). The regions involved in respiration have been

defined by their firing pattern and role in changing the respiratory cycle, which includes inspiration, post-inspiration, and late expiration. The output of the respiratory CPG provides synaptic drive for phrenic motor pools located in C3-C5 cervical region of the spinal cord and to intercostal motor neurons located in T1 – T12 thoracic region of the spinal cord that contract the diaphragm and intercostal muscles, respectively (Del Negro, Funk et al. 2018). Activation of phrenic motor neurons contracts the diaphragm and increases lung volume leading to inspiration. Phrenic drive then decreases, which stops the expansion of the lungs while upper airway muscles constrict during post-inspiration. Expiration follows when the intercostal muscles are activated (Bellingham 1998) This complex motor drive is controlled through specific components of the respiratory CPG.

1.4.4 Role of hindbrain nuclei in respiratory Central Pattern Generators

The ventral respiratory column (VRC), located in the lateral medulla, contains the structures that produce the main rhythms of the respiratory CPG. The structures of the VRC receive input from the retrotrapezoid nucleus/parafacial respiratory group (RTN/pFRG) as well as the additional neuronal populations located in the medulla and pons that influence rate of respiration. The VRC, located in the ventrolateral medulla, contains the Bötzinger Complex (BötC), pre Bötzinger Complex (pre BötC), as well as the rostral and caudal ventral respiratory groups (rVRG and cVRG). These structures are aligned sequentially in a rostral to caudal organization and have defined roles in controlling different stages of respiration (Ezure, Manabe et al. 1988, Ellenberger and Feldman 1990).

The RTN/pFRG is located rostral to the VRC and has two important roles in respiration – chemosensing and active expiration. One population of the RTN/pFRG links

environmental changes to increased inspiratory drive in the pre BötC. Located in the medial RTN/pFRG this Phox2B expressing population consists of approximately 2,000 chemosensing neurons that sense changes in the partial pressure of $C0_2$ ($pC0_2$) in the blood stream via proton receptors (Wang, Shi et al. 2013). Increased [H^+] is a product of increased $pC0_2$ which increases the excitatory activity of the RTN/pFRG. The RTN/pFRG provides excitatory drive to the pre BötC to increase the rate of inspiration and thus lower $pC0_2$. The chemosensing portion of the RTN/pFRG is not rhythmically active on its own (Mulkey, Stornetta et al. 2004, Guyenet, Mulkey et al. 2005, Guyenet, Stornetta et al. 2010). However, the lateral portion of the RTN/pFRG, which largely does not express Phox2B, has been postulated to provide the oscillatory behavior necessary in active expiration (Pagliardini, Janczewski et al. 2011).

The BötC is located caudal to the RTN/pFRG and is comprised primarily of inhibitory neurons that provide inhibition during post-inspiratory and expiratory phases (Ezure 1990, Jiang and Lipski 1990). The BötC has projections to pre BötC to inhibit inspiratory activity during expiration. The pre BötC is known to be the source of inspiratory rhythm generation in the respiratory CPG. This has been supported through physical and chemical manipulations to the pre BötC. Rats maintain a rhythmic inspiratory pattern following dissection of the brainstem just caudal to the pre BötC in a (Janczewski and Feldman 2006). In a separate study, explants of the rat pre BötC eliminated respiratory rhythm *in vivo,* yet the explanted pre BötC maintained rhythmic oscillating firing patterns when cultured *in vitro* (Smith, Ellenberger et al. 1991). Additionally, neurons of the pre BötC express neurokinin-1 receptor (NK1R) for which substance P (SP) is the ligand. Neurotoxic lesioning of pre BötC neurons by the toxin saproin, conjugated to SP resulted in

ataxic breathing in adult rats (Gray, Janczewski et al. 2001). Neurons of the pre BötC drive respiration through pre-motor and motor connectivity with the rVRG and hypoglossal nerve XII, respectively (Smith, Ellenberger et al. 1991, Feldman, Mitchell et al. 2003).

While the cellular composition of the pre BötC is heterogeneous, containing both excitatory and inhibitory neurons as well as astrocytes, it is the excitatory neurons that drive functional respiratory activity (Wallen-Mackenzie, Gezelius et al. 2006). One key excitatory population in the pre BötC responsible driving the respiratory rhythm generation is Dbx1 expressing interneurons (Vann, Pham et al. 2018). Dbx1 is a key transcription factor is necessary for pre BötC and V0 interneuron development. Similar to the spinal cord, $V0_D$ (inhibitory) and $V0_V$ (excitatory) are two subtypes of the V0 interneurons in the hindbrain. The excitatory $V0_V$ interneurons migrate and expand throughout the VRC and are thought to be the important population in the pre BötC (Wu, Capelli et al. 2017). Additionally, It has been recently demonstrated that the glial population is also important in the rhythmic activity produced by the pre BötC. Inhibiting vesicle release by astrocytes in the pre BötC results in attenuation of the rhythmicity implicating glial interaction in rhythm generation (Sheikhbahaei, Turovsky et al. 2018). Additionally, an inhibitory population in the pre BötC has been demonstrated to project to the BötC and RTN/pFRG and is active during inspiration to inhibit expiratory activity (Ausborn, Koizumi et al. 2018).

The rVRG is located caudal to and receives excitatory input from the pre BötC during inspiration as well as inhibitory input from the BötC during expiration. The rVRG contains excitatory bulbospinal neurons that connect the medulla to the spinal cord to provide excitatory drive to inspiratory phrenic and intercostal motor neurons (Bianchi,

Denavit-Saubie et al. 1995). Less has been identified about the cVRG though it is thought to be the expiratory counterpart to the rVRG (Ezure 1990). At this point, there has been little reported on the genetic make-up of these populations making subtype identification difficult.

Overall, several structures located in the ventrolateral medulla are active in a series of feedback loops to control the rhythmicity of respiration. The pre BötC is the main rhythm generator of the respiratory CPG, and it receives tonic input from the RTN/pFRG in response to changes in $pC0_2$. However, computation model of the respiratory CPG predicts that the pre BötC receives a tonic input (Rubin, Shevtsova et al. 2009). In a separate study, V2a interneurons located in the medial reticular formation were described to form glutamatergic synapses onto the soma of cells in the pre BötC (Crone, Viemari et al. 2012). This suggests that the V2a interneurons may function as an input to the respiratory CPG by providing the tonic input onto the pre BötC. While there have been great advancements in the understanding of the respiratory CPG, there is still a lot to be done to identify all the neurons involved as well as their transcriptional signatures. A deeper understanding of neuronal identity may lead to a better understanding of how to restore function following injury or developmental abnormalities.

1.5 Concluding Remarks

The neural tube is developed through a series of signaling gradients that pattern neural progenitors in the ventrodorsal as well as the rostrocaudal directions. These endogenous signaling pathways have been probed *in vitro* to direct PSCs into specific neuronal cell fates. Lastly, committed neural phenotypes, specifically those in the hindbrain

and spinal cord, mature to play a specific role in neural circuitry to control important motor functions including locomotion and respiration.

The following dissertation sits at a unique intersection of developmental stem cell biology and systems engineering approaches to define and build novel tissue systems from caudal interneuron populations. In summary, this work significantly adds to the field of developmental neurobiology and tissue engineering by describing new neural subtypes important in respiration from hPSCs. Given that the neurons involved in human respiration have not been interrogated due to lack of availability, the work presented here provides a significant advancement toward a platform to study how insult to the human respiratory system through disease and injury affects neural networks and therefore respiratory function.

1.6 Bibliography

Adil, M. M., T. Vazin, B. Ananthanarayanan, G. M. C. Rodrigues, A. T. Rao, R. U. Kulkarni, E. W. Miller, S. Kumar and D. V. Schaffer (2017). "Engineered hydrogels increase the post-transplantation survival of encapsulated hESC-derived midbrain dopaminergic neurons." Biomaterials **136**: 1-11.

Al-Mosawie, A., J. M. Wilson and R. M. Brownstone (2007). "Heterogeneity of V2-derived interneurons in the adult mouse spinal cord." Eur J Neurosci **26**(11): 3003-3015.
Amit, M., M. K. Carpenter, M. S. Inokuma, C. P. Chiu, C. P. Harris, M. A. Waknitz, J. Itskovitz-Eldor and J. A. Thomson (2000). "Clonally derived human embryonic stem cell lines maintain pluripotency and proliferative potential for prolonged periods of culture." Dev Biol **227**(2): 271-278.

Amoroso, M. W., G. F. Croft, D. J. Williams, S. O'Keeffe, M. A. Carrasco, A. R. Davis, L. Roybon, D. H. Oakley, T. Maniatis, C. E. Henderson and H. Wichterle (2013). "Accelerated high-yield generation of limb-innervating motor neurons from human stem cells." J Neurosci **33**(2): 574-586.

Amoyel, M., Y. C. Cheng, Y. J. Jiang and D. G. Wilkinson (2005). "Wnt1 regulates neurogenesis and mediates lateral inhibition of boundary cell specification in the zebrafish hindbrain." Development **132**(4): 775-785.

Ausborn, J., H. Koizumi, W. H. Barnett, T. T. John, R. Zhang, Y. I. Molkov, J. C. Smith and I. A. Rybak (2018). "Organization of the core respiratory network: Insights from optogenetic and modeling studies." PLoS Comput Biol **14**(4): e1006148.

Azim, E., J. Jiang, B. Alstermark and T. M. Jessell (2014). "Skilled reaching relies on a V2a propriospinal internal copy circuit." Nature **508**(7496): 357-363.

Bain, G., W. J. Ray, M. Yao and D. I. Gottlieb (1996). "Retinoic acid promotes neural and represses mesodermal gene expression in mouse embryonic stem cells in culture." Biochem Biophys Res Commun **223**(3): 691-694.

Bel-Vialar, S., N. Itasaki and R. Krumlauf (2002). "Initiating Hox gene expression: in the early chick neural tube differential sensitivity to FGF and RA signaling subdivides the HoxB genes in two distinct groups." Development **129**(22): 5103-5115.

Bellingham, M. C. (1998). "Driving respiration: the respiratory central pattern generator." Clin Exp Pharmacol Physiol **25**(10): 847-856.

Berggren, K., P. McCaffery, U. Drager and C. J. Forehand (1999). "Differential distribution of retinoic acid synthesis in the chicken embryo as determined by immunolocalization of the retinoic acid synthetic enzyme, RALDH-2." Dev Biol **210**(2): 288-304.

Bianchi, A. L., M. Denavit-Saubie and J. Champagnat (1995). "Central control of breathing in mammals: neuronal circuitry, membrane properties, and neurotransmitters." Physiol Rev **75**(1): 1-45.

Borghese, L., D. Dolezalova, T. Opitz, S. Haupt, A. Leinhaas, B. Steinfarz, P. Koch, F. Edenhofer, A. Hampl and O. Brustle (2010). "Inhibition of notch signaling in human embryonic stem cell-derived neural stem cells delays G1/S phase transition and accelerates neuronal differentiation in vitro and in vivo." Stem Cells **28**(5): 955-964.

Borowska, J., C. T. Jones, H. Zhang, J. Blacklaws, M. Goulding and Y. Zhang (2013). "Functional subpopulations of V3 interneurons in the mature mouse spinal cord." J Neurosci **33**(47): 18553-18565.

Britz, O., J. Zhang, K. S. Grossmann, J. Dyck, J. C. Kim, S. Dymecki, S. Gosgnach and M. Goulding (2015). "A genetically defined asymmetry underlies the inhibitory control of flexor-extensor locomotor movements." Elife **4**.

Brown, C. R., J. C. Butts, D. A. McCreedy and S. E. Sakiyama-Elbert (2014). "Generation of v2a interneurons from mouse embryonic stem cells." Stem Cells Dev **23**(15): 1765-1776.

Butts, J. C., D. A. McCreedy, J. A. Martinez-Vargas, F. N. Mendoza-Camacho, T. A. Hookway, C. A. Gifford, P. Taneja, L. Noble-Haeusslein and T. C. McDevitt (2017). "Differentiation of V2a interneurons from human pluripotent stem cells." Proc Natl Acad Sci U S A **114**(19): 4969-4974.

Cao, S. Y., Y. Hu, C. Chen, F. Yuan, M. Xu, Q. Li, K. H. Fang, Y. Chen and Y. Liu (2017). "Enhanced derivation of human pluripotent stem cell-derived cortical glutamatergic neurons by a small molecule." Sci Rep **7**(1): 3282.

Chambers, S. M., C. A. Fasano, E. P. Papapetrou, M. Tomishima, M. Sadelain and L. Studer (2009). "Highly efficient neural conversion of human ES and iPS cells by dual inhibition of SMAD signaling." Nat Biotechnol **27**(3): 275-280.

Chao, H. T., H. Chen, R. C. Samaco, M. Xue, M. Chahrour, J. Yoo, J. L. Neul, S. Gong, H. C. Lu, N. Heintz, M. Ekker, J. L. Rubenstein, J. L. Noebels, C. Rosenmund and H. Y. Zoghbi (2010). "Dysfunction in GABA signalling mediates autism-like stereotypies and Rett syndrome phenotypes." Nature **468**(7321): 263-269.

Cheah, C. S., F. H. Yu, R. E. Westenbroek, F. K. Kalume, J. C. Oakley, G. B. Potter, J. L. Rubenstein and W. A. Catterall (2012). "Specific deletion of NaV1.1 sodium channels in inhibitory interneurons causes seizures and premature death in a mouse model of Dravet syndrome." Proc Natl Acad Sci U S A **109**(36): 14646-14651.

Cheng, C., D. M. Fass, K. Folz-Donahue, M. E. MacDonald and S. J. Haggarty (2017). "Highly Expandable Human iPS Cell-Derived Neural Progenitor Cells (NPC) and Neurons for Central Nervous System Disease Modeling and High-Throughput Screening." Curr Protoc Hum Genet **92**: 21 28 21-21 28 21.

Crawford, T. Q. and H. Roelink (2007). "The notch response inhibitor DAPT enhances neuronal differentiation in embryonic stem cell-derived embryoid bodies independently of sonic hedgehog signaling." Dev Dyn **236**(3): 886-892.

Crone, S. A., K. A. Quinlan, L. Zagoraiou, S. Droho, C. E. Restrepo, L. Lundfald, T. Endo, J. Setlak, T. M. Jessell, O. Kiehn and K. Sharma (2008). "Genetic ablation of V2a ipsilateral interneurons disrupts left-right locomotor coordination in mammalian spinal cord." Neuron **60**(1): 70-83.

Crone, S. A., J. C. Viemari, S. Droho, A. Mrejeru, J. M. Ramirez and K. Sharma (2012). "Irregular Breathing in Mice following Genetic Ablation of V2a Neurons." J Neurosci **32**(23): 7895-7906.

Del Barrio, M. G., R. Taveira-Marques, Y. Muroyama, D. I. Yuk, S. Li, M. Wines-Samuelson, J. Shen, H. K. Smith, M. Xiang, D. Rowitch and W. D. Richardson (2007). "A regulatory network involving Foxn4, Mash1 and delta-like 4/Notch1 generates V2a and V2b spinal interneurons from a common progenitor pool." Development **134**(19): 3427-3436.

Del Negro, C. A., G. D. Funk and J. L. Feldman (2018). "Breathing matters." Nat Rev Neurosci.
Dessaud, E., A. P. McMahon and J. Briscoe (2008). "Pattern formation in the vertebrate neural tube: a sonic hedgehog morphogen-regulated transcriptional network." Development **135**(15): 2489-2503.

Dessaud, E., V. Ribes, N. Balaskas, L. L. Yang, A. Pierani, A. Kicheva, B. G. Novitch, J. Briscoe and N. Sasai (2010). "Dynamic assignment and maintenance of positional identity in the ventral neural tube by the morphogen sonic hedgehog." PLoS Biol **8**(6): e1000382.

Dessaud, E., L. L. Yang, K. Hill, B. Cox, F. Ulloa, A. Ribeiro, A. Mynett, B. G. Novitch and J. Briscoe (2007). "Interpretation of the sonic hedgehog morphogen gradient by a temporal adaptation mechanism." Nature **450**(7170): 717-720.

Diez Del Corral, R. and A. V. Morales (2017). "The Multiple Roles of FGF Signaling in the Developing Spinal Cord." Front Cell Dev Biol **5**: 58.

Dougherty, K. J., L. Zagoraiou, D. Satoh, I. Rozani, S. Doobar, S. Arber, T. M. Jessell and O. Kiehn (2013). "Locomotor rhythm generation linked to the output of spinal shox2 excitatory interneurons." Neuron **80**(4): 920-933.

Douvaras, P. and V. Fossati (2015). "Generation and isolation of oligodendrocyte progenitor cells from human pluripotent stem cells." Nat Protoc **10**(8): 1143-1154.

Du, Z. W., H. Chen, H. Liu, J. Lu, K. Qian, C. L. Huang, X. Zhong, F. Fan and S. C. Zhang (2015). "Generation and expansion of highly pure motor neuron progenitors from human pluripotent stem cells." Nat Commun **6**: 6626.

Eggenschwiler, J. T. and K. V. Anderson (2007). "Cilia and developmental signaling." Annu Rev Cell Dev Biol **23**: 345-373.

Eiraku, M., K. Watanabe, M. Matsuo-Takasaki, M. Kawada, S. Yonemura, M. Matsumura, T. Wataya, A. Nishiyama, K. Muguruma and Y. Sasai (2008). "Self-organized formation of polarized cortical tissues from ESCs and its active manipulation by extrinsic signals." Cell Stem Cell **3**(5): 519-532.

Elkouby, Y. M. and D. Frank (2010). Wnt/beta-Catenin Signaling in Vertebrate Posterior Neural Development. San Rafael (CA).

Ellenberger, H. H. and J. L. Feldman (1990). "Brainstem connections of the rostral ventral respiratory group of the rat." Brain Res **513**(1): 35-42.

Ezure, K. (1990). "Synaptic connections between medullary respiratory neurons and considerations on the genesis of respiratory rhythm." Prog Neurobiol **35**(6): 429-450.
Ezure, K., M. Manabe and H. Yamada (1988). "Distribution of medullary respiratory neurons in the rat." Brain Res **455**(2): 262-270.

Fandel, T. M., A. Trivedi, C. R. Nicholas, H. Zhang, J. Chen, A. F. Martinez, L. J. Noble-Haeusslein and A. R. Kriegstein (2016). "Transplanted Human Stem Cell-Derived Interneuron Precursors Mitigate Mouse Bladder Dysfunction and Central Neuropathic Pain after Spinal Cord Injury." Cell Stem Cell **19**(4): 544-557.

Feldman, J. L., C. A. Del Negro and P. A. Gray (2013). "Understanding the rhythm of breathing: so near, yet so far." Annu Rev Physiol **75**: 423-452.

Feldman, J. L., G. S. Mitchell and E. E. Nattie (2003). "Breathing: rhythmicity, plasticity, chemosensitivity." Annu Rev Neurosci **26**: 239-266.

Gordon, W. R., K. L. Arnett and S. C. Blacklow (2008). "The molecular logic of Notch signaling--a structural and biochemical perspective." J Cell Sci **121**(Pt 19): 3109-3119.

Gray, P. A., W. A. Janczewski, N. Mellen, D. R. McCrimmon and J. L. Feldman (2001). "Normal breathing requires preBotzinger complex neurokinin-1 receptor-expressing neurons." Nat Neurosci **4**(9): 927-930.

Griener, A., W. Zhang, H. Kao, C. Wagner and S. Gosgnach (2015). "Probing diversity within subpopulations of locomotor-related V0 interneurons." Dev Neurobiol **75**(11): 1189-1203.

Gupta, S., D. Sivalingam, S. Hain, C. Makkar, E. Sosa, A. Clark and S. J. Butler (2018). "Deriving Dorsal Spinal Sensory Interneurons from Human Pluripotent Stem Cells." Stem Cell Reports **10**(2): 390-405.

Guthrie, S., V. Prince and A. Lumsden (1993). "Selective dispersal of avian rhombomere cells in orthotopic and heterotopic grafts." Development **118**(2): 527-538.

Guyenet, P. G., D. K. Mulkey, R. L. Stornetta and D. A. Bayliss (2005). "Regulation of ventral surface chemoreceptors by the central respiratory pattern generator." J Neurosci **25**(39): 8938-8947.

Guyenet, P. G., R. L. Stornetta and D. A. Bayliss (2010). "Central respiratory chemoreception." J Comp Neurol **518**(19): 3883-3906.

Hookway, T. A., J. C. Butts, E. Lee, H. Tang and T. C. McDevitt (2016). "Aggregate formation and suspension culture of human pluripotent stem cells and differentiated progeny." Methods **101**: 11-20.

Hu, B. Y., Z. W. Du and S. C. Zhang (2009). "Differentiation of human oligodendrocytes from pluripotent stem cells." Nat Protoc **4**(11): 1614-1622.

Imayoshi, I., A. Isomura, Y. Harima, K. Kawaguchi, H. Kori, H. Miyachi, T. Fujiwara, F. Ishidate and R. Kageyama (2013). "Oscillatory control of factors determining multipotency and fate in mouse neural progenitors." Science **342**(6163): 1203-1208.

Imayoshi, I., M. Sakamoto, M. Yamaguchi, K. Mori and R. Kageyama (2010). "Essential roles of Notch signaling in maintenance of neural stem cells in developing and adult brains." J Neurosci **30**(9): 3489-3498.

Incardona, J. P., W. Gaffield, R. P. Kapur and H. Roelink (1998). "The teratogenic Veratrum alkaloid cyclopamine inhibits sonic hedgehog signal transduction." Development **125**(18): 3553-3562.

Iyer, N. R., J. E. Huettner, J. C. Butts, C. R. Brown and S. E. Sakiyama-Elbert (2016). "Generation of highly enriched V2a interneurons from mouse embryonic stem cells." Exp Neurol **277**: 305-316.

Janczewski, W. A. and J. L. Feldman (2006). "Distinct rhythm generators for inspiration and expiration in the juvenile rat." J Physiol **570**(Pt 2): 407-420.

Jiang, C. and J. Lipski (1990). "Extensive monosynaptic inhibition of ventral respiratory group neurons by augmenting neurons in the Botzinger complex in the cat." Exp Brain Res **81**(3): 639-648.

Jo, J., Y. Xiao, A. X. Sun, E. Cukuroglu, H. D. Tran, J. Goke, Z. Y. Tan, T. Y. Saw, C. P. Tan, H. Lokman, Y. Lee, D. Kim, H. S. Ko, S. O. Kim, J. H. Park, N. J. Cho, T. M. Hyde, J. E. Kleinman, J. H.

Shin, D. R. Weinberger, E. K. Tan, H. S. Je and H. H. Ng (2016). "Midbrain-like Organoids from Human Pluripotent Stem Cells Contain Functional Dopaminergic and Neuromelanin-Producing Neurons." Cell Stem Cell **19**(2): 248-257.

Jones-Villeneuve, E. M., M. A. Rudnicki, J. F. Harris and M. W. McBurney (1983). "Retinoic acid-induced neural differentiation of embryonal carcinoma cells." Mol Cell Biol **3**(12): 2271-2279.

Kadoshima, T., H. Sakaguchi, T. Nakano, M. Soen, S. Ando, M. Eiraku and Y. Sasai (2013). "Self-organization of axial polarity, inside-out layer pattern, and species-specific progenitor dynamics in human ES cell-derived neocortex." Proc Natl Acad Sci U S A **110**(50): 20284-20289.

Kirkeby, A., S. Grealish, D. A. Wolf, J. Nelander, J. Wood, M. Lundblad, O. Lindvall and M. Parmar (2012). "Generation of regionally specified neural progenitors and functional neurons from human embryonic stem cells under defined conditions." Cell Rep **1**(6): 703-714.

Kong, J. H., L. Yang, E. Dessaud, K. Chuang, D. M. Moore, R. Rohatgi, J. Briscoe and B. G. Novitch (2015). "Notch activity modulates the responsiveness of neural progenitors to sonic hedgehog signaling." Dev Cell **33**(4): 373-387.

Krencik, R. and S. C. Zhang (2011). "Directed differentiation of functional astroglial subtypes from human pluripotent stem cells." Nat Protoc **6**(11): 1710-1717.
Lai, E. C. (2004). "Notch signaling: control of cell communication and cell fate." Development **131**(5): 965-973.

Lancaster, M. A., M. Renner, C. A. Martin, D. Wenzel, L. S. Bicknell, M. E. Hurles, T. Homfray, J. M. Penninger, A. P. Jackson and J. A. Knoblich (2013). "Cerebral organoids model human brain development and microcephaly." Nature **501**(7467): 373-379.

Lanuza, G. M., S. Gosgnach, A. Pierani, T. M. Jessell and M. Goulding (2004). "Genetic identification of spinal interneurons that coordinate left-right locomotor activity necessary for walking movements." Neuron **42**(3): 375-386.

Li, W., W. Sun, Y. Zhang, W. Wei, R. Ambasudhan, P. Xia, M. Talantova, T. Lin, J. Kim, X. Wang, W. R. Kim, S. A. Lipton, K. Zhang and S. Ding (2011). "Rapid induction and long-term self-renewal of primitive neural precursors from human embryonic stem cells by small molecule inhibitors." Proc Natl Acad Sci U S A **108**(20): 8299-8304.

Li, X. J., Z. W. Du, E. D. Zarnowska, M. Pankratz, L. O. Hansen, R. A. Pearce and S. C. Zhang (2005). "Specification of motoneurons from human embryonic stem cells." Nat Biotechnol **23**(2): 215-221.

Li, X. J., B. Y. Hu, S. A. Jones, Y. S. Zhang, T. Lavaute, Z. W. Du and S. C. Zhang (2008). "Directed differentiation of ventral spinal progenitors and motor neurons from human embryonic stem cells by small molecules." Stem Cells **26**(4): 886-893.

Lippmann, E. S., C. E. Williams, D. A. Ruhl, M. C. Estevez-Silva, E. R. Chapman, J. J. Coon and R. S. Ashton (2015). "Deterministic HOX patterning in human pluripotent stem cell-derived neuroectoderm." Stem Cell Reports **4**(4): 632-644.

Liu, J. P., E. Laufer and T. M. Jessell (2001). "Assigning the positional identity of spinal motor neurons: rostrocaudal patterning of Hox-c expression by FGFs, Gdf11, and retinoids." Neuron **32**(6): 997-1012.

Maden, M., E. Sonneveld, P. T. van der Saag and E. Gale (1998). "The distribution of endogenous retinoic acid in the chick embryo: implications for developmental mechanisms." Development **125**(21): 4133-4144.

Mansour, A. A., J. T. Goncalves, C. W. Bloyd, H. Li, S. Fernandes, D. Quang, S. Johnston, S. L. Parylak, X. Jin and F. H. Gage (2018). "An in vivo model of functional and vascularized human brain organoids." Nat Biotechnol.

Mariani, J., G. Coppola, P. Zhang, A. Abyzov, L. Provini, L. Tomasini, M. Amenduni, A. Szekely, D. Palejev, M. Wilson, M. Gerstein, E. L. Grigorenko, K. Chawarska, K. A. Pelphrey, J. R. Howe and F. M. Vaccarino (2015). "FOXG1-Dependent Dysregulation of GABA/Glutamate Neuron Differentiation in Autism Spectrum Disorders." Cell **162**(2): 375-390.

Marklund, U., Z. Alekseenko, E. Andersson, S. Falci, M. Westgren, T. Perlmann, A. Graham, E. Sundstrom and J. Ericson (2014). "Detailed expression analysis of regulatory genes in the early developing human neural tube." Stem Cells Dev **23**(1): 5-15.

Maroof, A. M., S. Keros, J. A. Tyson, S. W. Ying, Y. M. Ganat, F. T. Merkle, B. Liu, A. Goulburn, E. G. Stanley, A. G. Elefanty, H. R. Widmer, K. Eggan, P. A. Goldstein, S. A. Anderson and L. Studer (2013). "Directed differentiation and functional maturation of cortical interneurons from human embryonic stem cells." Cell Stem Cell **12**(5): 559-572.

McCreedy, D. A., C. R. Brown, J. C. Butts, H. Xu, J. E. Huettner and S. E. Sakiyama-Elbert (2014). "A new method for generating high purity motoneurons from mouse embryonic stem cells." Biotechnol Bioeng **111**(10): 2041-2055.

Misra, K., H. Luo, S. Li, M. Matise and M. Xiang (2014). "Asymmetric activation of Dll4-Notch signaling by Foxn4 and proneural factors activates BMP/TGFbeta signaling to specify V2b interneurons in the spinal cord." Development **141**(1): 187-198.

Muguruma, K., A. Nishiyama, Y. Ono, H. Miyawaki, E. Mizuhara, S. Hori, A. Kakizuka, K. Obata, Y. Yanagawa, T. Hirano and Y. Sasai (2010). "Ontogeny-recapitulating generation and tissue integration of ES cell-derived Purkinje cells." Nat Neurosci **13**(10): 1171-1180.

Mulkey, D. K., R. L. Stornetta, M. C. Weston, J. R. Simmons, A. Parker, D. A. Bayliss and P. G. Guyenet (2004). "Respiratory control by ventral surface chemoreceptor neurons in rats." Nat Neurosci **7**(12): 1360-1369.

Mumm, J. S. and R. Kopan (2000). "Notch signaling: from the outside in." Dev Biol **228**(2): 151-165.

Nicholas, C. R., J. Chen, Y. Tang, D. G. Southwell, N. Chalmers, D. Vogt, C. M. Arnold, Y. J. Chen, E. G. Stanley, A. G. Elefanty, Y. Sasai, A. Alvarez-Buylla, J. L. Rubenstein and A. R. Kriegstein (2013). "Functional maturation of hPSC-derived forebrain interneurons requires an extended timeline and mimics human neural development." Cell Stem Cell **12**(5): 573-586.

Niederreither, K., P. McCaffery, U. C. Drager, P. Chambon and P. Dolle (1997). "Restricted expression and retinoic acid-induced downregulation of the retinaldehyde dehydrogenase type 2 (RALDH-2) gene during mouse development." Mech Dev **62**(1): 67-78.

Nordstrom, U., E. Maier, T. M. Jessell and T. Edlund (2006). "An early role for WNT signaling in specifying neural patterns of Cdx and Hox gene expression and motor neuron subtype identity." PLoS Biol **4**(8): e252.

Okada, Y., T. Shimazaki, G. Sobue and H. Okano (2004). "Retinoic-acid-concentration-dependent acquisition of neural cell identity during in vitro differentiation of mouse embryonic stem cells." Dev Biol **275**(1): 124-142.

Pagliardini, S., W. A. Janczewski, W. Tan, C. T. Dickson, K. Deisseroth and J. L. Feldman (2011). "Active expiration induced by excitation of ventral medulla in adult anesthetized rats." J Neurosci **31**(8): 2895-2905.

Pasini, A. and D. G. Wilkinson (2002). "Stabilizing the regionalisation of the developing vertebrate central nervous system." Bioessays **24**(5): 427-438.

Patten, I. and M. Placzek (2000). "The role of Sonic hedgehog in neural tube patterning." Cell Mol Life Sci **57**(12): 1695-1708.

Perrier, A. L., V. Tabar, T. Barberi, M. E. Rubio, J. Bruses, N. Topf, N. L. Harrison and L. Studer (2004). "Derivation of midbrain dopamine neurons from human embryonic stem cells." Proc Natl Acad Sci U S A **101**(34): 12543-12548.

Philippidou, P. and J. S. Dasen (2013). "Hox genes: choreographers in neural development, architects of circuit organization." Neuron **80**(1): 12-34.

Qian, X., H. N. Nguyen, M. M. Song, C. Hadiono, S. C. Ogden, C. Hammack, B. Yao, G. R. Hamersky, F. Jacob, C. Zhong, K. J. Yoon, W. Jeang, L. Lin, Y. Li, J. Thakor, D. A. Berg, C. Zhang, E. Kang, M. Chickering, D. Nauen, C. Y. Ho, Z. Wen, K. M. Christian, P. Y. Shi, B. J. Maher, H.

Wu, P. Jin, H. Tang, H. Song and G. L. Ming (2016). "Brain-Region-Specific Organoids Using Mini-bioreactors for Modeling ZIKV Exposure." Cell **165**(5): 1238-1254.

Rhinn, M. and P. Dolle (2012). "Retinoic acid signalling during development." Development **139**(5): 843-858.

Ribeiro, D., K. Ellwanger, D. Glagow, S. Theofilopoulos, N. S. Corsini, A. Martin-Villalba, C. Niehrs and E. Arenas (2011). "Dkk1 regulates ventral midbrain dopaminergic differentiation and morphogenesis." PLoS One **6**(2): e15786.

Rubin, J. E., N. A. Shevtsova, G. B. Ermentrout, J. C. Smith and I. A. Rybak (2009). "Multiple rhythmic states in a model of the respiratory central pattern generator." J Neurophysiol **101**(4): 2146-2165.

Rybak, I. A., K. J. Dougherty and N. A. Shevtsova (2015). "Organization of the Mammalian Locomotor CPG: Review of Computational Model and Circuit Architectures Based on Genetically Identified Spinal Interneurons(1,2,3)." eNeuro **2**(5).

Sances, S., L. I. Bruijn, S. Chandran, K. Eggan, R. Ho, J. R. Klim, M. R. Livesey, E. Lowry, J. D. Macklis, D. Rushton, C. Sadegh, D. Sareen, H. Wichterle, S. C. Zhang and C. N. Svendsen (2016). "Modeling ALS with motor neurons derived from human induced pluripotent stem cells." Nat Neurosci **19**(4): 542-553.

Schwartz, M. P., Z. Hou, N. E. Propson, J. Zhang, C. J. Engstrom, V. Santos Costa, P. Jiang, B. K. Nguyen, J. M. Bolin, W. Daly, Y. Wang, R. Stewart, C. D. Page, W. L. Murphy and J. A. Thomson (2015). "Human pluripotent stem cell-derived neural constructs for predicting neural toxicity." Proc Natl Acad Sci U S A **112**(40): 12516-12521.

Shaltouki, A., J. Peng, Q. Liu, M. S. Rao and X. Zeng (2013). "Efficient generation of astrocytes from human pluripotent stem cells in defined conditions." Stem Cells **31**(5): 941-952.

Sheikhbahaei, S., E. A. Turovsky, P. S. Hosford, A. Hadjihambi, S. M. Theparambil, B. Liu, N. Marina, A. G. Teschemacher, S. Kasparov, J. C. Smith and A. V. Gourine (2018). "Astrocytes modulate brainstem respiratory rhythm-generating circuits and determine exercise capacity." Nat Commun **9**(1): 370.

Shi, Y., P. Kirwan and F. J. Livesey (2012). "Directed differentiation of human pluripotent stem cells to cerebral cortex neurons and neural networks." Nat Protoc **7**(10): 1836-1846.
Shimojo, H., T. Ohtsuka and R. Kageyama (2008). "Oscillations in notch signaling regulate maintenance of neural progenitors." Neuron **58**(1): 52-64.

Smith, J. C., H. H. Ellenberger, K. Ballanyi, D. W. Richter and J. L. Feldman (1991). "Pre-Botzinger complex: a brainstem region that may generate respiratory rhythm in mammals." Science **254**(5032): 726-729.

Smith, J. L. and G. C. Schoenwolf (1989). "Notochordal induction of cell wedging in the chick neural plate and its role in neural tube formation." J Exp Zool **250**(1): 49-62.

Sternfeld, M. J., C. A. Hinckley, N. J. Moore, M. T. Pankratz, K. L. Hilde, S. P. Driscoll, M. Hayashi, N. D. Amin, D. Bonanomi, W. D. Gifford, K. Sharma, M. Goulding and S. L. Pfaff (2017). "Speed and segmentation control mechanisms characterized in rhythmically-active circuits created from spinal neurons produced from genetically-tagged embryonic stem cells." Elife **6**.

Takahashi, K. and S. Yamanaka (2006). "Induction of pluripotent stem cells from mouse embryonic and adult fibroblast cultures by defined factors." Cell **126**(4): 663-676.

Talpalar, A. E., J. Bouvier, L. Borgius, G. Fortin, A. Pierani and O. Kiehn (2013). "Dual-mode operation of neuronal networks involved in left-right alternation." Nature **500**(7460): 85-88.

Ungrin, M. D., C. Joshi, A. Nica, C. Bauwens and P. W. Zandstra (2008). "Reproducible, ultra high-throughput formation of multicellular organization from single cell suspension-derived human embryonic stem cell aggregates." PLoS One **3**(2): e1565.

van Straaten, H. W., J. W. Hekking, E. J. Wiertz-Hoessels, F. Thors and J. Drukker (1988). "Effect of the notochord on the differentiation of a floor plate area in the neural tube of the chick embryo." Anat Embryol (Berl) **177**(4): 317-324.

Vann, N. C., F. D. Pham, K. E. Dorst and C. A. Del Negro (2018). "Dbx1 Pre-Botzinger Complex Interneurons Comprise the Core Inspiratory Oscillator for Breathing in Unanesthetized Adult Mice." eNeuro **5**(3).

Verret, L., E. O. Mann, G. B. Hang, A. M. Barth, I. Cobos, K. Ho, N. Devidze, E. Masliah, A. C. Kreitzer, I. Mody, L. Mucke and J. J. Palop (2012). "Inhibitory interneuron deficit links altered network activity and cognitive dysfunction in Alzheimer model." Cell **149**(3): 708-721.

Wallen-Mackenzie, A., H. Gezelius, M. Thoby-Brisson, A. Nygard, A. Enjin, F. Fujiyama, G. Fortin and K. Kullander (2006). "Vesicular glutamate transporter 2 is required for central respiratory rhythm generation but not for locomotor central pattern generation." J Neurosci **26**(47): 12294-12307.

Wang, S., Y. Shi, S. Shu, P. G. Guyenet and D. A. Bayliss (2013). "Phox2b-expressing retrotrapezoid neurons are intrinsically responsive to H+ and CO2." J Neurosci **33**(18): 7756-7761.

Watanabe, M., J. E. Buth, N. Vishlaghi, L. de la Torre-Ubieta, J. Taxidis, B. S. Khakh, G. Coppola, C. A. Pearson, K. Yamauchi, D. Gong, X. Dai, R. Damoiseaux, R. Aliyari, S. Liebscher, K. Schenke-Layland, C. Caneda, E. J. Huang, Y. Zhang, G. Cheng, D. H. Geschwind, P. Golshani,

R. Sun and B. G. Novitch (2017). "Self-Organized Cerebral Organoids with Human-Specific Features Predict Effective Drugs to Combat Zika Virus Infection." Cell Rep **21**(2): 517-532.

Wataya, T., S. Ando, K. Muguruma, H. Ikeda, K. Watanabe, M. Eiraku, M. Kawada, J. Takahashi, N. Hashimoto and Y. Sasai (2008). "Minimization of exogenous signals in ES cell culture induces rostral hypothalamic differentiation." Proc Natl Acad Sci U S A **105**(33): 11796-11801.

Wichterle, H., I. Lieberam, J. A. Porter and T. M. Jessell (2002). "Directed differentiation of embryonic stem cells into motor neurons." Cell **110**(3): 385-397.

Wichterle, H., M. Peljto and S. Nedelec (2009). "Xenotransplantation of embryonic stem cell-derived motor neurons into the developing chick spinal cord." Methods Mol Biol **482**: 171-183.

Wilson, L. and M. Maden (2005). "The mechanisms of dorsoventral patterning in the vertebrate neural tube." Dev Biol **282**(1): 1-13.

Wizenmann, A. and A. Lumsden (1997). "Segregation of rhombomeres by differential chemoaffinity." Mol Cell Neurosci **9**(5-6): 448-459.

Wu, J., P. Capelli, J. Bouvier, M. Goulding, S. Arber and G. Fortin (2017). "A V0 core neuronal circuit for inspiration." Nat Commun **8**(1): 544.

Xu, H. and S. E. Sakiyama-Elbert (2015). "Directed Differentiation of V3 Interneurons from Mouse Embryonic Stem Cells." Stem Cells Dev **24**(22): 2723-2732.

Zhang, J., G. M. Lanuza, O. Britz, Z. Wang, V. C. Siembab, Y. Zhang, T. Velasquez, F. J. Alvarez, E. Frank and M. Goulding (2014). "V1 and v2b interneurons secure the alternating flexor-extensor motor activity mice require for limbed locomotion." Neuron **82**(1): 138-150.

Zhang, Y., S. Narayan, E. Geiman, G. M. Lanuza, T. Velasquez, B. Shanks, T. Akay, J. Dyck, K. Pearson, S. Gosgnach, C. M. Fan and M. Goulding (2008). "V3 spinal neurons establish a robust and balanced locomotor rhythm during walking." Neuron **60**(1): 84-96.

Zhao, Z., Y. Ma, Z. Chen, Q. Liu, Q. Li, D. Kong, K. Yuan, L. Hu, T. Wang, X. Chen, Y. Peng, W. Jiang, Y. Yu and X. Liu (2016). "Effects of Feeder Cells on Dopaminergic Differentiation of Human Embryonic Stem Cells." Front Cell Neurosci **10**: 291.

Zhong, G., S. Droho, S. A. Crone, S. Dietz, A. C. Kwan, W. W. Webb, K. Sharma and R. M. Harris-Warrick (2010). "Electrophysiological characterization of V2a interneurons and their locomotor-related activity in the neonatal mouse spinal cord." J Neurosci **30**(1): 170-182.

Zhong, G., K. Sharma and R. M. Harris-Warrick (2011). "Frequency-dependent recruitment of V2a interneurons during fictive locomotion in the mouse spinal cord." Nat Commun **2**: 274.

Chapter 2: Specification of V2a interneurons from human pluripotent stem cells

2.1 Introduction

Pluripotent stem cells (PSCs) provide a renewable source of cells that can differentiate into a variety of neurons, provided the necessary signaling cues are presented in an appropriate spatiotemporal manner. Different types of neurons, including forebrain and midbrain neural cell types (e.g. cortical neurons (Shi, Kirwan et al. 2012), dopaminergic neurons (Perrier, Tabar et al. 2004), and inhibitory interneurons from the medial ganglionic eminence (Maroof, Keros et al. 2013, Nicholas, Chen et al. 2013) have been differentiated from hPSCs, but, motor neurons are the only caudal neuronal population to be generated from hPSCs to date (Li, Du et al. 2005, Amoroso, Croft et al. 2013).

V2a spinal interneurons, in particular, are crucial to the transmission and coordination of motor and sensory functions (Butt, Harris-Warrick et al. 2002, Butt and Kiehn 2003). Glutamatergic V2a interneurons, identified by expression of the CHX10 transcription factor (Ericson, Rashbass et al. 1997), are distributed throughout the hindbrain and spinal cord in mammals and relay excitatory stimuli to central pattern generators that regulate motor function for breathing and locomotion (Al-Mosawie, Wilson et al. 2007, Crone, Quinlan et al. 2008, Zhong, Droho et al. 2010, Crone, Viemari et al. 2012, Azim, Jiang et al. 2014). Ablation of V2a interneurons in mice results in disruption of normal breathing patterns (Crone, Viemari et al. 2012), impaired forelimb reaching tasks

(Azim, Jiang et al. 2014), and loss of left-right hind-limb coordination (Crone, Quinlan et al. 2008, Zhong, Droho et al. 2010). Together, these studies suggest that V2a interneurons are critical population involved in motor function and could provide a potential cell therapy to restore motor function following injury or disease.

A combination of morphogenic signals are responsible for the patterning of the neural tube during development. The rostral-caudal location of spinal cell types is patterned by retinoic acid (RA) released from adjacent somites (Okada, Shimazaki et al. 2004). In parallel, an orthogonal ventral-dorsal gradient of sonic hedgehog (Shh), secreted from the floor plate and notochord, specifies independent progenitor domains (Marklund, Alekseenko et al. 2014) that yield mature cell types with distinct roles in motor function. In the ventral neural tube, excitatory V2a and inhibitory V2b interneurons arise coincidentally from the p2 domain (Karunaratne, Hargrave et al. 2002, Li, Misra et al. 2005) that is located immediately dorsal to the pMN domain. Notch signaling dictates the balance between V2a and V2b interneurons, with Notch signaling being necessary for the specification of V2b interneurons, whereas inhibition of Notch increases the proportion of V2a interneurons (Fig 2.1 A, (Del Barrio, Taveira-Marques et al. 2007)).

This objective of this study was to develop a protocol to differentiate V2a interneurons from hPSCs using small molecule agonists and antagonists of developmental signaling pathways. The resultant V2a interneuron protocol was specific and reproducible and the neurons matured into excitatory neurons *in vitro.* Transplantation into uninjured murine spinal cords resulted in survival and long extension of the V2a interneuron cultures. These results provide a robust source of human V2a interneurons that can be

used to further define their molecular profile and *in vitro* electrophysiological properties, as well as examine their therapeutic potential for repair of spinal cord injury.

2.2 Materials and methods

2.2.1 Human Pluripotent Stem Cell Culture

hPSCs—H7 and H1 hESCs (WiCell, Madison, WI), WTC and WTB iPSCs (generously donated by Bruce Conklin)—were grown to 70% confluence and passaged using Accutase (Accutase, San Diego, CA) to dissociate to single cells (incubated at 37°C for 5 minutes). Dissociated cells were replated on Matrigel-coated cultureware (hESC-qualified for ESCs and growth factor reduced for iPSCs) at a density of 10,000 cells per cm^2 with 10μM ROCK inhibitor (Y-27632, Selleckchem, Houston, TX) in mTeSR (StemCell Technologies, Vancouver, Canada). All work with human ESC and iPSC lines was approved by the University of California – San Francisco Human Gamete, Embryo and Stem Cell Research (GESCR) Committee.

2.2.2 V2a interneuron differentiation

hPSCs were seeded in mTeSR supplemented with 10μM ROCK inhibitor and dual SMAD inhibitors 0.2μM LDN193189 and 10μM SB431542 (StemGent, Cambridge, MA) at 5,000–100,000 cells/cm^2 onto 24-well plates coated with Matrigel. On day 3, medium was changed to mTeSR supplemented with dual SMAD inhibitors only. On day 5, the base medium was switched to neural induction medium (DMEM F:12 (Corning, Corning, NY), N2 supplement (Life Technologies, Carlsbad, CA), L-Glutamine (VWR), 2μg/ml heparin (Sigma

Aldrich, St. Louis, MO), non-essential amino acids (Mediatech INC, Manassas, VA), penicillin-streptomycin (VWR) supplemented with fresh 0.4µg/ml ascorbic acid (Sigma Aldrich) and 10ng/ml brain derived neurotrophin factor (BDNF, R&D Systems, Minneapolis, MN)) supplemented with dual SMAD inhibitors and 10nM–10µM retinoic acid (Sigma Aldrich). On day 7, dual SMAD inhibition was ceased and 10nM–10µM retinoic acid, 10nM–10µM pur (EMD Millipore, Darmstast, Germany) and 100nM–10µM N-[N-(3,5-difluorophenacetyl)-L-alanyl]-S-phenylglycine t-butyl ester (DAPT) were added to the neural induction medium. Medium was changed every 2–3 days throughout the differentiation, with fresh supplements added each time for up to 17 days.

2.2.3 Neuronal Maturation

On day 17 of differentiation, cultures were dissociated with Accutase (45 minutes at 37°C; triturated every 15 minutes) and plated at 100,000 cells/cm^2 on Matrigel-coated µ-slide 8 wells (ibidi, Martinsreid, Germany) or glass coverslips (Warner Instruments, Hamden CT) in neural induction medium containing 100nM RA, 100nM pur, and 1µM DAPT plus 10µM ROCK inhibitor. Three days later, the medium was switched to neural maturation medium (BrainPhys plus SM1 supplement (Stemcell Technologies (Bardy, van den Hurk et al. 2016)) supplemented with 10 ng/ml of BDNF, GDNF, CNTF, and IGF, R&D Systems). Medium was completely changed every 3–4 days for the remainder of the culture duration.

2.2.4 Real Time Quantitative Polymerase Chain Reaction

Samples were lysed and RNA was extracted using the E.Z.N.A. Total RNA Kit (Omega Biotek, Norcross, GA). RNA (500 ng) was reverse-transcribed into cDNA using the iScript cDNA

synthesis kit (BioRad, Hercules, CA). RT-qPCR was performed using Fast SYBR Green Master Mix (Life Technologies) and the primers listed in Table 2.1 were annealed at 61°C on the Step One Plus Real-Time PCR System (Life Technologies). Fold-changes were calculated using the $\Delta\Delta C_t$ method (Livak and Schmittgen 2001). For high-throughput gene expression analysis, Fluidigm was used. Preamplified cDNA samples and primers were mixed with Sso Fast EvaGreen Supermix (BioRad) then loaded onto a 96.96 Dynamic Array integrated fluidic circuit (IFC) and ran on a BioMark HD system.

2.2.5 Flow Cytometry

At day 17 of differentiation, cells were completely dissociated using Accutase and stained with the Transcription Factor Buffer Set, which includes a fixation/permeabilization (FP) and wash/permeabilization (WP) buffer (BD Biosciences, Franklin Lakes, NJ). Dissociated samples were first fixed for 45 minutes at 4°C in the FP buffer followed by a 20 minute block with WP buffer containing 5% normal donkey serum (NDS, Jackson Laboratory, Bay Harbor, ME). Primary antibodies against CHX10 and the proper matching species isotype control were added at the concentration shown in Table S3 into WP buffer containing 2% NDS and incubated at 4°C for 45 minutes. After two washes with WP buffer, secondary antibodies donkey anti-mouse IgG, Alexa Fluor 488 (Life Technologies), at a dilution of 1:200, were added to WP buffer and incubated at 4°C for 45 minutes. After two washes with WP buffer, samples were passed through a 35-µm filter before assessing with a BD Accuri C6 (BD) cytometer (minimum 20,000 events). Cytometry analysis was performed using FlowJo V10 (Flowjo, Ashland, OR).

2.2.6 *In Vitro* Immunocytochemistry and Imaging

Samples were fixed using 4% paraformaldehyde (VWR) for 30 minutes and permeabilized using 0.1% Triton-X in PBS for 15 minutes at 4° C before blocking for 1 hour at 4°C with PBS containing 5% NDS. Primary antibodies (Table 2.2) were diluted in PBS containing 2% NDS and incubated overnight. Samples were washed three times with PBS for 15 minutes at room temperature before incubating with secondary antibodies (Life Technologies) diluted in PBS containing 2% NDS. Hoechst was added to the samples for 10 minutes then washed and imaged using a Zeiss Axio Observer inverted wide-field microscope equipped with an Apotome structured light attachment. An average intensity projection was performed on Z-stack images to create a single two-dimensional image spanning the entire thickness of the observed field. Images were processed using Photoshop.

2.2.7 Single Cell RNA Sequencing

At Day 17 of culture, cells were dissociated with Accutase. Approximately 8,000 cells were prepared for single cell analysis through droplet encapsulation by the Chromium Controller and library preparation with the Chromium Single Cell 3' v1 Library and Gel Bead Kit (10x Genomics, San Francisco, CA). cDNA was sheared using a Covaris S2 sonicator and 12 PCR cycles were run during cDNA amplification. Libraries were sequenced on a NextSeq 500 (Illumina, San Diego, CA). Sequences were demultiplexed and aligned to human reference genome hg19 using the default settings of 10xGenomics *Cellranger* v 1.2. Genes were annotated using Ensembl version 70 (Dobin, Davis et al. 2013). After *Cellranger* filtering, >85 million valid reads remained with >70% mapping to the transcriptome. Downstream analysis was performed using *Seurat* (Macosko, Basu et al. 2015, Satija, Farrell et al. 2015)

and cells not expressing between 500 and 5000 unique genes were removed. A subset of high-variance genes was determined using Seurat's "MeanVarPlot" function (expression cutoff of ≥ 0.25; dispersion cutoff of ≥ 0.50) and used to group cells into clusters (principal components 1–12; cluster resolution parameter = 0.5) (van der Maaten LJP 2008). The top 20 differentially expressed genes for each cluster were plotted in the heatmap. Raw data is available at SRA under the accession number [upload in progress]. GO analysis was performed on statistically significant differentially expressed genes ($p \leq 0.05$) using PANTHER (Ashburner, Ball et al. 2000, Gene Ontology 2015) and GOrilla (Eden, Lipson et al. 2007, Eden, Navon et al. 2009).

2.2.8 Calcium Imaging and Analysis

Cultures were washed with PBS and the medium was replaced with Neurobasal plus Fluo4 AM (10μM, Life Technologies) for 30 minutes at 37° C. The cultures were then washed with fresh Neurobasal and allowed to recover for an additional 30 minutes at 37°C before recording on a Zeiss Axio Observer. To analyze wide field calcium videos, soma were identified from phase images and selected as regions of interest (ROI) in the corresponding fluorescent green channel. To assess calcium fluctuations, mean fluorescence intensity for each ROI was measured over time at a sampling rate of 2.38 frames per second using MATLAB (MathWorks, Natick, MA) to assess calcium fluctuations within the ROIs. To minimize noise, the median of all the traces was calculated and subtracted from each. A minimum of 20 ROIs were examined for each field of view.

2.2.9 Electrophysiological Testing

Neurons (days 27, 41, 63) were recorded in the whole-cell configuration using glass pipette electrodes filled with the internal solution ((mM): 100 K-gluconate, 20 KCl, 10 HEPES, 4 Mg-ATP, 0.3 Na-GTP, 10 Na-phosphocreatine, and 0.2% biocytin; osmolality 300 mOsm), while being perfused with warm artificial cerebrospinal fluid ((mM): 126 NaCl, 26 $NaHCO_3$, 3.0 KCl, 1.25 NaH_2PO_4, 2.0 $CaCl_2$, 2 $MgCl_2$, and 20 dextrose; osmolality 320 mOsm, T = 33ºC; bubbled with 95% O_2 + 5% CO_2 mixture, pH = 7.3–7.35). Resting membrane potential was measured immediately after achieving the whole-cell configuration. Action potentials were elicited by injecting a 1.5s long depolarizing current of 20pA and measuring the voltage response in current clamp (baseline voltage was held between -60 and -70 mV by injecting a small, constant, negative current). Action potentials were analyzed using custom-written software in IgorPro (Wavemetrics, Portland, OR).

2.2.10 Spinal Transplantation

All animal studies were performed in accordance with the Institutional Animal Care and Use Committee at the University of California, San Francisco. Day 17 cultures were dissociated for 45 minutes using Accutase, washed with PBS, resuspended in ice-cold DMEM at ~$5x10^5$ cells/µL, and maintained on ice until transplantation. Female C57Bl/6j SCID mice age 12 weeks were anesthetized using isoflurane and a dorsal laminectomy was performed at T9 to expose the spinal cord. The vertebral column was stabilized, and the dissociated cells were injected at four sites bilaterally in the ventral horns of the spinal cord at the rostral and caudal edges of the laminectomy site (~1.25x10^5 cells/site). The musculature over the exposed spinal cord was sutured closed and the skin was closed with surgical clips. Antibiotics (enrofloxacin) were delivery daily (I.P., 2.5 mg/kg) for 10 days.

After 2 weeks, animals were euthanized and transcardially perfused with PBS followed by 4% paraformaldehyde. A 2-cm segment of spinal cord tissue centered over the transplantation site was harvested and post-fixed overnight in 4% paraformaldehyde.

2.2.11 Murine Tissue Processing and Immunofluorescence

Spinal cords were embedded and 20 μm sections were obtained in the sagittal plane. Sections were permeabilized with 0.3% Triton-X in PBS for 15 minutes or ice-cold acetone for 10 minutes. All sections were then blocked with 10% NDS, 5% bovine serum albumin, and 0.1% Triton-X in PBS. Sections were incubated with primary antibodies found in Table 2.2. Sections were washed three times and incubated with the appropriate secondary antibodies (1:500) in blocking solution for 1 hour, then mounted with coverslips using Prolong Gold Antifade containing DAPI. Z-stack images (1 μm step size) were acquired using a Zeiss Axio Observer inverted wide-field microscope and an Apotome structured light attachment. For high resolution imaging of synaptic markers, Z-stack imaged were acquired using a Zeiss LSM 880 confocal microscope with Airyscan. Maximum intensity projection was performed on Z-stack images to create a single two-dimensional image spanning the entire thickness of the section.

Gene Symbol	Gene Description	Lineage	Alias	Forward Primer Sequence	Reverse Primer Sequence
RPS18	Ribosomal Protein S18	Ribosomal protein	*18S*	CTTCCACAGGAGGCCTACAC	CTTCGGCCCACACCCTTAAT
CHX10	Ceh-10 Homeodomain-Containing Homolog	V2a interneurons	*VSX2*	CGGCGACACAGGACAATCTT	CCTGTATCCTGTCTTCCGGC
FOXN4	Forkhead Box N4	p2 domain		CGTACAGCTGTCTGATCGCC	GGAGCCGCTCATCTTGTTCT
GATA3	GATA Binding Protein 3	V2b interneurons		TTGTGCTCGGAGGGTTTCTT	CAGCACAGGCTGCAGGAATA
OLIG2	Oligodendrocyte Lineage Transcription Factor 2	Progenitor motor neurons		CGCATCCAGATTTTCGGGTC	AAAAGGTCATCGGGCTCTGG
HB9	Homeobox Protein HB9	Committed motor neurons	*MNX1*	TCTCTTAACGGGAAGGGGCA	CTAATTCAGGGCGCTCTCGG
PAX6	Paired Box 6	Early neural		GAGCGAGCGGTGCATTTG	TCAGATTCCTATGCTGATTGGTGAT
TUBB3	Beta 3 Class III Tubulin	Immature neurons		GAACCCCAGGCAGCTAGAC	ACTGATGACTTCCCAGAACTGT
POU5F1	POU Class 5 Homeobox 1	Pluripotency	*OCT4*	ATGCATTCAAACTGAGGTGCCT	AACTTCACCTTCCCTCCAACCA
NES	Nestin	Early neural		CCACCCTGCAAAGGGAATCT	GGTGAGCTTGGGCACAAAAG
SOX14	SRY (Sex Determining Region Y)-Box 14	V2a interneurons		GAACCCTTGCACTCCCTACC	TCGATGTATGGCCGCTTCTC
SIM1	Single-Minded Family BHLH Transcription Factor 1	V3 interneurons		GGCTCTCACCGGCAGTATTT	TGAGCCATTACAGCCCAAGG
RBFOX3	Hexaribonucleotide Binding Protein 3 Neuronal Nuclei (NeuN)	Neuronal Nuclei		ACGATCGTAGAGGGACGGAA	AATTCAGGCCCGTAGACTGC
NEFL	Neurofilament (NF) Light Chain	Neurons		CATCAGCGCTATGCAGGACA	GTCTCCTCGCCTTCCAAGAG
PDGF-RA	Platelet-derived growth factor receptor, alpha peptide	Progenitor oligodendrocyte		CTGGACACTGGGAGATTCGG	CACGGCCTCCAATGATCTCT
CSPG4	Chondroitin Sulfate Proteoglycan 4	Progenitor oligodendrocyte		CACTCAGGACGAAGGAACCC	GGAGCAATACGGTACCCTGG
SOX10	SRY (Sex Determining Region Y)-Box 10	oligodendrocyte precursor		CACAAGAAAGACCACCCGGA	AAGTGGGCGCTCTTGTAGTG
GFAP	Glial Fibrillary Acidic Protein	Astrocytes		CAGTTATCAGGAGGCGCTGG	TTTGCCCCCTCGAATCTGC
THY1	Thy-1 Cell Surface Antigen	Retina		TGGATTAAGGATGAGGCCCG	TGGGGAGGTGCAGTCTGTAT
IRBP	Interphotoreceptor Retinoid-Binding Protein	Retina and photo receptor cells	*RBP3*	TATCTACAACCGCCCCTCCA	CTGGTGAGGACCACCACATC
CRX	Cone-Rod Homeobox	Retina		CCTTCTGACAGCTCGGTGTT	TGGTGTACTTCAGCGGTCAC

Table 2.1: Primer sequences for real-time quantitative PCR analysis

Antibody Target	Species	Vendor	Cat. Number	Dilution
CHX10	Mouse	Santa Cruz Biotechnology	sc-374151	1:1000
CHX10	Sheep	Abcam	ab16141	1:500
β_{III} Tubulin	Rabbit	BioLegend	MRB-435P	1:1000
Vesicular Glutamate Transporter 2 (VGlut 2)	Rabbit	Synaptic Systems	135 403	1:500
Neurofilament (NF)	Mouse	Developmental hybridoma studies bank	2H3	1:20
Neurofilament 200	Rabbit	Sigma-Aldrich	N4142	1:200
LHX3 (LIM3)	Mouse	Developmental hybridoma studies bank	67.4E12	1:500
OLIG2	Rabbit	Millipore (EMD)	AB9610	1:500
HB9	Mouse	Developmental hybridoma studies bank	81.5C10	1:20
Stem 121	Mouse	Clontech	Y40410	1:500
Human Nuclear Antigen	Mouse	Millipore (EMD)	MAB1281	1:200
GRP1	Rabbit	Abcam	ab25963	1:200
GABA	Rabbit	Sigma-Aldrich	A2052	1:2000
NeuN	Chicken	Millipore (EMD)	abN91	1:500
Oct-3/4	Goat	Santa Cruz Biotechnology	sc-8629	1:100
Ms isotype	Mouse	R&D Systems	MAB002	
NeuN	Rabbit	Millipore (EMD)	ABN91	1:1000
Synaptophysin	Rabbit	Synaptic Systems	101 002	1:200
HOMER	Rabbit	GeneTex	GTX103278	1:100

Table 2.2: Antibodies used for flow cytometry and immunostaining

2.2.12 Image Quantification

Quantification of *in vitro* maturation images was performed by rendering a 3D surface to define the regions positive for NF and β_{III} tubulin using Imaris 8.4 (Bitplane, Belfast, United Kingdom). Data was normalized by observed field area. For CHX10 counts, ImarisColoc was used to identify overlap of $CHX10^+$ cells with $Hoechst^+$ cells. A 3D surface to define the regions of overlap was created to quantify the number of $CHX10^+Hoechst^+$ cells as well as total $Hoechst^+$ cells. Quantification of transplanted V2a interneuron populations was performed by manual counting of 10 evenly spaced sagittal sections spanning the width of the spinal cord in Image J using the Cell Counter plugin.

2.2.13 Cryopreservation

To freeze the human V2a interneuron cultures, cells were dissociated in Accutase and centrifuged. The neurons were then resuspended at a concentration of one 24-well to one cryovial in 1 ml of a 5:4:1 mixture of neural induction media:fetal bovine serum (FSB):dimethyl sulfoxide (DMSO) solution. Cryovials were put into a Mr. Frosty and placed at -80°C overnight. The cryovials were then moved to the liquid nitrogen for long-term storage. To thaw, one vial was recovered in 4 ml neural induction medium supplemented with 10μM ROCK inhibitor and centrifuged. The cell pellet with resuspended in neural induction medium supplemented with 10μM ROCK inhibitor and seeded onto one well of a 24-well plate. V2a interneurons were then cultured for 3 days in neural induction medium before use.

2.2.14 Statistical Analysis

Statistical analysis was performed using Prism 6 software. The mean and ± standard deviation were calculated for a minimum of three biological replicates for all data unless otherwise noted. Unpaired t-tests were performed when comparing two groups. One-way analysis of variance (ANOVA) followed by appropriate post hoc pairwise comparisons Tukey's tests were used when three or more groups were specified. Specific statistical analysis is mentioned within the corresponding figure legend. Variances were confirmed to not differ significantly with the Brown-Forsythe test. In all comparisons, significance was defined as $p \leq 0.05$ (denoted as *).

2.3 Results

2.3.1 Induction of V2a Interneurons is Dependent on RA, Shh, and Inhibition of Notch

Motor neurons, which arise ventral to V2a interneurons, have been differentiated from hPSCs in ~3 weeks with dual SMAD inhibition followed by RA and Shh agonists (Amoroso, Croft et al. 2013). Thus, using a similar time course, the concentrations of known morphogens and signaling pathways that specify V2a commitment (RA, Shh, and Notch inhibitor, DAPT) in mouse embryonic stem cells (ESCs) (Brown, Butts et al. 2014, Iyer, Huettner et al. 2016) were sequentially varied independently, and the percentages of $CHX10^{+}$ cells differentiated from hPSCs at day 17 were examined (Fig 2.1 B). An RA concentration of 100nM starting at day 5 of culture with fixed concentrations of the Shh agonist, purmorphamine, (pur, 1μM) and DAPT (5μM) (both beginning on day 7) resulted

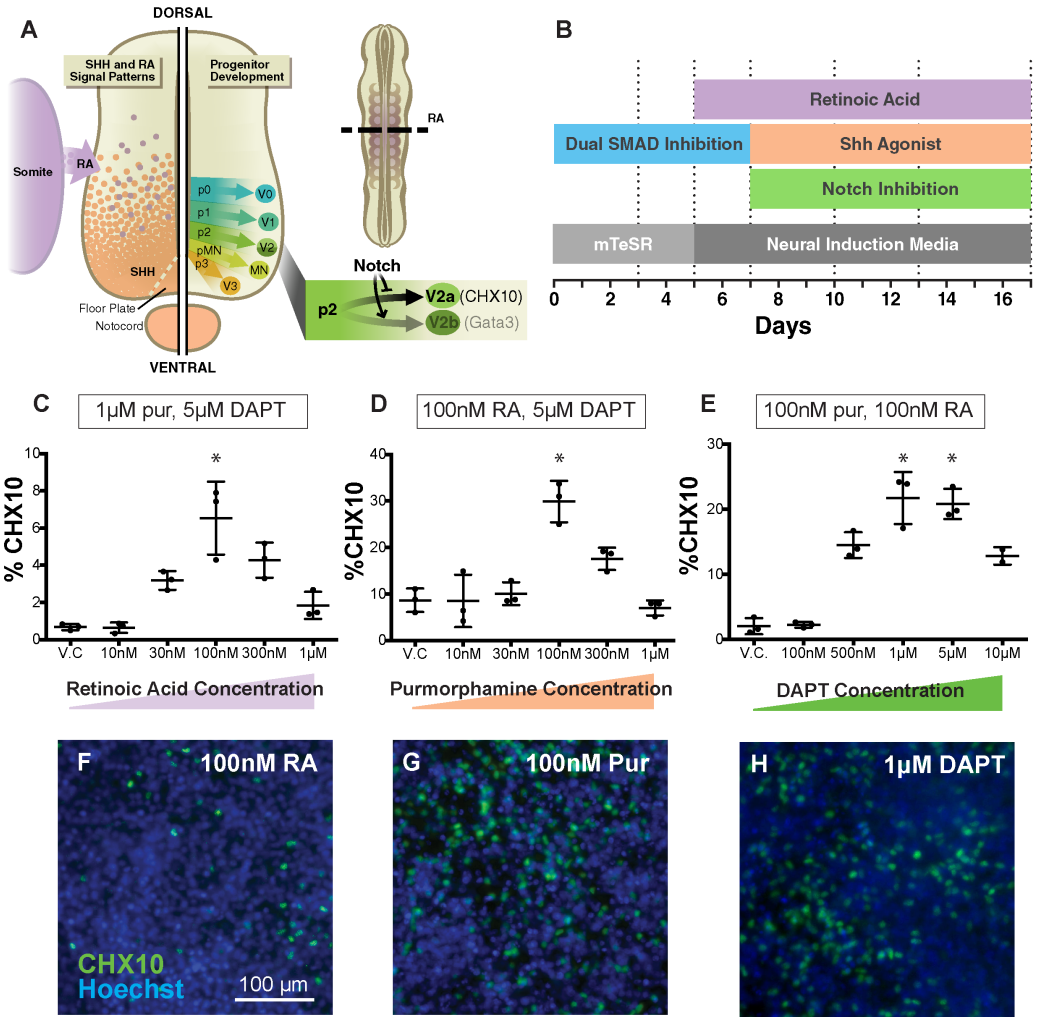

Figure 2.1: Morphogen concentrations modulate V2a interneuron population. *(A)* Schematic of the developing neural tube. Retinoic Acid (RA), released from the somites, and sonic hedgehog (Shh), released from the floorplate and notochord, pattern the different progenitor domains of the neural tube. Notch signaling is necessary for generating V2b interneurons, while Notch inhibition promotes V2a interneuron differentiation. *(B)* Timeline of V2a interneuron protocol. *(C)* Flow cytometry analysis of CHX10 expression as RA concentration was varied and Shh agonist, purmorphamine (pur), and DAPT were held constant. CHX10 expression using 100nM RA was greater ($p<0.05$, one-way ANOVA and Tukey post hoc comparison) than V.C, 10nM, 30nM, and 1 μ M groups. *(D)* Flow cytometry analysis of CHX10 expression as pur concentration was varied and RA and DAPT were held constant. CHX10 expression using 100nM pur was greater ($p<0.05$, one-way ANOVA and Tukey post hoc comparison) than all groups. *(E)* Flow cytometry of CHX10 expression as DAPT concentration was varied and RA and pur were held constant. CHX10 expression using 1 μ M and 5 μ M DAPT was more ($p<0.05$, one-way ANOVA and Tukey post hoc comparison) than V.C, 100nM, and 500nM groups. *(F-H)* Immunostaining for CHX10 (green) and nuclei labeling (blue) of differentiations with 100nM RA *(F)*, 100nM pur *(G)*, or 1μM DAPT *(H)*. Scale bar = 100μm, n = 3, data represented as mean ± standard deviation.

in the greatest CHX10$^+$ population at day 17 (~6%, Fig 2.1 C). Following that, treatment with 100nM pur beginning at day 7 with 100nM RA and 5μM DAPT resulted in ~30% CHX10$^+$ cells after 17 days of differentiation (Fig 2.1 D). Finally, the concentration of DAPT was varied beginning on day 7 with fixed RA and pur concentrations (100nM each) and 1μM and 5μM DAPT resulted in comparable CHX10$^+$ populations (~20%; Fig 2.1 E). Regardless of morphogen concentrations, CHX10$^+$ cells appeared to be evenly distributed throughout the differentiating cultures (Fig 2.1 F-H).

Since DAPT concentrations of 1μM and 5μM yielded similar efficiencies of V2a interneuron differentiation (Fig 2.2 A), the effects of these concentrations on the efficiency of CHX10$^+$ differentiation were examined. Since higher concentrations of small molecule inhibitors, such as DAPT, are often more cytotoxic (Lian, Zhang et al. 2013), the total number of cells and yield of CHX10$^+$ cells per input number of PSCs was examined. A lower DAPT concentration (1μM) yielded more viable cells than cultures treated with 5μM DAPT (4.40 million cells vs. 2.85 million cells per well of 24-well plate, Fig 2.2 B), resulting in a ~50% increase in the number of CHX10$^+$ cells per input PSC (Fig 2.2 C). Varying the onset of Notch inhibition by initiating DAPT treatment on day 5, 7, or 10 of differentiation (Fig 2.2 D) yielded similar percentages of CHX10$^+$ cells, so DAPT was added at day 7 for all subsequent studies, coinciding with the introduction of pur. In addition, with the H7 hESC cell line, a seeding density of 25,000 cells per cm^2 resulted in a greater percentage of CHX10$^+$ cells than 5,000 or 100,000 cells per cm^2 (Fig 2.2 E). Overall, these results demonstrate the ability of hPSCs to robustly differentiate into putative V2a interneurons by RA and Shh agonists in combination with Notch inhibition.

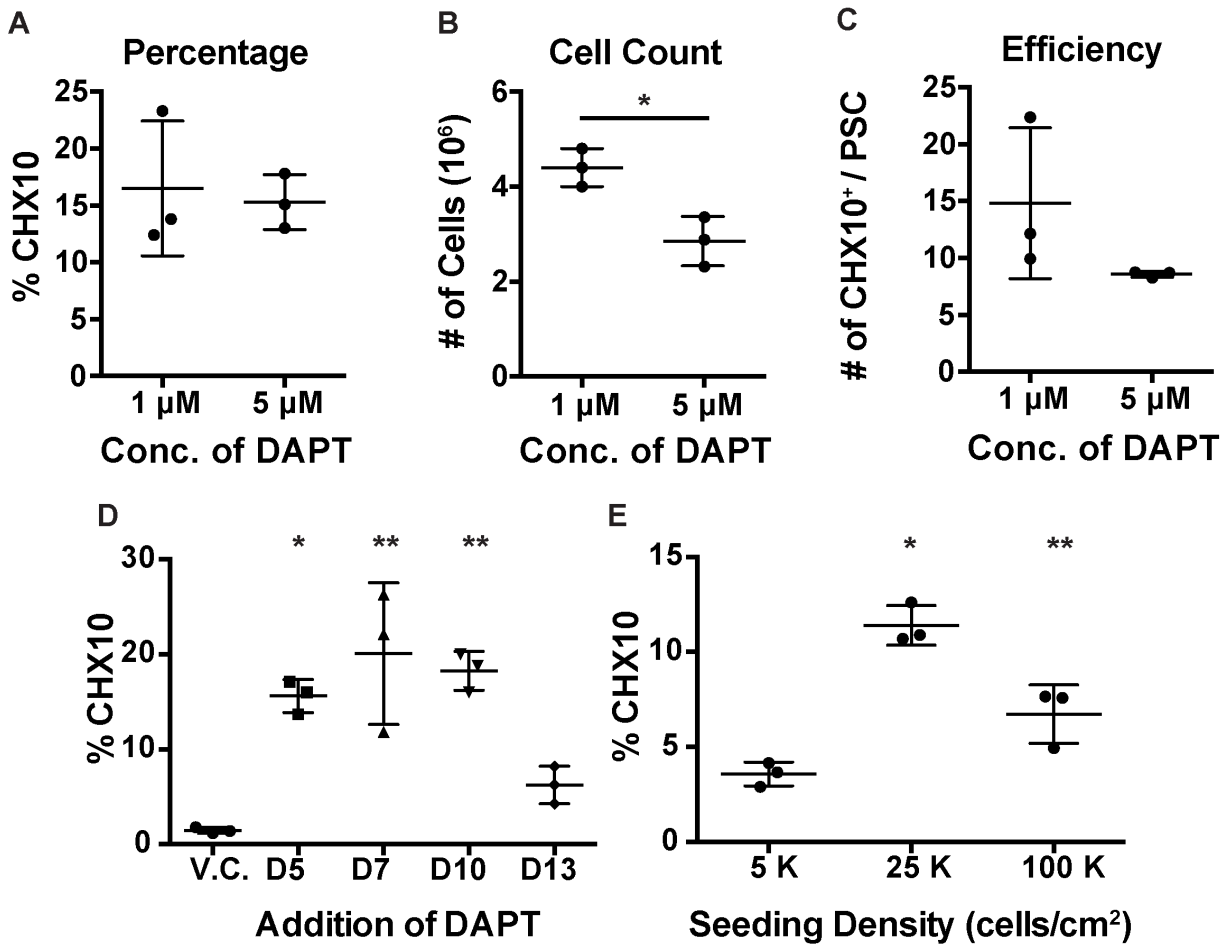

Figure 2.2: DAPT concentration effects V2a interneuron yield. *(A)* Flow cytometry analysis of CHX10 expression at Day 17 with 1μM and 5μM of DAPT. *(B)* Total number of cells per 24-well culture at day 17 of V2a interneuron differentiation with 1μM and 5μM DAPT (using 100nM RA and 100nM pur) is significantly different ($p<0.05$, unpaired t-test). *(C)* Total number of $CHX10^+$ cells at day 17 per input pluripotent stem cell. *(D)* Flow cytometry analysis of CHX10 at day 17 when DAPT was added on day 5, day 7, day 10, day 13, or vehicle control (V.C., DMSO). CHX10 expression adding DAPT on day 5 was significantly different (* = $p<0.05$, one-way ANVOA and Tukey post hoc comparison) than V.C. CHX10 expression adding DAPT on day 7 and day 10 was significantly different (** = $p<0.05$, one-way ANVOA and Tukey post hoc comparison) than V.C. and day 13. *(E)* Flow cytometry analysis of CHX10 at day 17 using three different initial seeding densities. CHX10 expression at a seeding density of 25k was significantly different (* = $p<0.05$, one-way ANVOA and Tukey post hoc comparison) compared to 5k and 100k. CHX10 expression at a seeding density of 100k was significantly different (** = $p<0.05$, one-way ANVOA and Tukey post hoc comparison) compared to 5k. Data represented as mean ± standard deviation.

To determine the reproducibility of V2a interneuron differentiation, the resulting protocol (i.e., 100nM RA, 100nM pur, and 1μM DAPT) was tested on several additional hPSC lines (H1 ESCs, WTC iPSCs, and WTB iPSCs). CHX10⁺ populations were robustly obtained in all of the lines examined, with efficiencies ranging from ~25%–50% (Fig 2.3 A). Expression of spinal neuronal markers was examined at day 17 for each of the hPSC cell lines, and *CHX10* levels were consistently high, whereas markers for early neural tube development (*PAX6*) and other neuronal subtypes (*HB9,* and *GATA3*) were low (Fig 2.3 B). No discernible spatial patterns were observed for CHX10⁺ cells in any of the differentiating cultures (Fig 2.3 C). These data demonstrate the establishment of a robust neuronal differentiation process that reproducibly yields enriched cultures of V2a interneurons from hPSCs.

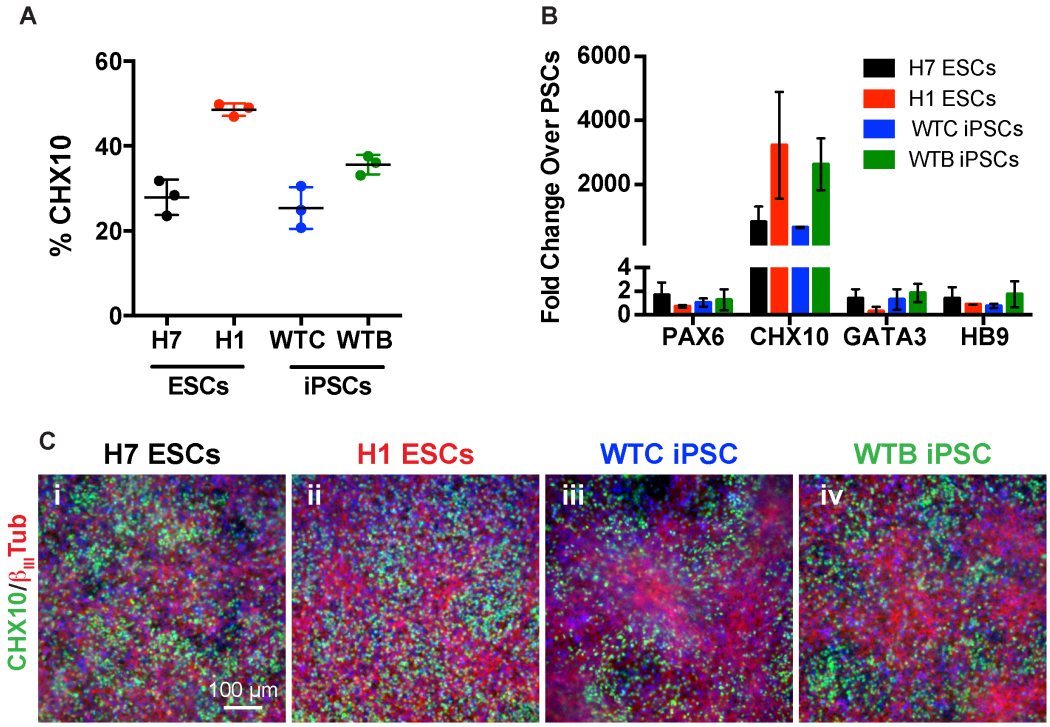

Figure 2.3: The V2a interneuron differentiation is reproducible in multiple cell lines. *(A)* CHX10 percentage of ESCs (H7, H1) and iPSCs (WTB and WTC) differentiated with the V2a interneuron protocol. *(B)* Gene expression at day 17 compared to PSCs. Data represented as mean ± standard deviation. *($C_{i\text{-}iv}$)* Immunostaining for CHX10 (green), β_{III} tubulin (red), and labeled nuclei (blue) of hPSCs differentiated using the V2a interneuron protocol. Scale bar is 100μm.

2.3.2 Differentiation of V2a Interneurons is Specific

Gene expression was analyzed throughout the first 17 days of differentiation to characterize the temporal changes of the V2a interneuron cell population (Fig 2.4 A). As expected, expression of the pluripotency gene *POU5F1* decreased by day 3 and remained significantly down-regulated through day 17. Early markers expressed during neural tube development increased by day 7 (*PAX6* and *NES*). Other markers of spinal cell types expressed in the ventral neural tube (*GATA3, OLIG2, HB9,* and *SIM1*) were detected as early as day 3, and continued to increase throughout differentiation. Expression of markers for the p2 domain (*FOXN4*) and committed V2a interneurons (*CHX10* and *SOX14*) began on day 10 and were highly upregulated by day 15. Expression of neuronal genes (*TUBB3*, *NEFL*) was significantly upregulated (~10- and ~70-fold respectively) whereas glial (*PDGFRA*, *CSPG4*, *SOX10*, and *GFAP*) and retinal (*THY1*, *IRBP,* and *CRX*) genes were not at day 17 (Fig 2.4 B). Altogether these results demonstrate that the observed gene expression profile of the population is consistent with the expected phenotype of V2a interneurons.

The specificity of the V2a interneuron protocol was examined by direct comparison to a common human motor neuron protocol ((Amoroso, Croft et al. 2013), Fig 2.5 A). After 17 days of differentiation, the V2a interneuron differentiation yielded ~30% $CHX10^+$ cells whereas the motor neuron differentiation yielded very few $CHX10^+$ cells (<1%, Fig 2.5 B). $CHX10^+$ nuclei and β_{III} tubulin expression were more abundant using the V2a interneuron differentiation protocol than the motor neuron conditions (Fig 2.5 $C_{i\text{-}ii}$). In addition, more $OLIG2^+$ (progenitor motor neuron marker) nuclei were yielded by the motor neuron differentiation conditions than the V2a interneuron protocol (Fig 2.5 $C_{iii\text{-}iv}$). Although, expression of neuronal genes (*NEFL*, *TUBB3*, and *PAX6*) was slightly elevated with the V2a

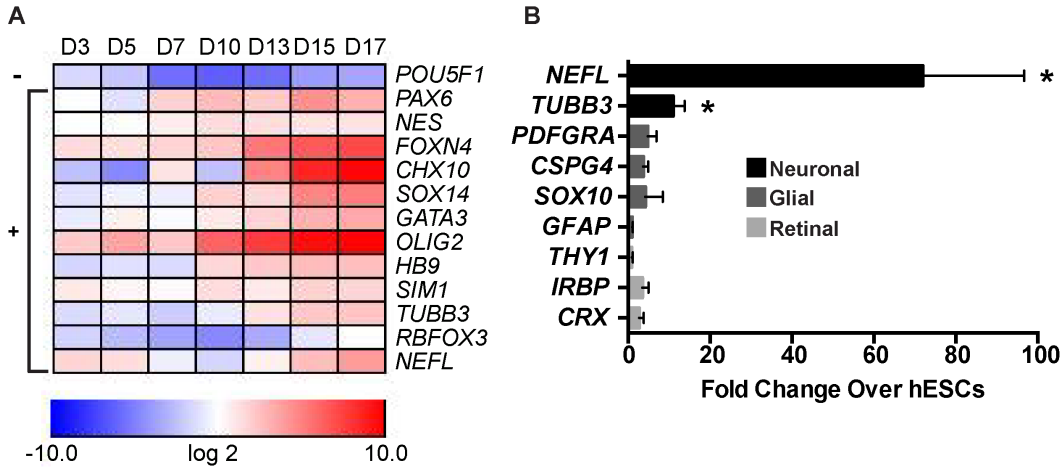

Figure 2.4: V2a interneuron protocol robustly increases hPSC neurogenesis. *(A)* Gene expression throughout V2a interneuron differentiation compared to undifferentiated H7 hESCs. - denotes gene expression is significantly downregulated (slope coefficient negative and different from 0, $p < 0.05$ using linear time-trend model) through culture duration. + denotes gene expression is significantly upregulated (slope coefficient positive and different from 0, $p < 0.05$ using linear time-trend model) through culture duration. *(B)* Neuronal, glial, and retinal gene expression at day 17 compared to H7 hESCs. NEFL and TUBB3 expression was increased greater than 2-fold ($p<0.05$, unpaired t-test).

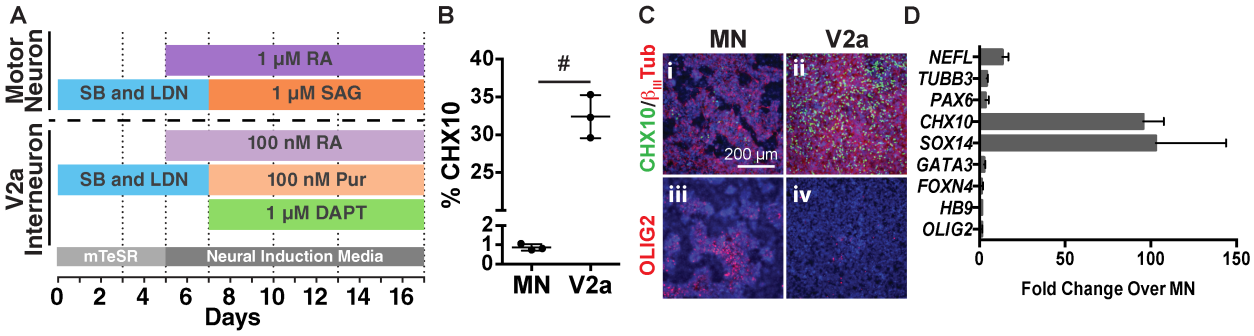

Figure 2.5: V2a interneuron protocol specifically increases V2a interneuron population. *(A)* Timeline contrasting the motor neuron and V2a interneuron differentiation protocols. *(B)* Flow cytometry analysis of CHX10 for motor neuron and V2a interneuron differentiation. CHX10 expression using the V2a interneuron differentiation was greater ($p<0.005$, by unpaired t-test) than motor neuron differentiation, n = 3. *(C)* Immunostaining for CHX10 (green) and nuclei (blue) *(C_{i-ii})* Immunostaining for β_{III} tubulin (red) in cultures differentiated with the motor neuron protocol (i) and V2a interneuron protocol (ii). *(C_{iii-iv})* Immunostaining for OLIG2 (red) in cultures differentiated with the motor neuron protocol (iii) and V2a interneuron protocol (iv). Scale bars = 200μm. *(D)* Gene expression of day 17 V2a interneuron cultures compared to day

interneuron differentiation, the V2a interneuron transcription factors (*CHX10* and *SOX14*) exhibited the greatest increase in expression (~100-fold) relative to motor neuron cultures. However, the expression of other lineage markers (*GATA3*, *FOXN4*, *OLIG2* and *HB9*) did not appear to differ between the two differentiation processes (Fig 2.5 D). Collectively, these results demonstrate that the V2a differentiation conditions specifically enrich for CHX10^{+} interneurons.

Single cell RNAseq analysis was performed to define the cellular composition of the heterogeneous cultures. Seven distinct clusters of cells (A-G) were identified by k-means clustering using 12 principal components (Fig 2.6 A) with 77% of *CHX10*$^{+}$ cells contained within cluster B (Fig 2.6 B). The top globally differentially expressed genes were used to distinguish the general phenotypes of the 7 clusters that defined the total population (Fig 2.6 C and Table 2.3). GO analysis and individual inspection of the top differentially expressed genes (Fig 2.7 – 2.9.) suggested that clusters A and B were committed neurons (*NEFM* and *NSG1*), cluster C was glial cells (*PLP1* and *TTHY1*), clusters D and E were neuron progenitors (*NEUROD1*), cluster F contained mitotically active neuronal cells (*FOXN4*, *PTTG1* and *UBE2C*), and cluster G consisted of mesenchymal/muscle cells (*TAGLN*, *COL1A1*, Fig 2.7 – 2.9). Overall, the single cell RNAseq data indicated that the vast majority of the culture was neuronal (~85%) at different stages of commitment (64% fully committed neurons, 15% neuronal progenitors, and 5% mitotic neuronal progenitors). Non-neuronal cells constituted the remaining fraction of differentiated cells (13% glial and 2% mesenchymal/muscle, Fig 2.10 A). Clusters A and B were the most closely related to one another (Fig 2.10 B), sharing many highly expressed genes (*GAP43* and *NEFM*) and GO terms (growth cone and axon). Cluster B, which contained the majority of the *CHX10*$^{+}$ cells,

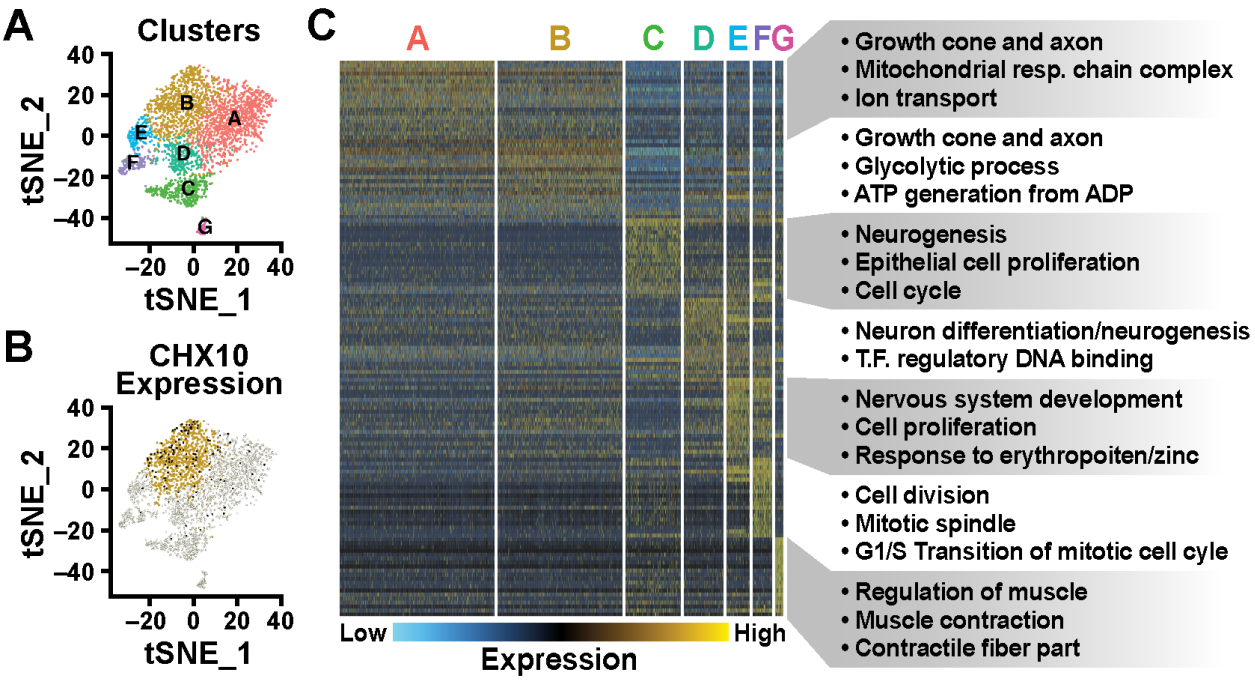

Figure 2.6: Single cell RNAseq of V2a interneuron cultures. *(A)* tSNE plot of V2a interneuron cultures indicating 7 clusters. *(B) CHX10* expression (black dots) overlaid on cluster B (gold dots). Open circles represent the rest of the population. *(C)* Heatmap of the top 20 globally differentially expressed genes for each cluster. Expression values are normalized for each individual gene with blue indicating low expression and yellow indicating high expression. GO terms for each cluster determined through global and pairwise comparisons.

	Cluster A	Cluster B	Cluster C	Cluster D	Cluster E	Cluster F	Cluster G
1	NEFL	CRABP2	VIM	C8orf46	HES6	UBE2C	TAGLN
2	NEFM	NRN1	FGFBP3	RGS16	MT1X	HMGB2	IGFBP3
3	STMN4	SNCG	ZFP36L1	GADD45G	CKB	MT2A	ACTA2
4	TUBB2B	STMN2	HES1	ARL4D	VSX1	HES6	ANXA1
5	PMEL	GNAS	MGST1	NEUROG1	MT2A	PTTG1	CTGF
6	GAP43	HOXB5	PLP1	HES6	GLRX	MT1X	NPPB
7	RTN1	PRR24	DLK1	TFDP2	NEUROG1	BIRC5	MYL9
8	MLLT11	CRABP1	TTYH1	GADD45A	CDH13	CCNA2	S100A11
9	TCEAL7	NEUROD1	SOX2	DLL3	PPP1R17	CCNB2	TPM1
10	GNG3	NSG1	ID3	PSTPIP1	ASCL1	NEK2	IGFBP5
11	RP11-834C11.4	PCP4	GPC3	MFNG	NEUROD1	CDC20	CALD1
12	AP1S2	HOTAIRM1	GSN	PHLDA1	DOK5	NUSAP1	CYR61
13	CLDN5	ISG15	GNG5	PRDX1	RASD1	TUBB4B	HSPB1
14	TSPAN7	COTL1	ARL4A	BTG1	FAM162A	PBK	SPARC
15	UCHL1	GLRX	NPC2	ELAVL4	B2M	CDKN3	ANXA2
16	CPE	DUSP1	MAD2L1	VIM	STC1	CCNB1	TNFRSF12A
17	SCG5	GNG3	HMGB2	RASD1	DLL3	CDK1	MYL12A
18	TM2D3	DANCR	SMS	ARL4A	PPP1R14C	CCNA1	LGALS1
19	HERPUD1	FOS	MEST	SH3BGRL3	GADD45G	VSX1	B2M
20	KLHL35		PTTG1	SOX2	BID	GPC3	C8orf4

Table 2.3: Top differentially expressed genes for each cluster from heatmap

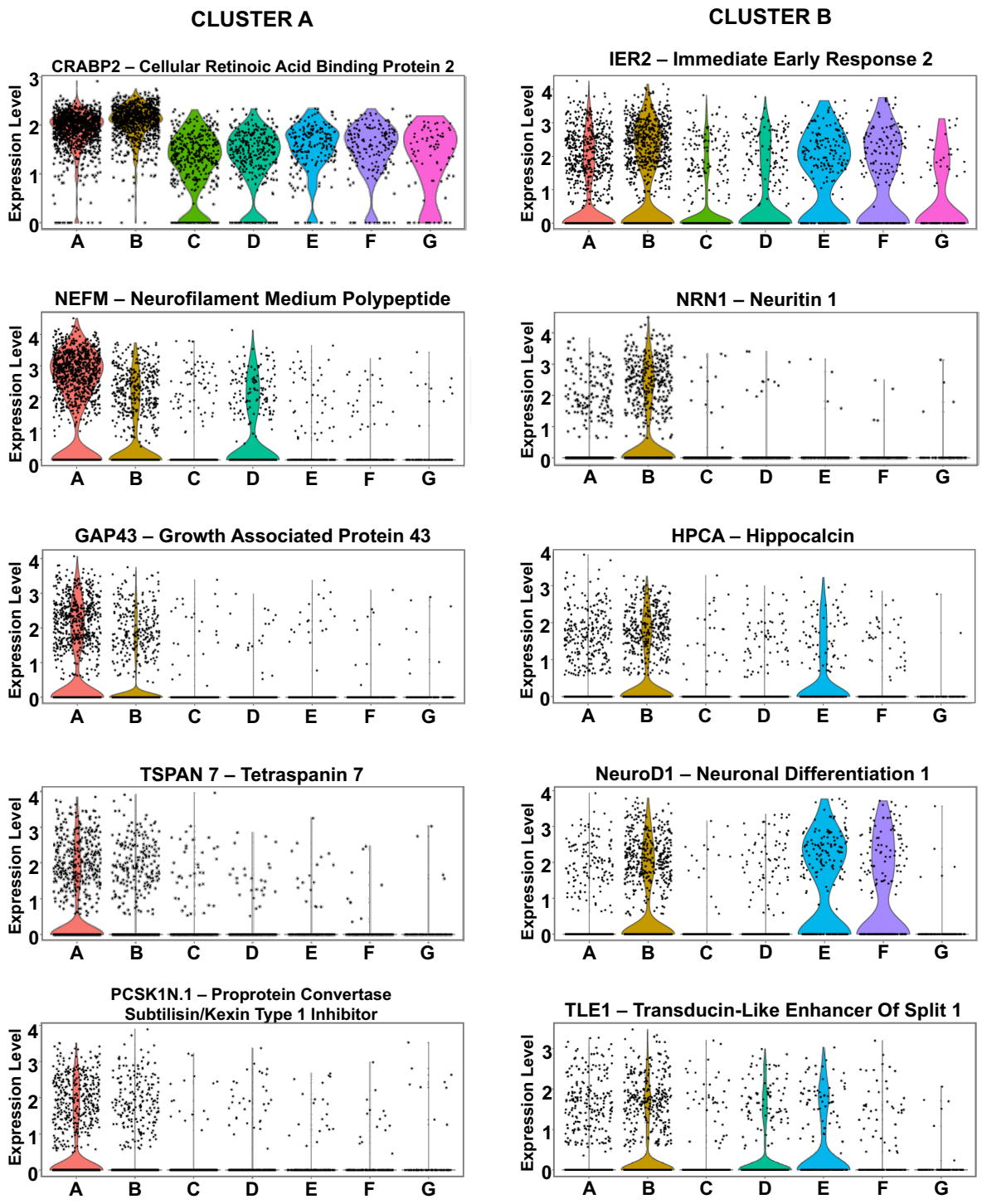

Figure 2.7: Select violin plots of genes that identify cluster A and cluster B. Representative genes for cluster A and B chosen from the top 50 differentially expressed genes from the A:B pair-wise comparison.

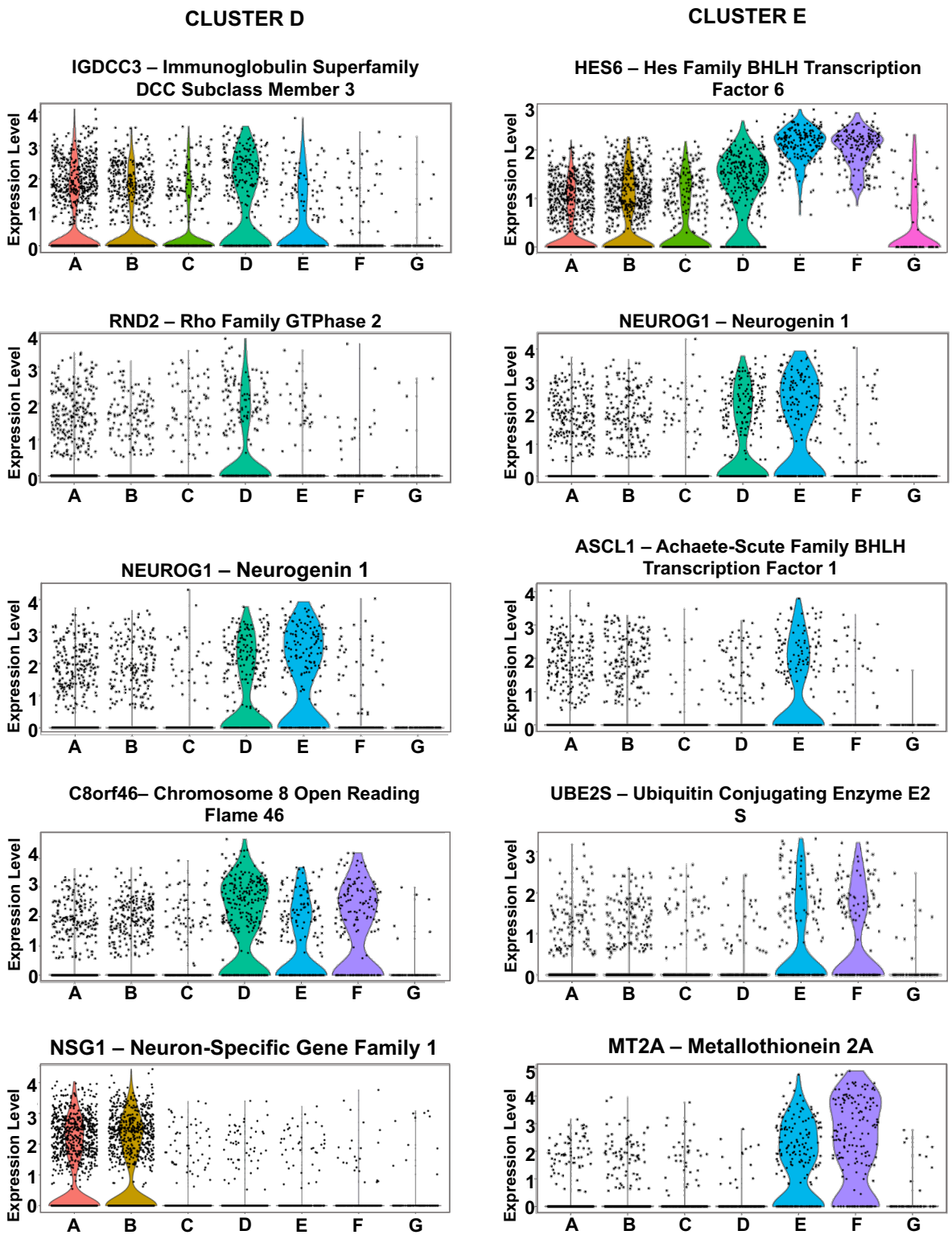

Figure 2.8: Select violin plots of genes that identify cluster D and cluster E. Representative genes for cluster D and E chosen from the top 50 differentially expressed genes from the D:B and E:B pair-wise comparison, respectively.

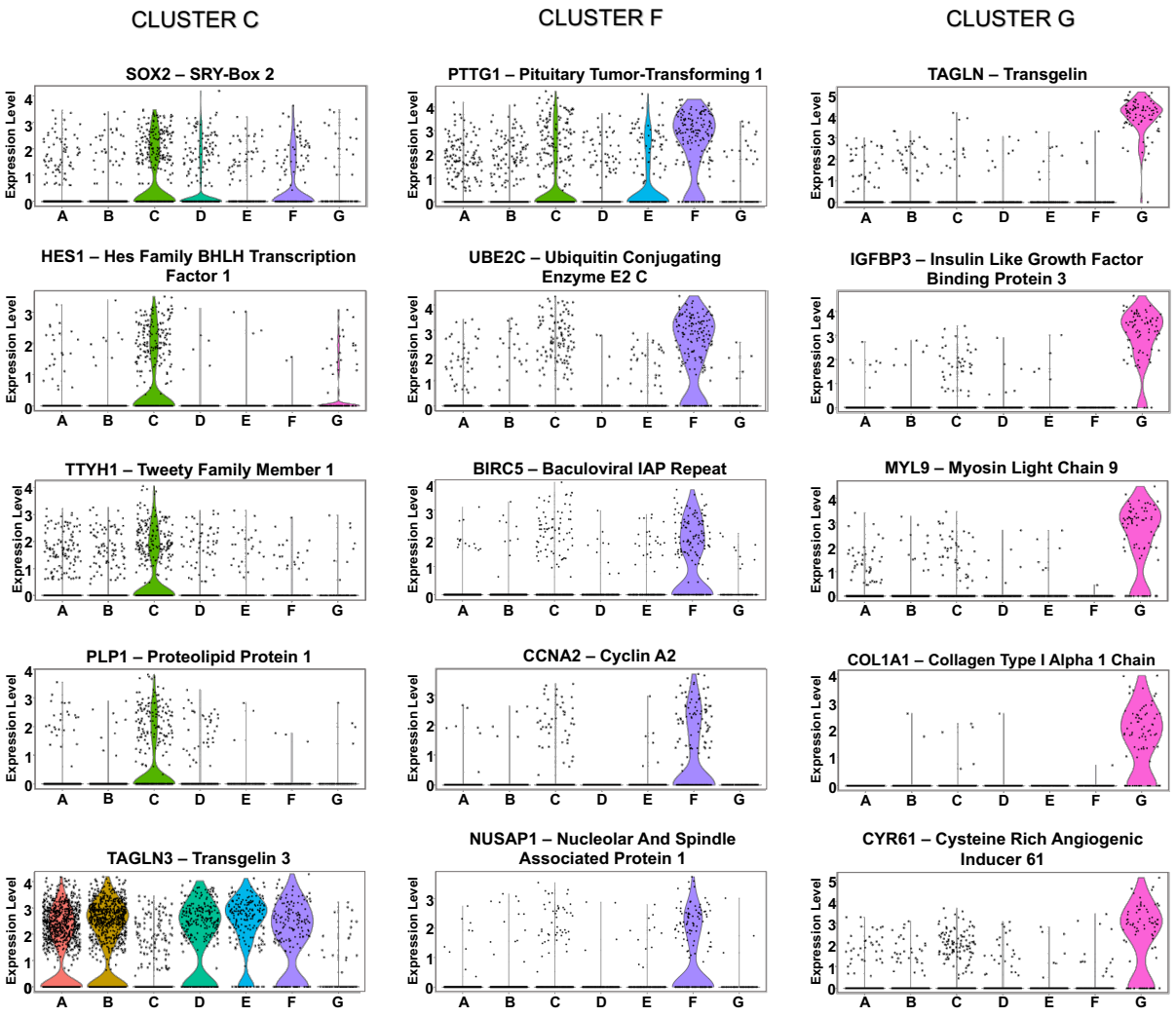

Figure 2.9: Select violin plots of genes that identify cluster C, cluster F and, cluster G. Representative genes for cluster C, F, and G chosen from the top 50 differentially expressed genes from the C:B, F:B, and G:B pair-wise comparison, respectively.

was comprised of cells that expressed a number of genes consistent with an excitatory V2a interneuron phenotype such as *SOX21*, *SHOX2*, *LHX3*, and *OAT,* as well as *HOX* genes consistent with a hindbrain/cervical identity *(HOXB5)* (Fig 2.11). Clusters D and E were both identified as early neurons (*NEUROG1),* however, cells in cluster D exhibited a more committed neuron phenotype (*RND2* and *IGDCC3)* compared to cells in cluster E (*UBE2S* and *MT2A*) (Fig 2.8). Further, 80% of cells expressing the p2 marker, *FOXN4,* were contained within the mitotically active cluster F (Fig 2.11). Altogether, these data collectively suggest that the V2a differentiation cultures (at day 17) yield primarily post-mitotic excitatory neurons (clusters A and B) that arise from a pool of neuronal progenitors (cluster D and E) and mitotic cells (cluster F) (Fig 2.10 C) and contain an enriched population of cells expressing markers consistent with a V2a interneuron phenotype.

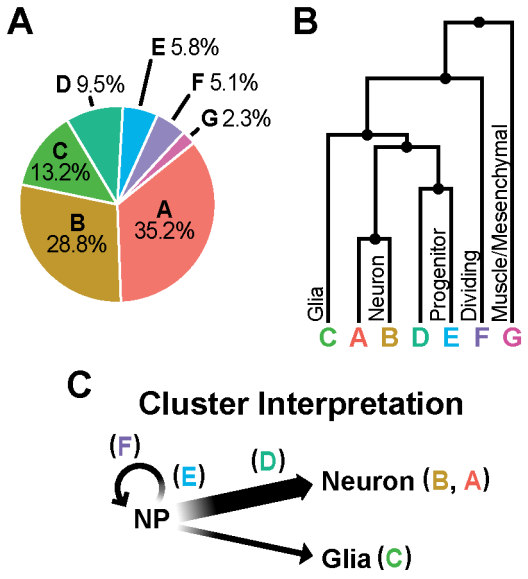

Figure 2.10 Cluster interpretation of Single cell RNAseq of V2a interneuron cultures. *(A)* Percentage of cells found in each cluster. *(B)* Dendrogram of the relationship between clusters. *(C)* Interpretation of the different cell types comprising V2a interneuron cultures based on cluster analysis.

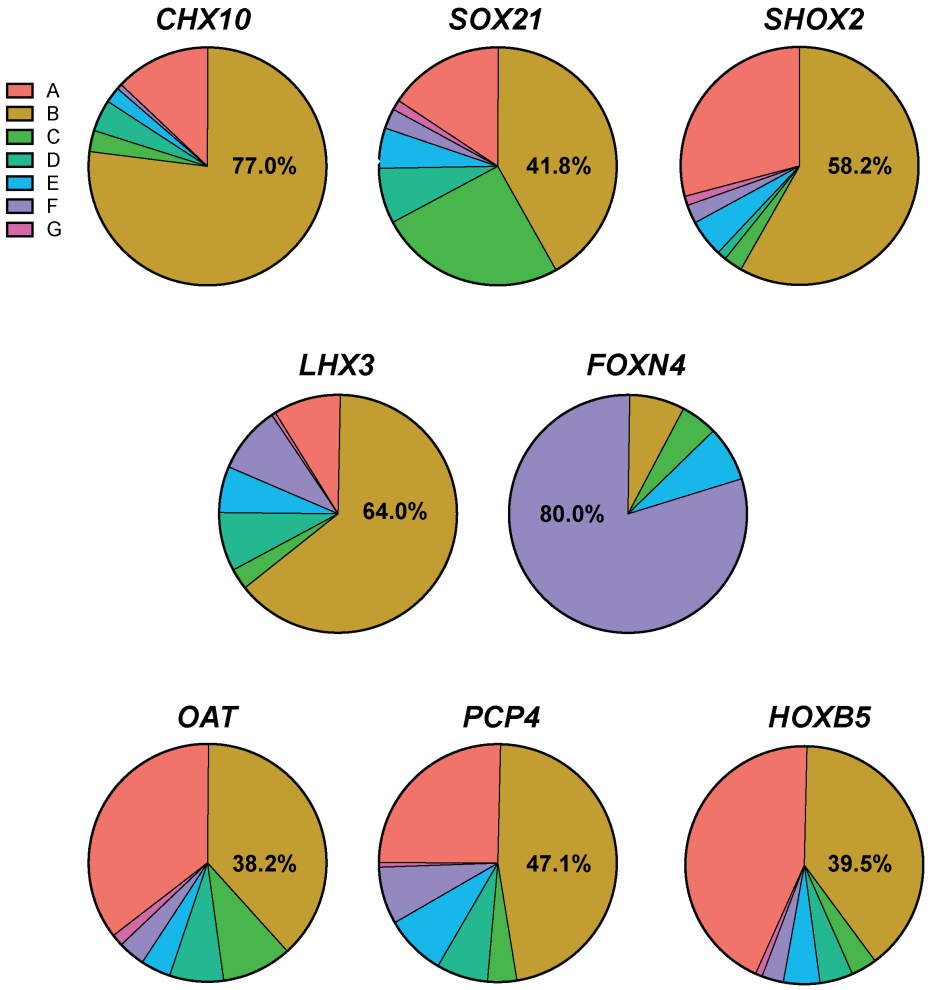

Figure 2.11: V2a interneuron genes and cluster identity. Each pie chart reports the number of cells with at least one read for the gene and its cluster identity. The percentage of cells found within cluster B is labeled on the chart for all genes except FOXN4, which labels the percentage of cells found in cluster F

2.3.3 Long-term Culture Increases the Maturation Profile of V2a Interneurons

To examine the maturation of V2a interneurons, differentiated cultures were dissociated after 17 days, re-plated, and analyzed on days 20, 30, 40, 50 and 60 of culture (Fig 2.12 A). By day 20, CHX10$^+$ cells expressed neuronal markers β_{III} tubulin (β_{III}Tub) and neurofilament (NF) and expression persisted throughout 60 days of culture (Fig 2.12 B-K and Fig 2.13 A-B). Some neuronal nuclei (NeuN) colocalized with CHX10$^+$ cells and NeuN expression continued through day 60 (Fig 2.12 L-P). Vesicular glutamate transporter 2 (VGlut2), a marker of glutamatergic neurons, was not detected early (Day 20, Fig 2.12 Q), but was abundant in later-stage cultures (day 60), indicating the adoption of a mature glutamatergic fate (Fig 2.12 Q-Y). Although many CHX10$^+$ nuclei were readily apparent initially (day 20, Fig 2.12 B), identification of CHX10$^+$ cells declined over time due to reduced expression as well as an increase in the total number of cells in the cultures (Fig 2.13 C-D). Altogether, the temporal phenotypic expression patterns support the progressive, albeit limited, maturation *in vitro* of the V2a interneuron cultures.

Calcium imaging was used to detect spontaneous electrical activity during extended culture as a functional indication of neuronal maturation. At different time points, individual soma of cells loaded with Fluo4 were visually identified (white arrows, Fig 2.14 A-B) and the average change in calcium transients was measured over time. Although calcium spikes were not observed initially (day 20), they were observed more often in older cultures (day 40), with increasing amplitudes and frequency (Fig 2.14 C). Whole-cell patch-clamp recordings of individual cells were used to assess electrophysiological properties of the differentiation over time. Although the resting membrane potential did not significantly change throughout culture duration (~ -40mV) (Fig 2.14 E), the action

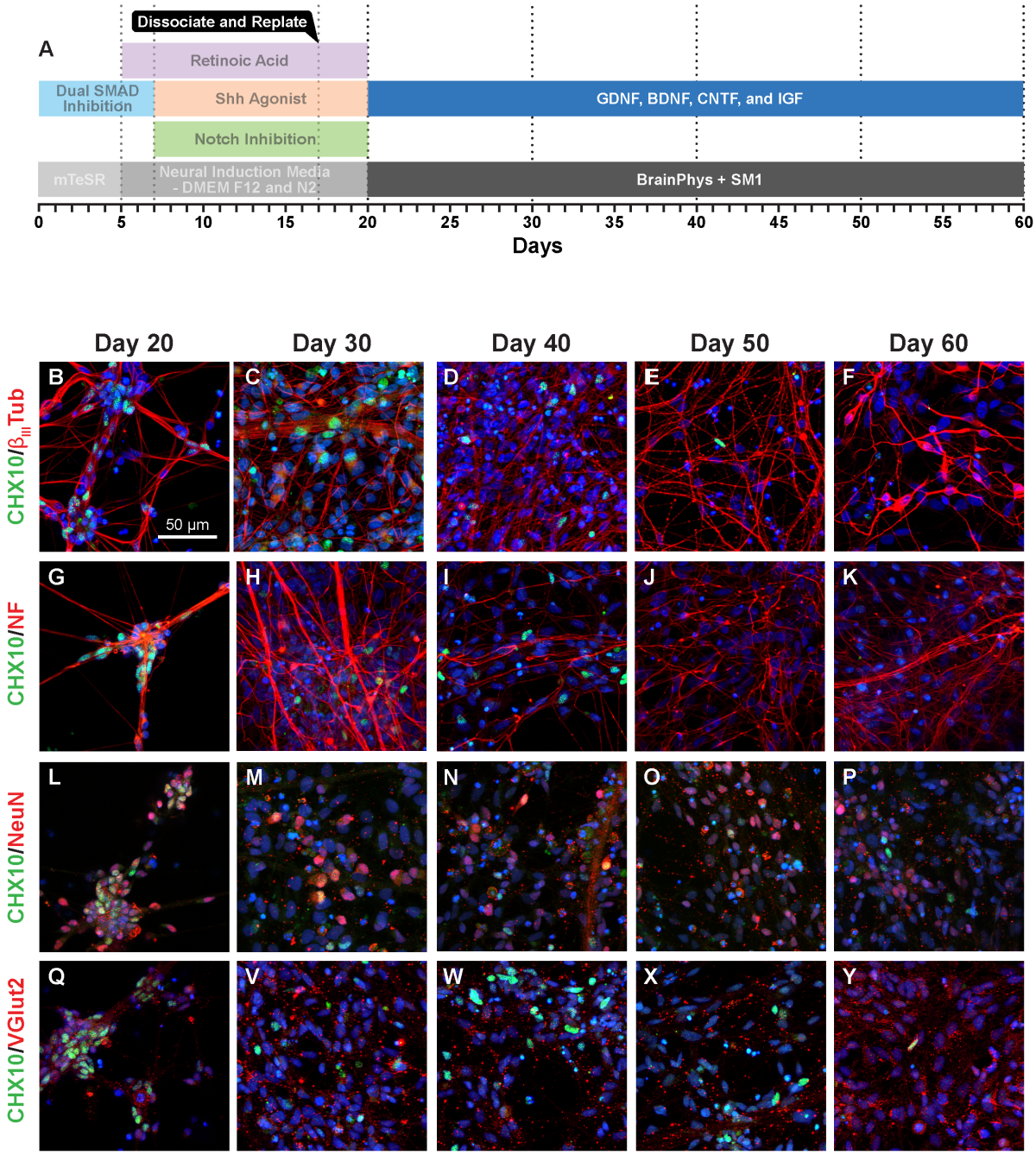

Figure 2.12: V2a interneuron maturation *in vitro.* *(A)* Timeline of V2a interneuron maturation cultures. *(B-Y)* Immunostaining for CHX10 (green) and nuclei labeling (blue) of V2a interneurons on day 20, 30, 40, 50 and 60 of culture. *(B-F)* Immunostaining for β_{III} tubulin (red). *(G-K)* Immunostaining for neurofilament (NF, red). *(L-P)* Immunostaining for NeuN (red). *(Q-Y)* Immunostaining of vesicular glutamate transporter 2 (VGLUT2, red). Scale bar = 50µm.

potential frequency of V2a cultures increased over time in response to current stimulation (20 pA, 1.5 s; Fig 2.14 E_{ii}). Consistent with the observed phenotypic expression patterns, the electrophysiological properties of the differentiated cells suggest some maturation of V2a interneuron cultures over time.

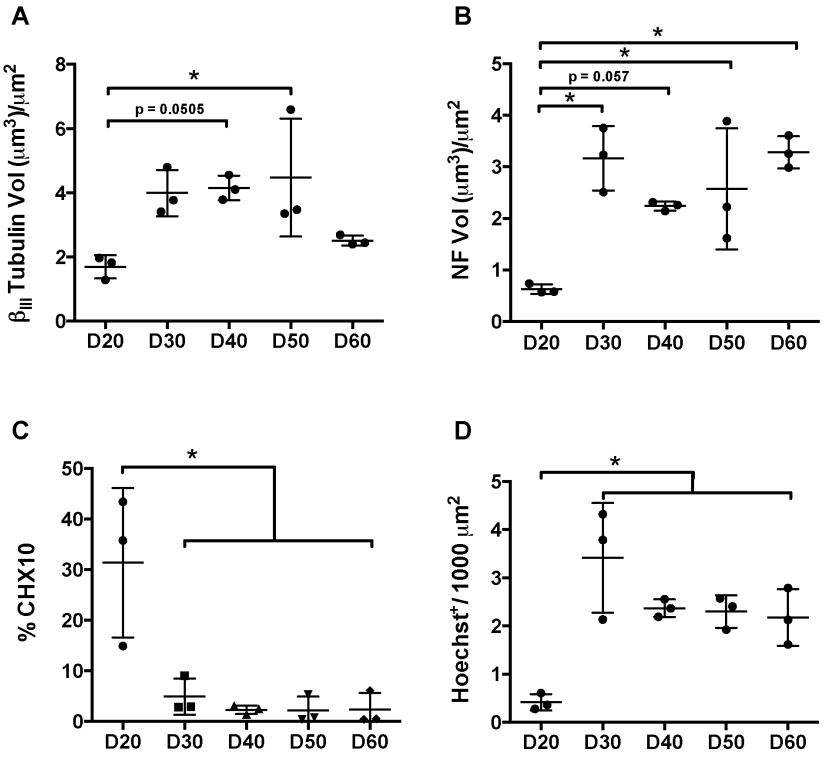

Figure 2.13: Quantification of *in vitro* maturation cultures. *(A)* Volume of β_{III} tubulin throughout culture duration normalized by observation view area. Day 50 volume was greater than day 20 volume ($p<0.05$, one-way ANOVA and Tukey post hoc comparison) *(B)* Volume of neurofilament throughout culture duration normalized by observation view area. Day 60, day 50, and day 30 volume was greater than day 20 volume ($p<0.05$, one-way ANOVA and Tukey post hoc comparison) *(C)* Percent $CHX10^+$ cells throughout culture duration. Day 20 percentage was greater than all other time points Day 50 volume was greater than day 20 volume ($p<0.05$, one-way ANOVA and Tukey post hoc comparison). *(D)* Number of $Hoechst^+$ cells throughout culture duration normalized by observation view area. Day 30 through day 60 were greater than day 20 Day 50 volume was greater than day 20 volume ($p<0.05$, one-way ANOVA and Tukey post hoc comparison).

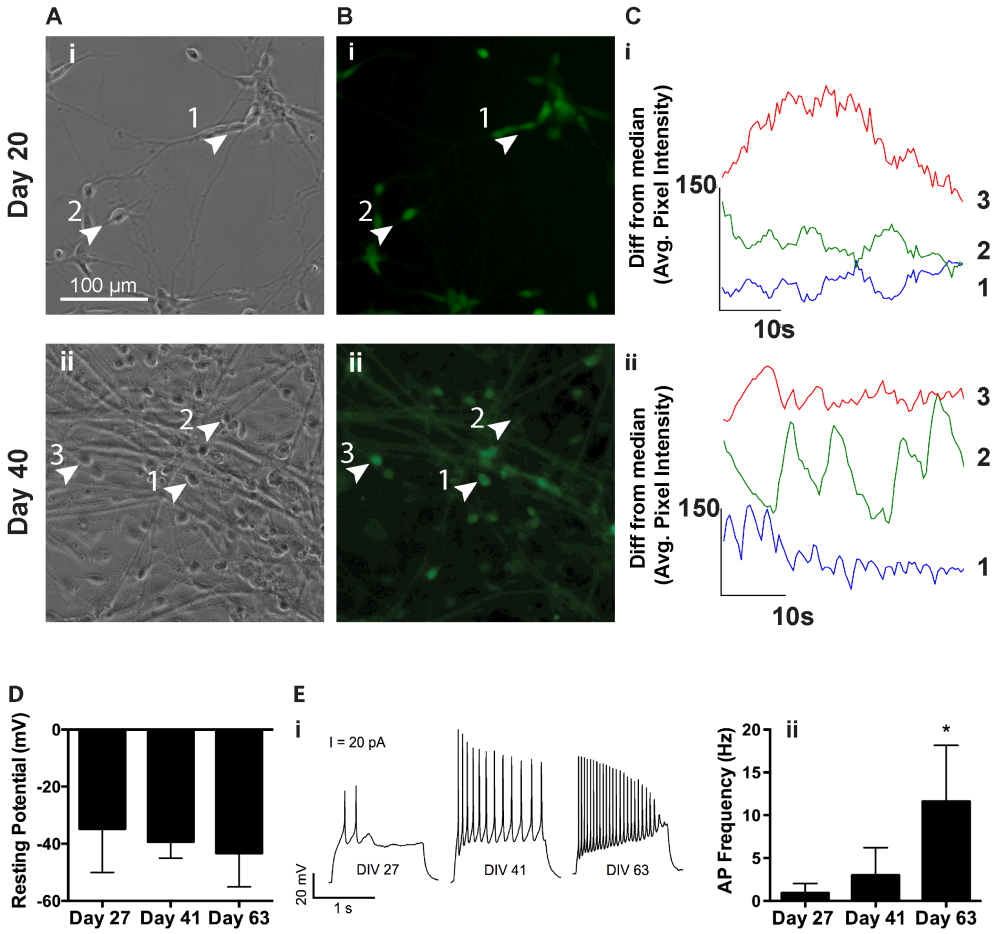

Figure 2.14: Electrophysiological properties show increased maturation with culture duration. *($A_{i\text{-}ii}$)* Representative phase images of cultures on days 20 and 40. *($B_{i\text{-}ii}$)* Representative fluorescent images of the calcium indicator Fluo4-loaded cells. White arrowheads indicate somas where the regions of interest were selected for calcium imaging. *($C_{i\text{-}ii}$)* Representative traces of fluorescence intensity over time. *(D)* Resting membrane potential of current-clamp patched neurons at Day 27, 41, and 63. *($E_{i\text{-}ii}$)* Representative action potential firing in response to 20 pA current stimulation at Day 27, 41, and 63 (i). Average action potential frequency at Day 27, 41, and 63. Action potential frequency on Day 63 is significantly different ($p<0.05$, one-way ANOVA and Tukey post hoc comparison) than Day 27 and 41 (ii). n = 5, 6, and 9 for Day 27, 41, and 63, respectively. Error bars indicate standard error of the mean.

2.3.4 Transplanted hPSC Derived V2a Interneurons Survive and Mature in the Uninjured Murine Spinal Cord

The physiological response of hPSC-derived V2a interneurons within the environment of the spinal cord was examined by transplanting differentiated cultures into naïve spinal cords of C57/SCID mice. V2a interneuron cultures (~45% $CHX10^+$ cells; Fig 2.15 A-B) were transplanted at thoracic vertebral level 9 (T9) and spinal cords were harvested 2 weeks later for histological analysis (Fig 2.15 C). Transplanted cells were identified in sagittal sections with antibodies for a human cytoplasmic protein (Stem121, Fig 2.15 D) and human nuclear antigen (HNA, Fig 2.15 E). HNA^+ nuclei remained predominantly at the transplant site with limited migration along the rostral/caudal axis of the spinal cord. $Stem121^+$ cells were observed at the transplant site (Fig 2.15 F) with processes extending over 5mm in both rostral and caudal directions (Fig 2.15 G).

To assess the phenotype of the transplanted cells, adult murine spinal cord was examined by immunohistological staining with a panel of different neuronal markers. Most of the HNA^+ cells co-expressed CHX10 (61.1% ± 10.8%), thus confirming the survival of transplanted V2a interneurons for at least 2 weeks (Fig 2.15 H-J). The majority of $CHX10^+$ cells expressed NeuN (Fig 2.15 K, 91.1% ± 4.6%, arrows and inset) and many expressed VGlut2 (Fig 2.15 L and inset), indicating maturation of V2a interneurons into a glutamatergic phenotype within the spinal cord environment. Occasional $GABA^+$ cells were found in the vicinity of the transplant site, but as expected, $CHX10^+/GABA^+$ cells were never detected (Fig 2.15 M and inset). In addition, no $OCT4^+$ cells or signs of potential teratoma formation were observed in any of the histological sections examined (Fig 2.16 A-D).

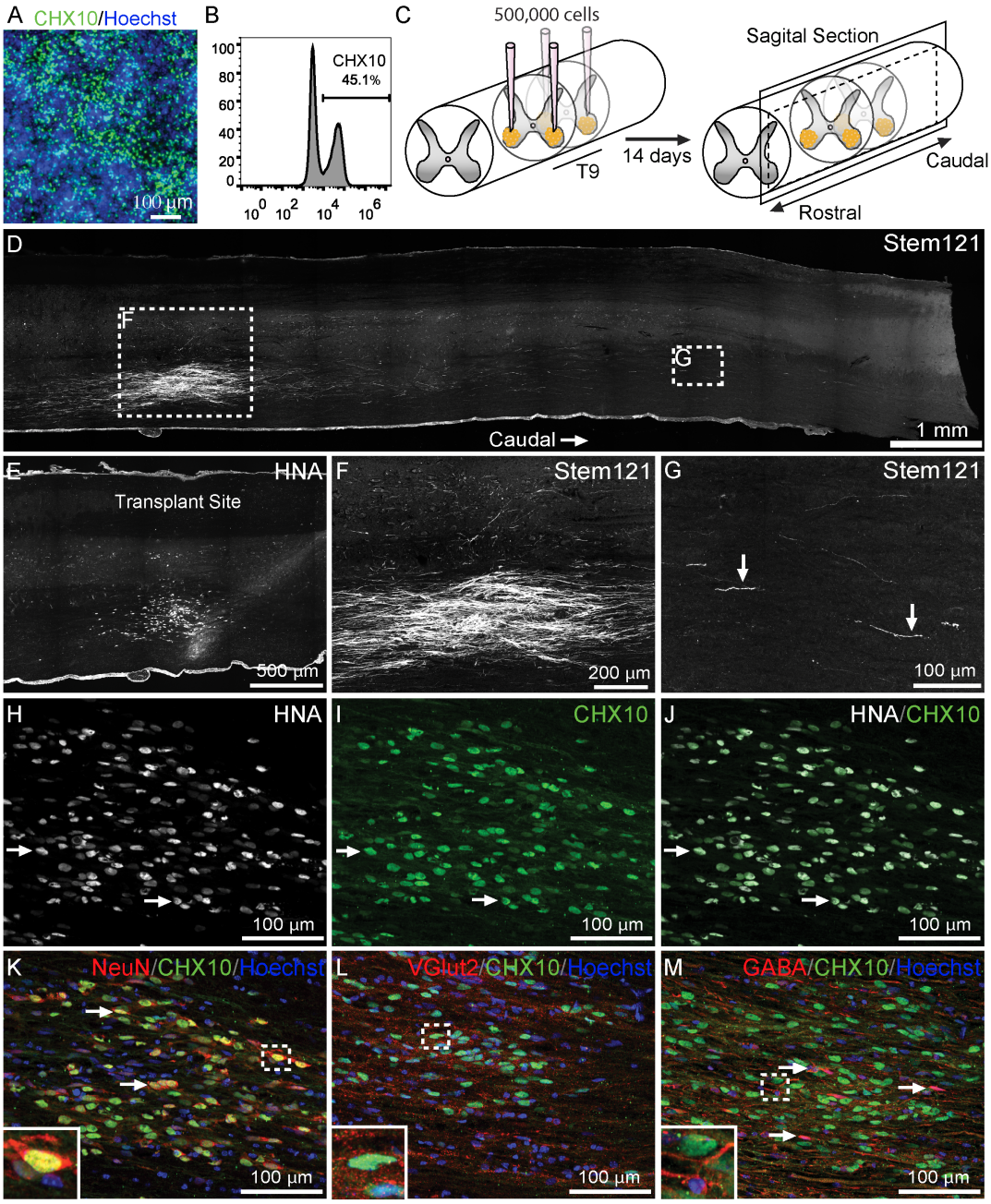

Figure 2.15: hPSC derived V2a interneurons survive and mature in the adult murine spinal cord. *(A)* Immunostaining of CHX10 (green) and Hoeschst labeling of nuclei (blue) in V2a interneuron cultures on day 17. *(B)* Flow cytometry analysis of CHX10 in V2a interneuron cultures used for transplantation. *(C)* Schematic of cell transplantation into the adult murine spinal cord and sectioning of harvested spinal cord tissue at 2 weeks post-transplantation. *(D)* Stem 121 (white) immunostaining in a sagittal tissue section caudal to T9. *(E)* HNA (white) immunostaining near the transplantation site. *(F)* Stem121 (white) immunostaining at the transplant site *(G)* and at 5mm away from the center of the transplantation site. *(H-J)* HNA (white) and CHX10 (green) immunostaining of V2a interneurons at the transplantation site. *(K-M)* CHX10 (green) immunostaining and nuclei labeling (blue) of transplanted V2a interneurons. Insets contain a higher magnification view. (K) NeuN (red) and inset of a $NeuN^{+}/CHX10^{+}$ nuclei. *(L)* VGLUT2 (red) and inset of VGlut2 labeling adjacent to the $CHX10^{+}$ nuclei of a transplanted V2a interneuron. *(M)* GABA (red) and inset of a $GABA^{+}/CHX10^{-}$ cell adjacent to a $GABA^{-}/CHX10^{+}$ cell.

Transplanted hPSC-derived V2a interneurons projected to multiple locations in the murine spinal cord (Fig 2.17 A). Stem121^{+} processes projected within the white matter and many branched into the adjacent gray matter as well (Fig 2.17 Ai). Transplanted neurons also projected axons between distinct transplantation sites (Fig 2.17 Aii). Putative synapse formations of the transplanted cell population with host cells were observed adjacent to the transplantation sites (Fig 2.17 Aiii). The post-synaptic marker, HOMER, was found on host neurons (NeuN^{+}) in direct proximity of abutting human cell neurites (Stem121^{+}), suggesting synapse formation of transplanted cells with the host tissue (Fig 2.17 B-E). In addition, human cell neurite endings expressing the pre-synaptic marker, synaptophysin, were observed directly adjacent to host neurons (Fig 2.17 F-I). Stem121^{+} cells also expressed the postsynaptic marker GRIP1 (Fig 2.17 J-M). These results demonstrate that transplanted hPSC-derived V2a interneurons integrate with the host tissue of the adult murine spinal cord.

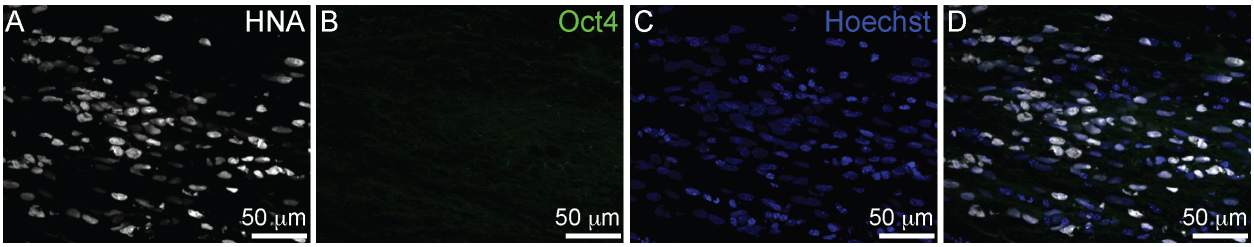

Figure 2.16: Transplanted cultures are not pluripotent. *(A-D)* Stem121 (white), Oct4 (green), and Hoechst labeled nuclei (blue) immunostaining of transplanted V2a interneurons.

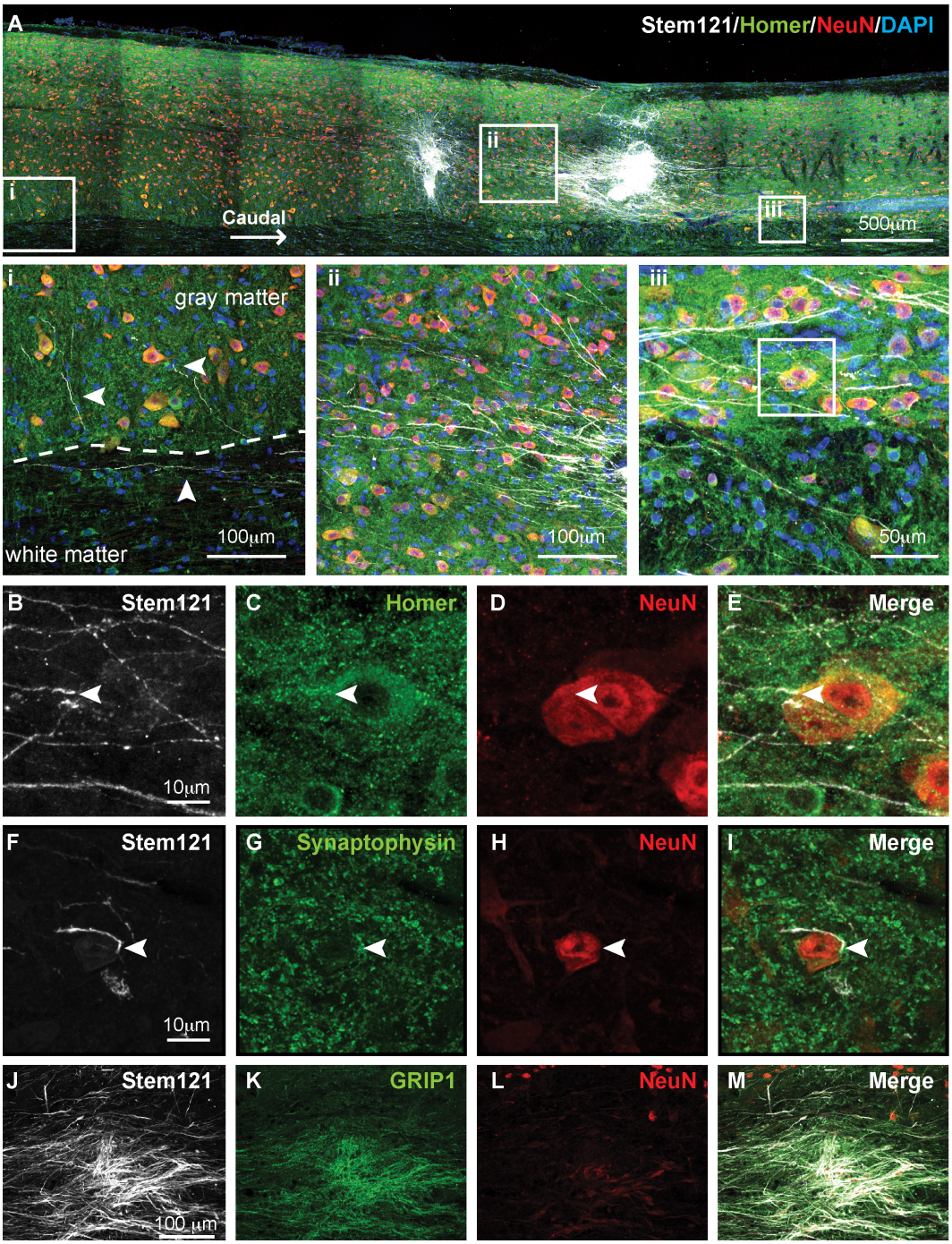

Figure 2.17: Transplanted cells extend projections and form putative synapses with host neurons. *(A_{i-iii})* Stem121 (white), Homer (green) and NeuN (red) immunostaining of transplanted V2a interneurons. (i) Inset of tissue rostral to the transplantation site. Horizontal arrows point to neurites that have extended into the gray matter. Vertical arrows point to neurites that have further extended into the white matter. (ii) Inset of tissue between the two transplantation sites. (iii) Inset of tissue caudal to the transplantation site. Box highlights the area shown in B-E. *(B-E)* Stem121 (white), Homer (green) and NeuN (red) immunostaining of transplanted V2a interneurons. Arrows point to colocalization of Stem121, Homer, and NeuN. *(F-I)* Stem121 (white), synaptophysin (green) and NeuN (red) immunostaining of transplanted V2a interneurons. Arrowheads point to colocalization of Stem121, synaptophysin, and NeuN. *(J-M)* Stem121 (white), NeuN (red), and GRIP1 (green) immunostaining of transplanted V2a interneurons.

2.3.5 Cryopreservation of V2a Interneurons

The V2a interneuron cultures were frozen to make batching of differentiations and future animal studies logistically feasible. Throughout the freeze/thaw process, the CHX10 percentage was maintained despite a ~30% decrease in overall cell yield (Fig 2.18 A-B). Immunocytochemistry revealed no great morphological differences between the day 17 and thawed populations except for cell density disparities due to cell survival (Fig 2.18 C-D). Gene expression analysis on a panel of neuronal genes as well as metabolic and heatshock genes (Table 2.4) revealed a slight shift of upregulated gene expression towards cells that had been dissociated and replated for 3 days compared to cells that had been dissociated, gone through a freeze/thaw cycle, and recovered for three days in culture (Fig 2.18 E). *CHX10* and *SOX14* (blue), two markers of V2a interneurons, were not robustly depleated during the freeze thaw process. Additionally, there was not up regulation of HSP60, HSP70, or HSP90 in response going through a freeze/thaw period. These results demonstrate the ability to freeze the V2a interneuron cultures at day 17 and recover the populations at a later time point to perform additional experiments without losing the integrity of the cells.

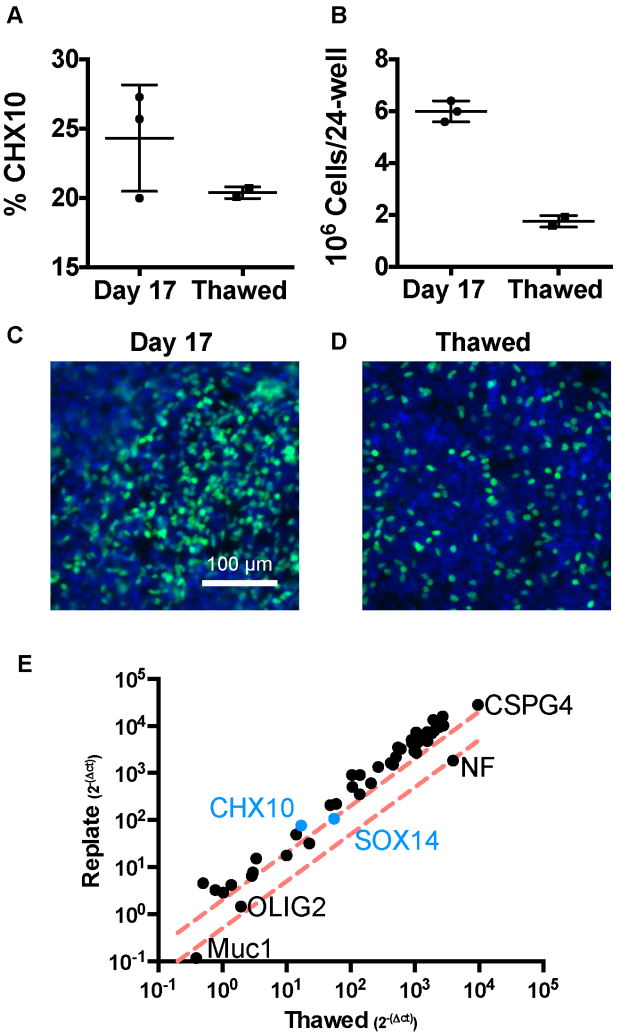

Figure 2.18: V2a interneuron cultures can be cryopreserved: Flow cytometry analysis of CHX10 percentage (A) and number of cells (B) at day 17 and after being frozen at day 17 and thawed for 3 days. B. Immunostaining for CHX10 (green) and nuclei (blue) at day 17 (C) and and after being frozen at day 17 and thawed for 3 days (D). E. qPCR of a panel of genes shown in Table 2.4 on cultures that were dissociated at day 17 and replated for 3 days (Replate) or frozen and thawed for 3 days (Thawed).

FOXG1	HOXD10	BCL2	EN	PDGFRA	POU5F1
HOXA1	HOXD11	CD38	EVX2	SOX14	SHH
HOXA2	HOXD9	HSP60	GATA3	THY-1	
HOXA7	LHX2	HSP70	HB9	DLL3	
HOXB1	NKX2.1	HSP90	IRBP	DLL4	
HOXB7	PAX5	MUC1	NES	HES1	
HOXA11	SIX3	NR4A2	NeuN	HES3	
HOXB9	HCN4	CHX10	NF	JAG1	
HOXC10	KCNA5	CRX	OLIG2	NOTCH 2	
HOXC9	SCN5A	CSPG4	PAX6	NOTCH 4	

Table 2.4: Genes assessed following cyropreservation

2.4 Discussion

This study describes the first successful differentiation of excitatory V2a interneurons from hPSCs using developmental signaling morphogens (RA and Shh agonists) to specify p2 progenitors in combination with Notch inhibition to direct V2a commitment. Initially, a combination of RA, pur, and DAPT concentrations was tested, similar to those used to promote V2a differentiation of murine ESCs (Brown, Butts et al. 2014), but applied over a comparable time scale for hPSC motor neuron differentiation (Amoroso, Croft et al. 2013). Compared to motor neuron differentiation, lower concentrations of RA (100nM vs. 1μM) increased the relative percentage of $CHX10^+$ cells (Fig 2.1 C-E). In addition to the well-known caudalizing effects of RA on hindbrain and spinal neuron populations (Kessel 1992, Okada, Shimazaki et al. 2004), dorsoventral RA signaling gradients can also impact progenitor domain specification during development (Pierani, Brenner-Morton et al. 1999, Okada, Shimazaki et al. 2004, Wilson, Gale et al. 2004). Additionally, a reduced concentration of Shh agonist (100nM), compared to that required for motor neuron differentiation (1μM), increased the relative percentage of $CHX10^+$ cells derived from hPSCs, analogous to dorsoventral patterning of the developing neural tube. Consistent with previous reports of PSC directed differentiation to neural lineages (Wichterle, Lieberam et al. 2002, Maroof, Keros et al. 2013), V2a fate specification is sensitive to subtle *in vitro* concentration changes of the signaling molecules that pattern the neural tube. The observed variability in the yield of $CHX10^+$ cells between experiments and different cell lines (Fig 2.3 A) could arise for a number of technical reasons that commonly afflict hPSC differentiation efficiency, such as genomic differences between cell lines, variable upstream isolation/derivation/culture methods prior to differentiation

studies, lack of synchrony among hPSCs at the start of differentiation, and variable concentrations of endogenously produced factors.

While coincident RA and Shh signaling pathways pattern progenitor domains in the developing neural tube, inhibition of Notch signaling is critical to specification of V2a interneurons (Fig 2.1 E). Notch inhibition effects on hPSC V2a interneuron differentiation are likely two-fold: 1) increased hPSC neurogenesis (β_{III} tubulin$^+$) when DAPT is first added and 2) promotion of V2a interneuron (CHX10$^+$, SOX14$^+$) specification, instead of V2b (GATA3$^+$) at later time points in the differentiation. Notch inhibition of PSCs undergoing neural differentiation generally enhances neurogenesis (Crawford and Roelink 2007, Borghese, Dolezalova et al. 2010). In our study, the proportion of neuronal cells was increased by inhibiting Notch in the V2a interneuron cultures compared to the motor neuron cultures that lacked DAPT treatment (Fig 2.5 Ci-ii and 3D). Notch signaling also regulates the balance between V2 committed cell types emanating from the p2 progenitor domain (Del Barrio, Taveira-Marques et al. 2007, Skaggs, Martin et al. 2011). Expression of the V2b marker, *GATA3*, was low (< two-fold increase over hPSCs) when Notch signaling was inhibited with DAPT (Fig 2.3 B) and expression of V2a transcription factors, *CHX10* and *SOX14*, was increased ~100-fold compared to motor neuron cultures that lacked Notch inhibition (Fig 2.5 D). Hence, inhibition of Notch signaling is critical to the specification of human V2a interneurons from hPSCs and exerts a compounded effect by increasing the neuronal pool in addition to specifying V2a interneurons from the p2 domain.

The duration of the human differentiation protocol (almost 3 weeks) can make logistical planning of long-term experiments difficult. Therefore, V2a interneuron cultures were frozen then thawed so that the differentiation protocol could be transiently

suspended soon after definitive commitment for experiments and analysis performed at later time points (i.e. electrophysiological testing, synaptogenesis experiments, cell transplantation).

A comprehensive analysis of the cell population at day 17 of the V2a interneuron differentiation was enabled by single cell RNAseq analysis. K-means clustering of 12 principal components revealed that $CHX10^{+}$ cells were contained largely within a single cluster (B, Fig 2.6 A-B) that was enriched with cells of an excitatory neuronal phenotype and hindbrain/cervical identity based upon coincident expression of several genes (*OAT*, *PCP4, HOXB5*). The majority of differentiated cells appeared to be committed to a neuronal fate with distinct sub-populations (clusters A, B, D, E, and F) differing largely on the basis of stage of differentiation or activity (i.e. metabolic, mitotic) (Fig 2.10 B-C), thus reflecting a snapshot of a dynamic differentiation process. It is not surprising that a small population of glial cells (cluster C) was detected along with a few non-neural cells (mesenchymal/muscle) when starting from PSCs, and glial cells can provide necessary support of neurons and promote maturation (Muller and Seifert 1982). Overall, single cell transcriptome results largely agreed with bulk gene analysis (Fig 2.4) and confirmed the effective differentiation of excitatory neurons with phenotypic properties of V2a interneurons. One difference between bulk and singling cell analysis was with the identification of the glial population. Using a handful of primers for glial markers for bulk PCR, it appeared as though there was not a glial population (Fig 2.4 B). However, the unbiased screening of genes with single cell analysis revealed the heterogeneous culture contained ~13% glial cells (Fig 2.10 A). Additionally, single cell analysis revealed populations that were missed with bulk analysis including the large progenitor and

mesenchymal populations. The insight revealing the progenitor populations suggests that if extending the duration of the differentiation protocol may increase the percentage of V2a interneurons as the neurons become committed neurons.

Maturation of hPSC-derived V2a interneurons is important to their physiological function and potential efficacy as a therapeutic cell type. However, a major challenge to the entire field of stem cell research is the relatively immature phenotype of most hPSC-derived cells, especially *in vitro* (Cornacchia and Studer 2015). Following V2a interneuron maturation over time was difficult to assess in heterogeneous cultures due to decreased expression of CHX10 and dilution by other neuronal and non-neuronal cell types (Fig 2.12 and 2.13). Electrophysiological analysis revealed that neurons in V2a cultures exhibited nascent signs of maturation over time, based upon increased action potential frequency in response to current injection (Fig 2.14 E_{ii}). Prospective studies on highly enriched populations of $CHX10^+$ cells or the use of an endogenous CHX10 reporter line will be necessary to rigorously define the phenotypic markers and electrophysiological properties of human V2a interneurons. Using a reporter line that labels cells that have expressed CHX10 would enable electrophysiological studies of specifically V2a interneurons to observe if the human-derived populations reflect what has been observed from *in vitro* and *in vivo* murine studies (Zhong, Droho et al. 2010, Iyer, Huettner et al. 2016).

To assess maturation beyond what is possible *in vitro,* hPSC-derived cardiomyocytes have been transplanted into adult rat hearts (Kadota, Pabon et al. 2017). Similarly, to examine survival and maturation within the native CNS environment, hPSC-derived V2a interneurons were transplanted into the adult murine spinal cord. Transplanted human cells in the spinal cord exhibited limited migration since the majority of HNA^+ and

Stem121^{+} cells were located within 1mm of the transplantation site. However, numerous Stem121+ processes resembling axons projected out from the sites of transplantation and were identified at least 5mm away, similar to endogenous murine V2a interneurons that can extend over four spinal segments (>2.5 mm) in the rostral and caudal direction (Dougherty and Kiehn 2010). The use of a CHX10 reporter line would enable tracking of V2a interneurons in the transplanted population to ensure that V2a interneurons are the long-descending population. Although transplanted CHX10^{+} human V2a interneurons matured into glutamatergic neurons expressing NeuN and VGlut2 it remains to be seen if human V2a interneurons adopt an appropriate laminar location and rostral/caudal phenotype depending on the site of transplantation. Functional integration of transplanted V2a interneuron cultures within spinal cord tissue was suggested by expression of pre-synaptic (synaptophysin) and post-synaptic (HOMER and GRIP1) markers at the interface of transplanted cell neurites and host neurons (Fig 2.17 B-M). In future studies, it will be necessary to functionally assess the electrical connectivity of human V2a interneurons with endogenous spinal neurons to determine whether proper synapses with motor circuits are formed. Previous studies have evaluated synaptic input connectivity of transplanted neural progenitors using photostimulation of the cortical spinal tract and whole cell recording of the transplanted population. This study revealed that the transplanted population had integrated with endogenous circuitry and was able to receive cortical input (Kadoya, Lu et al. 2016). A similar experiment could be performed wherein the transplanted V2a interneurons are stimulated and the activity of downstream motor neurons are recorded to evaluate synaptic connectivity.

The lack of teratoma formation and absence of $Oct4^+$ cells in histological sections indicated that non-purified, but highly enriched, V2a interneuron cultures were safe for transplantation. A preclinical safety study for hESC-derived oligodendrocyte precursors (AST-OPC1) demonstrated that the AST-OCP1 cells needed to be mixed with 10% pure PSCs during transplantation before a teratoma was detected, Further, even with 10% of the cells being pluripotent, a teratoma was detected only ~10% of the time (Priest, Manley et al. 2015). During the emergence of stem cell-derived therapies, teratoma formation following transplantation of PSC-derived cells was a prominent concern. However, studies are beginning to suggest the concern of teratoma formation has been mitigated as long as the transplanted population contains less than 10% pluripotent cells. Overall these data demonstrate that hPSC-derived V2a interneurons survive, adopt a glutamatergic phenotype, extend long distance axons and form putative synapses with host neurons when transplanted into the adult murine spinal cord.

2.5 Conclusion

In conclusion, this first study provides the first description and characterization of V2a interneurons differentiated from hPSCs through manipulation of RA, Shh, and Notch signaling pathways. The V2a interneuron protocol was specific in producing CHX10_ cells compared to previously published motor neuron studies and was also reproducible between multiple hPSC lines, which demonstrates robustness. The V2a interneuron cultures matured into glutamatergic neurons capable of producing action potentials and also displayed spontaneous Ca^{2+} activity. Further, transplanted V2a interneuron cultures survived, matured, and extended long distances in the uninjured murine spinal cord. These

cells enable new insights into the phenotypic properties of human V2a interneurons and represent a potent new candidate for regenerative cell therapies to treat CNS injuries and restore motor function.

2.6 Bibliography

Al-Mosawie, A., J. M. Wilson and R. M. Brownstone (2007). "Heterogeneity of V2-derived interneurons in the adult mouse spinal cord." Eur J Neurosci **26**(11): 3003-3015.

Amoroso, M. W., G. F. Croft, D. J. Williams, S. O'Keeffe, M. A. Carrasco, A. R. Davis, L. Roybon, D. H. Oakley, T. Maniatis, C. E. Henderson and H. Wichterle (2013). "Accelerated high-yield generation of limb-innervating motor neurons from human stem cells." J Neurosci **33**(2): 574-586.

Ashburner, M., C. A. Ball, J. A. Blake, D. Botstein, H. Butler, J. M. Cherry, A. P. Davis, K. Dolinski, S. S. Dwight, J. T. Eppig, M. A. Harris, D. P. Hill, L. Issel-Tarver, A. Kasarskis, S. Lewis, J. C. Matese, J. E. Richardson, M. Ringwald, G. M. Rubin and G. Sherlock (2000). "Gene ontology: tool for the unification of biology. The Gene Ontology Consortium." Nat Genet **25**(1): 25-29.

Azim, E., J. Jiang, B. Alstermark and T. M. Jessell (2014). "Skilled reaching relies on a V2a propriospinal internal copy circuit." Nature **508**(7496): 357-363.

Bardy, C., M. van den Hurk, B. Kakaradov, J. A. Erwin, B. N. Jaeger, R. V. Hernandez, T. Eames, A. A. Paucar, M. Gorris, C. Marchand, R. Jappelli, J. Barron, A. K. Bryant, M. Kellogg, R. S. Lasken, B. P. Rutten, H. W. Steinbusch, G. W. Yeo and F. H. Gage (2016). "Predicting the functional states of human iPSC-derived neurons with single-cell RNA-seq and electrophysiology." Mol Psychiatry **21**(11): 1573-1588.

Borghese, L., D. Dolezalova, T. Opitz, S. Haupt, A. Leinhaas, B. Steinfarz, P. Koch, F. Edenhofer, A. Hampl and O. Brustle (2010). "Inhibition of notch signaling in human embryonic stem cell-derived neural stem cells delays G1/S phase transition and accelerates neuronal differentiation in vitro and in vivo." Stem Cells **28**(5): 955-964.

Brown, C. R., J. C. Butts, D. A. McCreedy and S. E. Sakiyama-Elbert (2014). "Generation of v2a interneurons from mouse embryonic stem cells." Stem Cells Dev **23**(15): 1765-1776.

Butt, S. J., R. M. Harris-Warrick and O. Kiehn (2002). "Firing properties of identified interneuron populations in the mammalian hindlimb central pattern generator." J Neurosci **22**(22): 9961-9971.

Butt, S. J. and O. Kiehn (2003). "Functional identification of interneurons responsible for left-right coordination of hindlimbs in mammals." Neuron **38**(6): 953-963.
Cornacchia, D. and L. Studer (2015). "Back and forth in time: Directing age in iPSC-derived lineages." Brain Res.

Crawford, T. Q. and H. Roelink (2007). "The notch response inhibitor DAPT enhances neuronal differentiation in embryonic stem cell-derived embryoid bodies independently of sonic hedgehog signaling." Dev Dyn **236**(3): 886-892.

Crone, S. A., K. A. Quinlan, L. Zagoraiou, S. Droho, C. E. Restrepo, L. Lundfald, T. Endo, J. Setlak, T. M. Jessell, O. Kiehn and K. Sharma (2008). "Genetic ablation of V2a ipsilateral interneurons disrupts left-right locomotor coordination in mammalian spinal cord." Neuron **60**(1): 70-83.

Crone, S. A., J. C. Viemari, S. Droho, A. Mrejeru, J. M. Ramirez and K. Sharma (2012). "Irregular Breathing in Mice following Genetic Ablation of V2a Neurons." J Neurosci **32**(23): 7895-7906.

Del Barrio, M. G., R. Taveira-Marques, Y. Muroyama, D. I. Yuk, S. Li, M. Wines-Samuelson, J. Shen, H. K. Smith, M. Xiang, D. Rowitch and W. D. Richardson (2007). "A regulatory network involving Foxn4, Mash1 and delta-like 4/Notch1 generates V2a and V2b spinal interneurons from a common progenitor pool." Development **134**(19): 3427-3436.

Dobin, A., C. A. Davis, F. Schlesinger, J. Drenkow, C. Zaleski, S. Jha, P. Batut, M. Chaisson and T. R. Gingeras (2013). "STAR: ultrafast universal RNA-seq aligner." Bioinformatics **29**(1): 15-21.

Dougherty, K. J. and O. Kiehn (2010). "Firing and cellular properties of V2a interneurons in the rodent spinal cord." J Neurosci **30**(1): 24-37.

Eden, E., D. Lipson, S. Yogev and Z. Yakhini (2007). "Discovering motifs in ranked lists of DNA sequences." PLoS Comput Biol **3**(3): e39.

Eden, E., R. Navon, I. Steinfeld, D. Lipson and Z. Yakhini (2009). "GOrilla: a tool for discovery and visualization of enriched GO terms in ranked gene lists." BMC Bioinformatics **10**: 48.

Ericson, J., P. Rashbass, A. Schedl, S. Brenner-Morton, A. Kawakami, V. van Heyningen, T. M. Jessell and J. Briscoe (1997). "Pax6 controls progenitor cell identity and neuronal fate in response to graded Shh signaling." Cell **90**(1): 169-180.

Gene Ontology, C. (2015). "Gene Ontology Consortium: going forward." Nucleic Acids Res **43**(Database issue): D1049-1056.

Iyer, N. R., J. E. Huettner, J. C. Butts, C. R. Brown and S. E. Sakiyama-Elbert (2016). "Generation of highly enriched V2a interneurons from mouse embryonic stem cells." Exp Neurol **277**: 305-316.

Kadota, S., L. Pabon, H. Reinecke and C. E. Murry (2017). "In Vivo Maturation of Human Induced Pluripotent Stem Cell-Derived Cardiomyocytes in Neonatal and Adult Rat Hearts." Stem Cell Reports **8**(2): 278-289.

Kadoya, K., P. Lu, K. Nguyen, C. Lee-Kubli, H. Kumamaru, L. Yao, J. Knackert, G. Poplawski, J. N. Dulin, H. Strobl, Y. Takashima, J. Biane, J. Conner, S. C. Zhang and M. H. Tuszynski (2016).

"Spinal cord reconstitution with homologous neural grafts enables robust corticospinal regeneration." Nat Med **22**(5): 479-487.

Karunaratne, A., M. Hargrave, A. Poh and T. Yamada (2002). "GATA proteins identify a novel ventral interneuron subclass in the developing chick spinal cord." Dev Biol **249**(1): 30-43.
Kessel, M. (1992). "Respecification of vertebral identities by retinoic acid." Development **115**(2): 487-501.

Li, S., K. Misra, M. P. Matise and M. Xiang (2005). "Foxn4 acts synergistically with Mash1 to specify subtype identity of V2 interneurons in the spinal cord." Proc Natl Acad Sci U S A **102**(30): 10688-10693.

Li, X. J., Z. W. Du, E. D. Zarnowska, M. Pankratz, L. O. Hansen, R. A. Pearce and S. C. Zhang (2005). "Specification of motoneurons from human embryonic stem cells." Nat Biotechnol **23**(2): 215-221.

Lian, X., J. Zhang, S. M. Azarin, K. Zhu, L. B. Hazeltine, X. Bao, C. Hsiao, T. J. Kamp and S. P. Palecek (2013). "Directed cardiomyocyte differentiation from human pluripotent stem cells by modulating Wnt/beta-catenin signaling under fully defined conditions." Nat Protoc **8**(1): 162-175.

Livak, K. J. and T. D. Schmittgen (2001). "Analysis of relative gene expression data using real-time quantitative PCR and the 2(-Delta Delta C(T)) Method." Methods **25**(4): 402-408.

Macosko, E. Z., A. Basu, R. Satija, J. Nemesh, K. Shekhar, M. Goldman, I. Tirosh, A. R. Bialas, N. Kamitaki, E. M. Martersteck, J. J. Trombetta, D. A. Weitz, J. R. Sanes, A. K. Shalek, A. Regev and S. A. McCarroll (2015). "Highly Parallel Genome-wide Expression Profiling of Individual Cells Using Nanoliter Droplets." Cell **161**(5): 1202-1214.

Marklund, U., Z. Alekseenko, E. Andersson, S. Falci, M. Westgren, T. Perlmann, A. Graham, E. Sundstrom and J. Ericson (2014). "Detailed expression analysis of regulatory genes in the early developing human neural tube." Stem Cells Dev **23**(1): 5-15.

Maroof, A. M., S. Keros, J. A. Tyson, S. W. Ying, Y. M. Ganat, F. T. Merkle, B. Liu, A. Goulburn, E. G. Stanley, A. G. Elefanty, H. R. Widmer, K. Eggan, P. A. Goldstein, S. A. Anderson and L. Studer (2013). "Directed differentiation and functional maturation of cortical interneurons from human embryonic stem cells." Cell Stem Cell **12**(5): 559-572.

Muller, H. W. and W. Seifert (1982). "A neurotrophic factor (NTF) released from primary glial cultures supports survival and fiber outgrowth of cultured hippocampal neurons." J Neurosci Res **8**(2-3): 195-204.

Nicholas, C. R., J. Chen, Y. Tang, D. G. Southwell, N. Chalmers, D. Vogt, C. M. Arnold, Y. J. Chen, E. G. Stanley, A. G. Elefanty, Y. Sasai, A. Alvarez-Buylla, J. L. Rubenstein and A. R. Kriegstein

(2013). "Functional maturation of hPSC-derived forebrain interneurons requires an extended timeline and mimics human neural development." Cell Stem Cell **12**(5): 573-586.

Okada, Y., T. Shimazaki, G. Sobue and H. Okano (2004). "Retinoic-acid-concentration-dependent acquisition of neural cell identity during in vitro differentiation of mouse embryonic stem cells." Dev Biol **275**(1): 124-142.

Perrier, A. L., V. Tabar, T. Barberi, M. E. Rubio, J. Bruses, N. Topf, N. L. Harrison and L. Studer (2004). "Derivation of midbrain dopamine neurons from human embryonic stem cells." Proc Natl Acad Sci U S A **101**(34): 12543-12548.

Pierani, A., S. Brenner-Morton, C. Chiang and T. M. Jessell (1999). "A sonic hedgehog-independent, retinoid-activated pathway of neurogenesis in the ventral spinal cord." Cell **97**(7): 903-915.

Priest, C. A., N. C. Manley, J. Denham, E. D. Wirth, 3rd and J. S. Lebkowski (2015). "Preclinical safety of human embryonic stem cell-derived oligodendrocyte progenitors supporting clinical trials in spinal cord injury." Regen Med **10**(8): 939-958.

Satija, R., J. A. Farrell, D. Gennert, A. F. Schier and A. Regev (2015). "Spatial reconstruction of single-cell gene expression data." Nat Biotechnol **33**(5): 495-502.

Shi, Y., P. Kirwan and F. J. Livesey (2012). "Directed differentiation of human pluripotent stem cells to cerebral cortex neurons and neural networks." Nat Protoc **7**(10): 1836-1846.

Skaggs, K., D. M. Martin and B. G. Novitch (2011). "Regulation of spinal interneuron development by the Olig-related protein Bhlhb5 and Notch signaling." Development **138**(15): 3199-3211.

van der Maaten LJP, H. G. (2008). "Visualizing High-Dimensional Data Using t-SNE." Journal of Machine Learning Research **9**: 2579-2605.

Wichterle, H., I. Lieberam, J. A. Porter and T. M. Jessell (2002). "Directed differentiation of embryonic stem cells into motor neurons." Cell **110**(3): 385-397.

Wilson, L., E. Gale, D. Chambers and M. Maden (2004). "Retinoic acid and the control of dorsoventral patterning in the avian spinal cord." Dev Biol **269**(2): 433-446.

Zhong, G., S. Droho, S. A. Crone, S. Dietz, A. C. Kwan, W. W. Webb, K. Sharma and R. M. Harris-Warrick (2010). "Electrophysiological characterization of V2a interneurons and their locomotor-related activity in the neonatal mouse spinal cord." J Neurosci **30**(1): 170-182.

Chapter 3: Co-emergence of Respiratory Hindbrain Populations

3.1 Introduction

We have previously demonstrated that V2a interneurons can be induced from human pluripotent stem cells (Butts, McCreedy et al. 2017), however, the rostral-caudal identity and function of hPSC-derived V2a interneurons remains to be determined. Additionally, differentiation of V2a interneurons from hPSCs resulted in a heterogeneous population of cells including broad classes of committed neurons, neural progenitors, and glial populations. The specific neuronal cell types in the $CHX10^-$ fraction of the cultures have not been identified. The following study demonstrates that hPSC-derived V2a interneurons have a phenotype similar to endogenous V2a interneurons present in the medial reticular formation (mRF) of the hindbrain, which are involved in respiratory control. Additionally, other hindbrain populations have been identified in the heterogeneous hPSC-derived culture including chemosensing neurons and V0 interneurons, which are also critical to the control of respiration. This study demonstrates how a combination of signals delivered *in vitro* can recapitulate developmental processes to specify a regional identity, in this case the hindbrain, and result in the co-emergence of multiple functionally related cell types.

The hindbrain, which is comprised of the medulla, pons, and cerebellum, is involved in coordination of many autonomic functions including respiration and heart rate. The

neural tube gives rise to the hindbrain structures in response to sonic hedgehog (Shh), retinoic acid (RA), and WNT signaling (Ericson, Rashbass et al. 1997, Glover, Renaud et al. 2006, Elkouby and Frank 2010). Similar to the spinal cord, a ventrodorsal gradient of Shh patterns distinct progenitor domains of motor neuron and interneuron populations (Gray 2008). RA signaling and WNT activation specify the rostrocaudal identity of the hindbrain, marked by HOX 1-4 and rhombomere 3 – 7 expression (Gaunt, Krumlauf et al. 1989, Marshall, Nonchev et al. 1992, Krumlauf, Marshall et al. 1993, White, Nie et al. 2007). While these signaling events set up the transcription program to determine cell fate, the neural populations migrate and organize into clusters of neurons called nuclei that interact to perform a specific function including respiration in the medulla (Alheid, Gray et al. 2002).

Specific regions of the medulla have been identified to play a role in different phases of the respiration cycle. The Ventral Respiratory Column (VRC) is located in the ventrolateral medulla and contains important respiratory nuclei including the retrotrapezoid nucleus /prefacial respiratory group (RTN/pFRG) and preBötzinger complex (pre BötC) (Ezure, Manabe et al. 1988, Ellenberger and Feldman 1990). The neurons contained within these structures been classified by transcription factor expression during development and by neurotransmitter type as the neurons mature. The absence of these neurons through genetic manipulations demonstrates disruptions to and even absence of respiration. Here, the RTN/pFRG and pre BötC, the structures where the chemosensing and V0 interneurons reside, will be further described (Gray, Hayes et al. 2010).

The medial RTN/pFRG, located at the most rostral position of the VRC, is the connection between the environment and rate of respiration through chemosensing neurons (Mulkey, Stornetta et al. 2004, Stornetta, Moreira et al. 2006). This structure is composed primarily of cells that express the Phox2B transcription factor in the dorsal half of the neural tube and migrate to the ventral lateral medulla to the VRC (Sieber, Storm et al. 2007, Hernandez-Miranda and Birchmeier 2015). The Phox2B neurons mature into a glutamatergic phenotype that sense the partial pressure of $C0_2$ ($pC0_2$) in the blood stream through proton receptors (Wang, Shi et al. 2013). $Phox2B^{-/-}$ die in utero due to the absence of respiration while $Phox2B^{+/-}$ mice are born yet have early respiratory defects (Dauger, Pattyn et al. 2003). In addition, the RTN/pFRG, including the $Phox2B^{+}$ chemosensing population, transduce environmental information about $pC0_2$ to adjacent respiratory regions including the pre BötC (Bochorishvili, Stornetta et al. 2012).

The pre BötC, considered the main rhythm generator of respiration, is composed of cells that developmentally express the p0 transcription factor, Dbx1 (Smith, Ellenberger et al. 1991, Bouvier, Thoby-Brisson et al. 2010, Gray, Hayes et al. 2010). These cells then mature in to a variety of excitatory and inhibitory neurons including excitatory $V0_v$ interneurons (Gray 2008). The rhythm generating cells in the pre BötC have been identified to be glutamatergic, commissural, and express the neurokinin 1 receptor (NK1R) (Greer, Smith et al. 1991, Funk, Smith et al. 1993, Gray, Rekling et al. 1999, Wang, Stornetta et al. 2001). A recent single cell RNA sequencing analysis of Dbx1-expressing cells isolated from the pre BötC of P0 mice elucidated the transcriptional signature of $V0_V$ interneurons including expression of Lhx5, Pax2, and HoxA4 (Hayes, Kottick et al. 2017). Knockout of genes involved in the development of the pre BötC including *Dbx1*, *Mafb*, and *Pbx3* results

in severe respiratory deficits, reiterating its importance in control of respiration (Blanchi, Kelly et al. 2003, Rhee, Arata et al. 2004, Gray, Hayes et al. 2010). While the pre BötC receives input from the chemosensing neurons in the RTN/pFRG, it has also been demonstrated to receive input from medullary V2a interneurons (Crone, Viemari et al. 2012).

V2a interneurons do not reside in the VRC, however, they have been identified in the mRF of the medulla, adjacent to the pre BötC. Similar to the spinal cord, V2a interneurons in the mRF are glutamatergic and express CHX10. However, these medullary V2a interneurons have extensions to the pre BötC (Crone, Viemari et al. 2012). Complete ablation of medullary V2a interneurons results in embryonic death, and while partial ablation permits postnatal survival of mice, irregular breathing patterns in these newborn mice implicate the importance of this population in regulating respiration (Crone, Viemari et al. 2012).

While there are many cells involved in the control of respiration, V2a interneurons, V0 interneurons, and chemosensing neurons are important phenotypes in responding to environmental changes and generating the respiratory rhythm. These three cell types all arise from the developing neural tube in response to exposure to the same milieu of signaling molecules including Shh, RA, and WNT activation (Ericson, Rashbass et al. 1997, Glover, Renaud et al. 2006, Elkouby and Frank 2010). These cells migrate and mature into interconnected nuclei critical to respiratory control. In the following study, hPCS were exposed to a combination of morphogens similar to those present during development of these respiratory phenotypes, which has resulted in the co-emergence of V2a interneurons, V0 interneurons, and chemosensing neurons. When engineering a tissue composed of

many cell types from hPSCs, the individual cell types are differentiated separately then merged together. This study takes a unique approach to co-emerge multiple neuronal populations from one set of signaling molecules in a way that is more similar to native development. To our knowledge, this is the first description of these respiratory populations from hPSCs and one of the few reports of co-emergent differentiation systems. The concept of co-emergence explored in this study can be applied to other directed differentiation systems for any lineage that developmentally results in multiple subtypes.

3.2 Materials and Methods

3.2.1 Human Pluripotent Stem Cell Culture

hPSCs—WTC and WTB iPSCs (generously donated by Bruce Conklin)—were grown to 70% confluence and passaged using Accutase (Accutase, San Diego, CA) to dissociate to single cells (incubated at 37°C for 5 minutes). Dissociated cells were replated on Matrigel-coated cultureware (hESC-qualified for ESCs and growth factor reduced for iPSCs) at a density of 10,000 cells per cm^2 with 10μM ROCK inhibitor (Y-27632, Selleckchem, Houston, TX) in mTeSR (StemCell Technologies, Vancouver, Canada). All work with human ESC and iPSC lines have been approved by the University of California – San Francisco Human Gamete, Embryo and Stem Cell Research (GESCR) Committee.

3.2.2 V2a Interneuron Differentiation

hPSCs were seeded in mTeSR supplemented with 10μM ROCK inhibitor and dual SMAD inhibitors 0.2μM LDN193189 and 10μM SB431542 (StemGent, Cambridge, MA) at 5,000–

100,000 cells/cm^2 onto 24-well plates coated with Matrigel. On day 3, medium was changed to mTeSR supplemented with dual SMAD inhibitors only. On day 5, the base medium was switched to neural induction medium (DMEM F:12 (Corning, Corning, NY), N2 supplement (Life Technologies, Carlsbad, CA), L-Glutamine (VWR), 2μg/ml heparin (Sigma Aldrich, St. Louis, MO), non-essential amino acids (Mediatech INC, Manassas, VA), penicillin-streptomycin (VWR) supplemented with fresh 0.4μg/ml ascorbic acid (Sigma Aldrich) and 10ng/ml brain derived neurotrophin factor (BDNF, R&D Systems, Minneapolis, MN)) supplemented with dual SMAD inhibitors and 10nM–10μM retinoic acid (Sigma Aldrich). On day 7, dual SMAD inhibition was ceased and 10nM–10μM retinoic acid, 10nM–10μM pur (EMD Millipore, Darmstast, Germany) and 1μM N-[N-(3,5-difluorophenacetyl)-L-alanyl]-S-phenylglycine t-butyl ester (DAPT) were added to the neural induction medium. Medium was changed every 2–3 days throughout the differentiation, with fresh supplements added each time for up to 17 days.

3.2.3 Dissociation of V2a Interneuron Cultures

V2a interneuron cultures were dissociated by incubating each 24-well with 1 ml Accutase. Cultures were incubated for 45 minutes total with a trituration every 15 minutes. At the end of the incubation period, the dissociated cells were washed with PBS and centrifuged at 200 x g for 5 minutes to pellet the cells.

3.2.4 Enrichment with Replating

The day 17 cultures were replated by first dissociating the cultures as described in 3.2.3. The pelleted cells were resuspended in NIM supplemented with 0.4μg/ml AA, 10ng/ml

BDNF, 100nM RA, 100nM pur, 1μM DAPT and with 1μM or 10μM ROCK inhibitor and plated onto a fresh Matrigel-coated 24-well plate. While the exact cell density was not calculated, the total contents of one dissociated 24-well was replated back onto one 24-well. Cultures were incubated at 37°C for 3 days before analysis.

3.2.5 WNT Treatment

To examine pretreatment effects of WNT, hiPSCs were plated onto a Matrigel-coated 24-well plate at 125,000 cells/cm^2 in mTeSR supplemented with 10μM ROCK inhibitor and 2μM CHIR99021. Two days later, the cell layers were dissociated with Accutase and the differentiation was performed as described in 3.2.2 with the addition of 2μM CHIR99021. The CHIR99021 treatment was continued until day 7.

3.2.6 Single Cell RNA Sequencing

At Day 17 of culture, cells were dissociated with Accutase. Approximately 8,000 cells were prepared for single cell analysis through droplet encapsulation by the Chromium Controller and library preparation with the Chromium Single Cell 3' v2 Library and Gel Bead Kit (10x Genomics, San Francisco, CA). cDNA was sheared using a Covaris S2 sonicator and 12 PCR cycles were run during cDNA amplification. Libraries were sequenced on a HiSeq 4000 (Illumina, San Diego, CA). Sequences were demultiplexed and aligned to human reference genome GRCh38 using the default settings of 10xGenomics *Cellranger* v 1.2. Genes were annotated using Ensembl version 70 (Dobin, Davis et al. 2013). After *Cellranger* filtering, >85 million valid reads remained with >70% mapping to the transcriptome. Downstream analysis was performed using *Seurat* (Macosko, Basu et al. 2015, Satija, Farrell et al. 2015)

and cells not expressing between 200 and 6000 unique genes were removed. A subset of high-variance genes was determined using Seurat's "MeanVarPlot" function (expression cutoff of ≥ 0.0125; dispersion cutoff of ≥ 0.50) and used to group cells into clusters (principal components 1–15; cluster resolution parameter = 0.6) (van der Maaten LJP 2008). The top 20 differentially expressed genes for each cluster were plotted in the heatmap.

3.2.7 Flow Cytometry

At day 17 of differentiation, cells were completely dissociated as described in 3.3.3 and stained with the Transcription Factor Buffer Set, which includes a fixation/permeabilization (FP) and wash/permeabilization (WP) buffer (BD Biosciences, Franklin Lakes, NJ). Dissociated samples were first fixed for 45 minutes at 4°C in the FP buffer followed by a 20 minute block with WP buffer containing 5% normal donkey serum (NDS, Jackson Laboratory, Bay Harbor, ME). Primary antibodies against CHX10, LHX5, PHOX2A, and PHOX2B (Table 3.1) and the proper matching species isotype control were added at the concentration shown in Table S3 into WP buffer containing 2% NDS and incubated at 4°C for 45 minutes. After two washes with WP buffer, secondary antibodies donkey anti-mouse IgG, Alexa Fluor 488 (Life Technologies), at a dilution of 1:200, were added to WP buffer and incubated at 4°C for 45 minutes. After two washes with WP buffer, samples were passed through a 35-µm filter before assessing with a BD Accuri C6 (BD) cytometer (minimum 10,000 events). Cytometry analysis was performed using FlowJo V10 (Flowjo, Ashland, OR).

Antibody Target	Species	Vendor	Cat. Number	Application	Dilution
CHX10	mouse	Santa Cruz	sc-374151	Flow and ICC	1 to 1000
LHX5	goat	R&D	AF6290	Flow and ICC	1 to 250
PHOX2A	mouse	Santa Cruz	81978	Flow and ICC	1 to 250
PHOX2B	mouse	Santa Cruz	376997	Flow	1 to 500
PHOX2B	goat	R&D	AF4940	ICC	1 to 250
Mouse IgG1 Isotype Control	mouse	R&D	MAB002	Flow	Matched protein concentration
Normal Goat IgG Control	goat	R&D	AB-108-C	Flow	Matched protein concentration

Table 3.1: Antibodies used for flow cytometry and immunostaining

3.2.8 *In Vitro* Immunocytochemistry and Imaging

Samples were fixed using 4% paraformaldehyde (VWR) for 30 minutes and permeabilized using 0.1% Triton-X in PBS for 15 minutes at 4° C before blocking for 1 hour at 4°C with PBS containing 5% NDS. Primary antibodies (Table 3.2) were diluted in PBS containing 2% NDS and incubated overnight. Samples were washed three times with PBS for 15 minutes at room temperature before incubating with secondary antibodies (Life Technologies) diluted in PBS containing 2% NDS. Hoechst was added at 1:1000 to the samples for 10 minutes then washed and imaged using a Zeiss Axio Observer inverted wide-field microscope equipped with an Apotome structured light attachment. An average intensity projection was performed on Z-stack images to create a single two-dimensional image spanning the entire thickness of the observed field. Images were cropped using Photoshop.

3.2.9 Statistical Analysis

Statistical analysis was performed using Prism 6 software. The mean and ± standard deviation were calculated for a minimum of three biological replicates for all data unless otherwise noted. Unpaired t-tests were performed when comparing two groups. One-way

analysis of variance (ANOVA) followed by appropriate post hoc pairwise comparisons Tukey's tests were used when three or more groups were specified. Specific statistical analysis is mentioned within the corresponding figure legend. Variances were confirmed to not differ significantly with the Brown-Forsythe test. In all comparisons, significance was defined as $p \leq 0.05$.

3.3 Results

3.3.1 V2a Interneuron Enrichment Through Replating and WNT Activation

While Butts *et al* described a defined protocol to obtain V2a interneurons, identified through expression of the CHX10 transcription factor, the percentages consistently obtained from the protocol (~20%) left room for improvement. V2a interneuron cultures were dissociated and replated at day 17 in the presence of either 1 or 10μM ROCK inhibitor and cultured for an additional 3 days (Fig 3.1 A). In two different cells lines (WTB and WTC iPSCs), replating enriched the CHX10% over cultures differentiated for 17 days (Fig 3.1 B-C). Culturing for an additional 3 days (Day 20) without replating increased the percentage of $CHX10^+$ cells with the WTC cell line but not with the WTB indicating there are some differences in optimal culture duration between the two cell lines. The disparity between culture duration could be caused by differing growth rates between the cell lines causing confluency to be reached at different time points, which would effect endogenous signaling and rate of differentiation. This may suggest that a range of termination time points should first be tested for each cell line. However, with both cell lines, replating with 1μM ROCK inhibitor enriched the CHX10 percentage over D20 time-matched controls implicating that

replating step will enrich the CHX10 population regardless of baseline levels. However, It appears that the fold-increase of the enrichment is dependent on baseline differentiation levels. The CHX10 percentage was enriched ~3-fold and ~1.5-fold in the WTB and WTC10 cell lines, respectively. Therefore, if the baseline levels of CHX10 are low, replating can be performed to further enrich the V2a interneuron population.

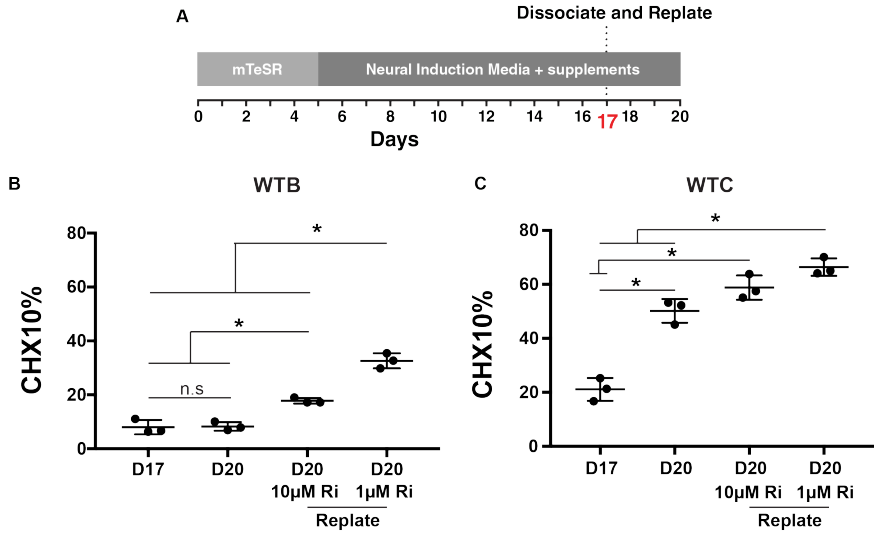

Figure 3.1: Replating enhances the V2a interneuron population. A. Schematic detailing experimental procedure. Cultures were dissociated and replated at day 17 and analysis occurred at day 20. B. and C. Flow cytometry analysis of CHX10 at day 17 and day 20 without replating as well as at day 20 with a replating step in the presence of 10μM or 1μM rock inhibitor (Ri)using the WTB (B) or WTC (C) hiPSC cell line. * = $p<0.05$, one-way ANVOA and Tukey post hoc comparison

Activation of the WNT signaling pathway has been demonstrated to promote neural induction and caudalization (Elkouby and Frank 2010, Li, Sun et al. 2011, Maury, Come et al. 2015). Activation of the the WNT pathway using the small molecule CHIR 99021 has been added into motor neuron differentiation protocols not only to caudalize the population but also increase the efficiency of differentiation (Du, Chen et al. 2015, Shimojo, Onodera et al. 2015). To test WNT activation in our differentiation, hiPSCs were plated at a high density in mTeSR supplemented with CHIR 99021 for two days. The cells were then dissociated and replated to begin the differentiation as previously described but CHIR 99021 was supplemented in the media for the first 7 days of the protocol (Fig 3.2 A). CHX10 percentage was increased when CHIR 99021 was added into the differentiation compared to the untreated (UT) controls in both WTB and WTC hPSCs (Fig 3.2 B-C). However, the effectiveness of the fold-change increase appeared to be cell line specific. Reports have demonstrated the response of hPSC cell lines to CHIR 99021 may depend on the concentration (Lippmann, Williams et al. 2015). Since this study only tested one concentration of CHIR 99021, it is possible that a higher concentration of CHIR may need to be used with the WTC cell line. These data support that the addition of WNT signaling could be used to enhance the V2a phenotype in the differentiation by either increasing the efficiency of neuralization or by defining a rostocaudal region that promotes V2a specification.

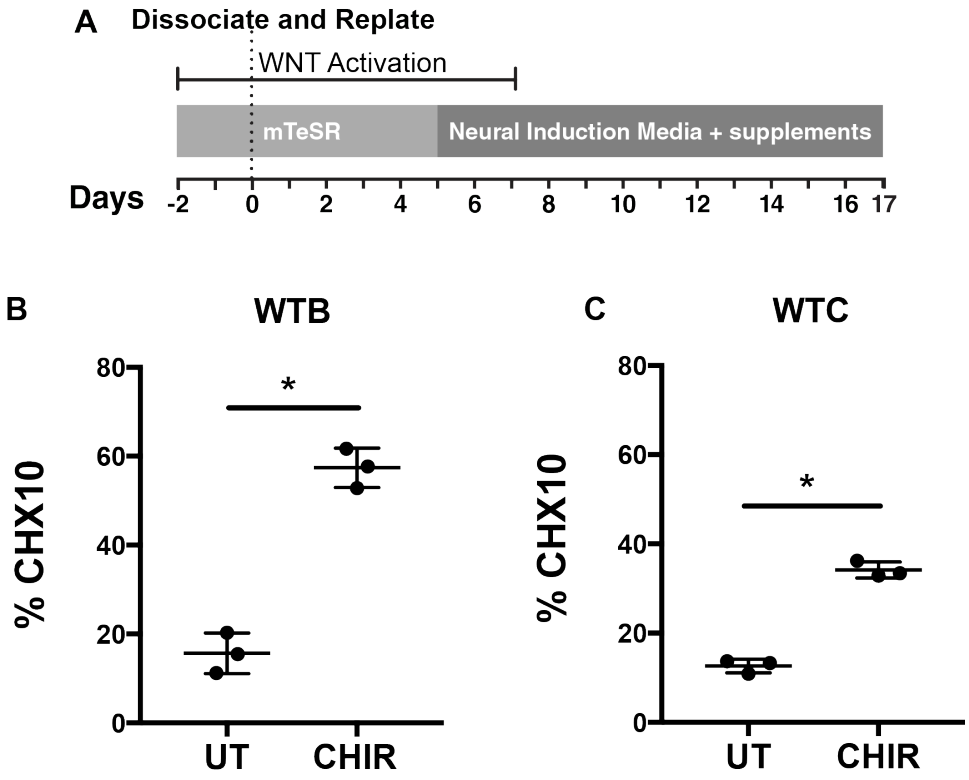

Figure 3.2: Early WNT activation enhances the V2a population. A. Schematic detailing experimental procedure. B. and C. Flow cytometry analysis of CHX10 following differentiation without WNT activation (untreated, UT) or with WNT activation (CHIR) using the WTB (B) or WTC (C) hiPSC cell line. * = $p<0.05$, un-paired t-test

3.3.2 Characterization of Heterogeneous V2a Interneuron Cultures

Single cell RNAseq was performed on the enriched V2a interneuron cultures that were replated for 3 days with 1μM ROCK inhibitor. For this data set, 561 cells were captured at 102,361 reads per cell and 4,138 genes per cell. Using 15 principle components and a resolution of 0.6, the tSNE plot revealed 5 distinct clusters that represented the heterogeneous population (Fig 3.3 A). The population appeared to be mainly neuronal as revealed through expression of neurofilament light and medium (*NEFL*, *NEFM*) (Fig 3.3 B-C). Dendrogram classification revealed that clusters 0, 1 and 2 are closely related while clusters 3 and 4 have more differences (Fig 3.3 D). Interestingly, when the number of genes per cell was plotted as a function of cluster (Fig 3.4), it was clear that cells in clusters 3 and 4 had fewer genes per cell (~1000) compared to clusters 0 to 2 (>4,000) meaning lower abundance genes such as transcription factors were not being sequenced making identification of neural subtype identity difficult. This disparity may be an artifact of library preparation or sequencing. For additional analysis, these two clusters could be filtered out.

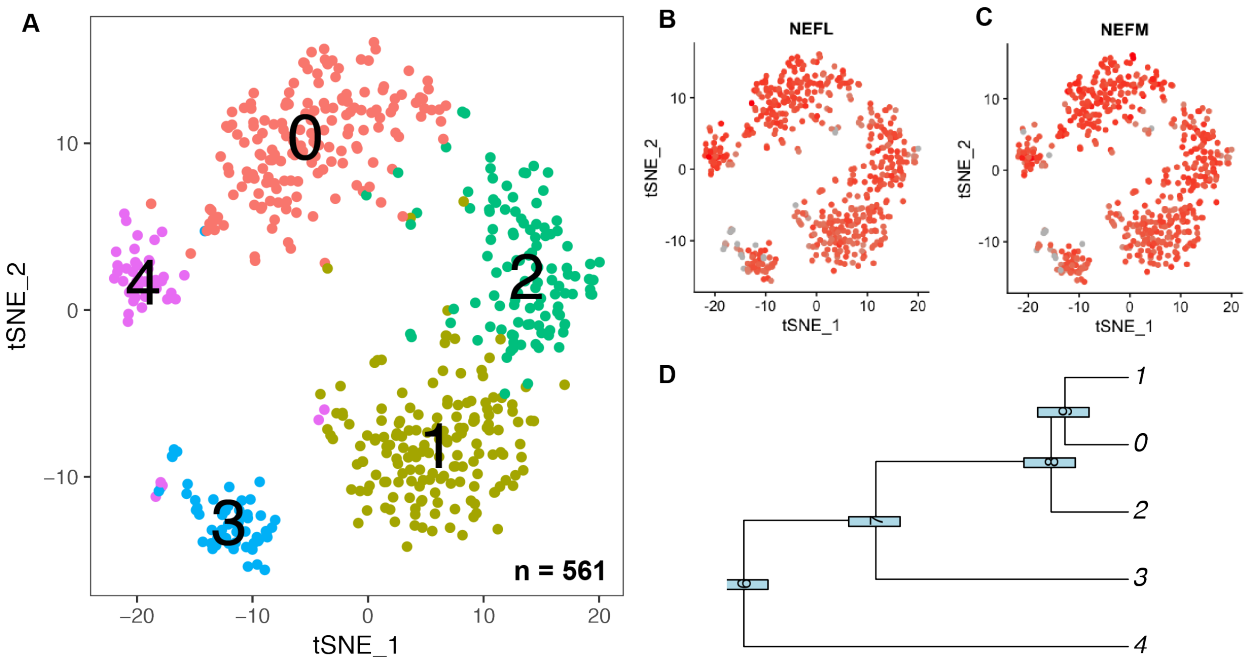

Figure 3.3: Single Cell RNA sequencing of replated differentiation. A. tSNE plot of replated V2a interneuron cultures indicating 5 clusters. B. Neurofilament light chain (*NEFL)* expression (red dots) C. Neurofilament Medium chain (*NEFM)* expression (red dots). D. Dendrogram of the relationship between clusters

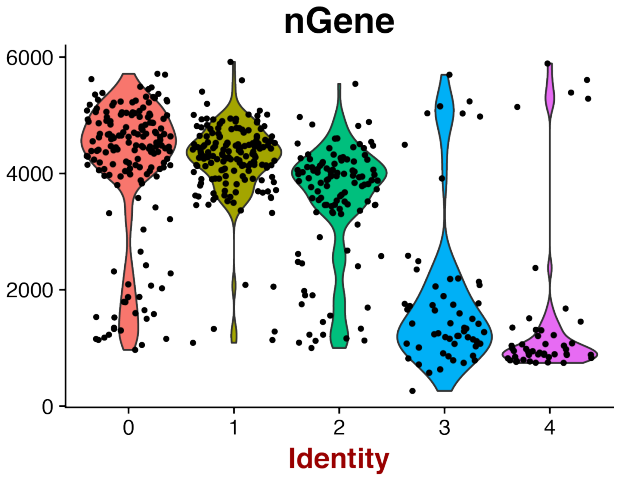

Figure 3.4 Imbalanced gene count between clusters. Clusters 3 and 4 have lower numbers of genes per cell making cluster identification difficult.

The V2a interneuron analyzed in the single cell analysis was approximately 36% CHX10^{+} via flow cytometry (Fig 3.5 A). Approximately 20% percent of cells were detected to express *CHX10* by single cell analysis and these cells were primarily contained within cluster 1 (Fig 3.5 B). Additional transcription factors that mark V2a interneurons including *SOX14* and *SOX21* were detected and contained within cluster 1 (Fig 3.5 C-E) reinforcing that cluster 1 represents the V2a interneurons in the cultures.

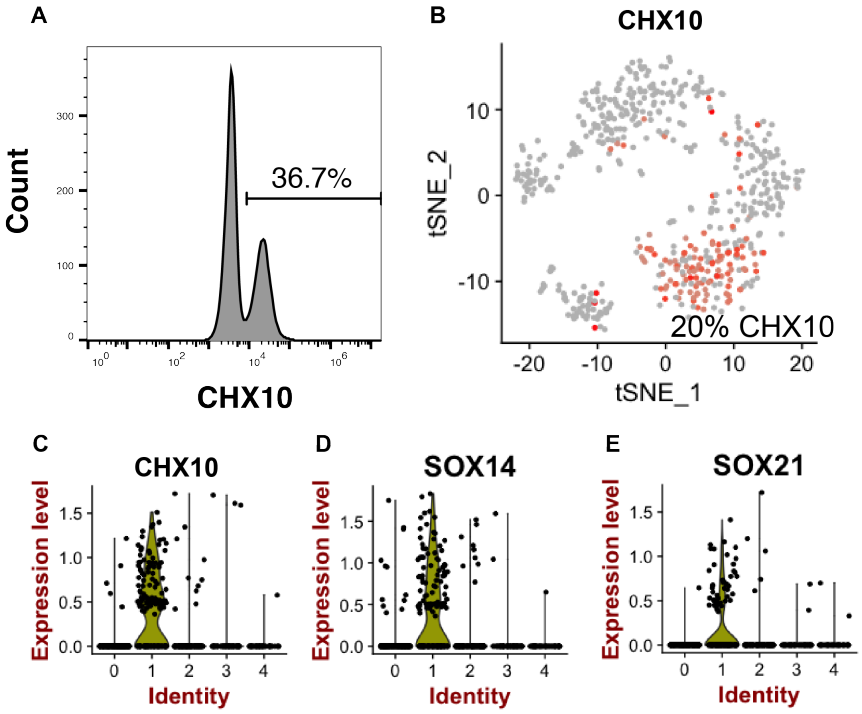

Figure 3.5: Identification of V2a interneuron population. A. Flow cytometry analysis of CHX10 from the V2a interneuron population analyzed by single cell RNA sequencing. B. *CHX10* expression (red dots). Gray dots represent remaining cells in the population. C. – E. Violin plot of *CHX10*, *SOX14*, and *SOX21* expression.

Physiologically, V2a interneurons are found throughout the rostral-caudal axis of the brainstem and spinal cord (Crone, Quinlan et al. 2008, Zhong, Droho et al. 2010, Crone, Viemari et al. 2012, Azim, Jiang et al. 2014) To identify the regional identity of the differentiated cultures, expression of a range of HOX markers from the hindbrain to the sacral region was analyzed. HOX genes present in the hindbrain (*HOXA2*, *HOXA3*, *HOXB2*, *HOXB1* and *HOXB4*) and cervical regions (*HOXA5*, *HOXB5*, *HOXB6*, *HOXB7*, and *HOXB8*) were detected in clusters 0 to 3 (Fig. 3.6). The midbrain gene (*OTX2*) and Hox genes for thoracic/lumbar regions (*HOXB9, HOXB10, HOXB11*) were not detected. This HOX profile indicates the cultures have expression patterns of a hindbrain/ high cervical regional identity.

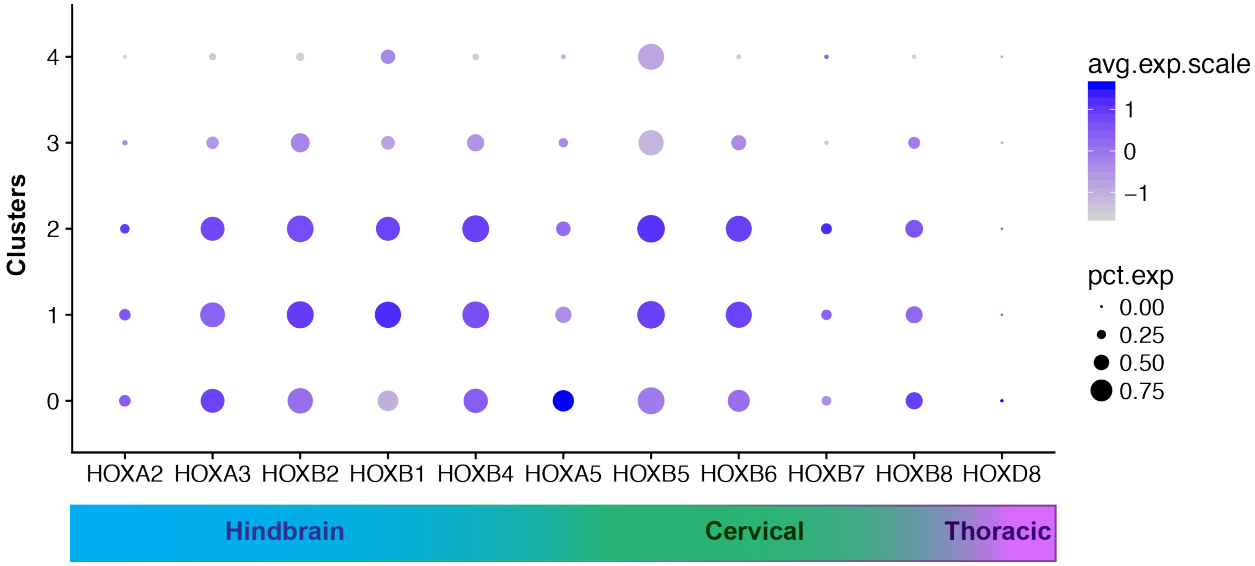

Figure 3.6: HOX expression profile. Expression level of various HOX genes in each cluster. The size of the dot correlates to the number of cells within the cluster that express the gene. The color of the dot correlates to the relative expression level.

3.3.3 Identification of Hindbrain Neuronal Populations

Cluster 1 was identified as the V2a interneurons, however, the identities of clusters 0, 2, 3 and 4 were unknown. Differential gene expression analysis was performed to detect genes that were upregulated in one cluster compared to all other clusters. The heatmap depicts the top 20 most differentially expressed genes for each cluster with the top 10 genes labeled for each cluster (Fig 3.7) For clusters 0 through 2, transcription factors present in the respiratory hindbrain circuit were highly upregulated (bold). More specifically, Cluster 0 expressed high levels of *PHOX2B*, *PHOX2A*, and *ADCYAP1,* which are markers of chemosensing neurons that are present in the retrotrapezoid nucleus (Fig 3.8 A). Cluster 1 expressed high levels of *CHX10*, *SOX14*, and *IRX3*, markers of committed and progenitor V2a interneurons (Fig 3.8 B). Cluster 2 expressed high levels of *LHX5*, *PAX2*, and *MAB21L2*, markers of V0 interneurons located in the pre BötC (Fig 3.8 C) (Hayes, Kottick et al. 2017). Additionally, clusters 0, 1 and 2 had high expression of markers found in respiratory hindbrain regions including the BötC and pre BötC (*HOXA4*, *PBX3*, *DACH1*, *LM04*, *SALL1*, Fig 3.9 A (Yackle, Schwarz et al. 2017) as well as genes that when mutated, lead to respiratory dysfunction (*PBX3*, *MAFB*, *MECP2*, *TSHZ3*, and *KDM6B*, Fig 3.9 B, (Amir, Van den Veyver et al. 1999, Shahbazian and Zoghbi 2001, Blanchi, Kelly et al. 2003, Rhee, Arata et al. 2004, Burgold, Voituron et al. 2012). Together, the single cell transcriptional analysis supports that the culture contains several different neural subtypes present in the respiratory hindbrain circuit.

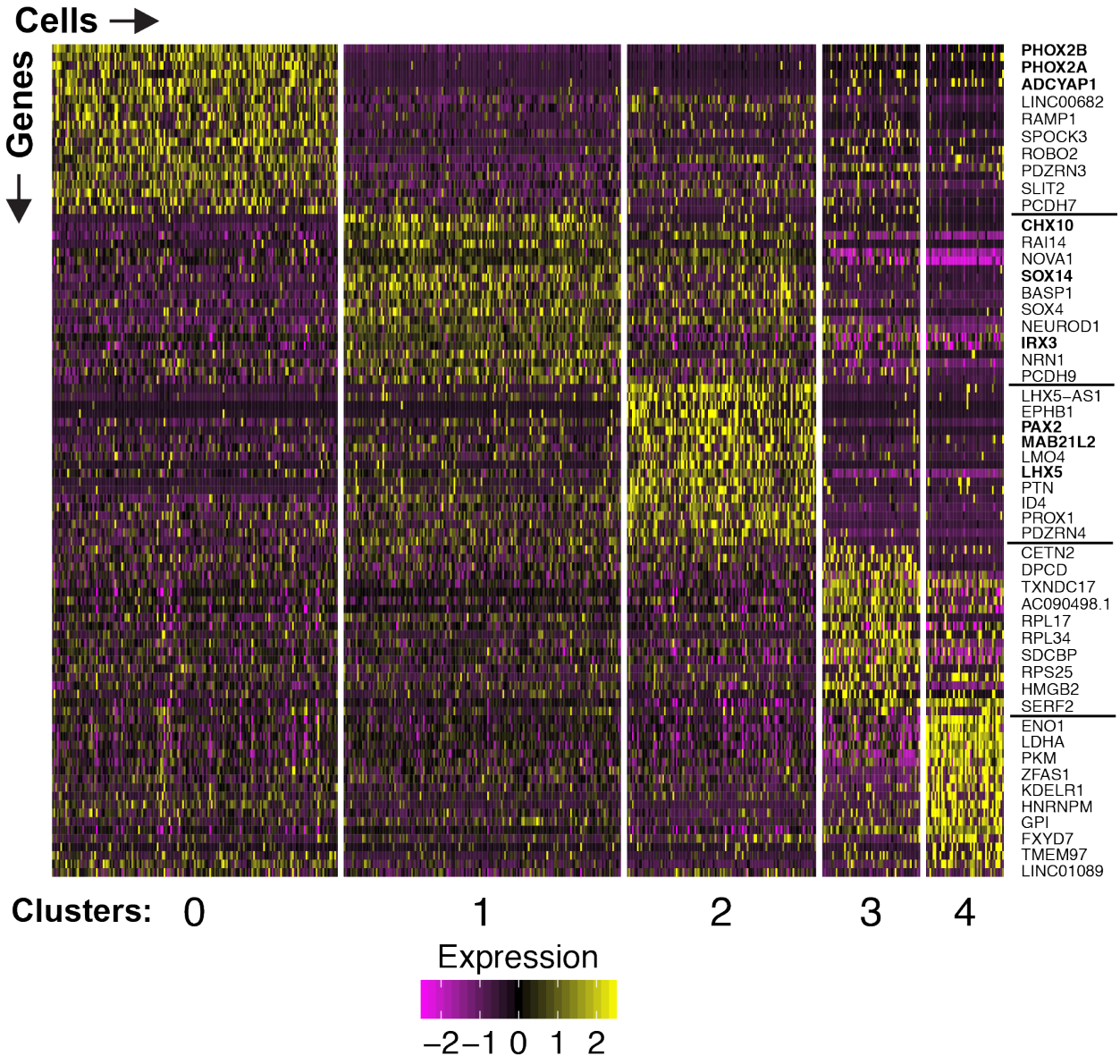

Figure 3.7: Heatmap of genes that define each cluster. Heatmap of the top 20 expressed genes for each cluster. Expression values are normalized for each gene with purple indicating low expression and yellow indicating high expression. The top 10 genes are listed for each cluster. Genes found in respiratory hindbrain populations are bolded.

	Cluster 0	Cluster 1	Cluster 2	Cluster 3	Cluster 4
1	PHOX2B	VSX2	LHX5-AS1	CETN2	ENO1
2	PHOX2A	RAI14	EPHB1	DPCD	LDHA
3	ADCYAP1	NOVA1	PAX2	TXNDC17	PKM
4	LINC00682	SOX14	MAB21L2	AC090498.1	ZFAS1
5	RAMP1	BASP1	LMO4	RPL17	KDELR1
6	SPOCK3	SOX4	LHX5	RPL34	HNRNPM
7	ROBO2	NEUROD1	PTN	SDCBP	GPI
8	PDZRN3	IRX3	ID4	RPS25	FXYD7
9	SLIT2	NRN1	PROX1	HMGB2	TMEM97
10	PCDH7	PCDH9	PDZRN4	SERF2	RPL12
11	EBF1	RND3	MYCBP2	GNG5	LINC01089
12	ID2	CCBE1	LAMP5	EEF1D	DOK5
13	TLN2	PPP2R2B	LHX1	EIF3E	CNN2
14	SPOCK1	CRNDE	LRRN1	ATP5I	FSTL1
15	SH3BGRL	CRABP2	ARL4C	TAGLN2	RPL39
16	ZFHX3	GNAS	TNRC6C	TIMP1	PPP1R1A
17	ZNF385D	KCNIP4	PIK3R1	SNRPG	WDR66
18	HOXA5	SYT1	ANOS1	B2M	S100A6
19	ASCL1	TLE1	TSHZ2	RPL12	PRPH
20	LMO3	RHOB	PCDH9	MTRNR2L12	NEAT1

Table 3.2: Top differentially expressed genes for each cluster from heatmap

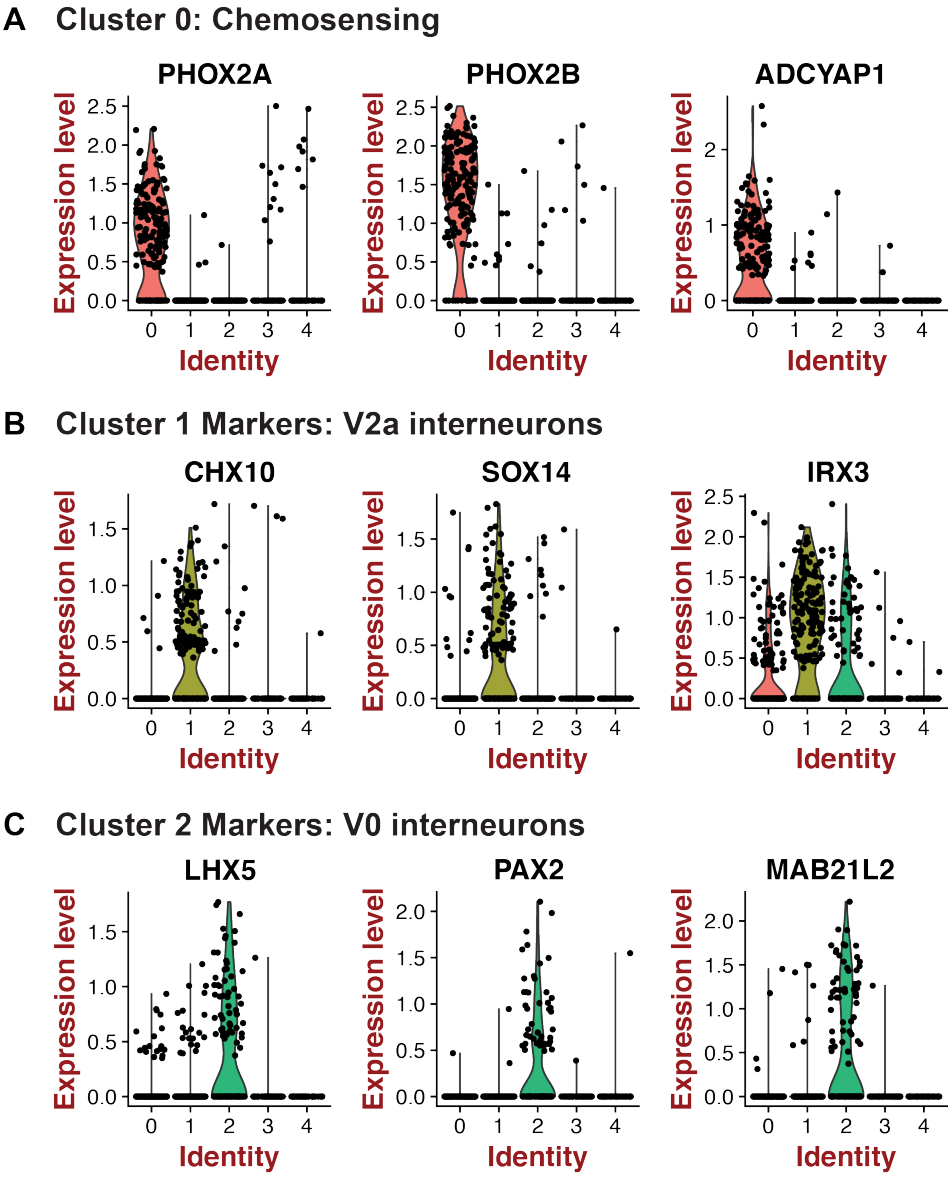

Figure 3.8 Clusters contain populations involved with respiratory control. Violin plots of genes from the top 10 genes that are expressed in A. chemosensing neurons, B. V2a interneurons, and C. V0 interneurons

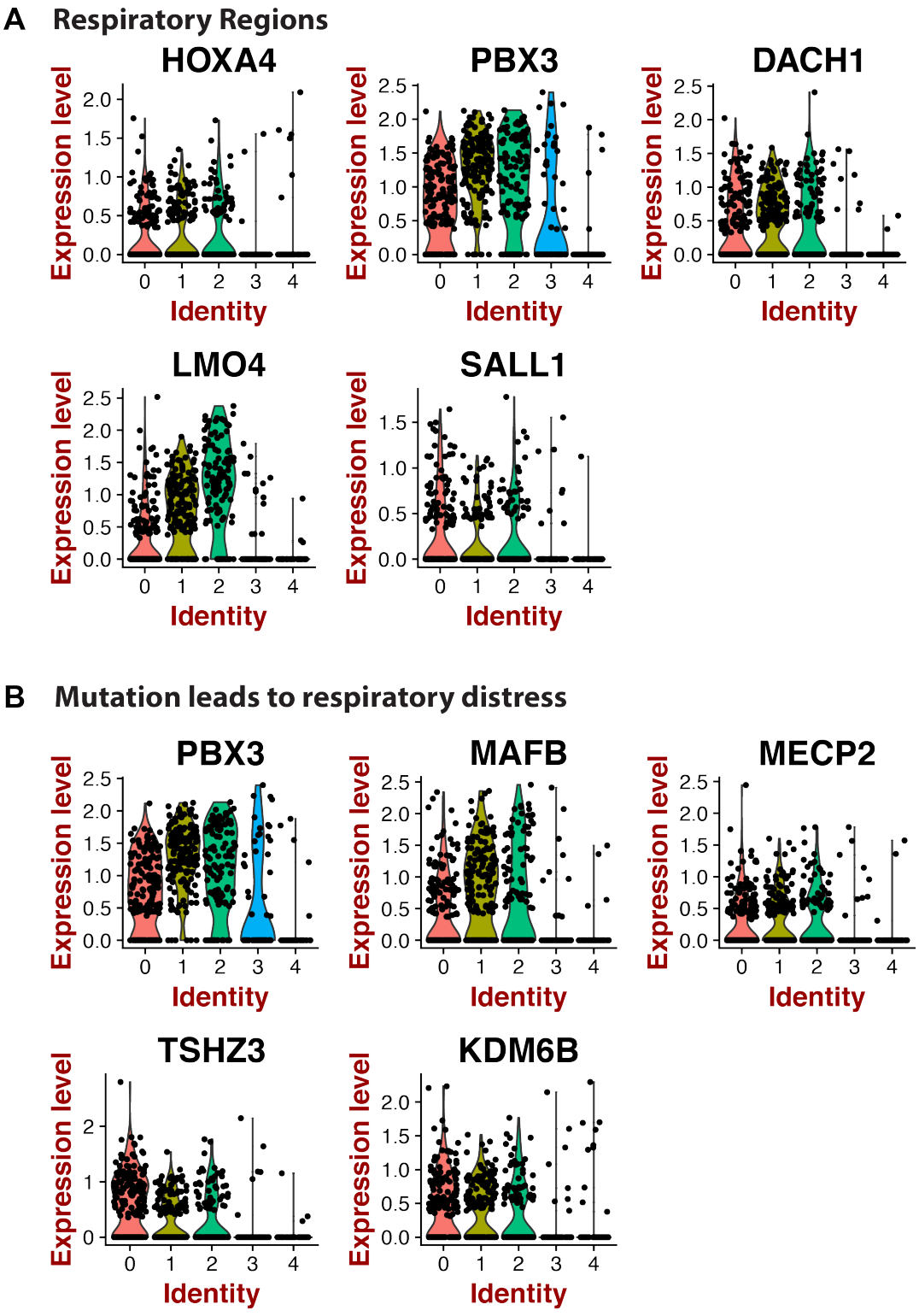

Figure 3.9: Confirmation of respiratory phenotype. A. Genes that are expressed in respiratory hindbrain regions including the Bötzinger Complex and the pre Bötzinger Complex. B. Genes implicated in respiratory distress.

3.3.4 *In Vitro* Confirmation of Hindbrain Populations

While the single cell RNA sequencing findings of a chemosensing and V0 interneuron were plausible given the signaling cues that were being provided, the results were confirmed in *in vitro* cultures. At day 17, CHX10, LHX5, PHOX2A, and PHOX2B were identified in the cultures at percentages similar to the single cell RNA sequencing representations (for cytometry: 23.6%, 11.2%, 24.6%, and 32.6%, respectively, Fig 3.10 A). Additionally, CHX10 and LHX5 were confirmed to be separate populations by dual staining and separation on the cytometry dot plot (Fig 3.10 B). Immunocytochemistry at day 17 confirmed the protein of all markers were present and distributed similarly throughout the dense cultures (Fig 3.10 C-D). Cultures were then dissociated and replated for 6 days to observe colocalization and neurite outgrowth. CHX10 and LHX5 expression was not co-localized, which visually confirmed the V2a and V0 interneurons as separate cell populations (Fig 3.10 E). As demonstrated by the single cell RNA sequencing, there was overlap of PHOX2A and PHOX2B expression (pointed arrowheads, Fig 3.10 F). However, $PHOX2A^-/PHOX2B^+$ (full arrowheads) but not $PHOX2A^+/PHOX2B^-$ cells were detected potentially indicating that PHOX2B expression precedes PHOX2A expression (Fig 3.10 F). All of these populations were expressed β_{III} Tubulin, a neuronal marker, and have extensive neurite outgrowth (Fig 3.10 E-F). *In vitro* confirmation of transcription factor expression identified in clusters 0 through 2 (PHOX2B and PHOX2A, CHX10, and LHX5) gives further support that the protocol yields V2a, V0, and chemosensing neurons.

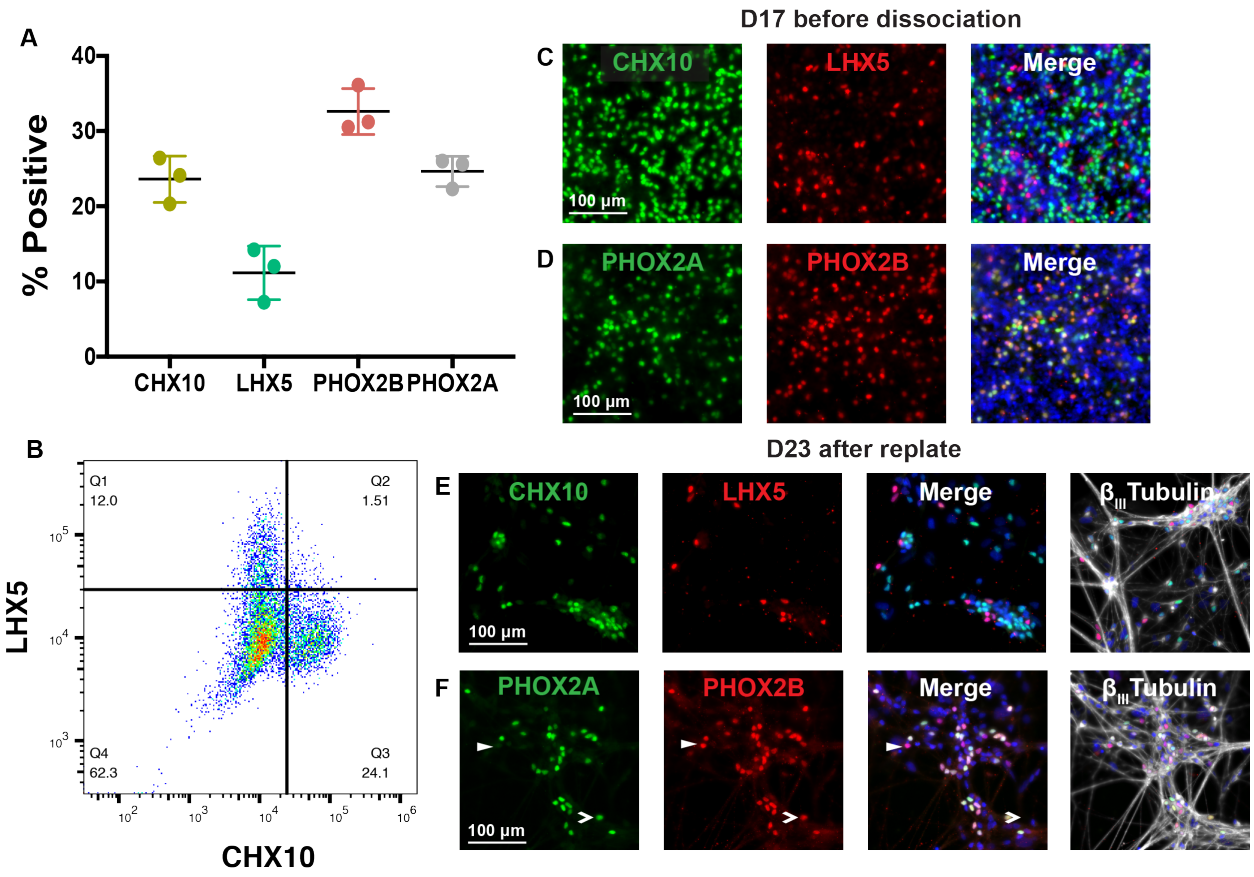

Figure 3.10: Confirmation of hindbrain respiratory populations *in vitro*. A. Flow cytometry analysis of CHX10, LHX5, PHOX2B, and PHOX2A in the hPSC-derived cultures. B. Dotplot of CHX10 and LHX5 co-staining. C. and D. Immunocytochemistry on *in vitro* cultures at day 17 of CHX10 (green) LHX5 (red) and nuclei labeling (blue, C) as well as PHOX2A (green), PHOX2B (red) and nuclei labeling (blue, D). E. and F. Immunocytochemistry on *in vitro* cultures that were dissociated at day 17 and replated for 6 days. Images show CHX10 (green), LHX5 (red), β_{III}Tubulin (white), and nuclei labeling (blue, E) as well as PHOX2A (red), PHOX2B (green), β_{III}Tubulin (white), and nuclei labeling (blue, F).

3.3.5 Manipulation of Hindbrain Interneuron Populations in Response to Shh and RA Treatment

The hindbrain interneuron populations arise in response to RA and a ventrodorsal gradient of Shh. If Shh and RA signaling modulate these populations developmentally, it was hypothesized that the relative proportion of V2a and V0 interneurons should shift in response to changes in RA and Shh concentration *in vitro*. The pur concentration was varied while keeping RA concentration at 100 nM. CHX10 percentage was greater at 30 and 100 nM pur ($p < 0.05$) while LHX5 percentage was increased at 10 and 30 nM pur compared to 100nM pur ($p < 0.05$, Fig 3.10 A). The RA concentration was then varied while keeping the pur concentration constant at 100nM. CHX10 percentage peaked at 30 – 100 nM while LHX5 percentage peaked at 10 nM (Fig 3.10 B). These studies confirm that changing concentration of pur and RA modulates relative proportions of V2a and V0 interneurons in a way predicted by developmental gradients.

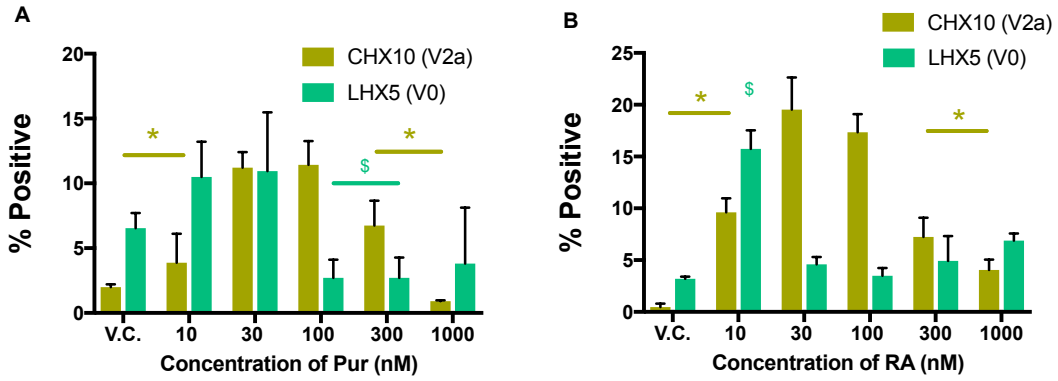

Figure 3.11: Modulation of V2a and V0 interneuron in response to purmorphamine and retinoic acid concentration. A. Flow cytometry analysis of CHX10 and LHX5 expression with varying purmorphamine (pur) concentration. * = $p<0.05$ compared to 30nM and 100nM, one-way ANVOA and Tukey post hoc comparison. $ = $p<0.05$ compared to 30nM and 30nM, one-way ANVOA and Tukey post hoc comparison. B. Flow cytometry analysis of CHX10 and LHX5 expression with varying RA concentration. * = $p<0.05$ compared to 30nM and 100nM, one-way ANVOA and Tukey post hoc comparison. $ = $p<0.05$ compared to all groups, one-way ANVOA and Tukey post hoc comparison.

3.4 Discussion

In this chapter, multiple hindbrain phenotypes including V2a and V0 interneurons as well as a chemosensing population were identified by single cell RNA sequencing to be differentiated from hPSCs in response to pur, RA, and DAPT. The three populations were then identified to exist in the *in vitro* cultures by protein and changing pur and RA concentration could modulate the relative proportions of interneurons.

This study initially described two ways to enhance the V2a phenotype – replating and WNT activation (Fig 3.1 and 4.2). Dissociation and replating steps have been utilized in differentiation protocols into other lineages, including cardiomyocytes, to purify the committed phenotype and deplete the stromal fraction (Burridge, Matsa et al. 2014). Following the replating step, there are some cells that do not attach. The hypothesis is that the neuronal phenotypes have a higher ability to reattach during replating and the more proliferative cell types (including the mesenchymal and glial fraction identified in a previous single cell RNA sequencing study) are depleted, at least temporarily. This idea is supported by the single cell RNA sequencing of a replated population presented in this study wherein the mesenchymal and glial fractions are absent. One potential reason for selective adhesion may be that the mesenchymal and glial populations do not survive the dissociation process as well as the neurons, however, further experimentation will need to be performed to elucidate the mechanism that enhances the neuronal pool after replating.

Early activation of the WNT pathway was also found to increase the V2a interneuron fraction (Fig 3.2 B). Initially, WNT activation was explored to specify a thoracic spinal phenotype (Lippmann, Williams et al. 2015). However, once the single cell analysis

revealed the hindbrain identity of the differentiation culture (Fig 3.5), alternative mechanisms for WNT signaling came to light. There is a dichotomy of WNT signaling at the interface of midbrain and hindbrain development where WNT activation specifies a hindbrain phenotype and WNT signaling is inhibited in the midbrain (Ciani and Salinas 2005). Further, in studies where WNT activation alone is used as the caudalizing agent, the resulting neurons have a hindbrain/cervical phenotype and are not able to obtain a more caudal identity. *In vivo*, FGF and GDF11 signaling is necessary for development of thoracic and more caudal identities. This has been further supported *in vitro* where addition of FGFs and GDFs may be necessary to obtain thoracic phenotypes (Lippmann, Williams et al. 2015). Early activation of the WNT pathway using CHIR99021 may aid in defining the regional specificity by reinforcing hindbrain development pathways established by RA and Shh signaling.

The development of single cell RNA sequencing technologies have become a highly valuable tool in identification of heterogeneous differentiation populations. Human PSCs-derived differentiations often result in heterogeneous cultures that are only partially defined. Traditionally, large panels of antibodies or PCR primers have been used to try to identify what additional populations are present in the cultures, however, this technique is inherently biased and under powered. Single cell analysis can provide information about 10^3 genes present in a single cell where standard 96-well or multiplexed quantitative real-time PCR analysis provides on the order of 10^1 to 10^2 genes in the whole population. Bulk RNA sequencing can provide information on 10^3 genes but there is no way to identify individual cell populations. However, single cell analysis does not come without its own caveats. The newness of single cell analysis means that the field is constantly improving the

strategies to determine the *in vivo* identity of neuronal populations. Traditionally, a few known genes have determined neuronal identity and the field is only now beginning to assign transcriptome profiles to different neuronal subpopulations at various time points in development (Hayes, Kottick et al. 2017, Lake, Chen et al. 2018, Rosenberg, Roco et al. 2018). This can make identification of hPSC derived populations inherently difficult not only because the exact developmental timeline is unknown and likely heterogeneous, but also because it is a different species origin. Fortunately, recent publication of single cell data sets from respiratory regions at different developmental stages has been an important resource for the identification of our iPSC-derived populations (Hayes, Kottick et al. 2017).

The data presented here corresponds with a data set derived from the pre BötC of P0 mice (Hayes, Kottick et al. 2017) . The study analyzed the transcriptional signature of cells that reside in the pre BötC and compared the cells that once expressed the V0 progenitor marker, Dbx1, and those that did not. In agreement with our data, the murine study identifies upregulation of Lhx5, Pax2, HoxA4, among others in the $Dbx1^{+}$ population. Additionally, Dbx1 transcript is not present in the P0 mice demonstrating that the marker turns off with maturation which supports why Dbx1 was not detected in the D17 cells. Further, PHOX2B is upregulated in the $Dbx1^{-}$ cells from the pre BötC region (Hayes, Kottick et al. 2017). This supports that PHOX2B expression is identified in a similar region yet separate from the V0 interneurons. Collectively, single cell transcriptomic analysis detected the presence of V0 interneurons and chemosensing neurons in the hPSC differentiated cultures.

In this study, three distinct populations were differentiated from one set of signaling molecules. The hindbrain originates as the neural tube and forms in response to a

ventrodorsal gradient of Shh (Marklund, Alekseenko et al. 2014). This gradient specifies different interneuron subtypes wherein V2a interneurons lie ventral to V0 interneurons. The rostrocaudal identity is influenced by RA concentration. The RA gradient appears to peak at the base of rhombomere formation and decrease in the rostral direction toward the hindbrain (Glover, Renaud et al. 2006). In the data presented here, the relative proportions of interneurons can be modulated by Shh signaling. Lower concentrations of pur induce higher percentages of V0 interneurons and lower amounts of V2a interneurons. Conversely, a higher concentration of pur results in higher percentages of V2a interneurons over V0 interneurons. Additionally, lower concentrations of RA induce higher percentages of V2a and V0 interneurons potentially indicating that the lower concentration of RA is recapitulating developmental signaling and specifies the hindbrain region which in turn increases the amount of V2a and V0s. These data indicate that developmental pathways were being probed *in vitro.* The initial intent of the study was to find the right combination of signaling molecules that resulted in the highest CHX10 percentage to induce V2a interneurons. However, a defined combination of chemical signals and culture conditions has induced a regional identity that contains the V2a interneurons, more specifically the respiratory control centers in the hindbrain. Along with that has come induction of additional cell types (V0 interneurons and chemosensing neurons) that are developmentally located in a similar region and function together as a tissue.

By definition, a tissue is composed of multiple cell populations that function together to perform a task. To engineer a functioning tissue *in vitro*, it is necessary that multiple cell types interact and operate as a unit. Traditional tissue engineering approaches have been to derive individual cell populations that compose the tissue separately and then combine

the defined cell populations together with a matrix or mold to form a tissue (Takebe, Sekine et al. 2013). However, because these cell population are derived or isolated separately, they may not mature at the same rate or contain proper support cell populations which therefore may not integrate to form the tissue-specific function. An alternate approach to *in vitro* tissue formation is co-emergence. Instead focusing on individual cell types separately, the concept of co-emergence is to differentiate multiple cell populations that arise from similar signaling mechanisms developmentally in one dish, which more accurately represents endogenous tissue formation (Sternfeld, Hinckley et al. 2017). In this study, a platform is demonstrated wherein multiple cell populations present in respiratory regions (Chemosensing, V2a and V0 interneurons) co-emerge from one developmentally relevant signaling environment. During development, differing neuronal populations arise from coordinated signaling events in combination with cell-cell signaling which is important to specification of neighboring cell types. Developmentally, V2a and V0 interneurons as well as the chemosensing population arise in the neural tube in response to Shh and RA signaling. The differentiation described here begins with a blank slate of PSCs that are first treated with dual SMAD inhibition to specify a neural progenitor state (Chambers, Fasano et al. 2009). Next, RA is added to promote a non-cortical phenotype and it is speculated that the concentration of RA used in this study is specifying a hindbrain/high cervical phenotype. Once the rostrocaudal identity is determined, Shh signaling drives the ventrodorsal identity (Dessaud, Ribes et al. 2010). At the stage where the Shh agonist is added to the *in vitro* culture, a multilayer cell sheet has formed therefore, it is possible that across the well, there are local regions of high and low Shh signaling that may specify different interneuron subtypes similar to the Shh gradient *in vivo*. This theory

was supported by observing the change in relative proportions of interneurons in response to concentration of pur (Fig 3.10). The mechanism of the chemosensing specification is still being investigated as developmentally, this population arises from the dorsal half of the neural tube in response to little Shh signaling (Sieber, Storm et al. 2007). However, the ability of these three populations to co-emerge in a dish and converge upon a combination of neurons that have a defined functional role *in vivo* seems to reflect that once the hPCSs have been pushed to a neural fate, the importance of cell-cell interactions are key in defining committed phenotypes.

3.5 Conclusion

Together, this work demonstrates how multiple neuronal populations that develop and function together *in vivo* can be differentiated from one set of signaling molecules *in vitro* from hPSCs. Single cell RNA-sequencing revealed the presence of multiple respiratory hindbrain populations in our cultures (Fig 3.6) and these findings were further confirmed by protein expression analysis (Fig 3.9). Additionally, the relative interneuron populations can be manipulated through changes in morphogen concentration demonstrating the ability to recapitulate the *in vivo* signaling environment *in vitro* (Fig 3.10). After identifying that the cultures contain multiple neurons that have genetic signatures similar to those that arise developmentally in the hindbrain and are involved in respiration, this platform presents an opportunity to explore how *in vivo* signaling pathways have be probed *in vitro.* While the work described here focuses on development of a hindbrain phenotype, a similar concept could be applied when developing directed differentiation protocols for any lineage that results in co-emergence of multiple cell types.

3.6 Bibliography

Alheid, G. F., P. A. Gray, M. C. Jiang, J. L. Feldman and D. R. McCrimmon (2002). "Parvalbumin in respiratory neurons of the ventrolateral medulla of the adult rat." J Neurocytol **31**(8-9): 693-717.

Amir, R. E., I. B. Van den Veyver, M. Wan, C. Q. Tran, U. Francke and H. Y. Zoghbi (1999). "Rett syndrome is caused by mutations in X-linked MECP2, encoding methyl-CpG-binding protein 2." Nat Genet **23**(2): 185-188.

Azim, E., J. Jiang, B. Alstermark and T. M. Jessell (2014). "Skilled reaching relies on a V2a propriospinal internal copy circuit." Nature **508**(7496): 357-363.

Blanchi, B., L. M. Kelly, J. C. Viemari, I. Lafon, H. Burnet, M. Bevengut, S. Tillmanns, L. Daniel, T. Graf, G. Hilaire and M. H. Sieweke (2003). "MafB deficiency causes defective respiratory rhythmogenesis and fatal central apnea at birth." Nat Neurosci **6**(10): 1091-1100.

Bochorishvili, G., R. L. Stornetta, M. B. Coates and P. G. Guyenet (2012). "Pre-Botzinger complex receives glutamatergic innervation from galaninergic and other retrotrapezoid nucleus neurons." J Comp Neurol **520**(5): 1047-1061.

Bouvier, J., M. Thoby-Brisson, N. Renier, V. Dubreuil, J. Ericson, J. Champagnat, A. Pierani, A. Chedotal and G. Fortin (2010). "Hindbrain interneurons and axon guidance signaling critical for breathing." Nat Neurosci **13**(9): 1066-1074.

Burgold, T., N. Voituron, M. Caganova, P. P. Tripathi, C. Menuet, B. K. Tusi, F. Spreafico, M. Bevengut, C. Gestreau, S. Buontempo, A. Simeone, L. Kruidenier, G. Natoli, S. Casola, G. Hilaire and G. Testa (2012). "The H3K27 demethylase JMJD3 is required for maintenance of the embryonic respiratory neuronal network, neonatal breathing, and survival." Cell Rep **2**(5): 1244-1258.

Burridge, P. W., E. Matsa, P. Shukla, Z. C. Lin, J. M. Churko, A. D. Ebert, F. Lan, S. Diecke, B. Huber, N. M. Mordwinkin, J. R. Plews, O. J. Abilez, B. Cui, J. D. Gold and J. C. Wu (2014). "Chemically defined generation of human cardiomyocytes." Nat Methods **11**(8): 855-860.

Butts, J. C., D. A. McCreedy, J. A. Martinez-Vargas, F. N. Mendoza-Camacho, T. A. Hookway, C. A. Gifford, P. Taneja, L. Noble-Haeusslein and T. C. McDevitt (2017). "Differentiation of V2a interneurons from human pluripotent stem cells." Proc Natl Acad Sci U S A **114**(19): 4969-4974.

Chambers, S. M., C. A. Fasano, E. P. Papapetrou, M. Tomishima, M. Sadelain and L. Studer (2009). "Highly efficient neural conversion of human ES and iPS cells by dual inhibition of SMAD signaling." Nat Biotechnol **27**(3): 275-280.

Ciani, L. and P. C. Salinas (2005). "WNTs in the vertebrate nervous system: from patterning to neuronal connectivity." Nat Rev Neurosci **6**(5): 351-362.

Crone, S. A., K. A. Quinlan, L. Zagoraiou, S. Droho, C. E. Restrepo, L. Lundfald, T. Endo, J. Setlak, T. M. Jessell, O. Kiehn and K. Sharma (2008). "Genetic ablation of V2a ipsilateral interneurons disrupts left-right locomotor coordination in mammalian spinal cord." Neuron **60**(1): 70-83.

Crone, S. A., J. C. Viemari, S. Droho, A. Mrejeru, J. M. Ramirez and K. Sharma (2012). "Irregular Breathing in Mice following Genetic Ablation of V2a Neurons." J Neurosci **32**(23): 7895-7906.

Dauger, S., A. Pattyn, F. Lofaso, C. Gaultier, C. Goridis, J. Gallego and J. F. Brunet (2003). "Phox2b controls the development of peripheral chemoreceptors and afferent visceral pathways." Development **130**(26): 6635-6642.

Dessaud, E., V. Ribes, N. Balaskas, L. L. Yang, A. Pierani, A. Kicheva, B. G. Novitch, J. Briscoe and N. Sasai (2010). "Dynamic assignment and maintenance of positional identity in the ventral neural tube by the morphogen sonic hedgehog." PLoS Biol **8**(6): e1000382.

Dobin, A., C. A. Davis, F. Schlesinger, J. Drenkow, C. Zaleski, S. Jha, P. Batut, M. Chaisson and T. R. Gingeras (2013). "STAR: ultrafast universal RNA-seq aligner." Bioinformatics **29**(1): 15-21.

Du, Z. W., H. Chen, H. Liu, J. Lu, K. Qian, C. L. Huang, X. Zhong, F. Fan and S. C. Zhang (2015). "Generation and expansion of highly pure motor neuron progenitors from human pluripotent stem cells." Nat Commun **6**: 6626.

Elkouby, Y. M. and D. Frank (2010). Wnt/beta-Catenin Signaling in Vertebrate Posterior Neural Development. San Rafael (CA).

Ellenberger, H. H. and J. L. Feldman (1990). "Brainstem connections of the rostral ventral respiratory group of the rat." Brain Res **513**(1): 35-42.

Ericson, J., P. Rashbass, A. Schedl, S. Brenner-Morton, A. Kawakami, V. van Heyningen, T. M. Jessell and J. Briscoe (1997). "Pax6 controls progenitor cell identity and neuronal fate in response to graded Shh signaling." Cell **90**(1): 169-180.

Ezure, K., M. Manabe and H. Yamada (1988). "Distribution of medullary respiratory neurons in the rat." Brain Res **455**(2): 262-270.

Funk, G. D., J. C. Smith and J. L. Feldman (1993). "Generation and transmission of respiratory oscillations in medullary slices: role of excitatory amino acids." J Neurophysiol **70**(4): 1497-1515.

Gaunt, S. J., R. Krumlauf and D. Duboule (1989). "Mouse homeo-genes within a subfamily, Hox-1.4, -2.6 and -5.1, display similar anteroposterior domains of expression in the

embryo, but show stage- and tissue-dependent differences in their regulation." Development **107**(1): 131-141.

Glover, J. C., J. S. Renaud and F. M. Rijli (2006). "Retinoic acid and hindbrain patterning." J Neurobiol **66**(7): 705-725.

Gray, P. A. (2008). "Transcription factors and the genetic organization of brain stem respiratory neurons." J Appl Physiol (1985) **104**(5): 1513-1521.

Gray, P. A., J. A. Hayes, G. Y. Ling, I. Llona, S. Tupal, M. C. Picardo, S. E. Ross, T. Hirata, J. G. Corbin, J. Eugenin and C. A. Del Negro (2010). "Developmental origin of preBotzinger complex respiratory neurons." J Neurosci **30**(44): 14883-14895.

Gray, P. A., J. C. Rekling, C. M. Bocchiaro and J. L. Feldman (1999). "Modulation of respiratory frequency by peptidergic input to rhythmogenic neurons in the preBotzinger complex." Science **286**(5444): 1566-1568.

Greer, J. J., J. C. Smith and J. L. Feldman (1991). "Role of excitatory amino acids in the generation and transmission of respiratory drive in neonatal rat." J Physiol **437**: 727-749.

Hayes, J. A., A. Kottick, M. C. D. Picardo, A. D. Halleran, R. D. Smith, G. D. Smith, M. S. Saha and C. A. Del Negro (2017). "Transcriptome of neonatal preBotzinger complex neurones in Dbx1 reporter mice." Sci Rep **7**(1): 8669.

Hernandez-Miranda, L. R. and C. Birchmeier (2015). "CO(2) in the spotlight." Elife **4**.
Krumlauf, R., H. Marshall, M. Studer, S. Nonchev, M. H. Sham and A. Lumsden (1993). "Hox homeobox genes and regionalisation of the nervous system." J Neurobiol **24**(10): 1328-1340.

Lake, B. B., S. Chen, B. C. Sos, J. Fan, G. E. Kaeser, Y. C. Yung, T. E. Duong, D. Gao, J. Chun, P. V. Kharchenko and K. Zhang (2018). "Integrative single-cell analysis of transcriptional and epigenetic states in the human adult brain." Nat Biotechnol **36**(1): 70-80.

Li, W., W. Sun, Y. Zhang, W. Wei, R. Ambasudhan, P. Xia, M. Talantova, T. Lin, J. Kim, X. Wang, W. R. Kim, S. A. Lipton, K. Zhang and S. Ding (2011). "Rapid induction and long-term self-renewal of primitive neural precursors from human embryonic stem cells by small molecule inhibitors." Proc Natl Acad Sci U S A **108**(20): 8299-8304.

Lippmann, E. S., C. E. Williams, D. A. Ruhl, M. C. Estevez-Silva, E. R. Chapman, J. J. Coon and R. S. Ashton (2015). "Deterministic HOX patterning in human pluripotent stem cell-derived neuroectoderm." Stem Cell Reports **4**(4): 632-644.

Macosko, E. Z., A. Basu, R. Satija, J. Nemesh, K. Shekhar, M. Goldman, I. Tirosh, A. R. Bialas, N. Kamitaki, E. M. Martersteck, J. J. Trombetta, D. A. Weitz, J. R. Sanes, A. K. Shalek, A. Regev

and S. A. McCarroll (2015). "Highly Parallel Genome-wide Expression Profiling of Individual Cells Using Nanoliter Droplets." Cell **161**(5): 1202-1214.

Marklund, U., Z. Alekseenko, E. Andersson, S. Falci, M. Westgren, T. Perlmann, A. Graham, E. Sundstrom and J. Ericson (2014). "Detailed expression analysis of regulatory genes in the early developing human neural tube." Stem Cells Dev **23**(1): 5-15.

Marshall, H., S. Nonchev, M. H. Sham, I. Muchamore, A. Lumsden and R. Krumlauf (1992). "Retinoic acid alters hindbrain Hox code and induces transformation of rhombomeres 2/3 into a 4/5 identity." Nature **360**(6406): 737-741.

Maury, Y., J. Come, R. A. Piskorowski, N. Salah-Mohellibi, V. Chevaleyre, M. Peschanski, C. Martinat and S. Nedelec (2015). "Combinatorial analysis of developmental cues efficiently converts human pluripotent stem cells into multiple neuronal subtypes." Nat Biotechnol **33**(1): 89-96.

Mulkey, D. K., R. L. Stornetta, M. C. Weston, J. R. Simmons, A. Parker, D. A. Bayliss and P. G. Guyenet (2004). "Respiratory control by ventral surface chemoreceptor neurons in rats." Nat Neurosci **7**(12): 1360-1369.

Rhee, J. W., A. Arata, L. Selleri, Y. Jacobs, S. Arata, H. Onimaru and M. L. Cleary (2004). "Pbx3 deficiency results in central hypoventilation." Am J Pathol **165**(4): 1343-1350.

Rosenberg, A. B., C. M. Roco, R. A. Muscat, A. Kuchina, P. Sample, Z. Yao, L. T. Graybuck, D. J. Peeler, S. Mukherjee, W. Chen, S. H. Pun, D. L. Sellers, B. Tasic and G. Seelig (2018). "Single-cell profiling of the developing mouse brain and spinal cord with split-pool barcoding." Science **360**(6385): 176-182.

Satija, R., J. A. Farrell, D. Gennert, A. F. Schier and A. Regev (2015). "Spatial reconstruction of single-cell gene expression data." Nat Biotechnol **33**(5): 495-502.

Shahbazian, M. D. and H. Y. Zoghbi (2001). "Molecular genetics of Rett syndrome and clinical spectrum of MECP2 mutations." Curr Opin Neurol **14**(2): 171-176.

Shimojo, D., K. Onodera, Y. Doi-Torii, Y. Ishihara, C. Hattori, Y. Miwa, S. Tanaka, R. Okada, M. Ohyama, M. Shoji, A. Nakanishi, M. Doyu, H. Okano and Y. Okada (2015). "Rapid, efficient, and simple motor neuron differentiation from human pluripotent stem cells." Mol Brain **8**(1): 79.

Sieber, M. A., R. Storm, M. Martinez-de-la-Torre, T. Muller, H. Wende, K. Reuter, E. Vasyutina and C. Birchmeier (2007). "Lbx1 acts as a selector gene in the fate determination of somatosensory and viscerosensory relay neurons in the hindbrain." J Neurosci **27**(18): 4902-4909.

Smith, J. C., H. H. Ellenberger, K. Ballanyi, D. W. Richter and J. L. Feldman (1991). "Pre-Botzinger complex: a brainstem region that may generate respiratory rhythm in mammals." Science **254**(5032): 726-729.

Sternfeld, M. J., C. A. Hinckley, N. J. Moore, M. T. Pankratz, K. L. Hilde, S. P. Driscoll, M. Hayashi, N. D. Amin, D. Bonanomi, W. D. Gifford, K. Sharma, M. Goulding and S. L. Pfaff (2017). "Speed and segmentation control mechanisms characterized in rhythmically-active circuits created from spinal neurons produced from genetically-tagged embryonic stem cells." Elife **6**.

Stornetta, R. L., T. S. Moreira, A. C. Takakura, B. J. Kang, D. A. Chang, G. H. West, J. F. Brunet, D. K. Mulkey, D. A. Bayliss and P. G. Guyenet (2006). "Expression of Phox2b by brainstem neurons involved in chemosensory integration in the adult rat." J Neurosci **26**(40): 10305-10314.

Takebe, T., K. Sekine, M. Enomura, H. Koike, M. Kimura, T. Ogaeri, R. R. Zhang, Y. Ueno, Y. W. Zheng, N. Koike, S. Aoyama, Y. Adachi and H. Taniguchi (2013). "Vascularized and functional human liver from an iPSC-derived organ bud transplant." Nature **499**(7459): 481-484.

van der Maaten LJP, H. G. (2008). "Visualizing High-Dimensional Data Using t-SNE." Journal of Machine Learning Research **9**: 2579-2605.

Wang, H., R. L. Stornetta, D. L. Rosin and P. G. Guyenet (2001). "Neurokinin-1 receptor-immunoreactive neurons of the ventral respiratory group in the rat." J Comp Neurol **434**(2): 128-146.

Wang, S., Y. Shi, S. Shu, P. G. Guyenet and D. A. Bayliss (2013). "Phox2b-expressing retrotrapezoid neurons are intrinsically responsive to H+ and CO2." J Neurosci **33**(18): 7756-7761.

White, R. J., Q. Nie, A. D. Lander and T. F. Schilling (2007). "Complex regulation of cyp26a1 creates a robust retinoic acid gradient in the zebrafish embryo." PLoS Biol **5**(11): e304.

Yackle, K., L. A. Schwarz, K. Kam, J. M. Sorokin, J. R. Huguenard, J. L. Feldman, L. Luo and M. A. Krasnow (2017). "Breathing control center neurons that promote arousal in mice." Science **355**(6332): 1411-1415.

Zhong, G., S. Droho, S. A. Crone, S. Dietz, A. C. Kwan, W. W. Webb, K. Sharma and R. M. Harris-Warrick (2010). "Electrophysiological characterization of V2a interneurons and their locomotor-related activity in the neonatal mouse spinal cord." J Neurosci **30**(1): 170-182.

Chapter 4: Generation of Respiratory Hindbrain Organoids

4.2 Introduction

Previous studies have defined a monolayer culture system wherein multiple respiratory populations that typically arise in the hindbrain including V2a and V0 interneurons as well as a chemosensing population co-emerged. These populations have been described to work in tandem to control respiration *in vivo*. Monolayer cultures provide a platform to test culture conditions in a high throughput manor, however, cell-cell interactions are limited. Therefore, we wanted to observe how these populations would organize and mature in a three-dimensional (3D) system where cell interactions are less constrained. The following study describes the formation of hindbrain organoids and evaluates the changes in morphology and cell-type specific markers during the induction and maturation processes. The organoids display synchronous activity as they mature similar to what has been reported from native respiratory structures. This study provides the first report of a hindbrain organoids system that contains cell populations critical to respiration.

3D cultures systems have been a common platform for neural stem cell differentiations since the onset of the field. The first directed motor neuron differentiation protocol began with spontaneous formation of the stem cells into clusters of cells called embyroid bodies (Wichterle, Lieberam et al. 2002). However, in recent years, 3D neural

culture has expanded to include organoids wherein stem cells are directed to a neural fate as multiple cell types co-emerge with some organization that resembles aspects of the native tissue. While 3D culture models have been explored since the early 1990s (Barcellos-Hoff, Aggeler et al. 1989, Petersen, Ronnov-Jessen et al. 1992), one of the first reports of an organoid system recapitulated cerebral development (Lancaster, Renner et al. 2013). In the last 10 years, many different neural organoids have been described that recapitulate a variety of neural structures including the retina, forebrain, midbrain cerebellum, and hypothalamus (Eiraku, Watanabe et al. 2008, Wataya, Ando et al. 2008, Muguruma, Nishiyama et al. 2010, Kadoshima, Sakaguchi et al. 2013, Jo, Xiao et al. 2016). Ideally, more than just structural similarity, an organoid would have a greater ability to generate a tissue-specific function that is not possible in a two dimensional system. To date, an organoid system that resembles the hindbrain and provides a platform to probe respiratory control has not been described. This study expands the previously described 2D culture conditions to co-emerge multiple hindbrain respiratory populations and provides a 3D hindbrain-like organoid system to model the neural circuits that control respiratory rhythm generation.

Respiration is a controlled closed-loop system that broadly incorporates neurons, the muscles that control lung volume, and the partial pressure of $C0_2$ ($pC0_2$) in the blood stream. The main sensor in this circuit is the chemosensing neuron in the hindbrains that sense changes in $pC0_2$, which provide input onto pre-inspiratory and pre-expiratory neurons in the medulla (Goridis, Dubreuil et al. 2010, Ruffault, D'Autreaux et al. 2015). The pre-inspiratory and pre-expiratory neurons then transduce signals to the phrenic motor neurons that form a neuro-muscular junction with the diaphragm and intercostal muscles

to control inspiration and expiration (Boulenguez, Gauthier et al. 2007). Oxygen exchange with the outside environment during inspiration and expiration alters $pC0_2$, which is then again sensed by the chemosensing population in the hindbrain, closing the respiration control circuit (Feldman, Mitchell et al. 2003, Guyenet, Stornetta et al. 2010). Researchers have worked to determine the phenotypic identity of the cells responsible for each of these critical circuit components.

The chemosensing neurons of the circuit are located in the retrotrapezoid nucleus/pre facial respiratory group (RTN/pFRG) (Mulkey, Stornetta et al. 2004, Stornetta, Moreira et al. 2006). This structure resides in the rostral aspect of the ventral respiratory group (VRG) in the ventrolateral medulla. The RTN is a nuclei of thousands of cells comprised of glutamatergic chemosensing neurons that express PHOX2B and detect pCO_2 in the bloodstream by a proton receptor (Wang, Shi et al. 2013). Together, the RTN/pFRG comprise the large majority of what have been called pre-inspiratory neurons in the respiratory rhythm generating circuit. The chemosensing neurons in the RTN are not rhythmic themselves but do form direct synapses with rhythmic inspiratory neurons located in the pre BötC (Mulkey, Stornetta et al. 2004, Guyenet, Mulkey et al. 2005).

The pre BötC is located caudal to the RTN in the VRG and is composed of a variety of cell types that are involved in respiratory rhythm generation as well as sighing behavior (Smith, Ellenberger et al. 1991). The cells of the pre BötC have been reported to be a combination of glutamatergic, glycinergic, and GABAergic neurons however, the excitatory signals are a necessary component for respiratory rhythm generation (Bouvier, Thoby-Brisson et al. 2010, Gray, Hayes et al. 2010). Consistent with their role in rhythm generation, neurons in the pre BötC produce a $Ca2^+$ flux that is synchronous and periodic

(Koizumi, Koshiya et al. 2013). Recent studies implicate commissural V0 interneurons that arise from Dbx1^{+} progenitors to be a critical neuronal subtype responsible for the pacing behavior of the pre BötC by providing a synchronous oscillatory output to pre motor populations (Wu, Capelli et al. 2017).

Medullary V2a interneurons located in the medial reticular formation also provide excitatory input into the pre BötC . The V2a interneurons are located at the same rostrocaudal level but medial to the pre BötC in the medulla. Ablation of these cells results in an irregular breathing pattern (Crone, Viemari et al. 2012). Electrophysiological analysis combined with synaptic tracing revealed V2a interneurons form excitatory synapses with tonic input onto cells in the pre BötC. While the synaptic target of the V2a interneurons in the pre BötC was not identified, it was hypothesized that the V0 interneurons are a potential target due to the known interactions of V2a and V0 interneurons in spinal motor circuits (Crone, Viemari et al. 2012). Together, chemosensing neurons in the RTN/pFRG and V2a interneurons in the mRF provide excitatory drive to the V0 interneurons in the pre BötC, which then produce a rhythmic output to control respiration. Together, the chemosensing, V2a, and V0 interneurons form a specific balanced neural circuit that one disrupted connection could lead to dysfunction.

Congenital central hypoventilation syndrome (CCHS) is a disease caused by a polyalanine expansion in *PHOX2B*, which disrupts the function of chemosensing neurons (Amiel, Laudier et al. 2003, Trochet, Hong et al. 2005). The lack of CO_2 sensing causes individuals to take shallow breaths and results in a build up of CO_2 and a lack of oxygen in the blood stream. Symptoms of CCHS are typically identified soon after birth and the current standard of care is a ventilator or a diaphragm pacemaker. While this disease is

considered to be rare, it has been identified as a potential cause of Sudden Infant Death Syndrome (SIDS) (Weese-Mayer, Berry-Kravis et al. 2008). Additionally, symptoms of CCHS can arise later in life without genetic mutation but in response to injury. In this study, we use a cell line with a Y14X mutation in the *PHOX2B* loci that diminishes the chemosensing population in our cultures to model CCHS in organoid culture (Workman, Mahe et al. 2017)

The following study describes the first report of a hindbrain organoid composed of neurons that are involved in respiratory control. The neurodevelopment of and function of the hindbrain interneuron populations can now be studied by assessing the differentiation, maturation, and function of these organoids. Additionally, as the organoids mature, they can be used as a model to assess how changes in respiratory circuit composition in response to injury or disease alters the functional output.

4.2 Materials and Methods

4.2.1 Human Pluripotent Stem Cell Culture

Human PSCs—WTC and WTB iPSCs (generously donated by Bruce Conklin)—were grown to 70% confluence and passaged using Accutase (Accutase, San Diego, CA) to dissociate to single cells (incubated at 37°C for 5 minutes). Dissociated cells were replated on Matrigel-coated cultureware (hESC-qualified for ESCs and growth factor reduced for iPSCs) at a density of 10,000 cells per cm^2 with 10μM ROCK inhibitor (Y-27632, Selleckchem, Houston, TX) in mTeSR (StemCell Technologies, Vancouver, Canada). All work with human ESC and iPSC lines have been approved by the University of California – San Francisco Human Gamete, Embryo and Stem Cell Research (GESCR) Committee.

4.2.2 V2a interneuron Differentiation in 3D Organoid Culture

Human PSCs were seeded at 125k cells/cm^2 in mTeSR supplemented with 10μM ROCK inhibitor and 2 μM CHIR99102. For WNT treated cells, CHIR was supplemented into the media at each feed through day 7. 48 hours later, cell layers were dissociated using Accutase and counted. For organoid culture, 800μm pyramidal PDMS inserts were placed into 24-well plates. 1 ml mTeSR containing 10μM ROCK inhibitor was added to the wells containing the molds and the plate was centrifuged at 2,000 x g for 3 minutes to get rid of any bubbles. Dissociated cells, either hPSCs or WNT pre-treated cells, were then added slowly into the wells at 10,000 cells per organoid in mTeSR supplemented with 10μM ROCK inhibitor, 0.2 LDN193189, and 10μM SB431542 (StemGent, Cambridge, MA). Twenty-four hours later, the organoids condensed to spheres and were washed out by gentle trituration with a p1000 pipette into a conical. After the organoids had settled, the spent media was aspirated and resuspended in mTeSR containing 10μM ROCK inhibitor, 0.2 LDN193189, and 10μM SB431542 and placed into 1 well of a 6-well plate. To change the media on the cells for the rest of the differentiation, the organoids were pipetted into a conical and allowed to settle. Old media was aspirated off and new media was used to resuspend the organoids and transfer them back to the 6 well. On day 3, medium was changed to mTeSR supplemented with dual SMAD inhibitors only. On day 5, the base medium was switched to neural induction medium (DMEM F:12 (Corning, Corning, NY), N2 supplement (Life Technologies, Carlsbad, CA), L-Glutamine (VWR), 2μg/ml heparin (Sigma Aldrich, St. Louis, MO), non-essential amino acids (Mediatech INC, Manassas, VA), penicillin-streptomycin (VWR) supplemented with fresh 0.4μg/ml ascorbic acid (Sigma Aldrich) and 10ng/ml brain derived neurotrophin factor (BDNF, R&D Systems,

Minneapolis, MN)) supplemented with dual SMAD inhibitors and 10nM–10μM retinoic acid (Sigma Aldrich). On day 7, dual SMAD inhibition was ceased and 10nM–10μM retinoic acid, 10nM–10μM pur (EMD Millipore, Darmstast, Germany) and 1μM N-[N-(3,5-difluorophenacetyl)-L-alanyl]-S-phenylglycine t-butyl ester (DAPT) were added to the neural induction medium. Medium was changed every 2 days throughout the differentiation, with fresh supplements added each time for up to 17 to 19 days.

4.2.3 Dissociation of V2a Interneuron Organoid Cultures

To dissociate organoid cultures, samples were collected and washed with 1 mL of PBS. The organoids were then transferred to 1 well of a 6-well plate with 2ml of accutase and incubated on the rotary at 37°C for 15 minutes. The organoids were triturated approximately 10 times every 15 minutes with a p1000 to break up cell clusters until the cells were completely dissociated – typically 45 minutes to 1 hour. The dissociated cells were then transpired to a 15 mL conical and diluted with 3 times the volume of PBS.

4.2.4 Neuronal Maturation

On day 17 of differentiation, organoids were switched to neural maturation medium (BrainPhys plus SM1 supplement (Stemcell Technologies (Bardy, van den Hurk et al. 2016)) supplemented with 10 ng/ml of BDNF, GDNF, CNTF, and IGF, R&D Systems). Medium was completely changed every 5 days for the remainder of the culture duration.

4.2.5 Flow Cytometry

At day 17 of differentiation, cells were completely dissociated using Accutase and stained with the Transcription Factor Buffer Set, which includes a fixation/permeabilization (FP) and wash/permeabilization (WP) buffer (BD Biosciences, Franklin Lakes, NJ). Dissociated samples were first fixed for 45 minutes at 4°C in the FP buffer followed by a 20 minute block with WP buffer containing 5% normal donkey serum (NDS, Jackson Laboratory, Bay Harbor, ME). Primary antibodies against CHX10, LHX5, PHOX2A, and PHOX2B (Table 4.1) and the proper matching species isotype control were added into WP buffer containing 2% NDS and incubated at 4°C for 45 minutes. After two washes with WP buffer, secondary antibodies donkey anti-mouse IgG, Alexa Fluor 488 (Life Technologies), at a dilution of 1:200, were added to WP buffer and incubated at 4°C for 45 minutes. After two washes with WP buffer, samples were passed through a 35-μm filter before assessing with a BD Accuri C6 (BD) cytometer (minimum 10,000 events). Cytometry analysis was performed using FlowJo V10 (Flowjo, Ashland, OR).

4.2.6 Organoid Tissue Processing

Organoids were first fixed with 4% paraformaldehyde for 1 hour at room temperature while rotating on a rotisserie. The paraformaldehyde was removed and the organoids were resuspended in PBS and stored at 4°C until embedding was performed. For embedding, the tissues were resuspended in 300 μl histogel (Thermo Scientific), dispensed into a tissue mold and solidified at 4°C for 1 hour. The histogel molds containing the organoids were then dispensed into tissue processing cassettes and processed into paraffin blocks. Tissue blocks were sectioned into 5 μm sections, placed onto microscope slides and incubated at 37 °C overnight before antigen retrieval and staining.

4.2.7 Histological Processing and Immunostaining of Organoid Tissue Sections

Slides containing the paraffin sections were deparaffinized prior to staining using a series of xylene and alcohol washes. Slides were then washed 3 times in PBS for 5 minutes at room temperature. For antigen retrieval, slides were incubated in antigen unmasking solution (Vector Laboratories) at 95 °C for 35 minutes and cooled for 25 minutes at room temperature. Slides were washed 3 times in PBS for 5 minutes at room temperature. The individual sections were then outlined using a wax pen. The samples were permeabilized briefly with 0.2% triton for 5 minutes at room temperature. Following 3 washes for 5 minutes, the samples were blocked in PBS containing 5% NDS. Primary antibodies were added to PBS containing 2% NDS at a dilution listed in Table 4.1 and incubated on the samples overnight at 4°C. Following three 15 minutes washes, secondary antibodies were added at a dilution of 1:200 in PBS containing 2% NDS and incubated at room temperature for 1 hour. Following a 10 minute incubation of Hoechst in PBS, slides were washed 3 times in PBS for 5 minutes. The slides were mounted with ProLong Gold (Life Technologies) and cover glass. For long-term storage, the cover glass was secured with nail polish and kept in 4°C.

For hematoxylin and eosin (H&E) staining, a standard protocol was followed. Briefly, slides were deparaffinized and re-hydrated followed by 5 minutes of Gill's Hematoxylin (Newcomersupply) and a series of washes. Slides were then counterstained in Eosin-Y (Newcomersupply) for 1 minute followed by a series of alcohol then zylene washes. Slides were then coversliped with Cytoseal (Richard-Allen Scientific). Florescent slides were imaged using a Zeiss Axio Observer inverted wide-field microscope equipped

with an Apotome structured light attachment. An average intensity projection was performed on Z-stack images to create a single two-dimensional image spanning the entire thickness of the observed field. H&E slides were imaged using the Zeiss Axio Imager upright microscope. Images were processed using Zen Blue and Photoshop.

4.2.8 Immunocytochemistry and Imaging of Whole Mount Organoids

Whole mount organoids were fixed using 4% paraformaldehyde (VWR) for 1 hour at room temperature. For all steps of the staining process, samples were rotating on a rotisserie. The samples were then permeabilized using 0.1% Triton-X in PBS for 15 minutes at 4° C before blocking for 1 hour at 4°C with PBS containing 0.1% bovine serum albumin (BSA) and 5% NDS. Primary antibodies (Table 4.1) were diluted in PBS containing 0.1 % BSA and 2% NDS then incubated overnight. Samples were washed three times with PBS for 15 minutes at room temperature before incubating with secondary antibodies (Life Technologies) diluted in PBS containing 0.1% BSA and 2% NDS. Hoechst was added to the samples for 10 minutes then washed. Organoids were imaged with a Zeiss LSM880 Confocal. Intensity levels were uniformly adjusted using Zen Blue.

4.2.9 Phase Imaging Quantification

Phase contrast images of the organoids were taken using the EVOS FL Imaging System. The size analysis performed in Fig 4.1 was performed manually using Image J. The size analysis performed in Fig 4.2 was done using a Python script to first segment the organoids using a watershed segmentation algorithm. The long and short axis was then extracted from the segmented image and plotted using Prism 7 software.

Antibody Target	Species	Vendor	Cat. Number	Application	Dilution
βIII Tubulin	rabbit	Covance	PRB-435P-100	ICC	1 to 1000
CHX10	mouse	Santa Cruz	sc-374151	Flow and ICC	1 to 1000
E-Cadherin	mouse	Abcam	AB1416	ICC	1 to 400
EVX1/2	mouse	DHSB	99.1-3A2	ICC	1 to 100
GABA	rabbit	Sigma-Aldrich	A2052	ICC	1 to 1000
Glial Fibrillary Acidic Protein (GFAP)	chicken	Aves Labs	GFAP	ICC	1 to 1000
GXB2	rabbit	Proteintech	21639-1-AP	ICC	1 to 50
Ki67	rabbit	Abcam	AB15580	ICC	1 to 500
LHX5	goat	R&D	AF6290	Flow and ICC	1 to 250
Myelin Basic Protein (MBP)	chicken	Thermo Fisher	PA1-10008	ICC	1 to 1000
N-Cadherin	rabbit	Abcam	AB76057	ICC	1 to 50
NESTIN	mouse	Santa Cruz	sc-23927	ICC	1 to 100
NeuN	chicken	Millipore (EMD)	abN91	ICC	1 to 200
NeuN	rabbit	Millipore (EMD)	ABN91	ICC	1 to 200
OCT4	goat	Santa Cruz	sc-8629	ICC	1 to 400
OLIG2	rabbit	Millipore (EMD)	AB9610	ICC	1 to 500
PAX6	mouse	Santa Cruz	sc-81352	ICC	1 to 200
PH3	mouse	Cell Signaling	33775	ICC	1 to 500
PHOX2A	mouse	Santa Cruz	81978	Flow and ICC	1 to 250
PHOX2B	mouse	Santa Cruz	376997	Flow	1 to 500
PHOX2B	goat	R&D	AF4940	ICC	1 to 250
SOX2	mouse	Abcam	AB79352	ICC	1 to 200
Synaptophysin	rabbit	Synaptic Systems	101 002	ICC	1 to 200
Tau	mouse	BioLegend	835201	ICC	1 to 250
VGLUT2	rabbit	Synaptic Systems	135 403	ICC	1 to 500
ZO1	mouse	Life Technologies	359100	ICC	1 to 400

Table 4.1: Antibodies used for flow cytometry and immunostaining

4.2.10 Calcium Imaging and Analysis

Endogenous GCaMP6 signal was used to detect calcium flux in differentiations performed with the WTC GCaMP6 cell line. Alternatively, cultures of cells that lacked GCaMP expression were washed with PBS and the medium was replaced with Neurobasal plus Fluo4 AM (5μM, Life Technologies) for 1 hour at 37° C. The cultures were then washed with fresh Neurobasal and allowed to recover for an additional 1 hour minutes at 37°C before recording on a Zeiss Axio Observer. To assess Ca^{2+} fluctuations, cultures were imaged at a rate of 17 frames per second. To analyze the results, ROI were selected by hand using Zen software. For organoids, the outer edge of the tissue was selected and for monolayer cultures, individual neurons were selected. The relative fluorescent units (RFU) measured at the ROIs were processed using Python3. A detrend function with a robust linear regression was performed for normalization and a 4 Hz lowpass Butterworth filter was applied to minimize noise.

4.2.11 Statistical Analysis

Statistical analysis was performed using Prism 6 software. The mean and ± standard deviation were calculated for a minimum of three biological replicates for all data unless otherwise noted. One-way analysis of variance (ANOVA) followed by appropriate post hoc pairwise comparisons Tukey's tests were used when three or more groups were specified. Specific statistical analysis is mentioned within the corresponding figure legend. Variances were confirmed to not differ significantly with the Brown-Forsythe test.

4.3 Results

4.3.1 3D Differentiation of Hindbrain Respiratory Populations

V2a interneurons, V0 interneurons, and chemosensing neurons are each important to respiratory control and were induced using a hindbrain differentiation in monolayer. In 2D culture systems, however, cell-cell interactions are limited as the cells are constrained to the surface of the plate. Here, a 3D differentiation platform is described to observe the self-organization and function of the hindbrain interneuron populations with culture duration. The hindbrain differentiation was performed in 3D to determine if the respiratory populations could be induced in suspension culture. For 3D organoid culture, hiPSCs were first pre-treated with CHIR99021 for two days in monolayer prior to aggregation. The cell layers were dissociated and plated into pyramidal molds overnight to create consistent organoids in a high throughput manner (Fig 4.1 A) The newly formed organoids were then transferred to a 10cm dish and cultured for the remainder of the differentiation in suspension (Fig 4.1 B). Visual inspection of phase imaging throughout the differentiation revealed the organoids were largest around day 12 and remain circular until later time points (Fig 4.1 C). Quantification of the phase images confirmed the organoids began approximately 300μm in diameter and grew to a peak diameter of approximately 700μm at day 12 (Fig 4.1 D). The organoid diameter began to decrease on day 14 and levels off at a diameter of approximately 500μm at day 17 (Fig 4.1 D). The organoids also became less circular at later time points of the differentiation, which may reflect morphogenic changes are occurring (Fig 4.1 E).

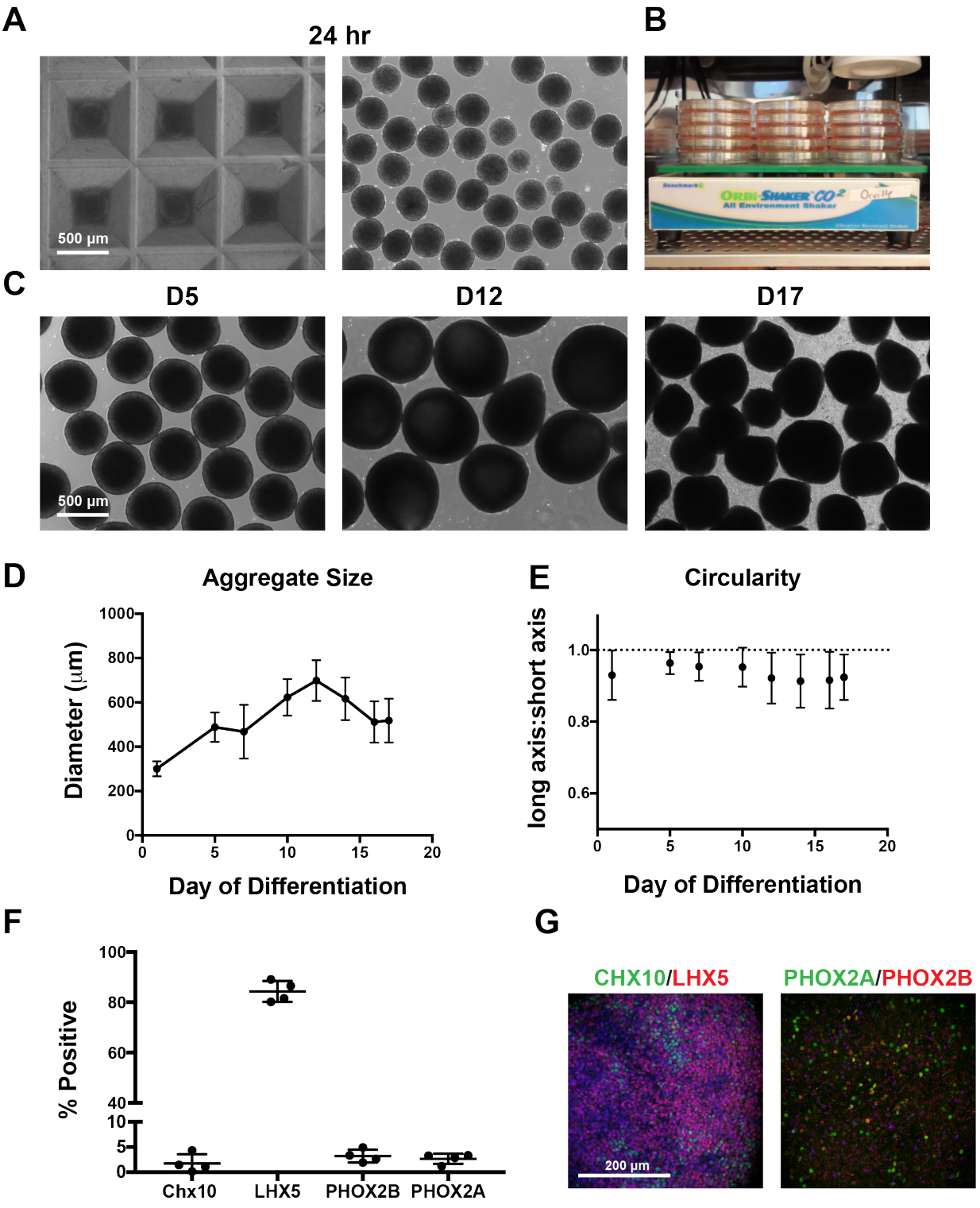

Figure 4.1: Hindbrain organoid differentiation: A. Formation of aggregates from hPSCs. B. Rotary orbital shaker for suspension culture. C. Phase contrast images of organoids at day 5, day 12, and day 17 of the differentiation. D. Diameter of the aggregates throughout the 17 day differentiation. E. Circularity, as calculated by the ratio of the long axis to the short axis, throughout the 17 day differentiation. F. Flow cytometry analysis of CHX10, LHX5, PHOX2B, and PHO2A at day 17. Immunocytochemistry of organoids at day 17.

Using the same concentrations of pur (100nM) and RA (100nM) that were defined as optimal concentrations for V2a interneurons in monolayer differentiations, the 3D culture system resulted in small percentages of $CHX10^+$, $PHOX2A^+$, and $PHOX2B^+$ cells (<5%) but high concentrations of $LHX5^+$ cells (~80%, Fig 4.1 F). The cytometry results were visually confirmed through whole mount immunostaining of the organoids (Fig 4.1 G). Not surprisingly, it appeared the effective concentration of the small molecules was different in monolayer vs. organoid cultures possibly due to different diffusion rates. Therefore, it was postulated that to define a more balanced population of the three cell types, different concentrations of signaling molecules might be needed in 3D compared to 2D.

4.3.2 Modulation of V2a and V0 Interneurons in Response to Sonic Hedgehog Signaling

Previous monolayer studies demonstrated that changing Shh signaling modulated relative proportions of V2a and V0 interneurons similar to the way progenitor domains develop in response to ventral-to dorsal Shh gradient. Therefore, it was postulated that the cellular composition of the organoids could be modulated similarly. The differentiation was performed using 10nM, 100nM, or 1μM pur. The organoids were homogenous and round at early stages of the differentiation (day 1 to day 7, Fig 4.2 A). However, by the end of the differentiation, the 10nM and 100nM pur groups were smaller than the 1μM pur group indicating the pur concentration is having some effect on organoid morphogenesis potentially through limiting proliferation (Fig 4.2 B). In this study, the size analysis of the

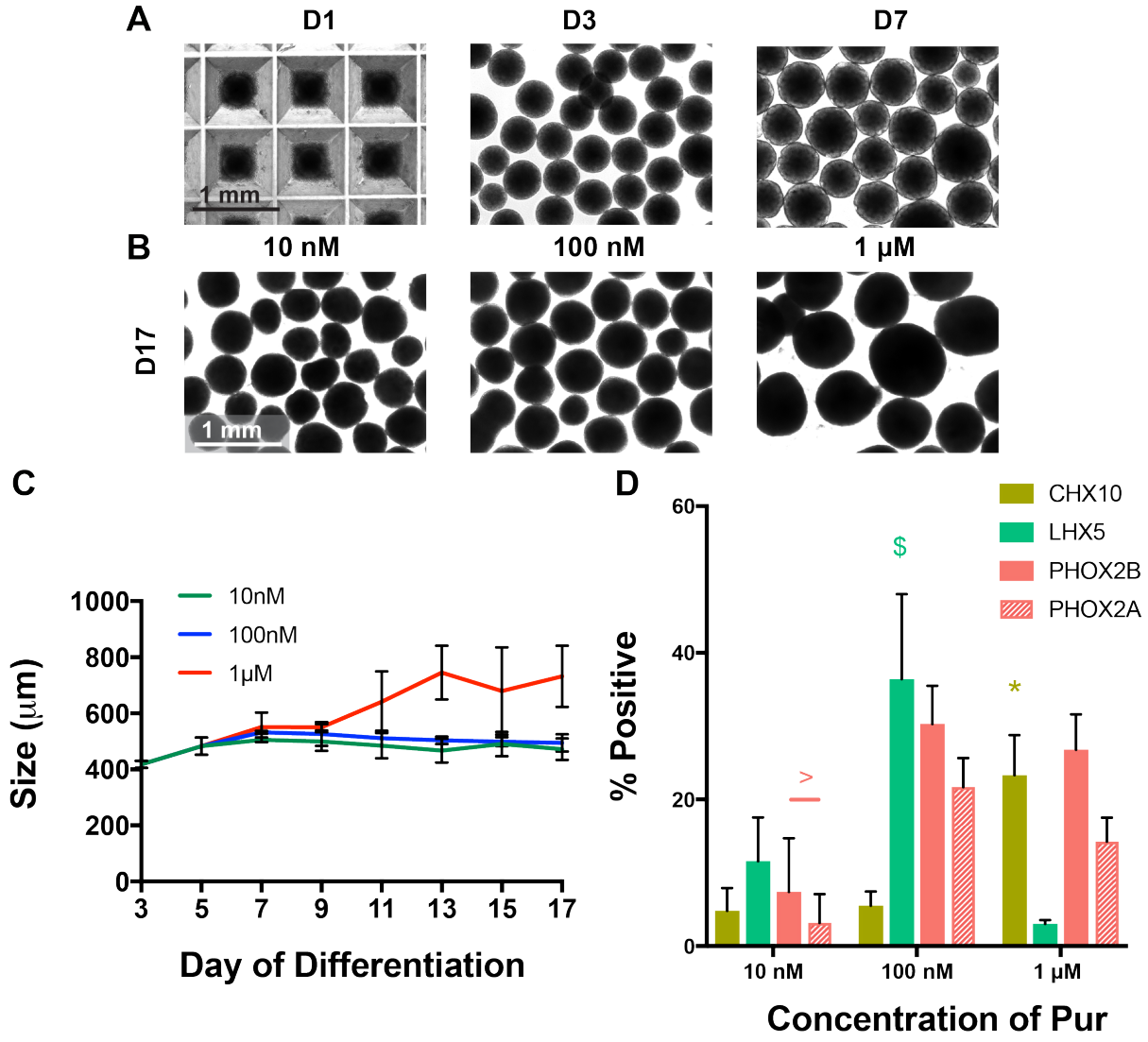

Figure 4.2: Cellular composition of the organoids is modulated by pur concentration. A. Phase contrast images of the organoids at day 1, day 3, and day 7. B. Phase contrast images of the organoids at day 17 treated with 10nM, 100nM, and 1µM. C. Diameter of the organoids throughout the differentiation. D. Flow cytometry analysis of CHX10, LHX5, PHOX2B, and PHO2A at day 17 of organoids treated with 10nM, 100nM, and 1µM pur. > $p < 0.05$ compared to 100nM and 1µM, $ $p < 0.05$ compared to 10nM and 1µM, * $p < 0.05$ compared to 10nM and 100M.

organoids was performed using a segmentation algorithm as a more unbiased approach than analysis by hand. Throughout the differentiation, the 10nM and 100nM pur groups maintained a relatively constant diameter (~500μm), but the 1μM pur group grew in size beginning on day 9 and was approximately 700μm by day 17 (Fig 4.2 C). To assess how pur concentration influenced cell fate determination, the relative proportions of V2a interneurons, V0 interneurons, and chemosensing neurons were analyzed on day 17 via flow cytometry (Fig 4.2 D). Using 10nM pur, low percentages of all subtypes were observed ($V0^{low}V2a^{low}$) suggesting the low amount of shh signaling was inefficient at driving neuronal commitment. 100nM pur resulted in high percentages of LHX5 (36.5%) and low percentages of CHX10 (3.5%, $V0^{high}V2a^{low}$), consistent with previous organoid experiments. 1μM pur resulted in low percentages of LHX5 (3.1%) and high percentages of CHX10 (23.3%, $V0^{low}V2a^{high}$). PHOX2A and PHOX2B percentages were highest in the 100nM and 1μM pur condition. This experiment demonstrates how relative proportions of the V2a and V0 interneurons can be modulated in response to Shh signaling, thus providing control over the population in order to probe how each of the interneurons affect the respiratory circuit.

4.3.3 Developmental Timeline of Organoid Culture

Self-organization is an important aspect of organoid culture. Therefore, we were interested in how these cell types emerge given a 3D environment. A longitudinal study was performed to assess how the V2a, V0 and chemosensing populations develop in the organoids, The analyzed organoids were treated with 1μM pur.

The organoids appeared to grow throughout the hindbrain differentiation process as visualized through phase imaging. Gross morphological changes in organoids where observed including a transition from smooth to irregular boundaries and a transient swirling pattern created by cell organization (Fig 4.3 A). During neural tube formation, the neuroepithelium elongates and compacts around the central canal then proliferates and differentiates to become the progenitor domains of the neural tube. In *in vitro* cell culture, a circular organization of condensed and proliferating progenitor cells that resembles early neural tube formation is identified as a neural rosette (Wilson and Stice 2006). H&E was performed to observed these morphological changes n tissue sections. Small lumens formed in the organoids by day 3 of the differentiation (Fig 4.3 Bi). By day 7, rosette-like structures were beginning to form as the lumens began to enlarge and nuclei around the lumen became more radially aligned (Fig 4.3 Bii). More developed rosette structures were apparent by day 11 as indicated by elongated nuclei arranged around the lumens (Fig 4.3 Biii). Additionally, the perimeter of the organoids became less smooth consistent with the phase images (Fig 4.3 Aiii). The rosette structures were still visible by day 13 but the regions adjacent to the lumens appear to become more filled with nuclei (Fig 4.3Biv). By day 17, the organoids became more round and the luminal spaces surrounded by rosettes became smaller (Fig 4.3 Bv). The H&E analysis demonstrated additional morphological changes, including the formation of rosette structures, thus expanding on observations obtained via phase imaging and revealing recapitulation of some aspects of neural development.

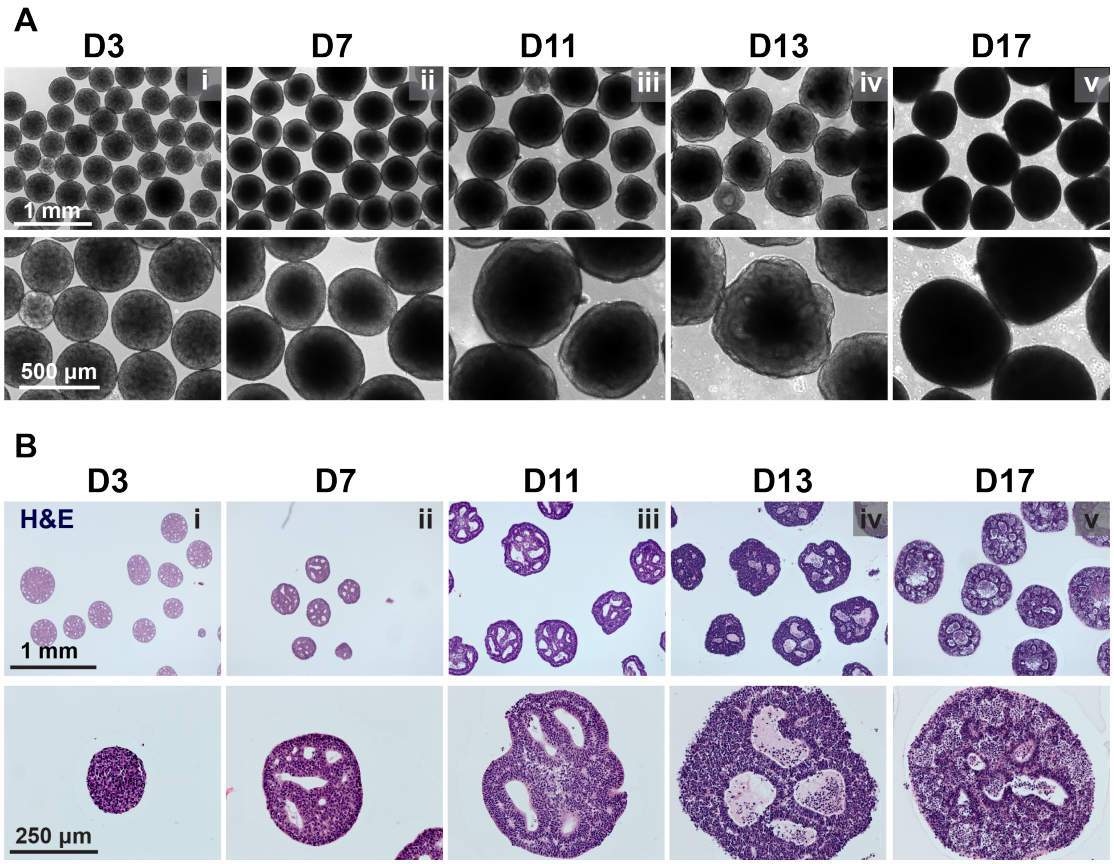

Figure 4.3 Phase contrast and H&E of organoids throughout the differentiation. A. Phase contrast images of the organoids at day 3, day 7, day 11, day 13, and day 17. H&E staining of sectioned organoids at day 3, day 7, day 11, day 13, and day 17.

The H&E results revealed structures that resembled neural rosettes, therefore additional analysis was performed to examine if the correct markers were expressed as the organoids developed. First, the expression of pluripotency and proliferation markers was assessed throughout the neural induction process. OCT4, a marker of pluripotency, was present in the organoids at day 3 and through day 7 but was absent by day 11 indicating the hPSCs were differentiating to a committed lineage (Fig 4.4 Ai). SOX2, a marker of pluripotency and early ectoderm was present and colocalized with OCT4 at day 3 and 7 (Fig 4.4 Aiii). By day 11, SOX2 expression persisted contrary to decreases in OCT4 confirming the emergence of a neuralectoderm phenotype. At day 17, SOX2 expression was present predominantly in the rosette-like structures indicating the many of the cells in these areas were still neural progenitors (Fig 4.4 Aii). Neural progenitors are a dividing cell population, therefore, the presence of proliferating cells was explored using Ki67. Most of the cells in the organoid were proliferating at day 3 but Ki67 expression began to diminish by day 11 (Fig 4.4 Bi). A small number of proliferating cells were present at day 17 but were localized to the rosette-like structures similar to SOX2 expression (Fig 4.4 Bi). Actively dividing cells, detected by phospho-histone H3 (PH3), were colocalized with Ki67 throughout the induction process but at lower frequency because the time a cell spends dividing is only a fraction of the cell cycle. By day 17 they were localized the rosette structures along with the Ki67 expression (Fig 4.4 Bii-iii). Together, at early time points, cells throughout the organoid are rapidly dividing but as cells begin to differentiate into committed lineages, the proliferation is more concentrated to the rosette structures.

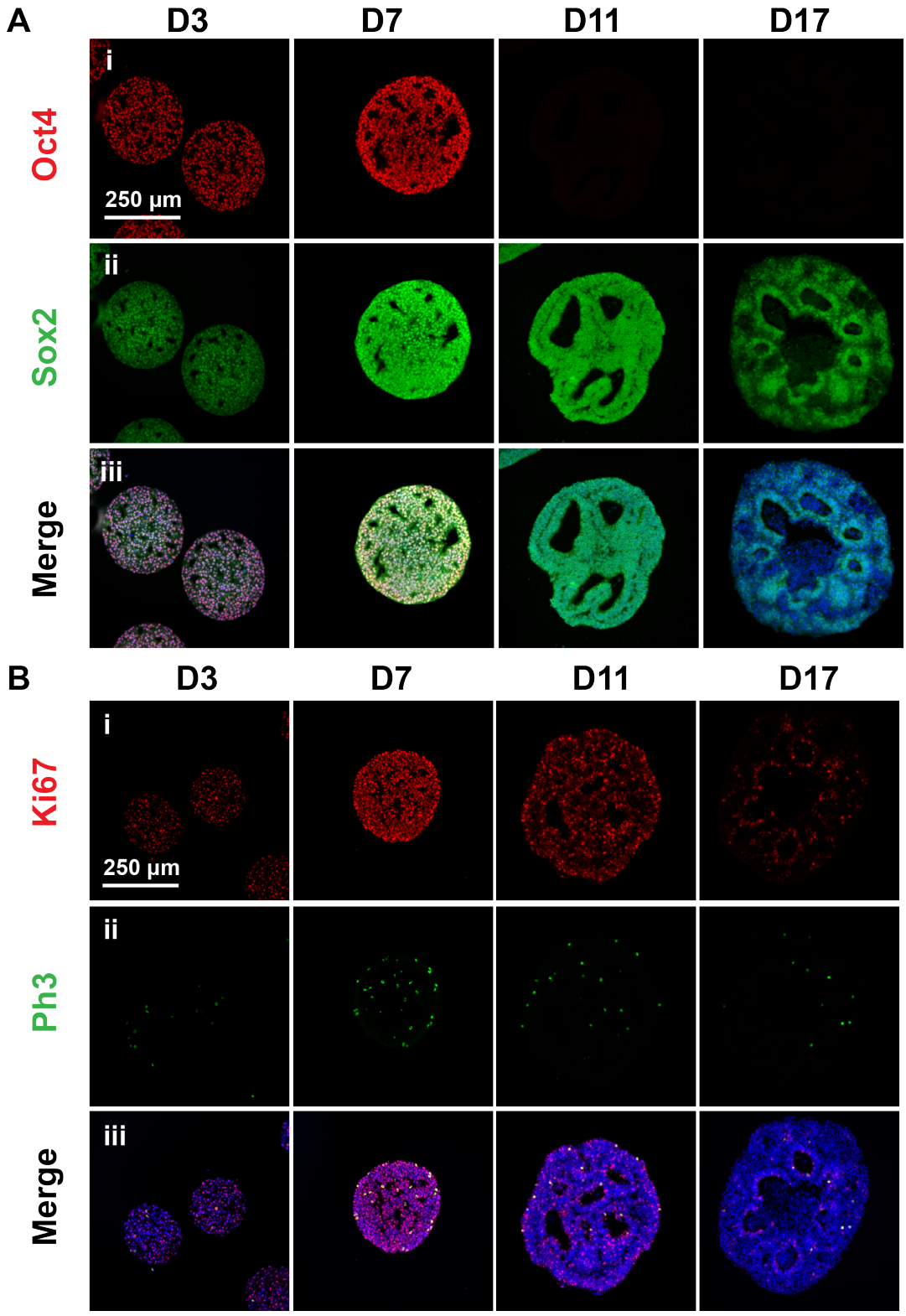

Figure 4.4: Analysis of pluripotency and proliferation in organoid sections throughout differentiation. A. Immunostaining for OCT4 and SOX2 at day 3, day 7, day 11, and day 17. B. Immunostaining for Ki67 and PH3 at day 3, day 7, day 11, and day 17.

To detect when different stages of neural commitment were occurring, the presence of early neural markers (Nestin and β_{III} Tubulin) as well as the transition from E-Cadherin expression to N-Cadherin expression was assessed. While Nestin and β_{III} Tubulin are early neural markers, Nestin is expressed by neural progenitors while β_{III} Tubulin continues to be expressed in committed, yet immature, neurons. Nestin and β_{III} Tubulin expression was robust by day 11 indicating a neural progenitor phenotype and continued throughout the duration of the culture period (Fig 4.5 Aiii). While Nestin and β_{III} Tubulin colocalized at day 11, by day 17, Nestin expression appeared to be more highly expressed within the rosette structures while β_{III} Tubulin was more diffuse throughout the organoid (Fig 4.5 Aiii). This change in expression pattern further confirmed the progenitor phenotype of the rosettes but also provided evidence that the cells outside of the neural rosettes were maturing to committed neurons. (Fig 4.5 Ai-ii). This fate transition was also demonstrated through a change in Cadherin expression. As cells differentiate down the neural lineage, there is a switch in Cadherin expression from E-Cadherin in pluripotent cells to N-Cadherin as cells commit to a neural fate (Hatta and Takeichi 1986, Detrick, Dickey et al. 1990). E-Cadherin outlined individual cells day 3 organoids but by day 7 became more colocalized to the luminal structures and turned off by day 11 (Fig 4.5 Bi). Little N-Cadherin expression was observed on day 7 but by day 11 it was located at the luminal structures and on the edges of the organoids (Fig 4.5 Bii). By Day 17, N-Cadherin was expressed more robustly and was observed throughout the organoids with a greater intensity of staining around the lumens (Fig 4.5 Bii). This data supports emergence of an early neural progenitor by day 7 that continues to mature throughout the induction.

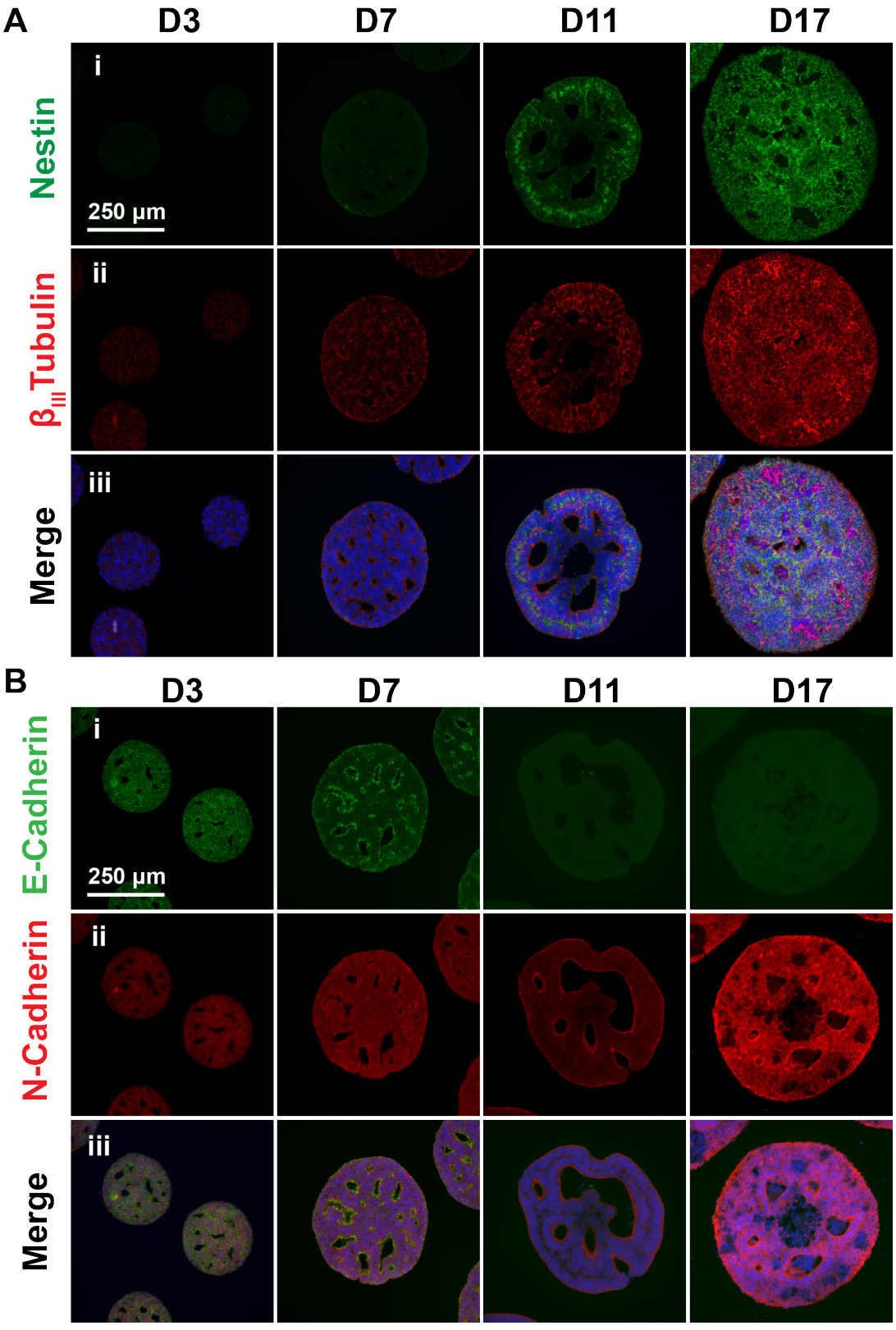

Figure 4.5: Analysis of neurogenesis in organoid sections throughout differentiation. A. Immunostaining for Nestin and β_{III}Tubulin at day 3, day 7, day 11, and day 17. B. Immunostaining for N-Cadherin and E-Cadherin at day 3, day 7, day 11, and day 17.

Two additional hallmarks of neural tube and neural rosette formation are the colocalization of ZO-1 with N-Cadherin at the apical surface of the lumen indicated of boundary formation and the presence of the neural progenitor marker, PAX6 (Aaku-Saraste, Hellwig et al. 1996). Diffuse expression of ZO-1, a tight junction marker, was present at the edges of the lumen at day 3 but condensed to form a tight luminal border by day 17. (Fig 4.6 Ai). ZO-1 expression colocalized with N-Cadherin on days 11 and 17 similar to what has been identified during neural tube formation (Fig 4.6 Aiii). PAX6, an early neural transcription factor was present at day 3 throughout the aggregates and began to turn off by day 11. At later time points, PAX6 was colocalized to the rosette structures (Fig 4.6 Bi). β_{III} Tubulin expression was highest at day 17 and could be identified around the $PAX6^{+}$ cells (Fig 4.6 Bii). The combination of nuclear organization with the expression of tight-junction, Cadherin, and neural progenitor markers reveals the presence of neural rosettes reminiscent of native neural tube development in the differentiating organoids.

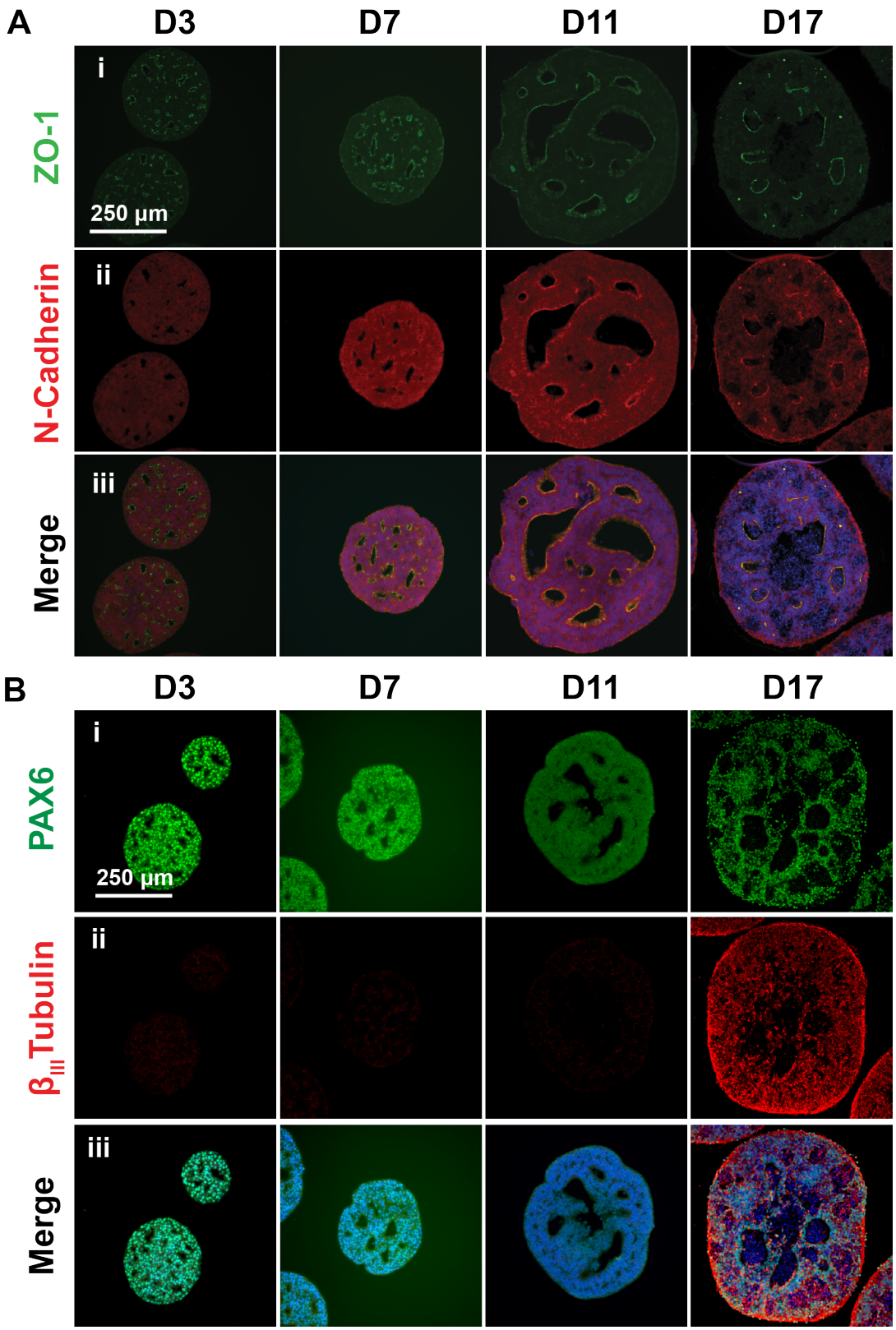

Figure 4.6: Analysis of rosette formation in organiod sections throughout differentiation. A. Immunostaining for N-Cadherin and ZO-1 at day 3, day 7, day 11, and day 17. B. Immunostaining for PAX6 and β_{III} Tubulin at day 3, day 7, day 11, and day 17.

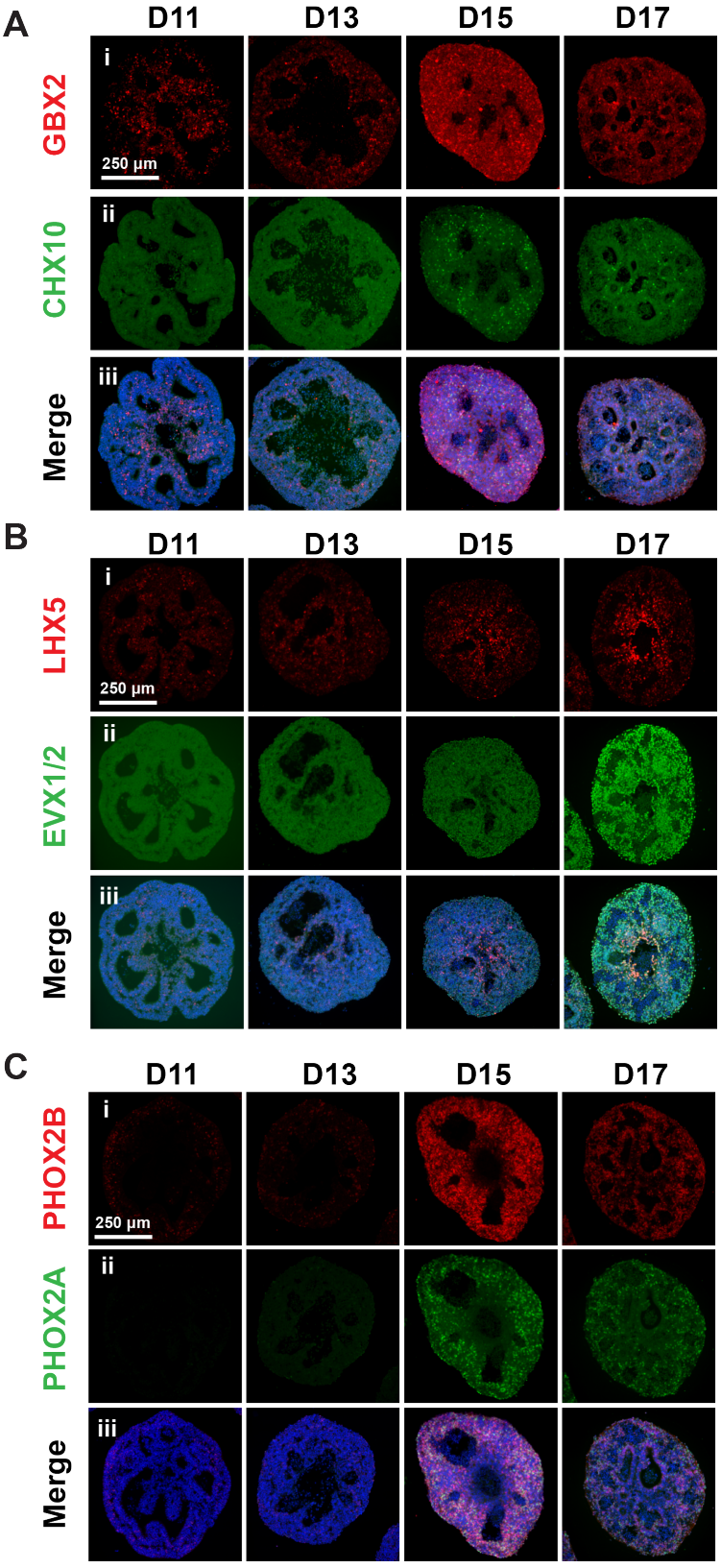

Figure 4.7: Analysis of committed phenotypes in organoid sections throughout differentiation. A. Immunostaining for OCT4 and SOX2 at day 3, day 7, day 11, and day 17. B. Immunostaining for Ki67 and PH3 at day 3, day 7, day 11, and day 17.

As the neural tube develops, neural progenitor domains expand near the central canal then migrate to more lateral positions in the spinal cord as the neurons mature into committed phenotypes. To determine the timing of how the respiratory populations (V2a, V0, and chemosensing) emerge in the organoid, the expression of more subtype-specific markers were examined. GBX2, a marker expressed in the developing hindbrain was identified at day 11 with expression localized mainly to the rosette regions. From day 13 to day 17, GBX2 expression diminishes and becomes more diffuse throughout the organoid (Fig 4.7 Ai). CHX10, marking the committed V2a population, was greatest at day 15 and appeared to be localized away from the rosette structures (Fig 7.7 Aii). CHX10 appeared to co-localize with GBX2 but not all $GBX2^+$ cells were $CHX10^+$ (Fig 4.7 Aiii). This result suggests that $CHX10^+$ cells have a hindbrain lineage and implies that GBX2 expression precedes the emergence of more committed hindbrain phenotypes within the organoid. LHX5, a marker of V0 interneurons, was expressed in the organoids at day 15 and was localized to the rosette structures (Fig 4.7 Bi). EVX1/2, a marker of committed V0 interneurons was robustly expressed by day 17 and was observed throughout the organoid (Fig 4.7 Bii). Further, LHX5 appeared to colocalize with EVX1/2 but not all $EVX1/2^+$ cells were $LHX5^+$, which might suggest LHX5 expression precedes EVX1/2 expression (Fig 4.7 Biii). PHOX2B, a marker for chemosensory neurons, was expressed at low levels at day 13 but increased by day 15 and continued through day 17. PHOX2A expression emerged later than PHOX2B at day 15 and also continued through day 17. Both PHOX2A and PHOX2B expression appeared to be located in the outer region of the organoid on day 15 and 17. The longitudinal examination of the induction process revealed the organoids undergo a differentiation program similar to what occurs in the developing neural tube from early

neural commitment to maturation into post-mitotic neurons of the respiratory hindbrain region.

4.3.4 Phenotypic Analysis of Maturing of Organoid Cultures

To observe how the organoids mature, samples described in Fig 4.1 were switched to BrainPhys medium supplemented with growth factors at D17. Via phase imaging, the organoids continued to grow and become more spherical after 17 days of culture before appearing to plateau in growth day 40 (Fig 4.8 A). A sample of organoids were taken every 10 days and processed for histological sectioning to assess maturation. H&E staining revealed a change in nuclear density as the organoids matured. The D17 organoids were very nuclear dense but the nuclei become more diffuse as the cultures matured. The sparse nuclei with increased extracellular space is more similar to native neural tissue which as less nuclear dense. Additionally, the size of the nuclei increased with culture duration indicative of maturation (Fig. 4.8 B). Interestingly, the lumens that form during the induction process where no longer observed.

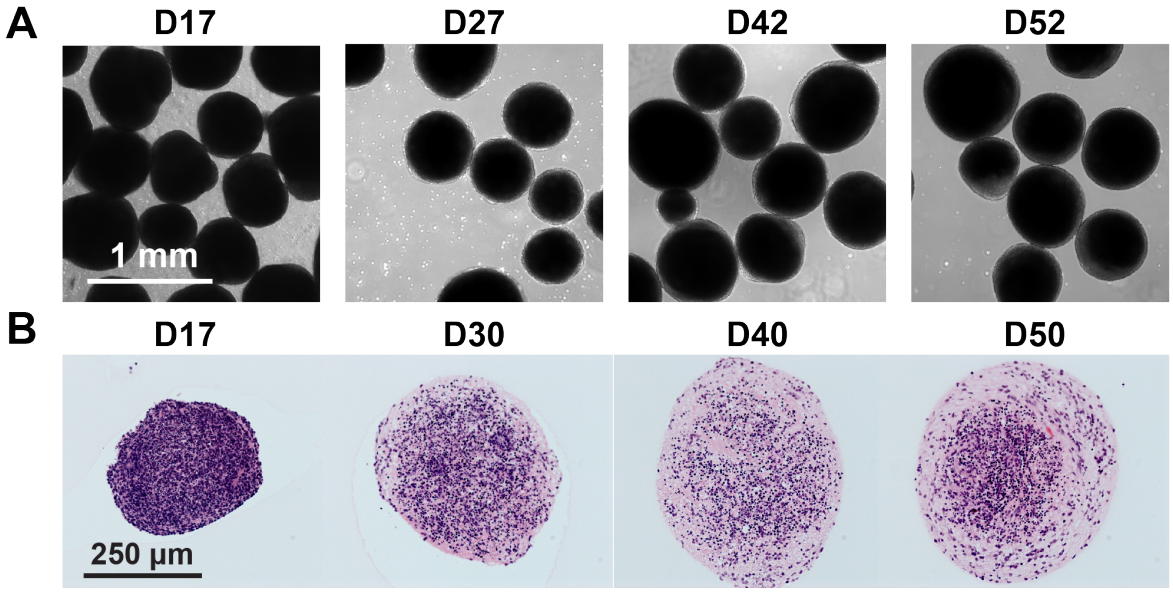

Figure 4.8: Phase contrast and H&E of organoids during maturation. Phase contrast images of the organoids at day 17, day 27, day 42, and day 52. H&E staining of sectioned organoids at day 17, day 30, day 40, and day 50.

Expression of a variety of mature markers were analyzed throughout the culture duration. Expression of β_{III} Tubulin, a marker of immature filaments, was highest at day 30 and appeared to decrease by day 50 (Fig 4.9 A). Tau, a marker of mature filaments, had low level of expression at day 17, but the expression became more robust by day 50 (Fig 4.9 B). This indicates that the immature filaments are being replaced by more mature axonal proteins with culture duration. Expression of NeuN, a marker of mature neurons, was present at low levels from day 17 to day 40 but expression was heavily distributed throughout the organoid by day 50 (Fig 4.9 C). The expression of vesicular glutamate

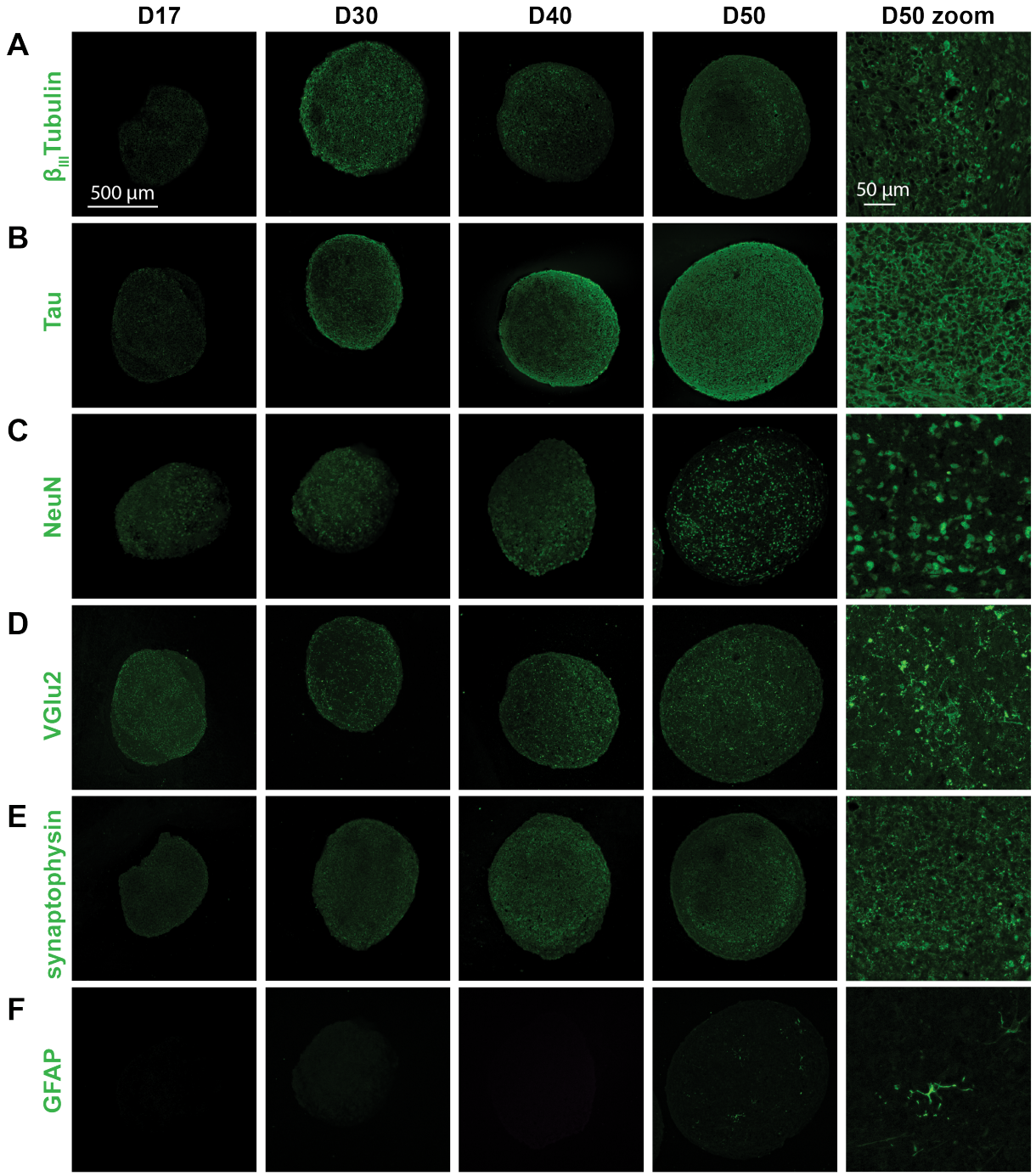

Figure 4.9 Assessment of early maturation in sectioned organoids. Immunostaining for (A) β_{III} Tubulin, (B) Tau, (C) NeuN, (D) VGlut2, (E) synaptophysin, (F) GFAP at days 17, 30, 40, and 50 of culture.

transporter 2 (VGLUT2), a marker of glutamatergic neurons, and synaptophysin, a pre-synaptic marker, were both expressed at day 40 became brighter and more abundant at day 50 (Fig 4.9 D and E) indicating the organoids expressed markers needed to be functional. Lastly, a few cells expressed glial fibrillary acidic protein (GFAP), indicative of astrocytes, by day 50 (Fig 4.9 F). While the main focus has been on neurons, the presence of glial phenotypes is key to a recapitulating native tissue, which contains both neuronal and glial phenotypes.

At 100 days of culture, the organoids had smooth edges with more cell-dense regions visible towards the center (Fig 4.10 A). H&E staining revealed nuclei are present throughout the organoids and a swirling pattern of nuclei appeared to have formed in some of the organoids (Fig 4.10 B). Analysis of mature neuronal markers was performed to observe how the organoids had matured by 100 days. Similar to D50 samples, the organoids contained $NeuN^+$ cells. However, at D100, there were many more $GFAP^+$ cells that appeared to intermingle with Tau^+ axons localized to the NeuN regions (Fig 4.10 C). GABA expression, marking inhibitory populations was present but interestingly largely localized to $NeuN^-$ regions (Fig 4.10 D). The organoids contained high abundance of the excitatory marker, VGlut2, a phenotype of the chemosensing population and the V2a and V0 interneurons (Fig 4.10 E). There also continued to be high abundance of synaptophysin indicating synapses are being formed (Fig 4.10 F). Not surprisingly, CHX10 was not present in the D100 culture but there was evidence of OLIG2, marking the presence of oligodendrocyte precursors (Fig 4.10 G). Staining for myelin basic protein (MBP) was minimal indicating that more time may be necessary for myelination to occur or there are too few $OLIG2^+$ cells (Fig 4.10 G). Together, the immunostaining results show that the

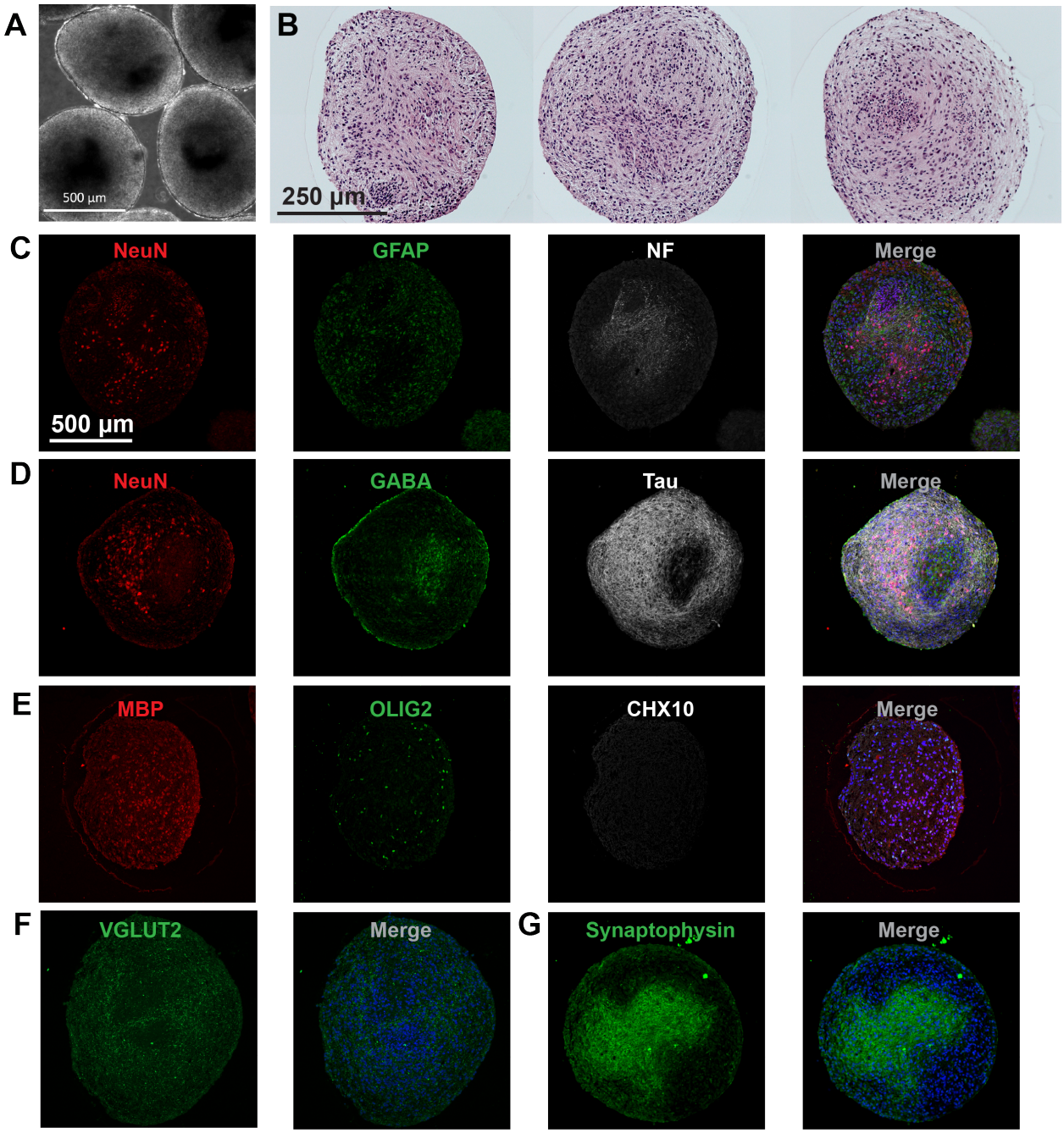

Figure 4.10: Assessment of maturation markers in 100 day old organoids. A. Phase contrast image at 100 days. B. H&E of sectioned organoids. C. Immunostaining for NeuN, GFAP, and Neurofilament (NF). D. Immunostaining for NeuN, GABA, and Tau. E. Immunostaining for myelin basic protein (MBP), OLIG2, and CHX10. F. Immunostaining for VGLUT2, G. Immunostaining for synaptophysin.

organoids are inducing a mature neuronal phenotype that is primarily glutamatergic with a small GABAergic population. Additionally, the presence of glia, including $GFAP^+$ astrocytes and progenitor oligodendrocytes, were potentially providing functional support to the neurons.

4.3.5 Functional Analysis of Maturing of Organoid Cultures

The maturation of the organoids was next assessed by measuring Ca^{2+} flux. The study was performed using the WTC11 GCaMP iPS cell line, which allowed for easy assessment of calcium flux every 5 to 6 days of the maturation process. At early time points (D17 to D38), little calcium flux was observed in individual organoids. However, at D42, whole organoids began to fire synchronously with a periodic rate (Fig 4.11 A). From that point onward, the organoids were imaged as a field of samples instead of as individual organoids. At day 52, all organoids were active but had different periodicities (Fig 4.11 B). The synchronous activity did stop after 3-5 minutes of the cultures being out of the incubator, suggesting potential sensitivity to ambient air and temperature (Fig 4.11 Bii). By day 69, the frequency of Ca^{2+} activity was more variable between organoids and by day 92, Ca^{2+} fluctuations were less common and less periodic. These changes in functional readout may be driven by changes in glial populations or increased synaptic connection, which correlate with the immunostaining results where few glial and synaptic populations are identified by day 50 but increase by day 100.

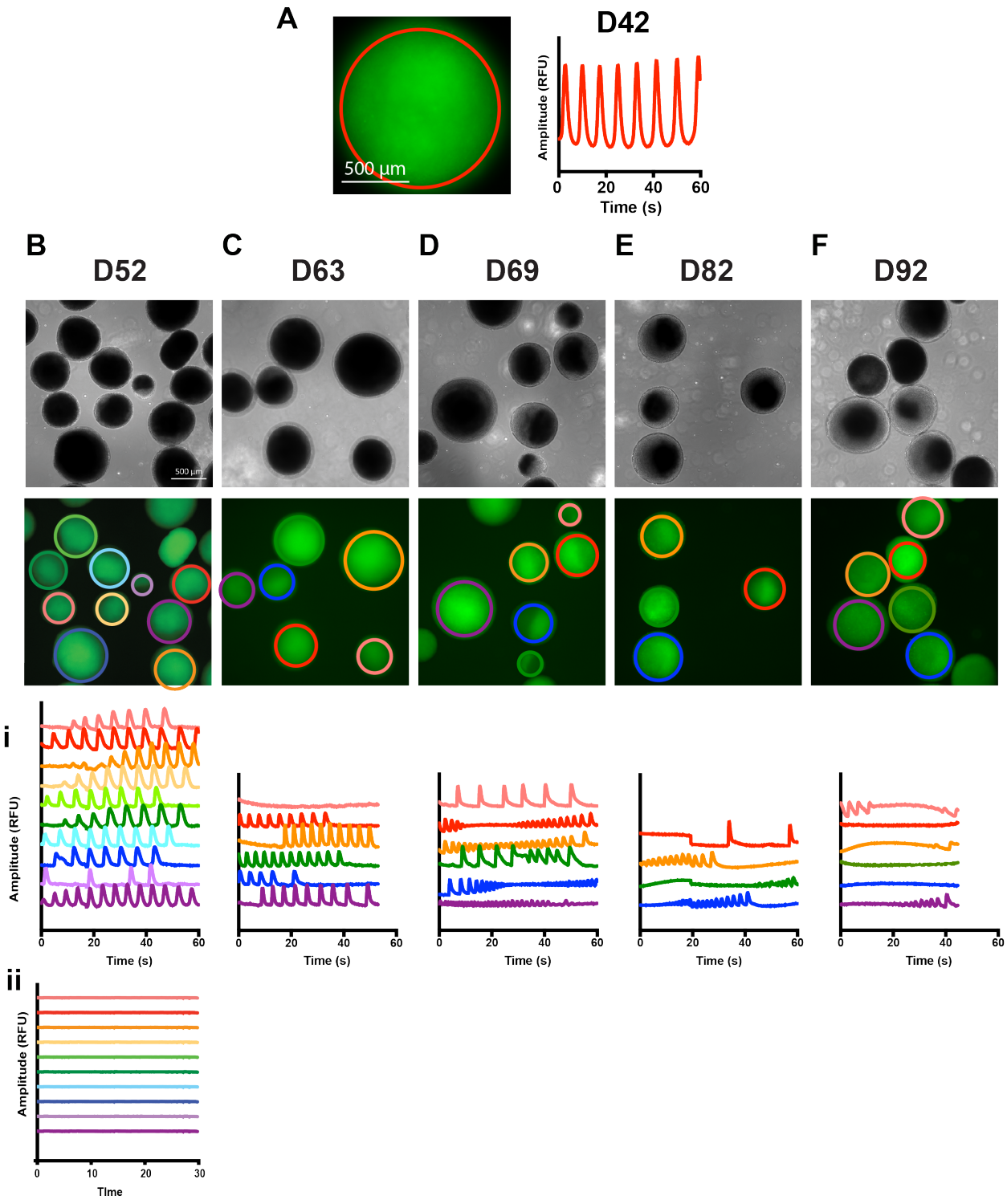

Figure 4.11 Synchronous Ca^{2+} fluctuations in the organoids throughout maturation. A. Ca^{2+} transients in one organoids at day 42. B. Ca^{2+} transients of a field of organoids taken right out of the incubator (i) and the same region 2 minutes later (ii). C-F. Ca^{2+} transients of a field of organoids at day 63, 69, 82, and 92. Colored circles demarcate regions of interest (ROI).

To observe if the cellular composition of the organoids was important to the periodic synchronous activity, Ca^{2+} flux was measured in the organoids differentiated with varying concentrations of pur. A functional comparison was made between the three samples that had different composition of interneurons: $V0^{low}V2a^{low}$ (10nM pur), $V0^{high}V2a^{low}$ (100nM pur), and $V0^{low}V2a^{high}$ 1μM pur). Calcium fluctuations were initially observed at day 33 and imaged every 5 to 6 days thereafter (Fig 4.12). The $V0^{low}V2a^{low}$ group had few periodic synchronous events throughout the measured time period (Fig 4.12 A). Both the $V0^{high}V2a^{low}$ and $V0^{low}V2a^{high}$ group displayed periodic synchronous Ca^{2+} fluctuations, though the $V0^{high}V2a^{low}$ group was more rhythmic overall and the $V0^{low}V2a^{high}$ appeared more sporadic (Fig 4.12 B and C). These results suggest the cellular composition does impact the functional response in that the interneurons are needed for the rhythmic activity and that more V0 interneurons increase the rhythmicity. This study probes the influence of the interneuron populations but not the PHOX2A/PHOX2B population, as it was not changed in response to Shh signaling, which is an important piece of the neural circuit.

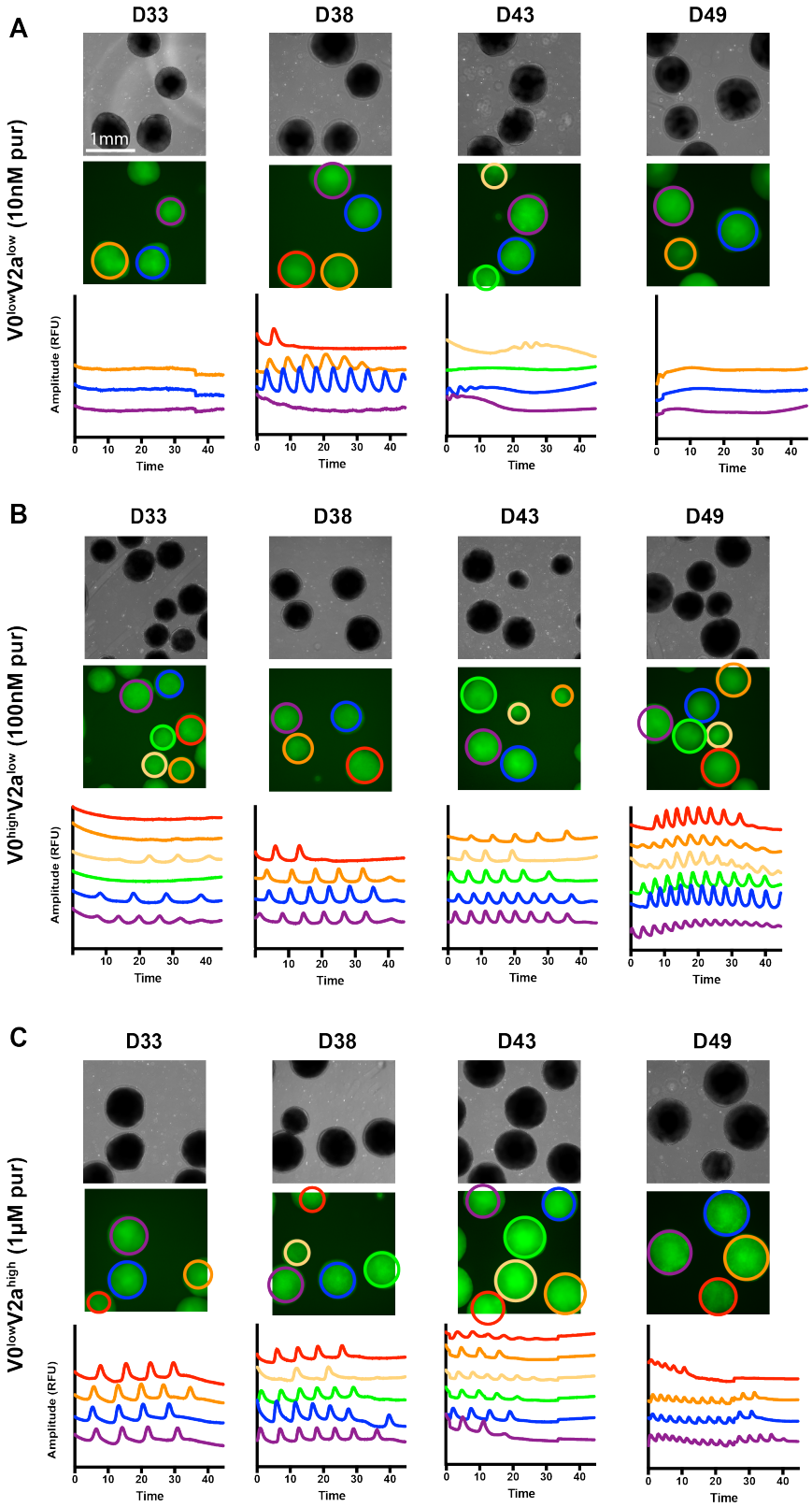

Figure 4.12: Synchronous Ca^{2+} fluctuations in the organoids are dependent on cellular composition. Ca^{2+} transients of a field of organoids at day 33, 38, 43, and 49 in aggregates trested with (A) 10nM, (B) 100nM, or (C) 1μM pur. Colored circles demarcate regions of interest (ROI).

4.3.6 Model of CCHS in organoid culture

CCHS is a disease caused by a PHOX2B mutation that results in the loss of CO_2 sensing and thus loss of respiratory control. The hindbrain differentiation was performed in organoid and monolayer culture simultaneously using a heterozygous and homozygous PHOX2B mutant hiPSC cell line ($PHOX2B^{+/Y14X}$ and $PHOX2B^{Y14X/Y14X}$) along with the isogenic control line ($PHOX2B^{+/+}$) (Workman, Mahe et al. 2017). All cell lines formed organoids normally and there were no discernable differences between the WT and mutant organoids via phase microscopy (Fig 4.12 A). On day 17 of organoid and monolayer culture, PHOX2B was detected in the $PHOX2B^{+/+}$ line (~20%) but was diminished in the $PHOX2B^{+/Y14X}$ and $PHOX2B^{Y14X/Y14X}$ lines (~5%) (Fig 4.12 B and C). Consequently, expression of PHOX2A was also diminished in the $PHOX2B^{+/Y14X}$ and $PHOX2B^{Y14X/Y14X}$ lines (~2%) compared to the $PHOX2B^{+/+}$ line (~15%). However, the effect of the mutation on V2a and V0 interneuron cultures differed in the organoid and monolayer cultures. In organoid culture, CHX10% was higher in the mutant lines (~45%) compared to the $PHOX2B^{+/+}$ line (~15%) but LHX5% was highest in the $PHOX2B^{+/+}$ (~35%) line compared to mutant lines (~15%). In monolayer culture, a different result was observed where LHX5% was highest in the mutant lines (~45%) compared to the $PHOX2B^{+/+}$ line (~20%). Similar percentages of CHX10 were detected across all lines in monolayer cultures. These relative percentages in organoid and monolayer culture were confirmed through immunostaining (Fig 4.13 E and F). This data suggests that the inhibition of PHOX2B does not adversely affect the differentiation of V2a and V0 interneurons and actually increased the differentiation efficiency of V2a interneurons in organoid culture and V0 interneurons in monolayer

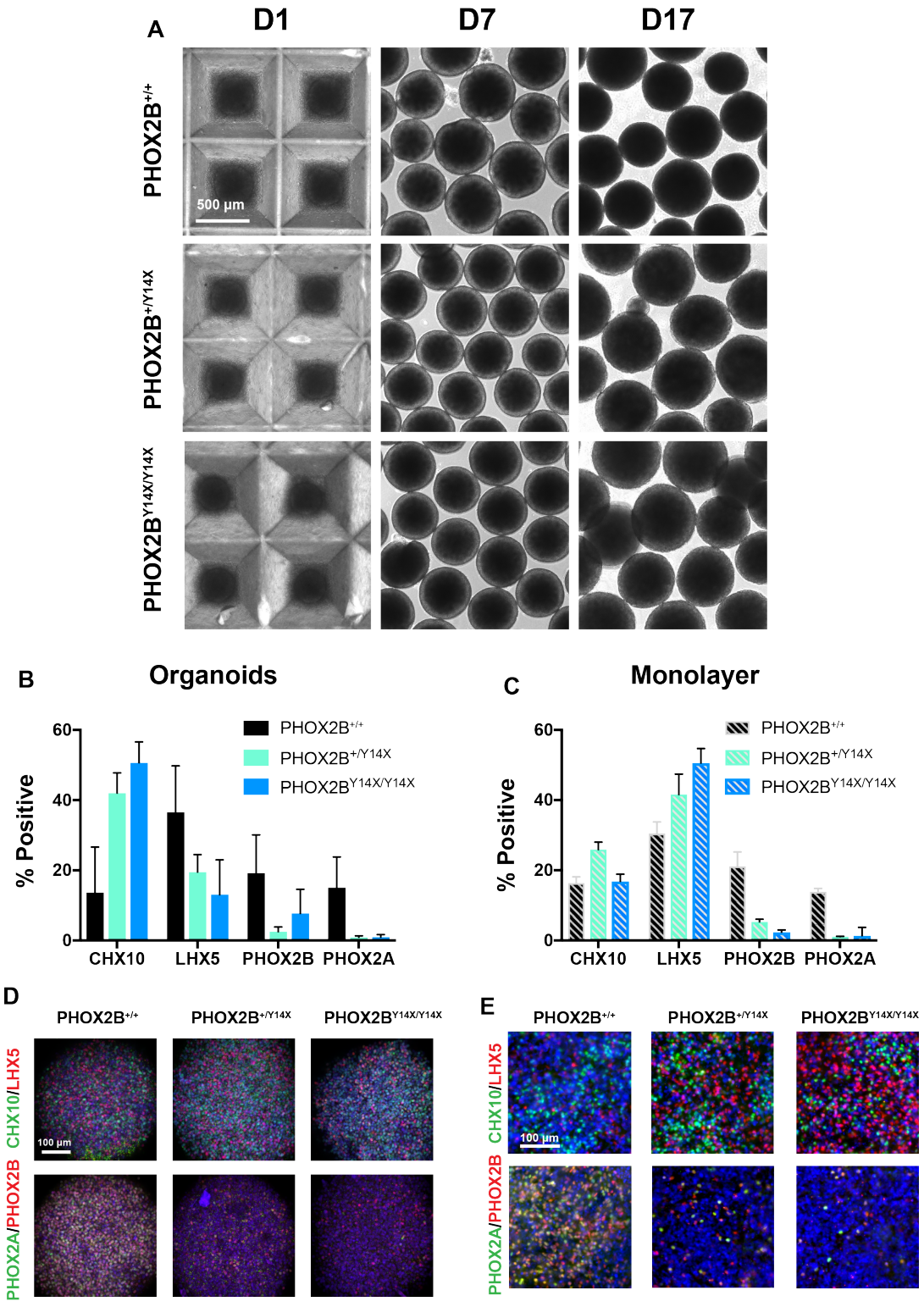

Figure 4.13: Disease modeling in hindbrain organoids. A. Phase contrast images of organoids made from PHOX2B$^{+/+}$, PHOX2B$^{+/Y14X}$, and PHOX2B$^{Y14X/Y14X}$ cell lines. Flow cytometry analysis of CHX10, LHX5, PHOX2B, and PHOX2A from PHOX2B$^{+/+}$, PHOX2B$^{+/Y14X}$, and PHOX2B$^{Y14X/Y14X}$ cell lines in aggregate (B) and monolayer (C) culture. Immunostaining analysis of CHX10, LHX5, PHOX2B, and PHOX2A from PHOX2B$^{+/+}$, PHOX2B$^{+/Y14X}$, and PHOX2B$^{Y14X/Y14X}$ cell lines in aggregate (D) and monolayer (E) culture.

culture potentially because the PHOX cells are no longer competing for signaling giving more opportunity for V2a and V0 development.

To assess how the organoid and monolayer cultures matured, the samples were switched to BrainPhys supplemented with growth factors. At day 38, both samples were treated with the Ca^{2+} dye, Fluo4, to observe if the mutant cell lines were capable of producing the periodic synchronous fluctuations. All organoid groups displayed some periodic synchronous activity with the fluctuations being more prevalent in the $PHOX2B^{+/Y14X}$ and $PHOX2B^{Y14X/Y14X}$ organoids (Fig 4.14 A). Interestingly, all monolayer cultures had active neurons as displayed through calcium flux but they appeared to not be synchronous (Fig 4.14 B). Together, these data suggest the PHOX2B population is not responsible for the synchronous activity and that the 3D structure is critical to synchronization.

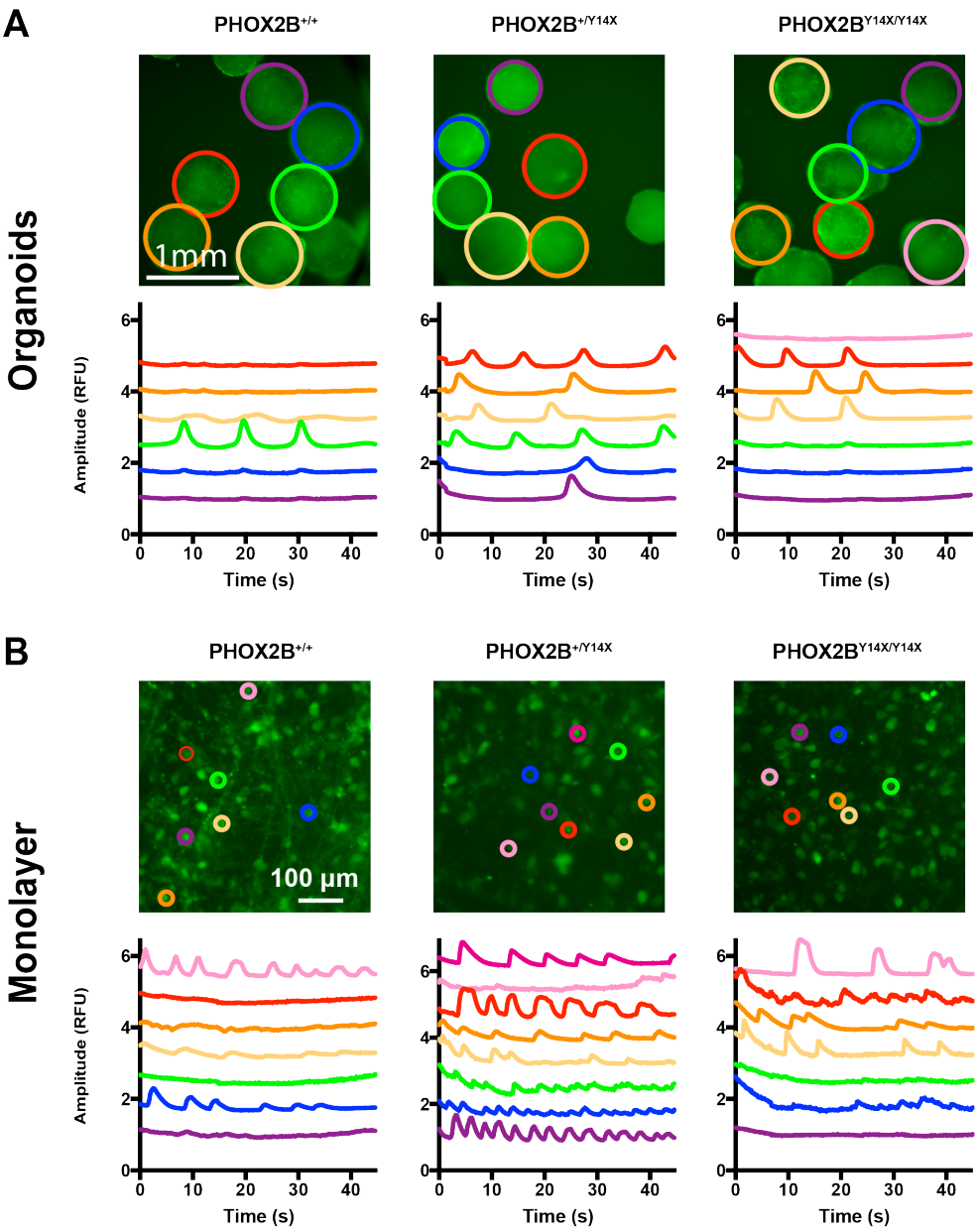

Figure 4.14: Synchronous Ca^{2+} fluctuations in PHOX2B mutant organoids. Ca^{2+} transients of (A) organoids and (B) individual cells in monolayer at day 38 in PHOX2B$^{+/+}$, PHOX2B$^{+/Y14X}$, and PHOX2B$^{Y14X/Y14X}$ cell lines. Colored circles demarcate regions of interest (ROI).

4.4 Discussion

This study describes a platform to differentiate respiratory hindbrain organoids from hPSCs. When transitioning from a monolayer to a 3D platform, the need for higher concentrations of signaling molecules to permeate the organoids was considered. The first organoid differentiation was performed with the same concentration of molecules as the monolayer system, which was optimized for V2a interneurons. Using the same concentration of pur as the monolayer differentiation (100nM), the percentage of V0 interneurons was high while percentage of CHX10 and PHOX2A/2B was very low (Fig 4.1 F). The ventrodorsal Shh gradient in the developing neural tube is organized such that the dorsal V0 interneurons receive lower amounts of signaling compared to the more ventral V2a interneurons. It was then hypothesized that a higher concentration of pur would result in an increased percentage of V2a interneurons in the organoids. This was confirmed through testing different concentrations of pur wherein a higher concentration (1μM) resulted in a higher V2a population at the expense of the V0 population (Fig 4.2 D). The implication of these results was two-fold. First, the relative proportions of interneurons could be controlled through developmentally inspired mechanisms and second, the small molecule kinetics may be slower in a $\sim 10^2$μm thick organoid compared to a $\sim 10^1$μm thick monolayer culture.

Histological sectioning of the organoids through time revealed distinct organizations that recapitulated neural development. Most interestingly, was the formation of neural rosette-like structures with open lumens observed through H&E (Fig 4.3 B). While the definition of neural rosettes comes from a phenomenon observed during hPSC *in*

vitro culture, they are believed to model neuroepithelium forming the neural tube *in vivo* (Wilson and Stice 2006*).* Expression of a variety of markers was used to further confirm the presence of neural rosettes. Developmentally, cells of the neural tube initially express E-Cadherin but as the neural tube forms, E-Cadherin expression stops and N-Cadherin expression begins (Hatta and Takeichi 1986, Detrick, Dickey et al. 1990). Similar transition of E-cadherin to N-Cadherin expression was observed in the organoids from days 3-7 (Fig 4.4 B. Next, condensation of N-Cadherin and the tight junction marker ZO-1 was observed at the luminal boarder in the organoids (Fig 4.5 A) similar to the condensation of these markers at the apical surface of neural tube formation (Aaku-Saraste, Hellwig et al. 1996) Additionally, the elongated nuclei comprising the rosettes in the center of the organoid were positive for neuroepithelial transcription factors SOX2 and PAX6, two defining populations of the early neural tube (Zhang, Huang et al. 2010) (Fig 4.4 A and Fig 4.6 B). Cells that make up the early neural tube are actively proliferating as the spinal cord develops. Similarly, proliferating cells are observed mainly in the rosette structures at later time points (Fig 4.4 B). Additionally, the hindbrain progenitor marker, GBX2, emerged closer to the rosette structures but the markers of committed neurons (CHX10, EVX1, PHOX2A, PHOX2B) are dispersed more throughout the organoid, away from the rosettes (Fig 4.7 A-C). LHX5 expression also appears to be closer to the rosettes potentially indicating that LHX5 expression is potentially an early marker for V0 interneurons before EVX1/2 expression begins.

The 3D differentiation recapitulates cell organization and temporal expression of neural development markers similar to that of the developing neural tube. The densely-packed elongated nuclear structures that are apparent after sectioning of the organoids

have been observed in our monolayer cultures before however, a lumen never appeared. This could result from the cells being constrained to the 2D surface whereas the 3D differentiation platform provides the necessary 3D cell-cell interactions to form a lumen. One consideration when interpreting the results is that the histological analysis was performed only on organoids that were treated with 1μM pur. We have demonstrated that different proportions of V2a, V0, and chemosensing neurons are induced in response to pur concentration; therefore future studies are needed to compare how cellular organization changes in response to pur concentration.

As the organoids culture for up to 100 days, they express markers of maturation. While NeuN is visible at D17, the expression increases throughout culture (Fig 4.9 C and 4.10 C). The high abundance of VGLUT2 confirms the glutamatergic phenotypes of V2a and V0 interneurons as well as the chemosensing population (Fig 4.10 E). The initial focus of the differentiation had been on neuronal phenotypes, however, functional neural tissues contain glial phenotypes that are critical for tissue function. There is early evidence of $GFAP^+$ cells at D50 but by 100 days of culture, there is a large population indicative of a potential astrocytic population (Fig 4.9 F and 4.10 C). Recently, astrocytes have been implicated as an important cell population in the Pre BötC in which astryocytic vesicle release influences rate of respiration (Sheikhbahaei, Turovsky et al. 2018). The high population of $GFAP^+$ cells may be recapitulating the predominance of astrocytes in the Pre BötC, which are a necessary part of the respiratory circuitry. Additionally, the cultures contain $OLIG2^+$ cells, which have the potential to mature into myelinating oligodendrocytes (Fig 4.10 F). The organoid cultures described here not only have a combination of neurons

important for respiratory control but also have the glial phenotypes needed for a functional tissue.

At around 40 days of culture, the organoids began to exhibit synchronous, periodic Ca^{2+} activity that is measurable and visible throughout the entire tissue (Fig 4.11). The synchrony was visible in organoid cultures but not in comparable monolayer cultures (Fig 4.14 B) indicating the importance of the 3D platform. However, it was not clear which population in the organoid was driving this activity. From literature, it is known the chemosensing population changes synaptic output in response to $pC0_2$ but the activity of $PHOX2B^{+}$ neurons are not rhythmogenic (Mulkey, Stornetta et al. 2004, Guyenet, Mulkey et al. 2005). The V2a and V0 interneurons, which are a part of the respiratory circuit that we have differentiated, have been described to have rhythmic activity (Crone, Viemari et al. 2012, Wu, Capelli et al. 2017). Explanted slice culture of the murine pre BötC, which contains V0 interneurons, retain the ability generate respiratory rhythms autonomously (Smith, Ellenberger et al. 1991, Feldman, Mitchell et al. 2003) Additionally, Ca^{2+} flux recordings of neurons in the rat pre BötC show similar periodicity that are observed in the organoid culture (Koizumi, Koshiya et al. 2013). The data shown in Fig 4.11 that displayed periodic synchronous activity was collected from organoids with a high population of V0 interneurons. Further, the more rhythmogenic activity was observed by the $V0^{high}V2a^{low}$ cultures compared to the $V0^{low}V2a^{low}$ and $V0^{low}V2a^{high}$ cultures overtime (Fig 4.12). Lastly, the synchronous activity was still detectable when the chemosensing population was absent using the $PHOX2B^{Y14X/Y14X}$ and $PHOX2B^{Y14X/Y14X}$ cell lines (Fig 4.12). All of this data suggests that the synchronous activity in the organoids may be a measure of the V0 interneuron activity. However, further experimentation in an environment that controls for

temperature and CO_2 as the organoids mature will aid in elucidating the role of each population in the organoid.

4.5 Conclusion

This study describes the first report of a hindbrain organoid that is composed of V2a interneurons, V0 interneurons, and a chemosensing population of neurons important in the control of respiration. Analysis of the induction process revealed the organoid develops through a process similar to native neural tube development. Control over the cellular composition of the organoid was demonstrated through changing the pur concentration. The organoids matured to contain neurons that were primarily glutamatergic with an astrocyte support population consistent with the cellular composition of the pre BötC. Lastly, the organoids displayed synchronous Ca^{2+} activity that is reminiscent of the native functioning pre BötC. This organoid platform could provide the first insight into human respiratory development and function. In the future, these organoids could potentially be used to track neural connectivity, assess how disease phenotypes affect respiratory output, and test new drug therapies during respiratory distress.

4.6 Bibliography

Aaku-Saraste, E., A. Hellwig and W. B. Huttner (1996). "Loss of occludin and functional tight junctions, but not ZO-1, during neural tube closure--remodeling of the neuroepithelium prior to neurogenesis." Dev Biol **180**(2): 664-679.

Amiel, J., B. Laudier, T. Attie-Bitach, H. Trang, L. de Pontual, B. Gener, D. Trochet, H. Etchevers, P. Ray, M. Simonneau, M. Vekemans, A. Munnich, C. Gaultier and S. Lyonnet (2003). "Polyalanine expansion and frameshift mutations of the paired-like homeobox gene PHOX2B in congenital central hypoventilation syndrome." Nat Genet **33**(4): 459-461.

Barcellos-Hoff, M. H., J. Aggeler, T. G. Ram and M. J. Bissell (1989). "Functional differentiation and alveolar morphogenesis of primary mammary cultures on reconstituted basement membrane." Development **105**(2): 223-235.

Bardy, C., M. van den Hurk, B. Kakaradov, J. A. Erwin, B. N. Jaeger, R. V. Hernandez, T. Eames, A. A. Paucar, M. Gorris, C. Marchand, R. Jappelli, J. Barron, A. K. Bryant, M. Kellogg, R. S. Lasken, B. P. Rutten, H. W. Steinbusch, G. W. Yeo and F. H. Gage (2016). "Predicting the functional states of human iPSC-derived neurons with single-cell RNA-seq and electrophysiology." Mol Psychiatry **21**(11): 1573-1588.

Boulenguez, P., P. Gauthier and A. Kastner (2007). "Respiratory neuron subpopulations and pathways potentially involved in the reactivation of phrenic motoneurons after C2 hemisection." Brain Res **1148**: 96-104.

Bouvier, J., M. Thoby-Brisson, N. Renier, V. Dubreuil, J. Ericson, J. Champagnat, A. Pierani, A. Chedotal and G. Fortin (2010). "Hindbrain interneurons and axon guidance signaling critical for breathing." Nat Neurosci **13**(9): 1066-1074.

Crone, S. A., J. C. Viemari, S. Droho, A. Mrejeru, J. M. Ramirez and K. Sharma (2012). "Irregular Breathing in Mice following Genetic Ablation of V2a Neurons." J Neurosci **32**(23): 7895-7906.

Detrick, R. J., D. Dickey and C. R. Kintner (1990). "The effects of N-cadherin misexpression on morphogenesis in Xenopus embryos." Neuron **4**(4): 493-506.

Eiraku, M., K. Watanabe, M. Matsuo-Takasaki, M. Kawada, S. Yonemura, M. Matsumura, T. Wataya, A. Nishiyama, K. Muguruma and Y. Sasai (2008). "Self-organized formation of polarized cortical tissues from ESCs and its active manipulation by extrinsic signals." Cell Stem Cell **3**(5): 519-532.

Feldman, J. L., G. S. Mitchell and E. E. Nattie (2003). "Breathing: rhythmicity, plasticity, chemosensitivity." Annu Rev Neurosci **26**: 239-266.

Goridis, C., V. Dubreuil, M. Thoby-Brisson, G. Fortin and J. F. Brunet (2010). "Phox2b, congenital central hypoventilation syndrome and the control of respiration." Semin Cell Dev Biol **21**(8): 814-822.

Gray, P. A., J. A. Hayes, G. Y. Ling, I. Llona, S. Tupal, M. C. Picardo, S. E. Ross, T. Hirata, J. G. Corbin, J. Eugenin and C. A. Del Negro (2010). "Developmental origin of preBotzinger complex respiratory neurons." J Neurosci **30**(44): 14883-14895.

Guyenet, P. G., D. K. Mulkey, R. L. Stornetta and D. A. Bayliss (2005). "Regulation of ventral surface chemoreceptors by the central respiratory pattern generator." J Neurosci **25**(39): 8938-8947.

Guyenet, P. G., R. L. Stornetta and D. A. Bayliss (2010). "Central respiratory chemoreception." J Comp Neurol **518**(19): 3883-3906.

Hatta, K. and M. Takeichi (1986). "Expression of N-cadherin adhesion molecules associated with early morphogenetic events in chick development." Nature **320**(6061): 447-449.

Jo, J., Y. Xiao, A. X. Sun, E. Cukuroglu, H. D. Tran, J. Goke, Z. Y. Tan, T. Y. Saw, C. P. Tan, H. Lokman, Y. Lee, D. Kim, H. S. Ko, S. O. Kim, J. H. Park, N. J. Cho, T. M. Hyde, J. E. Kleinman, J. H. Shin, D. R. Weinberger, E. K. Tan, H. S. Je and H. H. Ng (2016). "Midbrain-like Organoids from Human Pluripotent Stem Cells Contain Functional Dopaminergic and Neuromelanin-Producing Neurons." Cell Stem Cell **19**(2): 248-257.

Kadoshima, T., H. Sakaguchi, T. Nakano, M. Soen, S. Ando, M. Eiraku and Y. Sasai (2013). "Self-organization of axial polarity, inside-out layer pattern, and species-specific progenitor dynamics in human ES cell-derived neocortex." Proc Natl Acad Sci U S A **110**(50): 20284-20289.

Koizumi, H., N. Koshiya, J. X. Chia, F. Cao, J. Nugent, R. Zhang and J. C. Smith (2013). "Structural-functional properties of identified excitatory and inhibitory interneurons within pre-Botzinger complex respiratory microcircuits." J Neurosci **33**(7): 2994-3009.

Lancaster, M. A., M. Renner, C. A. Martin, D. Wenzel, L. S. Bicknell, M. E. Hurles, T. Homfray, J. M. Penninger, A. P. Jackson and J. A. Knoblich (2013). "Cerebral organoids model human brain development and microcephaly." Nature **501**(7467): 373-379.

Muguruma, K., A. Nishiyama, Y. Ono, H. Miyawaki, E. Mizuhara, S. Hori, A. Kakizuka, K. Obata, Y. Yanagawa, T. Hirano and Y. Sasai (2010). "Ontogeny-recapitulating generation and tissue integration of ES cell-derived Purkinje cells." Nat Neurosci **13**(10): 1171-1180.

Mulkey, D. K., R. L. Stornetta, M. C. Weston, J. R. Simmons, A. Parker, D. A. Bayliss and P. G. Guyenet (2004). "Respiratory control by ventral surface chemoreceptor neurons in rats." Nat Neurosci **7**(12): 1360-1369.

Petersen, O. W., L. Ronnov-Jessen, A. R. Howlett and M. J. Bissell (1992). "Interaction with basement membrane serves to rapidly distinguish growth and differentiation pattern of normal and malignant human breast epithelial cells." Proc Natl Acad Sci U S A **89**(19): 9064-9068.

Ruffault, P. L., F. D'Autreaux, J. A. Hayes, M. Nomaksteinsky, S. Autran, T. Fujiyama, M. Hoshino, M. Hagglund, O. Kiehn, J. F. Brunet, G. Fortin and C. Goridis (2015). "The retrotrapezoid nucleus neurons expressing Atoh1 and Phox2b are essential for the respiratory response to CO(2)." Elife **4**.

Sheikhbahaei, S., E. A. Turovsky, P. S. Hosford, A. Hadjihambi, S. M. Theparambil, B. Liu, N. Marina, A. G. Teschemacher, S. Kasparov, J. C. Smith and A. V. Gourine (2018). "Astrocytes modulate brainstem respiratory rhythm-generating circuits and determine exercise capacity." Nat Commun **9**(1): 370.

Smith, J. C., H. H. Ellenberger, K. Ballanyi, D. W. Richter and J. L. Feldman (1991). "Pre-Botzinger complex: a brainstem region that may generate respiratory rhythm in mammals." Science **254**(5032): 726-729.

Stornetta, R. L., T. S. Moreira, A. C. Takakura, B. J. Kang, D. A. Chang, G. H. West, J. F. Brunet, D. K. Mulkey, D. A. Bayliss and P. G. Guyenet (2006). "Expression of Phox2b by brainstem neurons involved in chemosensory integration in the adult rat." J Neurosci **26**(40): 10305-10314.

Trochet, D., S. J. Hong, J. K. Lim, J. F. Brunet, A. Munnich, K. S. Kim, S. Lyonnet, C. Goridis and J. Amiel (2005). "Molecular consequences of PHOX2B missense, frameshift and alanine expansion mutations leading to autonomic dysfunction." Hum Mol Genet **14**(23): 3697-3708.

Wang, S., Y. Shi, S. Shu, P. G. Guyenet and D. A. Bayliss (2013). "Phox2b-expressing retrotrapezoid neurons are intrinsically responsive to H+ and CO2." J Neurosci **33**(18): 7756-7761.

Wataya, T., S. Ando, K. Muguruma, H. Ikeda, K. Watanabe, M. Eiraku, M. Kawada, J. Takahashi, N. Hashimoto and Y. Sasai (2008). "Minimization of exogenous signals in ES cell culture induces rostral hypothalamic differentiation." Proc Natl Acad Sci U S A **105**(33): 11796-11801.

Weese-Mayer, D. E., E. M. Berry-Kravis, I. Ceccherini and C. M. Rand (2008). "Congenital central hypoventilation syndrome (CCHS) and sudden infant death syndrome (SIDS): kindred disorders of autonomic regulation." Respir Physiol Neurobiol **164**(1-2): 38-48.

Wichterle, H., I. Lieberam, J. A. Porter and T. M. Jessell (2002). "Directed differentiation of embryonic stem cells into motor neurons." Cell **110**(3): 385-397.

Wilson, P. G. and S. S. Stice (2006). "Development and differentiation of neural rosettes derived from human embryonic stem cells." Stem Cell Rev **2**(1): 67-77.

Workman, M. J., M. M. Mahe, S. Trisno, H. M. Poling, C. L. Watson, N. Sundaram, C. F. Chang, J. Schiesser, P. Aubert, E. G. Stanley, A. G. Elefanty, Y. Miyaoka, M. A. Mandegar, B. R. Conklin, M. Neunlist, S. A. Brugmann, M. A. Helmrath and J. M. Wells (2017). "Engineered human pluripotent-stem-cell-derived intestinal tissues with a functional enteric nervous system." Nat Med **23**(1): 49-59.

Wu, J., P. Capelli, J. Bouvier, M. Goulding, S. Arber and G. Fortin (2017). "A V0 core neuronal circuit for inspiration." Nat Commun **8**(1): 544.

Zhang, X., C. T. Huang, J. Chen, M. T. Pankratz, J. Xi, J. Li, Y. Yang, T. M. Lavaute, X. J. Li, M. Ayala, G. I. Bondarenko, Z. W. Du, Y. Jin, T. G. Golos and S. C. Zhang (2010). "Pax6 is a human neuroectoderm cell fate determinant." Cell Stem Cell **7**(1): 90-100.

Chapter 5: Future Considerations

The studies in this dissertation explore ways to control and direct stem cell fate into individual interneuron populations as well as into neural systems that function together. In chapter 2, a hPSC directed differentiation protocol for V2a interneurons, a neuron critical to control of respiration and left-right coordination, was described. Signaling morphogens present during development - sonic hedgehog (Shh), retinoic acid (RA), and a Notch inhibitor (DAPT) were sequentially varied to identify the treatment duration and concentration that resulted in the highest percentage of V2a interneurons. The V2a interneuron culture was demonstrated to mature into a glutamatergic phenotype *in vitro.* V2a interneurons cultures transplanted into uninjured murine spinal cords resulted in maturation and long extension of the hPSC-derived population. This study provided the first report of V2a interneurons from hPSCs. In chapter 3, single cell RNA sequencing revealed the heterogeneous V2a interneuron cultures had a hindbrain/cervical Hox expression pattern and also contained additional neural populations – V0 interneurons and chemosensing neurons – which are critical for control of respiration. Once the phenotypes were confirmed to be present in the *in vitro* cultures, changing RA and Shh agonist concentrations modulated the relative proportions of the different interneuron populations. In chapter 4, the differentiation was modified for a 3D culture platform to develop a method to create hindbrain organoids composed of neurons controlling respiration. At early time points in the differentiation, the organoids recapitulated cell organization and marker expression similar to neural tube development. The organoids

matured to contain glutamatergic neurons and astrocytes similar to the cellular composition of rhythm generating respiratory centers. The organoids displayed synchronous Ca^{2+} flux, a measurable functional response, which was modulated by relative proportions of V2a interneurons, V0 interneurons, and chemosensing neurons. Together, these three studies utilized principles of neural developmental biology and tissue engineering to direct hPSCs into multiple hindbrain populations. While these studies were able to define new phenotypes and a functioning organoid system, it also brings up additional questions and therefore studies that could be further explored.

5.1 Reporter lines for real-time differentiation assessment

Genetically modified cell lines with a fluorescent reporter expressed under the control of a specific target gene are a valuable tool to track and sort specific cell types. A reporter line would have utility in performing real-time assessment of differentiation progress, allow for purifying the population via sorting, and if constructed appropriately, – allow for tracking of a population as it matures and throughout transplantation studies.

The goal of a reporter line is to have expression of a particular reporter gene (typically a fluorescent protein) following expression of the target gene, typically a transcription factor that marks the specific cell population. This strategy has been used to track the progression of many different directed differentiation protocols including human motor neurons and MGE interneurons as well as mouse V2a interneurons (Di Giorgio, Boulting et al. 2008, Amoroso, Croft et al. 2013, Maroof, Keros et al. 2013, Iyer, Huettner et al. 2016). There are three broad strategies in making a reporter line. The most direct is to use the minimal promoter sequence of the gene of interest combined with a reporter and

randomly incorporate the construct into the genome. This strategy has been used to build robust reporter lines for Hb9, the transcription factor that identifies motor neurons (Di Giorgio, Boulting et al. 2008). There are some caveats to this strategy, mainly it requires that the minimal promoter sequence is known. Also, because the construct is randomly integrated, the risk of non-specificity or silencing with differentiation is heightened. An additional strategy is to place a reporter gene directly into the endogenous loci of the targeted gene. This strategy decreases the risk specificity and silencing but requires that the endogenous promoter sequence is sufficient to drive enough expression of the reporter gene that it is visible. One last targeting strategy is to use a cre-lox system. These strategies are used often for conditional knockouts in mice. Briefly, a cre gene is placed at the endogenous loci of the target gene and a lox-STOP-lox-reporter construct is placed in a safe harbor loci. Therefore, expression of the targeted gene would turn on cre and expression and thus the reporter gene. The caveat to this strategy is that it is the most time consuming to build because there are multiple targeting constructs. However, one main difference between this strategy and the previous two is that once a cell expresses the target gene, the reporter will always be expressed due to the change in the safe harbor loci. This could be an advantage or disadvantage depending on the experimental question. For this study, the cre-lox system would be the best strategy and could be utilized in the following experiments.

In this dissertation, the identity of the V2a interneurons, V0 interneurons, and chemosensing neurons were based on the presence and/or absence of specific transcription factors at day 17 of the differentiation. However, it is possible that this fixed time point is not really the point when transcription factor expression peaked. In fact, the

histological assessment of the aggregates in chapter 4 suggested that peak CHX10 expression was at day 15 instead of day 17. Due to batch-to-batch variability, it is also possible that peak transcription factor expression may fall within a window of ~48 hours between differentiation trials. Performing the differentiation with a CHX10 reporter line would allow for real-time temporal analysis of the differentiation progression so that downstream studies could take place at peak transcription factor expression. A reporter line would also make high throughput screening of different differentiation parameters feasible using a high content imaging system.

Another use for a reporter line would be purifying V2a interneurons using fluorescence activated cell sorting (FACS). One important application for sorting V2a would be in transplantation studies. To ensure that the effect of a potential behavioral response is really due to the V2a interneurons and not a different cell type in the heterogeneous population, it would be necessary to purify the V2a interneurons. While cell sorting can be achieved by surface markers there are no known specific surface markers for interneuron subtypes. Therefore, V2a interneurons could be sorted from the heterogeneous culture using an endogenous fluorescent reporter.

Additionally, a reporter cell line would make phenotypic assessment of the mature phenotype possible. There are difficulties with assessment of the mature V2a interneurons in our heterogeneous cultures mainly because the CHX10 transcription factor turns off as the neurons mature. A cre-lox reporter line would allow researchers to track V2a interneurons throughout the maturation process. This would allow for easier electrophysioloical assessment via patch clamp, assessment of neurite extension

properties, as well as provide a way to analyze the transcriptome of the mature V2a population.

Lastly, a reporter line would allow for in situ tracking of transplanted V2a interneurons in animal models The expression of the fluorescent reporter would be cytoplasmic if the cell line is built with the cre-lox strategy allowing for tracking of neurite extensions. Transplantation of V2a interneurons using a CHX10 reporter cell line would allow for the opportunities to confirm that the long neurite extension that was seen in the transplantation studies were from the V2a interneurons.

Together, the development of a reporter line to track the V2a interneurons would increase our understanding of the population on multiple levels. We attempted the construction of a CHX10 reporter line. Initially, the strategy of inserting a reporter construct directly at the CHX10 loci was attempted but the CHX10 promoter was not strong enough to drive visible expression of the fluorescent reporter. A project is on going to build the cre-lox CHX10 reporter line.

While focus in this section has been on the construction of a CHX10 reporter line to study V2a interneurons, it would be advantageous to build the necessary reporter lines to also study the V0 and chemosensing populations. Real-time assessment of all three populations would provide a powerful tool to assess development, self-organization, and connectivity.

5.2 Caudalization of interneuron phenotypes

In chapter 3 it was revealed that the V2a cultures were primarily of the hindbrain/cervical region via Hox expression. The initial hypothesis of the studies

presented here were that the addition of RA and WNT activation would be enough to shift the population to a thoracic spinal phenotype, which was not the case. In actuality the addition of RA and WNT activation shifted the population in the caudal direction away from the brain but only to the hindbrain/cervical region. Future studies could explore how to shift the culture to a more caudal phenotype (thoracic or lumbar regions). Differentiating cells of a thoracic phenotype could allow for study of the locomotor circuitry similar to how the respiratory circuitry is being studied in chapter 4. Further, while the populations have different functional roles *in vivo* (Crone, Quinlan et al. 2008, Crone, Viemari et al. 2012), there has not been a comparison of the electrophysiological properties of hPSC-derived interneurons with differing rostrocaudal identities. Lastly, there have been reports that survival and integration is increased when hPSC-derived populations have a similar rostrocaudal identity to the region where they are getting transplanted (Kadoya, Lu et al. 2016). Therefore, a future study could assess the functional response of transplanting a hindbrain-like V2a interneuron population compared to a more thoracic V2a interneuron population.

While there is motivation for differentiating a more caudal phenotype, future studies will need to determine how to create a caudal phenotype while still maintaining the V2a interneuron identity. One of the first signaling molecules to add to try to obtain a more caudal phenotype would be Fibroblast growth factor (FGF). Developmentally, FGF signaling is increased in the thoracic region of the spinal cord compared to RA concentration (Liu, Laufer et al. 2001). Further, addition of FGF8 and the WNT activator, CHIR before addition of RA when directing hPSCs to a neural lineage increased Hox expression found in the low cervical/high thoracic region (Lippmann, Williams et al. 2015). There are some obvious

signaling molecule candidates (FGFs and GDF11) that could be added to the protocol to differentiate a more caudal phenotype. However, the addition of two more molecules of which optimal concentration and duration need to be determined would make an already complex protocol more convoluted. Addition of new signaling paradigms to the protocol may warrant a more systematic approach to optimization such as design of experiment.

5.3 Optimization of differentiation using design of experiment

In chapter 2, a protocol to differentiate V2a interneurons from pluripotent stem cells as described that resulted in 25 to 50% $CHX10^{+}$ cells. To define the V2a interneuron protocol, three signaling molecules, RA, pur, and DAPT were varied one at a time while keeping the concentration of the other two molecules constant and only the duration of DAPT was explored. While this strategy was successful in differentiating V2a interneurons, a more systematic approach of sampling the experimental space would more accurately optimize the differentiation. The protocol currently uses 4 different signaling molecules at varying concentrations and exposure times leading to 8 testable parameters. An additional key variable of the monolayer differentiation is seeding density. Therefore, that leaves 9 parameters to be optimized for the current protocol. If two additional caudalization molecules are explored, that will bring the total to 13 to assess both concentration and signaling duration. Assessment of every combination of the 13 parameters with 3 conditions for each parameter would take 1,594,323 experiments. Since this is not feasible, fractional factorial design is a statistical a tool that can be used to systematically explore the experimental space without testing every possible combination. The model makes an assumption that some interactions between 3 or more factors are insignificant and

therefore do not need to be evaluated. The experiment is performed and reiterated on until peak expression of the output parameter is reached. For V2a interneurons, that would be CHX10 expression.

Progress has been made to make this experiment technically feasible. While fractional factorial design reduces the number of conditions that need to be tested, it is still more conditions than what was attempted in the previous studies. Therefore, the differentiation was scaled down from 24-well plates to 96-well plates. Also, evaluating CHX10 expression using flow cytometry from cell differentiated in a 96-well plate may be difficult and time-consuming so the use of a high-content imager to evaluate immunostaining of CHX10 on fixed samples will be used. However, the use of a reporter line, as described above would greatly stream line the process. Similar to above, while this process was described for optimization of V2a interneurons, the same process could be applied to optimize V0 interneurons and chemosensing neurons or even to identify a combination of molecules that results in a specific ratio of the three populations.

5.4 Conclusions

The results of this dissertation significantly add to the field of tissue engineering by providing a platform to derive new interneuron populations from hPSCs that can be further explored in a variety of different fields. These new cell types are new tools that can be used to explore a variety of different platforms including, probing developmental neurobiology, disease modeling, and cell therapeutics. For developmental purposes, this research provides a way to probe human phenotypes that were not possible before. The hindbrain organoid recapitulates some processes of development providing a platform for

researchers to probe different developmental pathways and explore how it changes cell fate. The end of chapter 4 describes one potential application of disease modeling using central congenital hypoventilation syndrome (CCHS). Models of ALS could be explored in the organoid models as V2a interneurons have been implicated to have a compensatory effect with ALS progression (Romer, Seedle et al. 2017). Additionally, this research demonstrates the ability to produce many new potential candidates for cell therapeutics. Studies are on-going evaluating the role of V2a interneurons in applications of thoracic spinal cord injury. Due to the hindbrain/cervical phenotype of the cells, it would be interesting to test these cells in a cervical injury model. Additionally the therapeutic benefit of the V0 interneurons and the chemosensing populations could be explored individually or in combination. While there are currently many ways to further explore the neural populations derived in this dissertation, as the roles of the interneuron and chemosensing populations continue to be elucidated, new opportunities for these cell populations may be uncovered.

5.5 Bibliography

Amoroso, M. W., G. F. Croft, D. J. Williams, S. O'Keeffe, M. A. Carrasco, A. R. Davis, L. Roybon, D. H. Oakley, T. Maniatis, C. E. Henderson and H. Wichterle (2013). "Accelerated high-yield generation of limb-innervating motor neurons from human stem cells." J Neurosci **33**(2): 574-586.

Crone, S. A., K. A. Quinlan, L. Zagoraiou, S. Droho, C. E. Restrepo, L. Lundfald, T. Endo, J. Setlak, T. M. Jessell, O. Kiehn and K. Sharma (2008). "Genetic ablation of V2a ipsilateral interneurons disrupts left-right locomotor coordination in mammalian spinal cord." Neuron **60**(1): 70-83.

Crone, S. A., J. C. Viemari, S. Droho, A. Mrejeru, J. M. Ramirez and K. Sharma (2012). "Irregular Breathing in Mice following Genetic Ablation of V2a Neurons." J Neurosci **32**(23): 7895-7906.

Di Giorgio, F. P., G. L. Boulting, S. Bobrowicz and K. C. Eggan (2008). "Human embryonic stem cell-derived motor neurons are sensitive to the toxic effect of glial cells carrying an ALS-causing mutation." Cell Stem Cell **3**(6): 637-648.

Iyer, N. R., J. E. Huettner, J. C. Butts, C. R. Brown and S. E. Sakiyama-Elbert (2016). "Generation of highly enriched V2a interneurons from mouse embryonic stem cells." Exp Neurol **277**: 305-316.

Kadoya, K., P. Lu, K. Nguyen, C. Lee-Kubli, H. Kumamaru, L. Yao, J. Knackert, G. Poplawski, J. N. Dulin, H. Strobl, Y. Takashima, J. Biane, J. Conner, S. C. Zhang and M. H. Tuszynski (2016). "Spinal cord reconstitution with homologous neural grafts enables robust corticospinal regeneration." Nat Med **22**(5): 479-487.

Lippmann, E. S., C. E. Williams, D. A. Ruhl, M. C. Estevez-Silva, E. R. Chapman, J. J. Coon and R. S. Ashton (2015). "Deterministic HOX patterning in human pluripotent stem cell-derived neuroectoderm." Stem Cell Reports **4**(4): 632-644.

Liu, J. P., E. Laufer and T. M. Jessell (2001). "Assigning the positional identity of spinal motor neurons: rostrocaudal patterning of Hox-c expression by FGFs, Gdf11, and retinoids." Neuron **32**(6): 997-1012.

Maroof, A. M., S. Keros, J. A. Tyson, S. W. Ying, Y. M. Ganat, F. T. Merkle, B. Liu, A. Goulburn, E. G. Stanley, A. G. Elefanty, H. R. Widmer, K. Eggan, P. A. Goldstein, S. A. Anderson and L.

Studer (2013). "Directed differentiation and functional maturation of cortical interneurons from human embryonic stem cells." Cell Stem Cell **12**(5): 559-572.

Romer, S. H., K. Seedle, S. M. Turner, J. Li, M. L. Baccei and S. A. Crone (2017). "Accessory respiratory muscles enhance ventilation in ALS model mice and are activated by excitatory V2a neurons." Exp Neurol **287**(Pt 2): 192-204.

Publishing Agreement

It is the policy of the University to encourage the distribution of all theses, dissertations, and manuscripts. Copies of all UCSF theses, dissertations, and manuscripts will be routed to the library via the Graduate Division. The library will make all theses, dissertations, and manuscripts accessible to the public and will preserve these to the best of their abilities, in perpetuity.

I hereby grant permission to the Graduate Division of the University of California, San Francisco to release copies of my thesis, dissertation, or manuscript to the Campus Library to provide access and preservation, in whole or in part, in perpetuity.

Author Signature 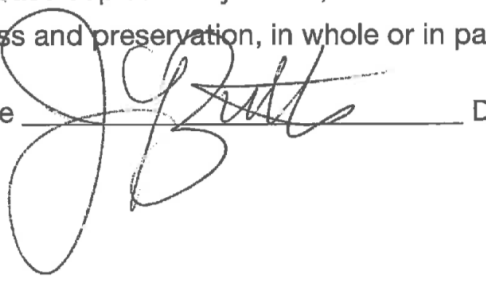 Date 6/11/18